

Crystal Nucleation in Molecular Liquids and Glasses: Effects of  
the Liquid/Vapor Interface, Polymers, and Surfactants

By  
Xin Yao

A dissertation submitted in partial fulfillment of  
the requirements for the degree of

Doctor of Philosophy  
(Pharmaceutical Sciences)

at The  
UNIVERSITY OF WISCONSIN-MADISON  
2022

Date of Final Oral Examination: August 02, 2022

This dissertation is approved by the following members of the Final Oral Committee:

Lian Yu, Professor, Pharmacy and Chemistry (Dissertation Advisor)

Glen Kwon, Professor, Pharmacy

Sandro Mecozzi, Professor, Pharmacy

Mark D. Ediger, Professor, Chemistry

*To my family*

## Acknowledgements

When I am writing this thesis in the lab office, where I spent the most of my time in the past 5 years, I realize that I am walking toward the end of my Ph.D. journey at the University of Wisconsin-Madison. Before reaching the termination, I look back, with a compacted and convoluted feeling flowing into my chest and caressing my heart. When I try to deconvolute the feeling as a scientist, I find I am probably dealing with another thesis topic. But I clearly see the most important part: my appreciation to all the people who helped and supported me in my training and life as mentors, teachers, collaborators, mentees, friends, and families.

I cannot thank Prof. Lian Yu enough for his training and help. We met even before I came to the UW-Madison in the front of Beiyisanyuan, where he was wearing a blue cap as the sign for me to find him. I can still recall that hot and humid day, and my enthusiasm of introducing my research to him. That first meeting led to my rotating and finally joining in his lab for studying solid-state chemistry in late 2017. In the past five years, my appreciation to him has been growing with the growth of myself. When I read my own slides and manuscript drafts 3-4 years ago, I cannot say how patient and tolerant Lian is to his students. When one looking at such products, huge courage is needed to train the student and believe in him. Lian did. He tirelessly exhorted me to kill typos and other sloppy mistakes in writing, to structure stories and sentences logically and smoothly, and to trim the product to show highlights with concision. With his training I stepped into a new world of writing with astonishing how far away I am to a good scientific writer and presenter. Besides scientific communication, he also trained me to be a careful and productive scientist who can design and perform valid experiments, evaluate the validation of results, analyze data, and draw right conclusions, by focusing the value and aim of research. In life, he is a good friend from the same hometown as mine and a respectable elder like a family. He gave his students great happiness and company by hosting home parties with his wife Karren and his son Patrick. I appreciate all his strict but kind training in science, and great help and company in life.

I would like to thank my committee members, Prof. Glen Kwon, Prof. Sandro Mecozzi, Prof. Mark Ediger and Prof. Ronald Burnette (retired). They and Lian show me how to be a good scientist. They spent time with me during my committee meetings and exams, gave me suggestions about science and career, asked insightful questions, and encouraged me to dive deeper into my study. Mark and Ron gave me excellent lectures on polymer physics and pharmacokinetics respectively. What I learned in their courses really helps me with my research and career, and encourages me to keep learning. I feel grateful to my committee members who encouraged me to do good sciences, watched me growing, and supported me in my training and career development.

I thank my collaborators. All the publications would not happen without their contributions. Dr. Geoff Zhang and Dr. Chenyang Shi brought our collaboration with AbbVie to study crystal nucleation, and provided suggestions and comments at our quarter meetings. Prof. Bu Wang and Qitong Liu really provided great help with their expertise on molecular dynamics simulations. Dr. Ilia Guzei and Michael Aristov contributed excellent work on crystal structure solutions in my projects. Dr. Niya Bowers, Dr. Phil Goliber, Mrs. Ellen Harrington, Dr. Francisco Alvarez, and Dr. David Monteith from the Bill & Melinda Gates Foundation offered helpful discussions on formulating amorphous drugs for global health. It is so exciting that the formulation we developed will be tested in animals. Dr. Mark Sacchetti and Ms. Karen Jones in Zeeh Pharmaceutical Experimental Station at the University of Wisconsin-Madison School of Pharmacy helped me with facilities and suggestions on studying drug dissolution.

I also owe thanks to my colleagues in Yu lab. We covered each other's back in research and life. M is a great friend and a good guide to exploring Madison and Chicago. Chengbin guided me when I started my research and shared a lot of tips and experiences with me sincerely. Zhenxuan helped me a lot and hosted wonderful parties in the group. Yue supported me in life and collaborated with me on several projects. Yuhui joined the group in the same year as me. We helped each other and went through a lot of things together. Junguang helped my research with XPS experiments and cooked yummy moon cakes. Amy worked with me on the Gates project and cooked desserts for the group. Kennedy managed all the

orders and safety regulations in the group, and worked with me on nucleation projects. Thanks to her, everyone's life in the lab becomes easier. Caroline joined the group in my last year here, but also encouraged me with her efforts in the lab. Dr. Zeng, Changlin, Hao and Chengyu also brought joy to my life and new views to my research. I really appreciate all the help, support, and company of you. I believe all the good memories with you will be projected like a movie in my mind when I revisit the photos we took together.

Thanks to my mentors and group members during my summer internship at AbbVie. Dr. Geoff Zhang, Dr. Chenyang Shi, Xiaochun, Gosia, Joe, and Socrates at AbbVie really supported me in my research and life there. Thanks to my mentees, Emily Benson, Soojin Kim, and Erin McCann. They tolerated my mature mentoring, taught me how to be a good mentor, and contributed to my research projects. All of them are pursuing doctor degrees now. Wish them great success in their own research and career.

I would have much more headache if without my great friends in Madison. I met Xiaolei and Ri at Peking University, with their company I landed on this faraway and unfamiliar land to start a brand-new life. I cannot say enough thanks to them for their help and friendship all the time. Qinying and Jerry (Zihui) are good friends of me and Yue. We had so many wonderful memories together during travelling and exercising. Zhongrui and Miyang are my roommates and made my life much easier. Thank Jinshan, Lauren, Chris, Hye Jin, Arielis, Cassie, Zack, Ao, and Bin. for their help and company especially in my first two years in Madison. I especially thank Dr. Melgardt De Villiers and Mrs. Bonnie Fingerhut. I cannot forget their kind help and patient explanations when I knew little about this country and the compounding lab, and cannot forget the fun time at our lunch-meal meetings.

Finally, I thank my parents for their love. I am always ready to face challenges because I can recharge my batteries by chatting with them when I am tired, frustrated, and despaired. Commencement is just a start of my career. I foresee a much harder journey in the future, and I do feel the required courage and strength to step forward, to keep learning, and to discovery the world. At the end, I appreciate all the experiences at UW-Madison. It is great to be a curious, brave, and tough badger.

## Table of Contents

Acknowledgements.....	ii
Abstract.....	viii
Chapter 1. Introduction .....	1
1.1. Overview.....	2
1.2. Crystal Nucleation .....	4
1.3. Polymorphism.....	13
1.4. Anisotropic Environment at the Surface and the Impact on Crystallization.....	16
1.5. Effect of a Second Component on Crystal Nucleation and Growth .....	17
1.6. Contributions of This Thesis.....	19
1.7. References.....	22
Chapter 2. Anisotropic Molecular Organization at a Liquid/Vapor Interface Promotes Crystal Nucleation with Polymorph Selection.....	28
2.1. Abstract.....	29
2.2. Introduction.....	29
2.3. Results and Discussion .....	30
2.4. Conclusions.....	42
2.5. Materials and Methods.....	43
2.6. Acknowledgements.....	47
2.7. Supporting Information.....	47
2.8. References.....	54
Chapter 3. Surface-Enhanced Crystal Nucleation and Polymorph Selection in Amorphous Posaconazole .....	58
3.1. Abstract.....	59
3.2. Introduction.....	60
3.3. Materials and Methods.....	63
3.4. Results and Discussion .....	65

3.5. Conclusions.....	79
3.6. Acknowledgements.....	80
3.7. Supporting Information.....	80
3.8. References.....	85
Chapter 4. Effect of Polymers on Crystallization in Glass-Forming Molecular Liquids: Equal Suppression of Nucleation and Growth and Master Curve for Prediction .....	89
4.1. Abstract .....	90
4.2. Introduction.....	90
4.3. Materials and Methods.....	93
4.4. Results.....	95
4.5. Discussion .....	107
4.6. Conclusions.....	111
4.7. Acknowledgements.....	112
4.8. Supporting Information.....	112
4.9. References.....	115
Chapter 5. Surfactants Accelerate Crystallization of Amorphous Nifedipine by Similar Enhancement of Nucleation and Growth Independent of Hydrophilic-Lipophilic Balance .....	117
5.1. Abstract .....	118
5.2. Introduction.....	119
5.3. Materials and Methods.....	122
5.4. Results.....	123
5.5. Discussion .....	130
5.6. Conclusions.....	134
5.7. Acknowledgments.....	135
5.8. Supporting Information.....	136
5.9. References.....	138
Chapter 6. Amorphous Drug-Polymer Salt with High Stability under Tropical Conditions and Fast Dissolution: The Challenging Case of Lumefantrine-PAA .....	140

6.1. Abstract.....	141
6.2. Introduction.....	142
6.3. Materials and Methods.....	145
6.4. Results.....	148
6.5. Discussion.....	159
6.6. Conclusions.....	162
6.7. Acknowledgments.....	163
6.8. Supporting Information.....	163
6.9. References.....	165
Chapter 7. Amorphous Drug–Polymer Salts.....	169
7.1. Abstract.....	170
7.2. Introduction.....	170
7.3. Polyelectrolyte Coating.....	174
7.4. Amorphous Drug–Polymer Salts in the Bulk.....	180
7.5. Concluding Remarks.....	187
7.6. Acknowledgments.....	189
7.7. References.....	189
Chapter 8. Conclusions and Future Work.....	194
8.1. Surface Nucleation in Different Molecular Liquids.....	195
8.2. Effect of Dopants on Surface Nucleation.....	199
8.3. Effects of Molecular Weight, Drug Loading, and Synthesis Process on the Protonation Ratio and Performance of Amorphous Drug-Polymer Salts.....	200
8.4. References.....	201



## Abstract

This thesis considers crystal nucleation in the liquids and glasses of organic molecules. Crystal nucleation together with crystal growth defines the phase and microstructure of a crystalline material and therefore its properties. Crystal nucleation has been extensively studied for many decades, but many unanswered questions remain. Here, we focus on two situations: Crystal nucleation (1) at the Liquid/Vapor interface and (2) in the presence of a second dissolved component (dopant).

We demonstrate that nucleation at the surface of a pure liquid, D-arabitol, is vastly enhanced, by 12 orders of magnitude, and selects a different polymorph (Chapter 2). Similarly, surface nucleation of posaconazole is vastly enhanced over bulk nucleation, by approximately 9 orders of magnitude, and selects a different polymorph from the bulk (Chapter 3). The phenomenon likely results from the anisotropic organization at the surface and its similarity to the surface-nucleating polymorph. A comparison of these two systems with two other systems (water and acetaminophen) whose surface nucleation has been studied suggests that a strong surface effect on nucleation requires (1) significant reconstruction at the surface and (2) the existence of a different polymorph whose structure is similar to that of the liquid surface.

We study the effect of a dopant (a polymer or a surfactant) on crystal nucleation and growth of the host molecules under deep supercooling. The polymer PVP slows the nucleation and growth by a similar factor when doped in D-sorbitol or D-arabitol (Chapter 4). The surfactants (Tween 80, Span 80, Triton X-100, and poloxamer) doped in amorphous nifedipine enhance its nucleation and growth by a similar factor (Chapter 5). These results indicate that crystal nucleation and growth in a deeply supercooled liquid are both limited by mobility and a dopant at low concentrations (<15%) essentially acts as a mobility

modifier (enhancer or inhibitor), altering the two rates by a similar factor. This allows the prediction of hard-to-measure nucleation rates from easy-to-measure growth rates in multi-component systems.

We show that the formation of a drug-polymer salt can effectively stabilize an amorphous drug against crystallization under the highly stressful tropical conditions (high temperature and high humidity), without sacrificing fast dissolution. Lumefantrine (LMF), a basic and easy-to-crystallize WHO drug for treating malaria, and poly(acrylic acid) (PAA) are presented as a test case (Chapter 6), followed by a general discussion of the state of the art (Chapter 7).

## **Chapter 1. Introduction**

Xin Yao

## 1.1. Overview

The same molecules can exist in different condensed phases, e.g., liquids, glasses, and crystals. The phases are distinguished by their kinetic and structural features. Liquids and glasses are distinguished by their kinetic difference. In liquids, molecules are still mobile within human consciousness (structural relaxation time  $\tau_\alpha < 100$  s,<sup>1</sup> viscosity  $\eta < 10^{12}$  Pa.s,<sup>2</sup> and self-diffusion coefficient  $D > 10^{-20}$  m<sup>2</sup>/s),<sup>3</sup> allowing liquids to flow and fill a container. Glasses, however, cannot within conscious time and are taken as solids. In glasses, molecules move so slow as being steady, in other words, reach kinetic arrest. Additionally, unlike liquids, glasses are not an equilibrated state due to kinetic arrest. The structure of a glass keeps changing overtime, or so-called glass aging. Despite the kinetic difference, both liquids and glasses lack long-range order and are the so-called amorphous materials. Such isotropic or quasi-isotropic packing allow glasses to be macroscopically homogeneous for important applications, from optical microscopes to eyeglasses. This structural feature of glasses differs from crystals, which have regular molecular packing organized through specific and repeating intermolecular interactions. This structural difference can be readily characterized under X-ray radiation. Crystals show sharp X-ray diffraction peaks because the regularly packed molecules are the diffraction grating for X-ray following Bragg's law, but

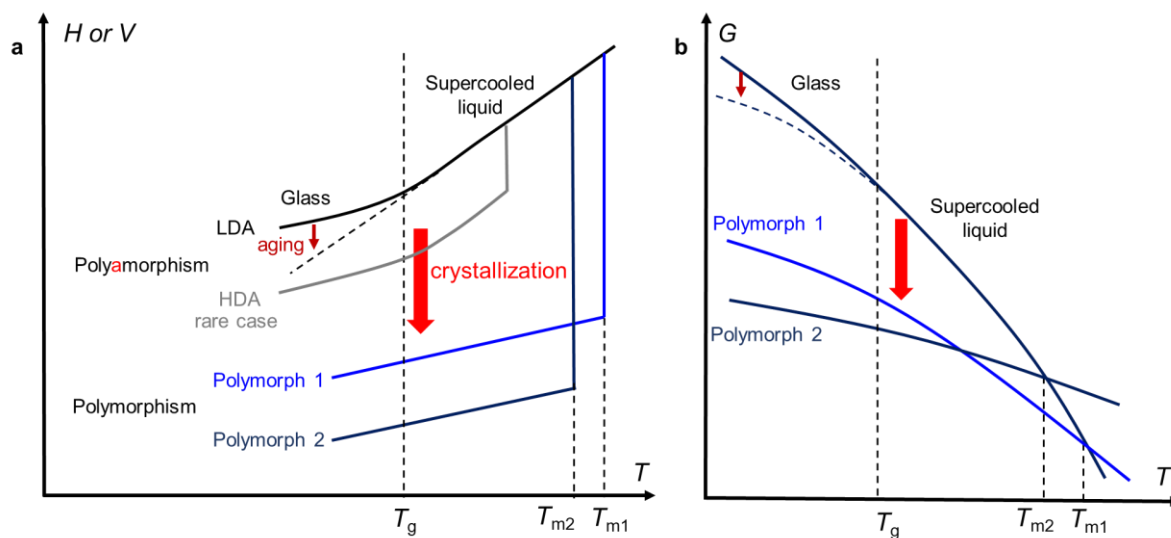


**Figure 1.** (a) Enthalpy ( $H$ ) or volume ( $V$ ) (b) the Gibbs free energy ( $G$ ) of liquids, glass and crystals as a function of temperature ( $T$ ). Crystallization can spontaneously happen below melting temperature.

glasses and liquids only show broader scattering peak(s). The structural and kinetic differences among the phases lead to different thermodynamic properties. The phases are distinguished in the plots of enthalpy ( $H$ ) or volume ( $V$ ) vs. temperature ( $T$ ), and the Gibbs free energy ( $G$ ) vs. temperature, as shown in Figure 1a and 1b.

Crystallization can happen in the supercooled liquids or glasses, as shown in Figure 1. A liquid is more stable than its crystal above a melting temperature ( $T_m$ ). Those liquids widely exist in our life, e.g., water, soybean oil, and gasoline. However, liquids can spontaneously convert into crystals below  $T_m$ , as the icing of water below freezing point. The relative stability between liquids and the crystals are rooted in their structural difference. The lack of long-range order and weaker intermolecular integration allow liquids to have higher entropy ( $S$ ) and lower enthalpy ( $H$ ) than crystals, thus more stable than crystals at high temperatures, but less stable at low temperatures according to the equation of the Gibbs free energy ( $G = H - ST$ ). Crystallization can happen, but may not happen in a certain time, or never happen at all. If crystallization does not happen when we cool a liquid below  $T_m$ , we can get a supercooled liquid, a metastable phase. If we keep cooling a supercooled liquid without crystallization, molecules move slower and slower and eventually will reach kinetic arrest at glass transition temperature ( $T_g$ ) and form a glass. Due to the unequilibrated state of glass, the conventional glasses by melt-quench usually have higher energy than the hypothetical supercooled liquids at the same temperature, and obviously can crystallize. This thesis focuses on studying the crystallization kinetics in supercooled liquids or glasses. Crystallization happens in a sequence of two steps, crystal nucleation and growth. Crystal growth inevitable happens and is mainly diffusion controlled. The crystal growth rate can be predicted fairly well with given viscosity or diffusion coefficient.<sup>3,4</sup> Compared with crystal growth, crystal nucleation is not well understood due to its additional energy barrier for generating an interface,<sup>5,6</sup> and is the center of this thesis.

The beauty of nature arises from its extraordinary variety developed from limited elements. In the condensed phases, it is astonishing that the same molecules not only can exist in liquid, glass and crystal states, but also exist in different liquids,<sup>7, 8</sup> glasses,<sup>9-12</sup> and crystals.<sup>13</sup> Since glasses are not equilibrated due to kinetic arrest, the different structures can remain after they are initially packed through different preparation methods.<sup>9-12</sup> Additionally, different crystalline (amorphous) phases separated by first-order transition can exist. This phenomenon is called polymorphism (polyamorphism). Figure 1 shows the example of the phases with their enthalpy differences. Polyamorphism is rare relative to polymorphism. Only few systems are known to have polyamorphs, e.g., water,<sup>8</sup> mannitol,<sup>7</sup> triphenyl phosphite (TPP).<sup>14</sup> As a contrast, one in three compounds in the Cambridge Structural Database (CSD) has polymorphs,<sup>15</sup> and ROY (5-methyl-2-[(2-nitrophenyl)amino]-3-thiophenecarbonitrile) has the crown by having 13 known polymorphs,<sup>6</sup> there could be even more polymorphs undiscovered for any molecules. To study crystallization kinetics, it becomes evidently important to distinguish the polymorphs and understand their different crystallization kinetics.

This thesis studies the effects of liquid/vapor (L/V) interface and dopant on crystal nucleation and growth, the control of crystallization in drug development, and the polymorphism of the studied systems.

## 1.2. Crystal Nucleation

Crystal nucleation is the initial step of crystallization and decides how long a supercooled liquid can last because crystal growth happens following nucleation inevitably. More importantly, crystal nucleation impacts the grain size and the polymorph of crystals, which decide the properties of crystalline material everywhere, e.g., metals, silicon chips, and drugs. For example, fine grain size of metals and alloys gives greater strength and toughness. Refinement of grain size is achieved by doping certain ingredients which form dense heterogenous nuclei.<sup>16</sup> Differently, silicon chips are manufactured using single crystal of

silicon instead of polycrystals because the boundary of silicon crystals can lower the conductivity and a uniform film is desired. A single crystal is grown by seeding and avoiding crystal nucleation. In drug industry, solution crystallization is the first choice to purify compounds in large scales. During crystallization processes, crystal nucleation needs to be controlled<sup>17</sup> to generate desired polymorph, particle morphology and size distribution to achieve good physical stability, powder flowability, and compressibility for later processes. These are but three examples of many in which crystal nucleation plays an important role.

Crystal nucleation can be classified into homogeneous or heterogeneous nucleation by whether nucleation appears in a single phase or at the interfaces respectively. Further, heterogeneous nucleation can happen through different mechanisms depending on the structure and the curvature of the interface.<sup>18</sup> For example, nucleation induced by crystal/liquid interface is usually attributed to the lattice match or specific intermolecular interactions between the crystal surface and the nucleating crystal.<sup>19-21</sup> A rare and special case of heterogeneous nucleation is cross-nucleation, that a second polymorph heterogeneously nucleate on an initial polymorph.<sup>22-24</sup> Among the varied situations, the effect of Liquid/Vapor<sup>25</sup> and Crystal/Liquid interface<sup>26</sup> attract great attention for their universality in nature and the potential applications. In this thesis, we discuss the Liquid/Vapor interface (the free surface) on crystal nucleation in chapter 2 and 3.

### 1.2.1. Current methodologies of studying crystal nucleation

For measuring the nucleation rates, methods are used differently between fast and slow-crystallizing systems. In fast-crystallizing systems, e.g., water, alkanes, and metals, the crystal growth rate is so fast that a sample will fully crystallize when one nucleus appears. To measure nucleation rate, samples are dispersed into separated droplets in vapor or liquid matrix so that droplets do not interfere each other when crystallizing. The ratio of crystallized droplets among the total droplets is analyzed based on the size distribution of the droplets, following 0 order of Poisson distribution. This method inevitably involves large interface to the sample. To know the nucleation type, the sample sizes need to be varied to test

whether the interface causes significant differences (heterogeneous) or not (homogeneous). During the analyses, complicated model and wide distribution of particle size can be involved to fit the data, leading to some uncertainties.<sup>25</sup> Actually, even for water, the most studied system, the analysis is not solid enough to conclude whether the liquid/vapor interface induces nucleation or not,<sup>25</sup> and the discrepancy is huge under deep supercooling.<sup>27</sup>

In this method, the way of generating droplet dispersions includes condensing vapor phase through a supersonic nozzle,<sup>28</sup> atomizing,<sup>29</sup> injecting droplets in an elevated chamber<sup>30</sup> or flowing through detectors,<sup>27</sup> emulsifying,<sup>31, 32</sup> dispersing droplets on a hydrophobic solid surface.<sup>33</sup> Among the methods, droplets injection, atomizer, and emulsion usually give particles with narrow particle-size-distribution, which is desired to reduce measurement error. Smaller droplet size is desired for pushing up the measurement limit of nucleation rates under even deeper supercooling. Among all the methods, condensing vapor phase<sup>28</sup> can generate smallest droplets (with radii between 3 and 6 nm). But condensing method requires water molecule to go through a long tunnel where condensation and crystallization happen in a sequence. During that, temperature and droplet size distribution although can be monitored but keep changing all the time, leading to complexity of interpreting data relative to other methods. To get the nucleation rate, the fraction of crystallized droplets can be measured for analyzing the accumulated signal of all the droplets together using Fourier transform infrared (FTIR) spectroscopy,<sup>28, 29</sup> and differential scanning calorimetry (DSC),<sup>31</sup> or measuring the counts of crystallized droplets over the total counts using light microscopy,<sup>32, 33</sup> synchrotron X-ray scattering,<sup>27</sup> and light scattering.<sup>34</sup>

For slow-crystallizing materials, since multiple nuclei can exist in the same sample before full crystallization, nucleation rates can be measured by monitoring crystal density over time. This method is used widely in the ceramic glasses<sup>35</sup> and recently in glass-forming molecular liquids.<sup>5, 6</sup> Crystals can be developed at a single nucleation temperature when crystal growth is fast enough ( $>10^{-11}$  m/s). If crystals grow too slowly at a nucleation temperature, a second stage is needed to grow nuclei to a visible size at a



higher temperature. Then, the nucleation time can be plotted with the crystal densities, the slope at a steady state is the frequency of generating nuclei, thus the nucleation rate. Without complicated model fitting, this method can give accurate nucleation rates, and distinguish homogeneous and heterogeneous nucleation by varying the bulk volume/interface area ratio. Multiple examples are shown in the Chapter 2-3. Another method to extract nucleation rates is measuring the total crystallinity and crystal growth rates as a function of time. Since the nucleation and growth rates decide the total crystallinity, given the geometry of the crystals and crystal growth rates, nucleation rates can be extracted from the total crystallization rate by fitting all the data into the Avrami equation,<sup>36, 37</sup> which is derived by assuming nuclei appear randomly and the volume increment that forms during each time increment is proportional to the amorphous volume remaining in the sample. However, the error from growth rates and geometry constrictions can be enlarged during the fitting to calculate nucleation rates.

Nowadays, great interests are shown in describing the assembling process of nucleation by observing nuclei evolution directly using advanced electron microscopies. Nucleation process has been observed using atomic electron tomography<sup>38</sup> for FePt nanoparticles, time-resolved cryo-transmission electron microscopy (Cryo-TEM) for proteins solution,<sup>39</sup> and in situ transmission electron microscopy (TEM) for calcium carbonate ( $\text{CaCO}_3$ ) solution.<sup>40</sup> Observing crystal nucleation of small molecules could be more challenging than the above cases due to that the constituent atoms (C, N, O) scatter electrons similarly and much more weakly than heavy atoms do, and the molecule size is much smaller than proteins. However, with the improvement of spatiotemporal resolution, it is reasonable to expect observing crystal nucleation of small molecules in the future.

Computer simulations are also applied to study crystal nucleation. Compared with experiments, the advantages of computer simulations are obvious: The nucleation process can be observed as it happens and at atomic scales, and many physical properties can be followed and analyzed during nucleation. However, there are also significant limitations of simulations for studying crystal nucleation, which is a

rare event.<sup>41</sup> Thus, the limitations are mainly the simulation cost depending on simulation time and system size, and the accuracy of the simulation model. Nowadays, the typical simulation time is in nanosecond range.<sup>42</sup> The state-of-the-art simulation time is on scales of milliseconds,<sup>43</sup> and the typical box sizes is  $1000 \text{ nm}^3$ . Only when nucleation rate is faster than  $10^{27} / \text{m}^3/\text{s}$ , one nucleus can be observed in a  $1000 \text{ nm}^3$  simulation box in 1 millisecond. But many important nucleation processes are far slower than this rate. To gain good statistics, either the simulation box, or simulation time, or simulation runs needs to be increased by 10-100 times, and the simulation cost is unaffordable for a lot of materials without simplifying the simulation model. To solve this problem, enhanced sampling methods are usually used to accelerate the nucleation process by applying an external bias potential or enhancing the naturally occurring fluctuations of the system.<sup>41</sup> However, one concern is that the simulation results can depend on the force field used.<sup>44</sup> All the order parameters, enhanced sampling methods, and force field parameters can influence the final results. The more accurate the model is, the higher the simulation cost is. A balance between simulation cost and accuracy is needed, and sometimes can be tricky because the validation of simulations needs to be tested using experimental results. Overall, it is still challenging to study crystal nucleation using computational simulations.

### 1.2.2. Crystal nucleation rates in glasses and supercooled liquids

There are several systems whose nucleation rates have been experimentally measured in their glasses and supercooled liquids. We plot them in Figure 2. As poor glass-forming materials, water,<sup>27,33</sup> alkanes,<sup>45</sup> and Ni<sup>46</sup> show fast nucleation rates at relative high temperatures. It is worth noting that their nucleation rates have not been measured at the left wing of the nucleation-temperature curve, and the measurement temperatures are far above their glass transition temperatures. Among those materials, water has been studied most extensively. However, significant discrepancies exist,<sup>27,47</sup> likely due to the varied droplet size and different analysis models. It has been suggested the large discrepancies are due to the crystal nucleation induced by the liquid-vapor interface.<sup>47</sup> Besides water, metals (Fe, Au, and Ni) can be supercooled much deeper when the gas interface is avoided by sealing the melts in molten glass.<sup>46,48</sup>

Alkanes show supercooling in emulsions but not in the air environment.<sup>31,49</sup> All those results indicate that the vapor interface can play an important role in the nucleation of weak glass-forming materials. More careful studies are needed to investigate whether the measured nucleation rates are real homogeneous nucleation, or surface-induced nucleation.

Nucleation has been also measured for glass-forming materials, including silicate glasses<sup>50-52</sup> and organic liquids.<sup>6, 53</sup> Different from the earlier cases, the nucleation rates in the glass-forming liquids can be measured covering the nucleation rate maximum. The measured nucleation rates are within the range of  $10^3$ – $10^{13}$  / $m^3/s$ , a combined result of measurement time and sample volume. One important feature is that all the nucleation maximum temperatures are within the range of 1.0–1.2  $T/T_g$ . It is important to know whether this is also true for poor glass-forming materials. Overall, the known data about nucleation is still not sufficient to predict nucleation rates for an arbitrary system. It is interesting to measure nucleation rates at wider temperature and rate ranges.

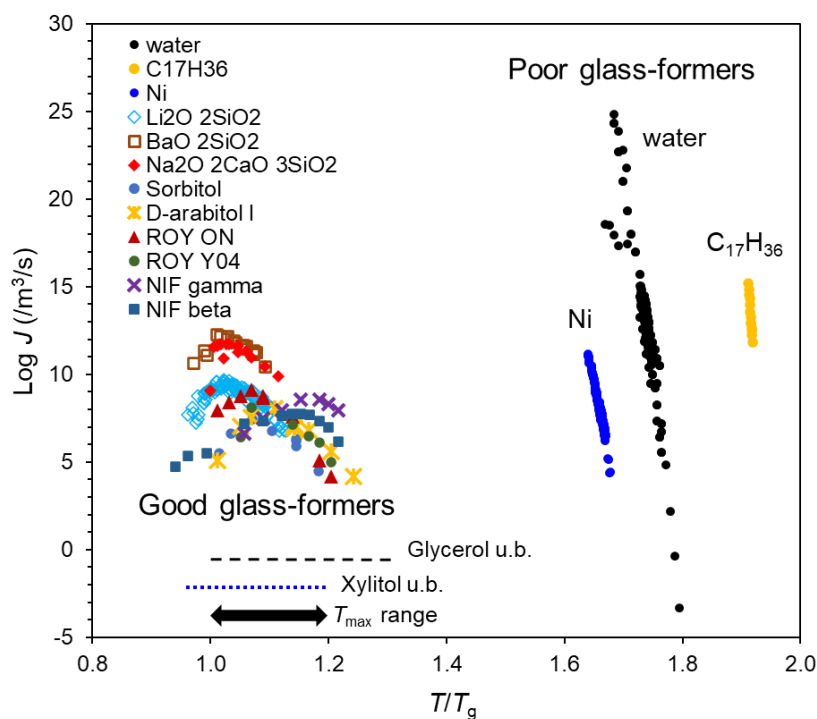


**Figure 2.** Crystal nucleation rates in the glasses or supercooled liquids of water, C17 alkane, Ni, silicate glasses, and organic molecules. Plotted from the data in Ref. 6, 27, 33, 45, 46, 50-53.

### 1.2.3. The classical nucleation theory (CNT)

The classical nucleation theory (CNT) describes nucleation rate by two terms: (1) Kinetic term ( $k_j$ ) describes the attempt frequency at which nucleating units join the nuclei. It depends on the density of nucleating units and their kinetic barrier to join a nucleus; (2) Thermodynamic term describes the possibility of a nucleus to survive or shrink, and it depends on both the driving force from generating a more stable phase and the energy penalty due to creating an interface. The equation can be derived by taking nucleation as a series of reversible reaction.<sup>54</sup> The steady-state nucleation rate can be written as  $J = k_j \times \exp(-W_c/kT)$ . This equation is discussed in detail below.

The kinetic term ( $k_j$ ) can be described by a liquid dynamic value ( $D$ ,  $\eta$ , or  $\tau$ ) and a corresponding constant ( $f$ ),  $k_j = f_D \times D$ ,  $k_j = f_\eta \times \eta$ , or  $k_j = f_\tau \times \tau_\alpha$ , where  $f$  is the corresponding constant,  $D$  is the diffusion coefficient,  $\eta$  is the viscosity, and  $\tau_\alpha$  is the structure relaxation time.<sup>5</sup> The corresponding constant depends on the density of nucleating units. For a given supercooled liquid or glass, the corresponding constant can be treated as a constant independent of temperature due to the small density change (< 50%). Recently, Huang et al. showed crystal nucleation and growth share similar kinetic barrier and suggested growth rate ( $u$ ) can describe the  $k_j$  term better because crystal nucleation and growth both involve crystal-liquid interface, but the liquid dynamic values do not. They tested  $k_j = f_u \times u$  with other three formats and found growth rate ( $u$ ) gives better fitting.<sup>5</sup>

The thermodynamic term is  $\exp(-W_c/kT)$ , where  $k$  is the Boltzmann constant,  $T$  is the nucleation temperature, and  $W_c$  is the critical energy barrier, equal to the free energy maximum. The free energy of a nucleus with given volume and area parameters ( $A$  and  $B$ ) can be written as a function of nucleus size ( $L$ ):

$$\Delta G = volume \times \Delta G_v + area \times \sigma = AL^3 \Delta G_v + BL^2 \sigma$$

where  $\sigma$  is the interfacial tension and  $\Delta G_v$  is the free energy difference between the nucleating crystal phase and the liquid phase. If the shape of the nuclei does not change ( $A$  and  $B$  are constant),  $\sigma$  is a constant, and the nuclei have the same structure as the mature crystal, then, the free energy maximum known as the critical energy barrier ( $W_c$ ), as shown in Figure 3, can be calculated at the critical size ( $L_c = -\frac{2B\sigma}{3A\Delta G}$ ) as:

$$W_c = \frac{4B^3\sigma^3}{27A^2\Delta G^2}$$

Commonly, the shape of nuclei is assumed as sphere,  $A = \frac{4}{3}\pi$ ,  $B = 4\pi$ ,  $L_c = r$  (radius of a spherical nucleus). Thus,  $W_c = \frac{16\pi\sigma^3}{3\Delta G^2}$  for spherical nuclei.

The CNT provides a good framework to think about crystal nucleation. When temperature is high, the driving force is too low to generate stable nuclei although kinetic term is high. With cooling, the thermodynamic term increases due to the increase of driving force, but the kinetic term decreases due to

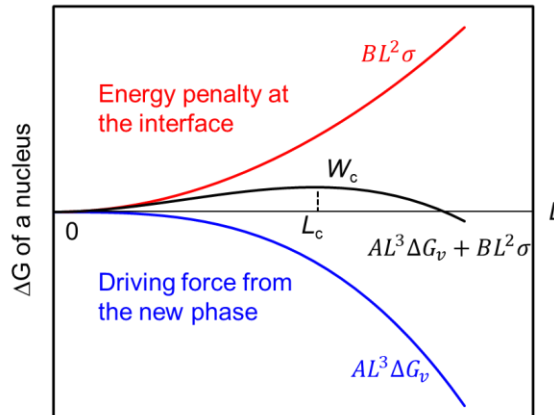


**Figure 3.** Total free energy ( $\Delta G$ ) of a nucleus (black) as a function of nucleus size ( $L$ ). It is the sum of a bulk term (blue) and an interfacial term (red).

the increase of kinetic barrier. In other words, although the possibility to form stable nuclei increases with cooling, nucleating units move slower and the attempt frequency of nucleating units to join nuclei decreases. Thus, the CNT predicts that the nucleation rate in a supercooled liquid should be low near the

melting temperature, and increase with cooling but later decrease again due to the limited mobility at low temperatures. Experimental data from many systems, e.g., silicate glasses,<sup>55</sup> organic molecules,<sup>5, 6</sup> and water,<sup>27</sup> has been fitted into this model successfully. It is worth noticing that the CNT is only a fitting model. Due to the unknown parameters ( $f$ ,  $\sigma$ ,  $A$ , and  $B$ ), the validation of the model cannot be tested, and the physical meaning of the fitted values can be different from the assumptions.

Despite its fitting validity, the CNT has limitations. The CNT is derived based on several assumptions. Some assumptions are not accurate enough, *especially for molecules*: (1) The surface tension of a nucleus is assumed a constant value for the entire interface between a nucleus and the liquid. This is likely not true, because crystals are naturally anisotropic, and have different facets. Each facet can have very different interfacial tension. (2) The shape of nuclei is assumed as the same and independent of the size of the nuclei. However, the shape of nuclei can involve overtime, based on simulation<sup>41</sup> and experimental observations.<sup>39</sup> Since the facets and the shape of nuclei are neither uncertain, the calculation of the interfacial tension as a function of nucleus size can be difficult or impossible. (3) The structure of nuclei is assumed as that of the mature crystal. This assumption can fairly describe the real situation, but it is unknown that whether the structure of nuclei evolves overtime. (4) Most importantly, when Turnbull derived the nucleation rate, he assumed all nucleating units are isotropic spheres, and the thermodynamic barrier is the same between any two nucleating units.<sup>54</sup> This assumption is fairly good for metals but likely cannot be accurate for flexible and anisotropic organic molecules. Organic molecules can adopt different conformation and diversify the interaction between neighbors. Besides that, an organic molecule can have very anisotropic potential energy surface based on the arrangement of their chemical groups. Thus, a molecule with given conformation can still have very diversified interaction with their neighbors. Following Turnbull's work,<sup>54</sup> if we treat nucleation as a series of reaction with their neighbors, each unique combination between two molecules should have a very different reaction barrier. Thus, the nucleation in organic liquids is much more complicated than assumed. A distribution of intermolecular states needs to be considered when we derive the nucleation rate following Turnbull's idea. Thus, the  $f$

value not only depends on the concentration of molecules, but more importantly depends on the concentration of certain intermolecular combinations having low barrier for crystal nucleation, leading to a too wide range of  $f$  value among different molecules to be explained by the variation of molecular density. The bigger and more flexible a molecule is, the lower the  $f$  value should be due to the increased possibility of intermolecular combinations. This hypothesis could be tested by measuring the structural entropy and the  $f$  value from the CNT fitting. If the hypothesis is right, the structural entropy should be negatively correlated with  $f$ . Although some deviation may exist when the main combination of molecules in a liquid is not the good-for-nucleation combination, but a trend between structural entropy and  $f$  should exist.

### **1.3. Polymorphism**

Polymorphs are different crystal forms with unique molecular packings, exhibiting different properties, such as solubility, melting point, density, stability, hardness, morphology, color and chemical reactivity.<sup>13</sup> Because of that, polymorphs are important and are intensively studied in many areas. For example, drug polymorphs are studied extensively in drug development under the regulation of the U.S. Food and Drug Administration (FDA). Compared with a more stable polymorph, a less stable polymorph can have higher solubility and dissolution rate, leading to the higher absorption of oral dosed drugs (bioavailability). For that benefit, a new polymorph can be patented and generate profits. Although a less stable polymorph gives higher solubility, in drug industry, the most stable polymorph is usually chosen for drug development, and extensive screening is performed to search the most stable polymorph. Such decision is made to avoid any risk of physical stability and is learned from extraordinary losses. The most famous lesson was given by Ritonavir,<sup>56, 57</sup> an antiviral active pharmaceutical ingredient (API) for the treatment of AIDS. Ritonavir was first marketed in 1996 by Abbott as Form I. However, 2 years later, a more stable polymorph, Form II appeared, causing the failure of manufacturing the original formulation, and the company was forced to withdraw the drug and redevelop the formulation using Form II. The cost for

missing the most stable polymorph is nearly one billion dollars. Polymorphism is not only important for reliable drugs, but also for tasty foods. The polymorph of chocolate needs to be controlled as the second stable Form V ( $T_m = 33.8\text{ }^\circ\text{C}$ ) among the six known polymorphs to achieve glossy appearance at room temperature as crystals, rich flavor and silky taste through sharp melting in mouth.<sup>16</sup> Polymorphism even plays a role in sustainable development and species diversity.<sup>58,59</sup> The polymorphs of insecticides show different efficacy. The metastable polymorphs (IV, VI and IX) of imidacloprid have much lower  $IC_{50}$  for mosquitos than stable polymorph (I). The higher efficacy allows less amount of an insecticide unleashed to the environment, thus lowers the harm to pollinators and maintains species diversity.

To study crystal polymorphs, the most important task is to distinguish them. Several conventional methods are X-ray diffraction, thermo-analysis, Infrared and Raman spectra, and crystal morphologies. Due to the regular packing of molecules, crystals can diffract X-ray. Different polymorphs possess their specific molecular packing and can diffract X-ray differently. The powder X-ray diffraction peaks can be taken as the fingerprint of a polymorph, and provide the gold standard for distinguishing polymorphs. Different polymorphs can have different melting points and heat of fusions. Those features can be captured using Differential Scanning Calorimetry (DSC). Among those thermodynamic features, melting point is the most used, and can be observed under a microscope with a hot stage. Compared with X-ray, thermal analyses usually destroy the sample, and should be performed as the last. Each polymorph also shows its specific IR absorption and Raman shifts, which also contain fingerprint regions for distinguishing polymorphs. Compared with X-ray, these methods are secondary standards. However, Raman and IR spectra can be collected faster than X-ray diffraction using conventional equipment, and the analyzing area can be well controlled to micrometers using a confocal microscope. Because of those advantages, Raman spectroscopy is usually used in high throughput analysis for polymorph screening.<sup>60</sup> Finally, the morphology of crystals is formed due to the habits of crystal growth. Although the evidence given by morphology is not strong as other technologies, different crystal morphologies can give the first indication of different polymorphs. By combining with other analysis, the morphology can be used to



distinguish polymorphs reliably. This method is very important for finding new polymorphs and studying crystal nucleation.<sup>5, 6</sup>

Polymorph screening is important but time-consuming, as the famous statement by McCrone, ‘the number of forms known for a given compound is proportional to the time and money spent in research on that compound’. In polymorph screening, nucleation is the key. Without the first nucleus, a new polymorph cannot be observed. Polymorphs are screened by varying the conditions of crystal nucleation. The most used method in industry is solution crystallization, in which diverse nucleation conditions are created by varying solvents, pH, temperature process, concentrations, and agitation. The screening can be performed in a high-throughput way in 96-well plates.<sup>60</sup> Recently, melt crystallization shows the advantage in discovering new polymorphs, especially metastable polymorphs.<sup>61</sup> For example, 4 out of the 13 known polymorphs of 5-Methyl-2-[(2-nitrophenyl)amino]-3-thiophnecarbonitrile (ROY, the model molecule for studying polymorphism) are found from its melt.<sup>62</sup> Other nucleation conditions can be created by inducing solid interface,<sup>20</sup> polymer,<sup>63</sup> high pressure,<sup>64</sup> and space confinement.<sup>65</sup> Besides the experimental methods, computational crystal structure prediction (CSP) is increasingly applied in exploring polymorphs. CSP usually has three parts: crystal structure generation, lattice energy calculation, and crystal structure refinement. CSP usually generates more crystal structures than experimental observations, possibly because simulation methods lack sufficient accuracy for calculating the structure energy and some theoretical polymorphs using conventional methods cannot be experimentally nucleated.

All the screening methods we discussed above are about generating nuclei by varying the nucleation conditions. However, a more fundamental question remains unanswered: for a given molecular supercooled liquid, how do we predict the nucleating polymorph? It is surprising that there is not much understanding regarding this fundamental question. This lack of knowledge is part of the reason for that polymorph screening cannot be performed in a systematic way that guarantees all the possible polymorphs to be found.<sup>13</sup> The widely-known empirical observation is the Ostwald rule, the least stable

polymorph nucleates and then converts to the next least stable polymorph.<sup>66</sup> This has been rationalized on the basis of minimizing entropy production.<sup>67</sup> However, there are many exceptions to this rule.<sup>5, 68, 69</sup> Instead of using the free energy as the predictor, Gui et al.<sup>6</sup> observed that the polymorphs with low density and high energy tend to nucleate first in several organic liquids (nifedipine, ROY, D-arabitol, and D-sorbitol).

In Chapters 2 and 3, a new avenue to polymorph selection through anisotropic liquid-vapor interfaces is discussed. The nucleating polymorphs in the bulk and at the surface vary significantly in the studied cases due to the anisotropic organization at liquid surfaces.

#### **1.4. Anisotropic Environment at the Surface and the Impact on Crystallization**

The surface environment of a liquid is anisotropic, and molecules may adopt very different organization from that in the bulk to minimize surface tension. In a pure liquid, surface organization can differ from the bulk with in-plane layering and preferred orientation. Molecules or atoms tend to have the center of mass constrained in one plane, instead of being randomly distributed as in the bulk. This surface layering effect has been observed by experiments<sup>70, 71</sup> and simulations.<sup>72</sup> Additionally, surface molecules can exhibit preferred orientation to minimize surface tension. Glycerol and alcohols are known to point -OH groups inside the liquid and -CH<sub>x</sub> groups toward the vapor phase.<sup>73, 74</sup> Some rod-like molecules tend to have the long axis slightly vertical to the surface.<sup>10, 72</sup> In multicomponent systems, the composition can vary from the surface to the bulk. For example, in a surfactant-water solution, the surfactant can form a monolayer at the surface when its concentration is higher than the critical micelle concentration. In drug-surfactant systems, surfactants can enrich at the drug surface as well.<sup>75</sup> Besides the structural and composition differences, molecules or atoms at the surface can diffuse much faster than in the bulk because surface molecules or atoms lack some neighbors on the vapor side and have lower kinetic barrier to diffuse. For molecular glasses without extensive hydrogen bonds, Li et al. showed that fast surface

diffusion is related to the penetration depth,<sup>76</sup> allowing the prediction of surface diffusivity from the molecular structure and bulk diffusivity.

The surface structure of liquids and glasses has been studied by sum frequency generation vibrational spectroscopy,<sup>73, 77</sup> near-edge X-ray absorption fine structure (NEXAFS) spectroscopy,<sup>10, 78</sup> molecular dynamics simulations,<sup>72</sup> X-ray or neutron reflectivity,<sup>71, 79</sup> surface tensiometry,<sup>80</sup> X-ray photoelectron spectroscopy (XPS),<sup>75, 79</sup> and atomic force microscopy (AFM).<sup>81</sup>

All those differences between surface and bulk can potentially lead to different crystallization behavior. The diffusion coefficients and crystal growth rates at the surface have been measured for multiple systems and show a linear correlation between the two rates,<sup>3</sup> indicating fast surface diffusion supports fast surface crystal growth. Another interesting phenomenon is surface freezing. Surface molecules or atoms can form a monolayer crystal at the liquid surface above the melting temperature. This phenomenon happens in long-chain alkanes<sup>80</sup>, alcohols<sup>82</sup>, and metal alloys.<sup>83</sup> Surface freezing is favored by energy. In the thermodynamic framework, when a liquid cannot wet a crystal surface at all, surface freezing can happen.<sup>25</sup> Despite those achievements in understanding surface effect on crystal growth and surface freezing, surface effect on crystal nucleation is poorly understood. Given the importance of nucleation, it is important to understand surface effect on crystal nucleation. The results and understandings regarding that are shown in Chapter 2 and 3.

## **1.5. Effect of a Second Component on Crystal Nucleation and Growth**

One advantage of glasses is that multiple components can be dissolved in a single phase to tailor the physical properties. When a second component is introduced, one important consideration is the effect of the dopant on crystallization of glasses. A second component can influence the crystallization of the host molecules by lowering the driving force for crystallization and by modifying the mobility of the host molecules.

To inhibit crystal nucleation, we can increase the concentration of the second component until the driving force is too low for nucleation. This effect usually is more significant when temperature is slightly below the melting point, and driving force dominates the nucleation rate. However, under deep supercooling, driving force for nucleation is high, but the mobility of molecules is low, both the crystal nucleation and growth finally are dominated by kinetics. Under such deep supercooling, a second component could affect nucleation and growth rate by altering the mobility of host molecules, a hypothesis to be tested in this work. This study is important for amorphous drugs, which are usually stored under deep-supercooling conditions.

An amorphous drug provides the highest solubility among all its solid phases but also has the lowest stability. To stabilize amorphous drugs or improve dissolution further, amorphous drugs commonly contain a dissolved polymer and a surfactant. The effect of polymers and surfactants on crystallization is important for designing stable amorphous formulations. The polymer and surfactant effects are better understood on crystal growth than on nucleation. At a low concentration of 1 wt % and under deep supercooling, a polymer can strongly influence the rate of crystal growth, from a 10-fold increase to a 10-fold decrease, depending on the polymer's segmental mobility relative to the host molecules.<sup>53, 84, 85</sup> In contrast to this detailed understanding, a comparable progress is yet to be made on crystal nucleation. In chapter 5 and 6, we consider the effect of polymers and surfactants at low concentrations (<15%) under deep supercooling on crystal nucleation and growth.

It is still challenging to achieve high drug loading and high stability against crystallization at the same time for many easy-to-crystallize drugs. The solution requires inhibiting crystallization in the most efficient way: lowering both the driving force and the molecular mobility for crystallization through forming strong drug-polymer ionic interactions. In chapter 7, we show lumefantrine (LMF), an easy-to-

crystallize antimalaria drug, as an example of amorphous drug-polymer salt with high physical stability against crystallization under tropical conditions.

## 1.6. Contributions of This Thesis

In Chapter 2 and 3, the effect of Liquid-Vapor interfaces on crystal nucleation was quantitatively demonstrated by measuring crystal nucleation rate independently at the surface and in the bulk. Chapter 2 shows the case of D-arabitol. D-arabitol nucleates much faster at the surface than in the bulk by 12 orders of magnitude on a per-molecule basis, and the surface nucleation selects a different polymorph (Form II) than the bulk nucleation (Form I). Crystal structure of Form II was solved to understand its selectivity at the surface. The two polymorphs have significant molecular packing: Form I has 3D H-bond network while Form II has 2D H-bond layers and no H-bond between layers in (001) plane. On the other hand, the liquid structure has been studied by molecular dynamics (MD) simulations. The surface organization of liquid D-arabitol is anisotropic and is similar to that of Form II but not Form I. Additionally, Form II crystals have strong preferred orientation with (001) plane being parallel to the surface. All the results indicate that the anisotropic packing at the surface liquid of D-arabitol templates the Form II crystals. In Chapter 3, the surface effect on posaconazole (POS) nucleation is demonstrated. Surface nucleation of POS is much faster than the bulk nucleation, by 9 orders of magnitude on a per-molecule bases, and selectively nucleates Form II different from the bulk (Form I). Form II crystal structure is solved in this work, and compared with Form I: Both polymorphs are composed of smectic-like layers. In each layer, molecules are parallel in Form II, but antiparallel to their neighbors in Form I. The selective and fast nucleation of Form II at the surface is likely because the anisotropic surface organization of liquid POS mimics the molecular layer in POS Form II. In contrast to D-arabitol and POS, the surface enhancement effect is weaker on crystal nucleation in acetaminophen and water and causes no polymorph switch. Based on the cases studied, we find strong enhancement requires (1) major structural reconstruction at the surface relative to the bulk and (2) existence of a crystal polymorph whose structure resembles the surface molecular packing with respect to preferred orientation and layering. Our results highlight that the

anisotropic packing at the surface can both alter the nucleation rate and the nucleating polymorph by self-templating effect. The understanding is relevant to the materials with large surface/volume ratio, e.g., atmospheric water, nanodroplets of metals, and pharmaceutical powders.

In Chapters 4 and 5, the effect of polymers and surfactants on crystal nucleation and growth has been studied. We found that a second component, a dissolved polymer or surfactant, alters the nucleation and growth rate of the host material by a similar factor mainly through modifying the mobility of host molecules at low concentrations (< 15%) under deep supercooling. In chapter 4, we focus on the polymer effect. The effect was studied by measuring the crystal nucleation and growth rates in D-arabitol and D-sorbitol liquids with the presence of polyvinylpyrrolidones (PVPs), and comparing the results with that in the pure D-arabitol and D-sorbitol liquids. The results show that the presence of PVPs decreases both the nucleation and growth rates by a similar factor (~10 times). Additionally, the glass transition temperature ( $T_g$ ) was tested as a function of PVP concentration. We found that polymer PVPs increase the  $T_g$  of D-arabitol and D-sorbitol, indicating PVPs decrease the mobility of the host molecules. Our results argue that nucleation and growth in these viscous liquids are both mobility-limited and that a polymer solute functions mainly as a mobility modifier, suppressing nucleation and growth to a similar degree. In chapter 5, we show the effect of surfactants on nifedipine crystallization. Four surfactants were chosen to have similar  $T_g$  but different structures with a wide range of hydrophilic-lipophilic balance (HLB) value. The nucleation and growth rates in NIF with 10% surfactants were measured and compared with the rates in pure NIF. The four surfactants increase the crystal nucleation and growth rates by a similar factor (~30 times) independent of the HLB values. Additionally, the four surfactants decrease the  $T_g$  of NIF by a similar degree, indicating they enhance the mobility of host molecules similarly. Again, these results indicate that nucleation and growth in a deeply supercooled liquid are both mobility-limited, and common surfactants tested are all mobility enhancers and enhance the crystallization of amorphous drugs. Overall, a dopant mainly functions as a mobility modifier (enhancer or suppressor depending on the dopant) and

alters nucleation and growth rates by a similar factor under deep supercooling. Since crystal nucleation and growth are promoted or depressed by a similar factor, a generic prediction is given to predict the hard-to-measure nucleation rates using the easy-to-measure growth rates, and is tested and validated in 11 systems covering 7 orders of magnitude. The results and understanding are relevant to the design of multicomponent glasses, especially amorphous drug formulations.

In chapter 6, we focus on how crystallization can be avoided efficiently in the application of amorphous drugs for global health without sacrificing dissolution performance. An easy-to-crystallize antimalaria drug, lumefantrine (LMF), is formulated into stable amorphous drug-polymer salt to improve its bioavailability for saving the lives vulnerable to malaria infection. To inhibit crystallization, the most efficient way is to decrease both the driving force and molecular mobility for crystallization by forming strong interaction between drug and polymer. We tested the strategy by formulating lumefantrine (a base) with poly(acrylic acid) (PAA, acidic polymer). The ionic interaction has been indicated by the extraordinary levigated  $T_g$  of LMF and the peak shift assigned to -COOH and -COO<sup>-</sup> groups. The amorphous LMF-PAA salt shows outstanding stability against crystallization: the amorphous salt remained pure amorphous after one and half year under the accelerating condition (40 °C/75% RH) while other ASDs (LMF-HPMCAS and LMF-PVP) crystallized in one week. Additionally, LMF-PAA reached higher concentration than crystalline LMF by 30 times in simulated gastric fluid (SGF), and 200 times in Fasted State Simulated Gastric Fluid (FaSSIF), likely due to the formation of colloidal particles during dissolution. Amorphous LMF-PAA salt, therefore, is a promising solution to malaria in the tropical and subtropical regions. Amorphous drug-polymer salt inhibits crystallization by lowering molecular mobility and the driving force for crystallization, and enhances dissolution via forming colloidal particles. Amorphous drug-polymer salt can be a promising and generic solution to the oral delivery of drugs with low water solubility and high crystallization tendency. The states of the art and the future directions of amorphous drug-polymer salt are further discussed in Chapter 7.

Overall, this thesis considers crystal nucleation and growth, specifically focusing on the effect of liquid-vapor interfaces and second components on crystal nucleation and growth, and amorphous drug-polymer salts for global health by avoiding crystallization. The results and understanding in this thesis can be relevant to polymorph screening and crystallization control in systems having large surface/volume ratio or in multi-component glasses.

## 1.7. References

1. Angell, C., Liquid fragility and the glass transition in water and aqueous solutions. *Chemical reviews* **2002**, *102* (8), 2627-2650.
2. Angell, C. A., Formation of glasses from liquids and biopolymers. *Science* **1995**, *267* (5206), 1924-1935.
3. Huang, C.; Ruan, S.; Cai, T.; Yu, L., Fast surface diffusion and crystallization of amorphous griseofulvin. *The Journal of Physical Chemistry B* **2017**, *121* (40), 9463-9468.
4. Ediger, M. D.; Harrowell, P.; Yu, L., Crystal growth kinetics exhibit a fragility-dependent decoupling from viscosity. *The Journal of chemical physics* **2008**, *128* (3), 034709.
5. Huang, C.; Chen, Z.; Gui, Y.; Shi, C.; Zhang, G. G.; Yu, L., Crystal nucleation rates in glass-forming molecular liquids: D-sorbitol, D-arabitol, D-xylitol, and glycerol. *The Journal of chemical physics* **2018**, *149* (5), 054503.
6. Gui, Y.; Huang, C.; Shi, C.; Zhang, G. G. Z.; Yu, L., Polymorphic Selection in Crystal Nucleation. *The Journal of chemical physics* **2022**, doi: 10.1063/5.0086308.
7. Zhu, M.; Wang, J.-Q.; Perepezko, J. H.; Yu, L., Possible existence of two amorphous phases of d-mannitol related by a first-order transition. *The Journal of Chemical Physics* **2015**, *142* (24), 244504.
8. Mishima, O.; Suzuki, Y., Propagation of the polyamorphic transition of ice and the liquid-liquid critical point. *Nature* **2002**, *419* (6907), 599-603.
9. Swallen, S. F.; Kearns, K. L.; Mapes, M. K.; Kim, Y. S.; McMahon, R. J.; Ediger, M. D.; Wu, T.; Yu, L.; Satija, S., Organic glasses with exceptional thermodynamic and kinetic stability. *Science* **2007**, *315* (5810), 353-356.
10. Bishop, C.; Thelen, J. L.; Gann, E.; Toney, M. F.; Yu, L.; DeLongchamp, D. M.; Ediger, M. D., Vapor deposition of a nonmesogen prepares highly structured organic glasses. *Proceedings of the National Academy of Sciences* **2019**, *116* (43), 21421-21426.
11. Teerakapibal, R.; Huang, C.; Gujral, A.; Ediger, M. D.; Yu, L., Organic glasses with tunable liquid-crystalline order. *Physical review letters* **2018**, *120* (5), 055502.



12. Chen, Z.; Bishop, C.; Thoms, E.; Bock, H.; Ediger, M. D.; Richert, R.; Yu, L., Controlling the Columnar Order in a Discotic Liquid Crystal by Kinetic Arrest of Disc Tumbling. *Chemistry of Materials* **2021**, *33* (12), 4757-4764.
13. Bernstein, J., *Polymorphism in Molecular Crystals 2e*. International Union of Crystal: 2020; Vol. 30.
14. Cohen, I.; Ha, A.; Zhao, X.; Lee, M.; Fischer, T.; Strouse, M. J.; Kivelson, D., A low-temperature amorphous phase in a fragile glass-forming substance. *The Journal of Physical Chemistry* **1996**, *100* (20), 8518-8526.
15. Cruz-Cabeza, A. J.; Reutzel-Edens, S. M.; Bernstein, J., Facts and fictions about polymorphism. *Chemical Society Reviews* **2015**, *44* (23), 8619-8635.
16. Kelton, K. F.; Greer, A. L., *Nucleation in condensed matter: applications in materials and biology*. Elsevier: 2010.
17. Chen, J.; Sarma, B.; Evans, J. M.; Myerson, A. S., Pharmaceutical crystallization. *Crystal growth & design* **2011**, *11* (4), 887-895.
18. Lupi, L.; Hudait, A.; Molinero, V., Heterogeneous nucleation of ice on carbon surfaces. *Journal of the American Chemical Society* **2014**, *136* (8), 3156-3164.
19. Last, J. A.; Hooks, D. E.; Hillier, A. C.; Ward, M. D., The physicochemical origins of coincident epitaxy in molecular overlayers: Lattice modeling vs potential energy calculations. *The Journal of Physical Chemistry B* **1999**, *103* (32), 6723-6733.
20. Mitchell, C. A.; Yu, L.; Ward, M. D., Selective nucleation and discovery of organic polymorphs through epitaxy with single crystal substrates. *Journal of the American Chemical Society* **2001**, *123* (44), 10830-10839.
21. Zielke, S. A.; Bertram, A. K.; Patey, G. N., A molecular mechanism of ice nucleation on model AgI surfaces. *The Journal of Physical Chemistry B* **2015**, *119* (29), 9049-9055.
22. Chen, S.; Xi, H.; Yu, L., Cross-nucleation between ROY polymorphs. *Journal of the American Chemical Society* **2005**, *127* (49), 17439-17444.
23. Tao, J.; Yu, L., Kinetics of cross-nucleation between polymorphs. *The Journal of Physical Chemistry B* **2006**, *110* (14), 7098-7101.
24. Tao, J.; Jones, K. J.; Yu, L., Cross-nucleation between D-mannitol polymorphs in seeded crystallization. *Crystal Growth and Design* **2007**, *7* (12), 2410-2414.
25. Haji-Akbari, A.; Debenedetti, P. G., Perspective: Surface freezing in water: A nexus of experiments and simulations. *The Journal of chemical physics* **2017**, *147* (6), 060901.
26. Marcolli, C.; Nagare, B.; Welti, A.; Lohmann, U., Ice nucleation efficiency of AgI: review and new insights. *Atmospheric Chemistry and Physics* **2016**, *16* (14), 8915-8937.
27. Laksmono, H.; McQueen, T. A.; Sellberg, J. A.; Loh, N. D.; Huang, C.; Schlesinger, D.; Sierra, R. G.; Hampton, C. Y.; Nordlund, D.; Beye, M., Anomalous behavior of the homogeneous ice nucleation rate in “no-man’s land”. *The journal of physical chemistry letters* **2015**, *6* (14), 2826-2832.
28. Manka, A.; Pathak, H.; Tanimura, S.; Wölk, J.; Strey, R.; Wyslouzil, B. E., Freezing water in no-man's land. *Physical Chemistry Chemical Physics* **2012**, *14* (13), 4505-4516.

29. Kuhn, T.; Earle, M.; Khalizov, A.; Sloan, J., Size dependence of volume and surface nucleation rates for homogeneous freezing of supercooled water droplets. *Atmospheric Chemistry and Physics* **2011**, *11* (6), 2853-2861.
30. Weidinger, I.; Klein, J.; Stöckel, P.; Baumgärtel, H.; Leisner, T., Nucleation behavior of n-alkane microdroplets in an electrodynamic balance. *The Journal of Physical Chemistry B* **2003**, *107* (15), 3636-3643.
31. Kraack, H.; Sirota, E.; Deutsch, M., Measurements of homogeneous nucleation in normal-alkanes. *The Journal of Chemical Physics* **2000**, *112* (15), 6873-6885.
32. Riechers, B.; Wittbracht, F.; Hüthen, A.; Koop, T., The homogeneous ice nucleation rate of water droplets produced in a microfluidic device and the role of temperature uncertainty. *Physical Chemistry Chemical Physics* **2013**, *15* (16), 5873-5887.
33. Murray, B.; Broadley, S.; Wilson, T.; Bull, S.; Wills, R.; Christenson, H.; Murray, E., Kinetics of the homogeneous freezing of water. *Physical Chemistry Chemical Physics* **2010**, *12* (35), 10380-10387.
34. Duft, D.; Leisner, T., Laboratory evidence for volume-dominated nucleation of ice in supercooled water microdroplets. *Atmospheric Chemistry and Physics* **2004**, *4* (7), 1997-2000.
35. Fokin, V. M.; Zanutto, E. D.; Yuritsyn, N. S.; Schmelzer, J. W., Homogeneous crystal nucleation in silicate glasses: A 40 years perspective. *Journal of Non-Crystalline Solids* **2006**, *352* (26-27), 2681-2714.
36. Cheng, S.; McKenna, G. B., Isothermal Crystallization and Time-Temperature Transformation of Amorphous Nifedipine: A Case of Polymorphism Formation and Conversion. *Molecular Pharmaceutics* **2021**, *18* (7), 2786-2802.
37. Fultz, B., *Phase transitions in materials*. Cambridge University Press: 2020.
38. Zhou, J.; Yang, Y.; Yang, Y.; Kim, D. S.; Yuan, A.; Tian, X.; Ophus, C.; Sun, F.; Schmid, A. K.; Nathanson, M., Observing crystal nucleation in four dimensions using atomic electron tomography. *Nature* **2019**, *570* (7762), 500-503.
39. Van Driessche, A. E.; Van Gerven, N.; Bomans, P. H.; Joosten, R. R.; Friedrich, H.; Gil-Carton, D.; Sommerdijk, N. A.; Sleutel, M., Molecular nucleation mechanisms and control strategies for crystal polymorph selection. *Nature* **2018**, *556* (7699), 89-94.
40. Nielsen, M. H.; Aloni, S.; De Yoreo, J. J., In situ TEM imaging of CaCO<sub>3</sub> nucleation reveals coexistence of direct and indirect pathways. *Science* **2014**, *345* (6201), 1158-1162.
41. Sosso, G. C.; Chen, J.; Cox, S. J.; Fitzner, M.; Pedevilla, P.; Zen, A.; Michaelides, A., Crystal nucleation in liquids: Open questions and future challenges in molecular dynamics simulations. *Chemical reviews* **2016**, *116* (12), 7078-7116.
42. Walsh, M. R.; Koh, C. A.; Sloan, E. D.; Sum, A. K.; Wu, D. T., Microsecond simulations of spontaneous methane hydrate nucleation and growth. *Science* **2009**, *326* (5956), 1095-1098.
43. Lane, T. J.; Shukla, D.; Beauchamp, K. A.; Pande, V. S., To milliseconds and beyond: challenges in the simulation of protein folding. *Current opinion in structural biology* **2013**, *23* (1), 58-65.
44. Haji-Akbari, A.; DeFever, R. S.; Sarupria, S.; Debenedetti, P. G., Suppression of sub-surface freezing in free-standing thin films of a coarse-grained model of water. *Physical Chemistry Chemical Physics* **2014**, *16* (47), 25916-25927.
45. Turnbull, D.; Cormia, R. L., Kinetics of crystal nucleation in some normal alkane liquids. *The Journal of Chemical Physics* **1961**, *34* (3), 820-831.

46. Bokeloh, J.; Rozas, R. E.; Horbach, J.; Wilde, G., Nucleation barriers for the liquid-to-crystal transition in Ni: experiment and simulation. *Physical review letters* **2011**, *107* (14), 145701.
47. Tabazadeh, A.; Djikaev, Y. S.; Reiss, H., Surface crystallization of supercooled water in clouds. *Proceedings of the National Academy of Sciences* **2002**, *99* (25), 15873-15878.
48. Wilde, G.; Sebright, J.; Perepezko, J., Bulk liquid undercooling and nucleation in gold. *Acta materialia* **2006**, *54* (18), 4759-4769.
49. Sirota, E., Supercooling, nucleation, rotator phases, and surface crystallization of n-alkane melts. *Langmuir* **1998**, *14* (11), 3133-3136.
50. Kelton, K. F., Crystal nucleation in liquids and glasses. In *Solid state physics*, Elsevier: 1991; Vol. 45, pp 75-177.
51. Narayan, K. L.; Kelton, K. F., First measurements of time-dependent nucleation as a function of composition in Na<sub>2</sub>O·2CaO·3SiO<sub>2</sub> glasses. *Journal of non-crystalline solids* **1997**, *220* (2-3), 222-230.
52. Gupta, P. K.; Cassar, D. R.; Zanutto, E. D., Role of dynamic heterogeneities in crystal nucleation kinetics in an oxide supercooled liquid. *The Journal of Chemical Physics* **2016**, *145* (21), 211920.
53. Huang, C.; Powell, C. T.; Sun, Y.; Cai, T.; Yu, L., Effect of low-concentration polymers on crystal growth in molecular glasses: a controlling role for polymer segmental mobility relative to host dynamics. *The Journal of Physical Chemistry B* **2017**, *121* (8), 1963-1971.
54. Turnbull, D.; Fisher, J. C., Rate of nucleation in condensed systems. *The Journal of chemical physics* **1949**, *17* (1), 71-73.
55. Zanutto, E. D.; Fokin, V. M., Recent studies of internal and surface nucleation in silicate glasses. *Philosophical Transactions of the Royal Society of London. Series A: Mathematical, Physical and Engineering Sciences* **2003**, *361* (1804), 591-613.
56. Bauer, J.; Spanton, S.; Henry, R.; Quick, J.; Dziki, W.; Porter, W.; Morris, J., Ritonavir: an extraordinary example of conformational polymorphism. *Pharmaceutical research* **2001**, *18* (6), 859-866.
57. Chemburkar, S. R.; Bauer, J.; Deming, K.; Spiwek, H.; Patel, K.; Morris, J.; Henry, R.; Spanton, S.; Dziki, W.; Porter, W., Dealing with the impact of ritonavir polymorphs on the late stages of bulk drug process development. *Organic Process Research & Development* **2000**, *4* (5), 413-417.
58. Zhu, X.; Hu, C. T.; Erriah, B.; Vogt-Maranto, L.; Yang, J.; Yang, Y.; Qiu, M.; Fella, N.; Tuckerman, M. E.; Ward, M. D., Imidacloprid crystal polymorphs for disease vector control and pollinator protection. *Journal of the American Chemical Society* **2021**, *143* (41), 17144-17152.
59. Yang, J.; Erriah, B.; Hu, C. T.; Reiter, E.; Zhu, X.; López-Mejías, V.; Carmona-Sepúlveda, I. P.; Ward, M. D.; Kahr, B., A deltamethrin crystal polymorph for more effective malaria control. *Proceedings of the National Academy of Sciences* **2020**, *117* (43), 26633-26638.
60. Morissette, S. L.; Soukasene, S.; Levinson, D.; Cima, M. J.; Almarsson, Ö., Elucidation of crystal form diversity of the HIV protease inhibitor ritonavir by high-throughput crystallization. *Proceedings of the National Academy of Sciences* **2003**, *100* (5), 2180-2184.
61. Yao, C.; Guzei, I. A.; Jin, Y.; Ruan, S.; Sun, G.; Gui, Y.; Wang, L.; Yu, L., Polymorphism of piroxicam: new polymorphs by melt crystallization and crystal structure Prediction. *Crystal Growth & Design* **2020**, *20* (12), 7874-7881.

62. Gui, Y., *Phase Transitions in Molecular Solids: Understanding Polymorphic Transformation and Crystal Nucleation, and Engineering Amorphous Drugs for Global Health*. The University of Wisconsin-Madison: 2021.
63. Price, C. P.; Grzesiak, A. L.; Matzger, A. J., Crystalline polymorph selection and discovery with polymer heteronuclei. *Journal of the American Chemical Society* **2005**, *127* (15), 5512-5517.
64. Guerin, M., A review on high pressure experiments for study of crystallographic behavior and polymorphism of pharmaceutical materials. *Journal of Pharmaceutical Sciences* **2020**, *109* (9), 2640-2653.
65. Ha, J.-M.; Wolf, J. H.; Hillmyer, M. A.; Ward, M. D., Polymorph selectivity under nanoscopic confinement. *Journal of the American Chemical Society* **2004**, *126* (11), 3382-3383.
66. Ostwald, W., Studien über die Bildung und Umwandlung fester Körper. *Zeitschrift für physikalische Chemie* **1897**, *22* (1), 289-330.
67. Van Santen, R., The Ostwald step rule. *The Journal of Physical Chemistry* **1984**, *88* (24), 5768-5769.
68. Germann, L. S.; Arhangelskis, M.; Etter, M.; Dinnebier, R. E.; Friščić, T., Challenging the Ostwald rule of stages in mechanochemical cocrystallisation. *Chemical science* **2020**, *11* (37), 10092-10100.
69. Hedges, L. O.; Whitlam, S., Limit of validity of Ostwald's rule of stages in a statistical mechanical model of crystallization. *The Journal of chemical physics* **2011**, *135* (16), 164902.
70. Magnussen, O.; Ocko, B.; Regan, M.; Penanen, K.; Pershan, P. S.; Deutsch, M., X-ray reflectivity measurements of surface layering in liquid mercury. *Physical review letters* **1995**, *74* (22), 4444.
71. Regan, M.; Kawamoto, E.; Lee, S.; Pershan, P. S.; Maskil, N.; Deutsch, M.; Magnussen, O.; Ocko, B.; Berman, L., Surface layering in liquid gallium: An X-ray reflectivity study. *Physical review letters* **1995**, *75* (13), 2498.
72. Haji-Akbari, A.; Debenedetti, P. G., Thermodynamic and kinetic anisotropies in octane thin films. *The Journal of chemical physics* **2015**, *143* (21), 214501.
73. Oh-e, M.; Yokoyama, H.; Baldelli, S., Structure of the glycerol liquid/vapor interface studied by sum-frequency vibrational spectroscopy. *Applied physics letters* **2004**, *84* (24), 4965-4967.
74. Superfine, R.; Huang, J. Y.; Shen, Y., Nonlinear optical studies of the pure liquid/vapor interface: Vibrational spectra and polar ordering. *Physical review letters* **1991**, *66* (8), 1066.
75. Yu, J.; Li, Y.; Yao, X.; Que, C.; Huang, L.; Hui, H.-W.; Gong, Y. G.; Yu, L., Surface Enrichment of Surfactants in Amorphous Drugs: An X-Ray Photoelectron Spectroscopy Study. *Molecular pharmaceutics* **2022**, *19* (2), 654-660.
76. Li, Y.; Zhang, W.; Bishop, C.; Huang, C.; Ediger, M.; Yu, L., Surface diffusion in glasses of rod-like molecules posaconazole and itraconazole: Effect of interfacial molecular alignment and bulk penetration. *Soft Matter* **2020**, *16* (21), 5062-5070.
77. Even, M. A.; Lee, S.-H.; Wang, J.; Chen, Z., Detection and spectral analysis of trifluoromethyl groups at a surface by sum frequency generation vibrational spectroscopy. *The Journal of Physical Chemistry B* **2006**, *110* (51), 26089-26097.
78. Genzer, J.; Sivaniah, E.; Kramer, E. J.; Wang, J.; Körner, H.; Xiang, M.; Char, K.; Ober, C. K.; DeKoven, B. M.; Bubeck, R. A., The orientation of semifluorinated alkanes attached to polymers at the surface of polymer films. *Macromolecules* **2000**, *33* (5), 1882-1887.

79. Tanaka, K.; Kawaguchi, D.; Yokoe, Y.; Kajiyama, T.; Takahara, A.; Tasaki, S., Surface segregation of chain ends in  $\alpha$ ,  $\omega$ -fluoroalkyl-terminated polystyrenes films. *Polymer* **2003**, *44* (15), 4171-4177.
80. Wu, X.; Ocko, B.; Sirota, E.; Sinha, S.; Deutsch, M.; Cao, B.; Kim, M.-W., Surface tension measurements of surface freezing in liquid normal alkanes. *Science* **1993**, *261* (5124), 1018-1021.
81. Tian, X.; Song, D.; He, X.; Liu, H.; Wang, W.; Li, Z., Investigation of micro-surface potential of coals with different metamorphism by AFM. *Measurement* **2021**, *172*, 108915.
82. Gang, O.; Wu, X.; Ocko, B.; Sirota, E.; Deutsch, M., Surface freezing in chain molecules. II. Neat and hydrated alcohols. *Physical Review E* **1998**, *58* (5), 6086.
83. Shpyrko, O. G.; Streitl, R.; Balagurusamy, V. S.; Grigoriev, A. Y.; Deutsch, M.; Ocko, B. M.; Meron, M.; Lin, B.; Pershan, P. S., Surface crystallization in a liquid AuSi alloy. *Science* **2006**, *313* (5783), 77-80.
84. Kestur, U. S.; Taylor, L. S., Role of polymer chemistry in influencing crystal growth rates from amorphous felodipine. *CrystEngComm* **2010**, *12* (8), 2390-2397.
85. Kothari, K.; Ragoonanan, V.; Suryanarayanan, R., The role of drug-polymer hydrogen bonding interactions on the molecular mobility and physical stability of nifedipine solid dispersions. *Molecular pharmaceutics* **2015**, *12* (1), 162-170.

## **Chapter 2. Anisotropic Molecular Organization at a Liquid/Vapor Interface Promotes Crystal Nucleation with Polymorph Selection**

Xin Yao, Qitong Liu, Bu Wang, Janguang Yu, Michael M. Aristov, Chenyang Shi, Geoff G. Z.

Zhang, Lian Yu

As published in:

*Journal of the American Chemical Society* **2022**

DOI: 10.1021/jacs.2c02623

## 2.1. Abstract

The molecules at the surface of a liquid have different organization and dynamics from those in the bulk, potentially altering the rate of crystal nucleation and polymorphic selection, but this effect remains poorly understood. We present the first demonstration that nucleation at the surface of a pure liquid, D-arabitol, is vastly enhanced, by 12 orders of magnitude, and selects a different polymorph. The surface effect intensifies with cooling and can be inhibited by a dilute, surface-active second component. This phenomenon arises from the anisotropic molecular packing at the interface and its similarity to the surface-nucleating polymorph. Our finding is relevant for controlling the crystallization and polymorphism in any system with a significant interface such as nanodroplets and atmospheric water.

## 2.2. Introduction

Crystal nucleation is important in many areas of science and technology,<sup>1-5</sup> but important unanswered questions remain.<sup>6</sup> One such question concerns the effect of a liquid/vapor interface on nucleation, which is relevant for understanding ice formation from atmospheric water<sup>7</sup> and the crystallization of metallic nano-droplets,<sup>8, 9</sup> silicon,<sup>10</sup> and organic liquids.<sup>11, 12</sup> There have been reports of interface-induced nucleation with polymorph control<sup>13-15</sup> but surprisingly little is known about the role of the vapor interface of a pure liquid. A liquid/vapor interface has a different structure from the bulk liquid, exhibiting layering,<sup>16, 17</sup> preferred orientation,<sup>18-20</sup> and enhanced mobility.<sup>21, 22</sup> These features potentially alter the nucleation rate, but our understanding of the effect is very limited. According to the Classical Nucleation Theory (CNT),<sup>23</sup> the rate of nucleation depends on the thermodynamic barrier to create a new interface and the molecular mobility available, and both factors are modified by the interfacial environment. It is difficult,

however, to use the CNT to make quantitative predictions because of the unknown parameters in the theory. Surface-initiated crystal nucleation has been observed by simulations,<sup>8-10</sup> the results are generally obtained for nanodroplets or thin films and are often sensitive to the force fields used.<sup>24-26</sup> To our knowledge, there has been no experimental demonstration that a single-component liquid can have different nucleation rates in the bulk and at the surface. In the case of water, there is considerable interest<sup>7</sup> and ongoing debate over the role of surface water on ice crystallization.<sup>27</sup> Given the importance of crystal polymorphs and their control,<sup>28</sup> a further question in this area is whether surface nucleation selects a different polymorph from the bulk nucleation.

Here we report the first experimental demonstration where nucleation at the liquid/vapor interface is vastly enhanced, by 12 orders of magnitude, and selects a different polymorph. This phenomenon arises from the similarity of the surface molecular packing to the surface-nucleating polymorph and can be inhibited by a dilute, surface-active second component. Our results demonstrate that the anisotropic molecular packing at an interface can significantly alter both the rate and the polymorph of nucleation.

### **2.3. Results and Discussion**

**Crystal Structures and Molecular Conformations of D-Arabitol.** Our model system is D-arabitol (Figure 1), a glass-forming polyol derived from carbohydrates.<sup>29</sup> Polyols have applications in cryoprotection,<sup>30</sup> food and drug formulations, and energy storage.<sup>31</sup> Two polymorphs of D-arabitol are known at present: I<sup>32</sup> and II (structure solved in this work; see the Crystallographic Information File in the SI and Table S1). The polymorphs have similar



molecular conformations conforming to Jeffrey's Rule<sup>33</sup> but different molecular packing and hydrogen-bond (HB) networks. As Figure 1 shows, Form I has a 3-dimensional HB network, while Form II consists of 2-dimensional HB layers with no HBs between the layers. As we show later, the structural difference leads to different polymorphic preference of bulk and surface nucleation. Being a chiral molecule, the two termini of D-arabitol (C1 and C5) are inequivalent and the terminal CO group is persistently bent relative to the carbon chain at the C5 end and either bent or extended at the C1 end, consistent with CSD statistics (Table S2).

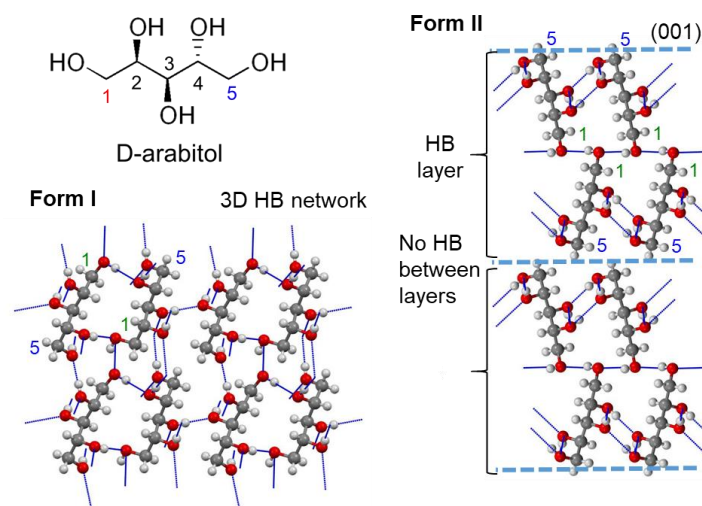


**Figure 1.** Crystal structures of D-arabitol. Form I has a 3D HB network; Form II has HB layers with no HB between layers. The two termini (C1 and C5) are inequivalent.

**Nucleation Rates at the Surface and in the Bulk.** To investigate the effect of a liquid/vapor interface on nucleation, we have measured the nucleation rates in the bulk of liquid D-arabitol and at its free surface. In a bulk experiment (Figure 2a), a liquid film is sandwiched between two coverslips and no vapor interface is present in the region of observation. In a surface experiment (Figure 2b), the top coverslip is absent, thus creating a free surface. The sample was protected from moisture with a blanket of dry nitrogen. In both cases, the film thickness was nominally 50

$\mu\text{m}$  and was varied to test the mechanism of nucleation as described below. Figures 2c and 2d

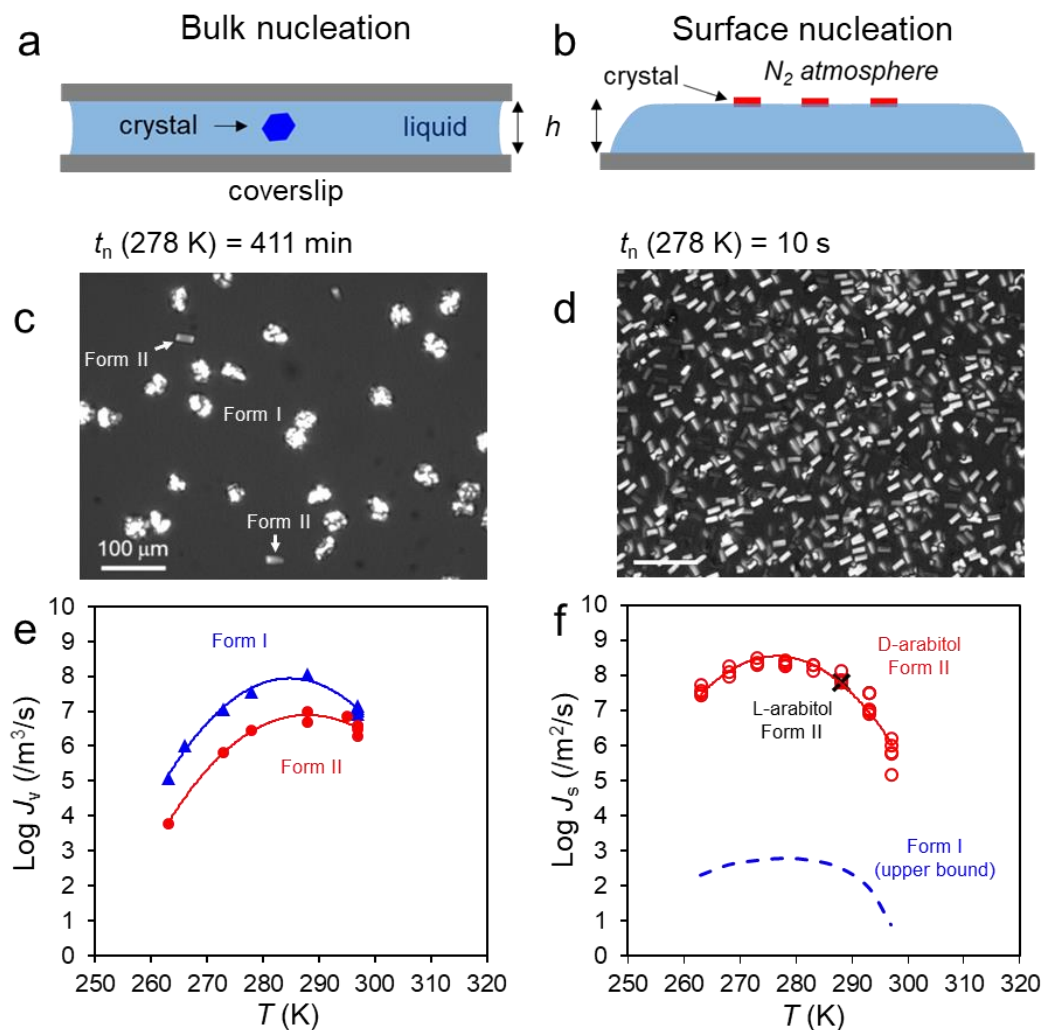


**Figure 2.** (a, b) Bulk- and surface-nucleation experiments. The thickness of the liquid film  $h$  is nominally  $50 \mu\text{m}$ . (c, d) Comparison of the densities of bulk- and surface-nucleated crystals at 278 K. After nucleation at 278 K, each sample spent 60 s at 323 K for the nuclei to grow. Surface nucleation created more crystals in 10 s than bulk nucleation in 411 min. Furthermore, surface nucleation yielded Form II while bulk nucleation mainly Form I (10 % Form II). (e, f) Bulk- and surface-nucleation rates,  $J_v$  and  $J_s$ , vs. temperature. In (f), the black X is a data point for L-arabitol which agrees with the D-isomer value. The curves are guide to the eye.

show the qualitative difference between the number of crystals created without and with a vapor interface. Each sample was nucleated at 278 K for a chosen time and heated to 323 K for 1 min to grow the nuclei to visible size. (Without the heating step, or only with the heating step, no

crystals were observed indicating nucleation occurred at 278 K.) We find that in the presence of a vapor interface, nucleation was significantly faster: far more crystals nucleated in 10 s in the free-surface sample (Figure 2d) than in 411 min in the bulk sample (2c). Furthermore, by varying the thickness of the open liquid film  $h$  from 30 to 240  $\mu\text{m}$ , we observed no significant effect on the number of crystals per surface area, consistent with surface nucleation.

An important feature of the surface nucleation in D-arabitol is its different polymorphic preference from bulk nucleation. Bulk nucleation produced mainly Form I, with Form II being a minor component (10 %), whereas surface nucleation produced only Form II, with no detectable Form I. The two polymorphs are readily distinguished by their morphologies, melting points (376 K for I and 356 K for II), and X-ray diffraction patterns (Figure 3). The X-ray pattern also indicates that surface-nucleated crystals have a preferred orientation: the observed peaks are all

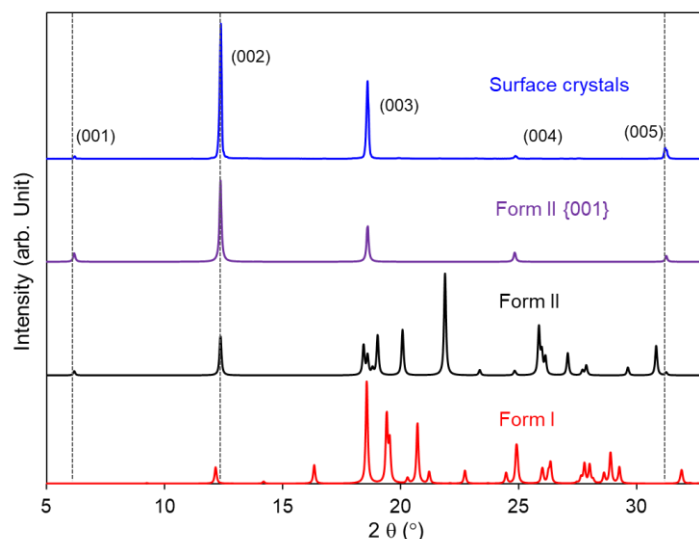


**Figure 3.** X-ray diffraction pattern of surface-nucleated crystals (top) and predicted patterns of Forms I and II from their crystal structures. The observed pattern matches that of Form II (see the vertical lines indicating peaks unique to Form II) and all the peaks correspond to  $(00l)$ , indicating the  $(00l)$  plane is parallel to the liquid/vapor interface.

(00 $l$ ) reflections, indicating the (001) plane is parallel to the liquid/vapor interface. Real-time observation of surface crystallization showed no crystal rotation during growth, suggesting that the surface crystals nucleated in the preferred orientation. As we discuss below, this result is consistent with the selective nucleation Form II at the surface.

Figures 2e and 2f show the bulk and surface nucleation rates in D-arabitol. The development method<sup>34</sup> was used for this purpose where the number of crystals was measured as a function of nucleation time (see Figure S1 for typical data). We find that in the bulk, Form I nucleates faster than Form II by approximately a factor of 10, whereas at the surface, only Form II nucleates and Form I is never observed. We estimate the surface nucleation of Form I to be at least 5 orders of

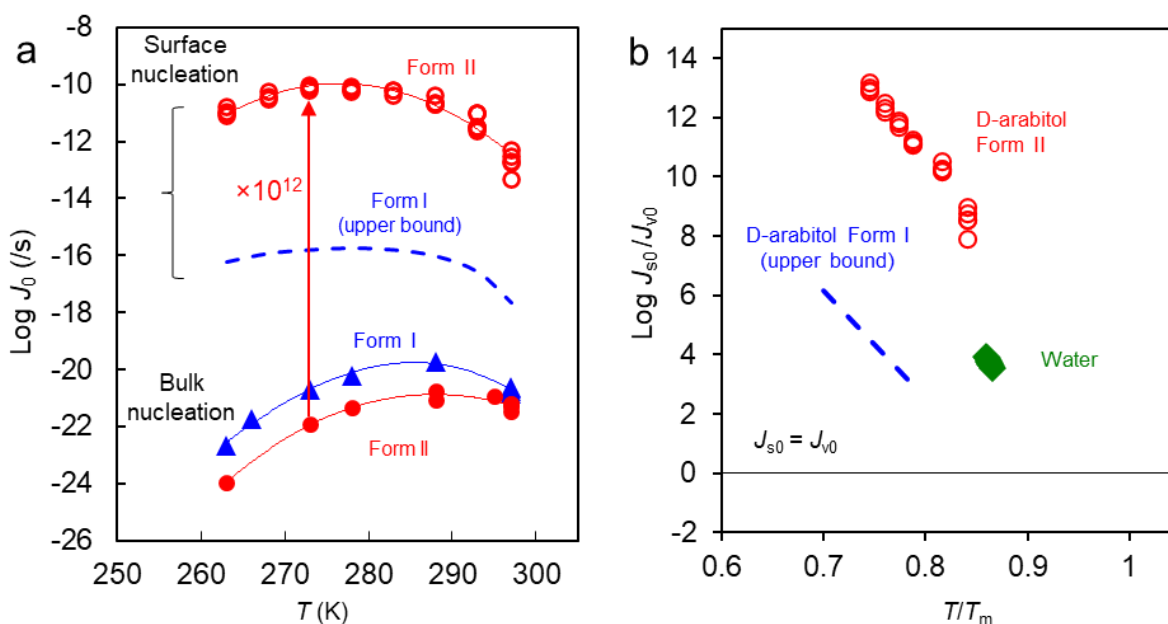


**Figure 4.** (a) Per-molecule rates of surface and bulk nucleation. Surface nucleation of D-arabitol Form II is vastly faster than bulk nucleation while the difference is smaller for Form I. (b)  $J_{s0}/J_{v0}$  ratios for D-arabitol and water, where  $J_{s0}$  and  $J_{v0}$  are the per-molecule rates of surface and bulk nucleation. The ratio increases with cooling. The horizontal line at bottom indicates the condition that surface and bulk nucleation are equally productive on a per-molecule basis.

magnitude slower than that of Form II (dashed curve in Figure 2f). This estimate is based on the non-observation of Form I crystals in all the experiments performed:  $J_s$  (Form I)  $< 1/(A_{\text{total}} t_{\text{total}})$ , where  $A_{\text{total}}$  is the total area of the melt sample examined and  $t_{\text{total}}$  is the total time of the experiment. In addition to D-arabitol, Figure 2f contains a data point on L-arabitol. Being mirror images of each other, D- and L-arabitol should exhibit the same surface nucleation phenomenon, and this was indeed observed.

The results above indicate a strong surface effect on crystal nucleation. We now show that surface nucleation is vastly faster than bulk nucleation when compared on a per-molecule basis. Because of the different units of  $J_v$  ( $1/\text{m}^3/\text{s}$ ) and  $J_s$  ( $1/\text{m}^2/\text{s}$ ), the two rates cannot be compared directly. To compare them, we convert each to the per-molecule value:  $J_{v0} = J_v \Omega_0$  and  $J_{s0} = J_s A_0$ , where  $\Omega_0$  is the volume occupied by one molecule and  $A_0$  is the surface area occupied by one molecule.  $J_{v0}$  ( $J_{s0}$ ) is the number of nucleation events per second in the volume (area) occupied by one molecule. Defined on a per-molecule basis, the values of  $J_{v0}$  and  $J_{s0}$  are exceedingly small, but this should not cause confusion since the base can be enlarged to one mole of molecules so that  $J_{v0}$  ( $J_{s0}$ ) is the frequency of nucleation per molar volume (molar surface area). For D-arabitol,  $\Omega_0 = 0.2 \text{ nm}^3$  from its bulk density, and  $A_0 \approx \Omega_0^{2/3} = 0.3 \text{ nm}^2$ . In Figure 4a, the  $J_{v0}$  and  $J_{s0}$  values are plotted against temperature, and we observe a large difference between these values for Form II. For example, at 273 K (arrow),  $J_{s0}/J_{v0} = 10^{12}$  for Form II, meaning surface nucleation outpaces bulk nucleation by 12 orders of magnitude when compared on a per-molecule basis. In contrast,  $J_{s0}/J_{v0} < 10^5$  for Form I. This quantifies the strong polymorphic preference of surface nucleation.

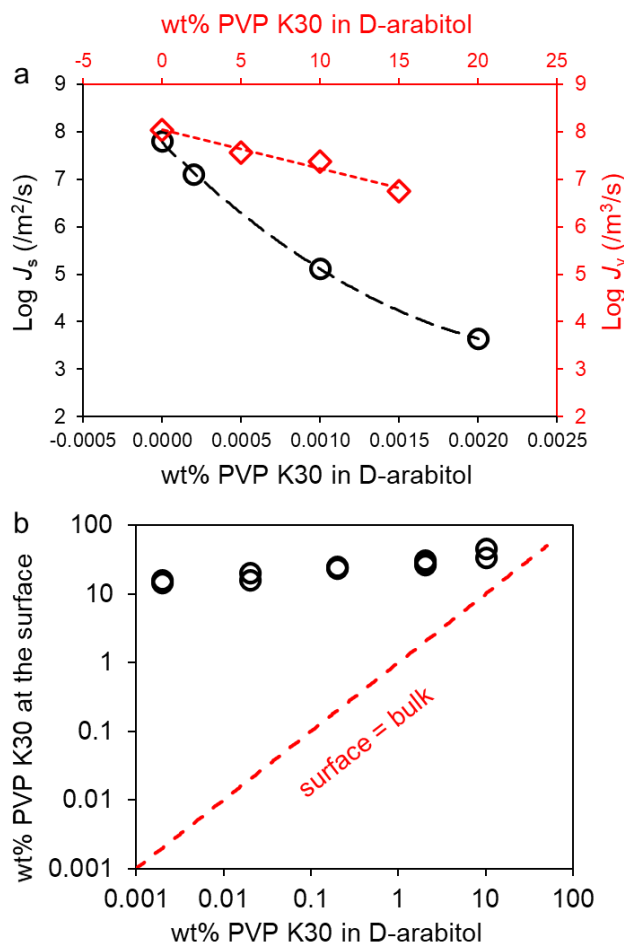


**Figure 5.** (a) Surface and bulk nucleation rates vs. the wt% of PVP K30. Inhibition of surface nucleation occurs at much lower concentrations (lower x axis) than that of bulk nucleation (upper x axis). (b) wt% of PVP at the surface (measured by XPS) vs. wt% of PVP in the bulk, showing a strong surface enrichment effect. The diagonal line indicates the condition of equal surface and bulk concentrations.

In Figure 4b, we plot the surface-enhancement factor  $J_{s0}/J_{v0}$  as a function of temperature and compare the result with that of water. For this comparison, the temperature has been scaled by the crystal melting point  $T_m$ . The horizontal line indicates the condition  $J_{s0} = J_{v0}$ , that is, surface and bulk nucleation are equally productive on a per-molecule basis. Above this line, nucleation is enhanced by the surface and below this line, inhibited. For D-arabitol Form II,  $J_{s0}/J_{v0} = 10^8 - 10^{13}$  in the temperature range investigated and increases with cooling. This means that surface nucleation is more productive than bulk nucleation at lower temperatures, likely a result of

greater surface ordering observed by MD simulations (see below). For water,<sup>35,36</sup> droplets larger than tens of micrometers show predominantly bulk nucleation, whereas surface nucleation is important for micrometer-sized droplets. From these results, Kuhn et al. extracted water's surface and bulk nucleation rates.<sup>36</sup> Their result indicates  $J_{s0}/J_{v0} = 10^3 - 10^4$ , smaller than the value for D-arabitol Form II and comparable to the upper bound estimated for Form I, and the limited data on water also suggest that the surface-enhancement of nucleation increases with cooling.

**A Dilute Surface-Active Component Inhibits Surface Nucleation.** The strong effect of a liquid/vapor interface on nucleation suggests an ability to disrupt the process through a second component that is enriched at the interface like a surfactant in water. This effect was indeed observed for D-arabitol doped with polyvinylpyrrolidone (PVP, molecular-weight grade K30). PVP is a polymer miscible with D-arabitol and at low concentrations (<1 %), has no effect on bulk nucleation.<sup>37</sup> We observed, however, that at only 20 ppm (0.0002 wt%), PVP can significantly inhibit surface nucleation and the effect increases with PVP concentration (Figure 5). This effect arises because PVP can enrich at the liquid/vapor interface of D-arabitol. Using X-ray Photoelectron Spectroscopy (XPS), we determined the surface concentration of PVP (see Figure S2 for typical data).<sup>38</sup> The result (Figure 5b) indicates that the surface concentration of PVP is substantially higher than its bulk concentration, consistent with its greater hydrophobicity and lower surface tension. This would reduce the surface concentration of D-arabitol and its driving force to crystallize. The surface enrichment of PVP could also alter the local structure that promotes surface nucleation. This result confirms our assignment of the nucleation mechanism (via the liquid/vapor interface) and provides a tool to control the process.

It is important to rule out the possibility of surface contamination in the surface nucleation process. Here we summarize the evidence against this possibility. Surface analysis by XPS observed only the elements present in D-arabitol. Throughout the experiment, the sample was sealed in a chamber purged with high-purity nitrogen. We observed uniform distribution of the nuclei on the surface unrelated to the flow direction of nitrogen and longer purging did not alter the nucleation rate. Replacing the nitrogen purge with vacuum (10 mTorr) had no significant effect on the results. The nucleation process showed an extended steady state (Figure S1); had it been catalyzed by contaminants, the nucleation rate should be fast initially but quickly plateau without an extended steady state. The enrichment of PVP at the liquid/vapor interface (Figure 5b) substantially reduced the rate of nucleation (Figure 5a). Different batches of D-arabitol from multiple suppliers and recrystallized by different cycles showed no significant difference in nucleation rate (Figure 2f contains data from different batches). The simplest explanation for this is that all the batches were sufficiently pure and surface nucleation is an intrinsic property of the material.

**Structure of Liquid Surface by Molecular Dynamics Simulations.** Having established the significant effect of the liquid/vapor interface on nucleation and polymorph selection experimentally, we now investigate the structural origin of the phenomenon by MD simulations. For this purpose, the Force Field (FF) was a modified version of AMBER BCFF (Table S3 and S4), which has been applied with success to the smaller polyol, glycerol.<sup>39</sup> The FF was validated by reproducing the experimental crystal structures (Table S5) and the expected conformers based on crystal structures (Table S2). After equilibration, 84 % of the molecules have the



conformations observed in crystals, that is, the carbon backbone is an extended zigzag and the terminal CO is bent relative to the backbone at C5 and either bent or extended at C1. This provides another validation of our FF.

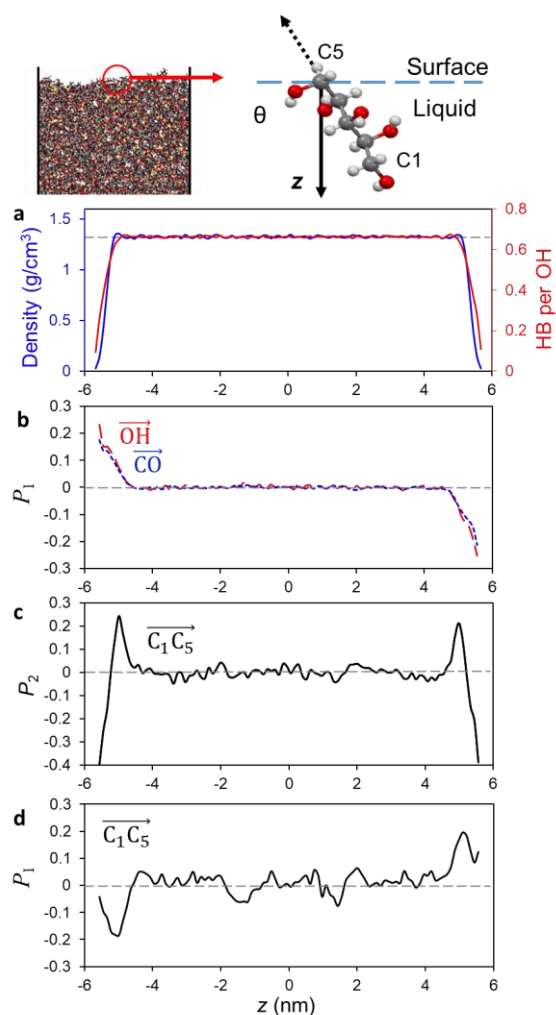


**Figure 6.** Order parameters vs depth  $z$ . (a) Density and HB density. (b)  $P_1$  order parameters of the OH and CO vectors. (c, d)  $P_2$  and  $P_1$  order parameters of the  $C_1C_5$  vector.

Figure 6 shows how structure varies across the liquid/vapor interface of D-arabitol. The density profile (Figure 6a) defines the thickness of the liquid film. Figure 6a also shows the probability for each OH group to participate in HB. The HB profile closely matches the density profile,

indicating that the molecule forms roughly the same number of HBs in the surface region as in the bulk. This is expected since the HB is the strongest interaction in the liquid and molecules organize themselves to maximize the number of HBs regardless of their physical environment. This conclusion is supported by the preferred orientation of the OH and CO vectors into the film (Figure 6b).

In Figure 6b, we plot the order parameter  $P_1 = \langle \cos \phi \rangle$  for the angle  $\phi$  between the OH or CO vector and the surface normal.  $P_1$  is positive at the top vapor interface and negative at the bottom, indicating that CO and OH groups tend to point into the liquid. This orientation allows these polar groups to form intermolecular HBs. Our result agrees with that on glycerol<sup>18</sup> for which surface molecules expose the non-polar  $\text{CH}_x$  groups to air and point their CO and OH groups down or sideways to maximize the number of HBs.

Figure 6c and 6d characterize the backbone orientation using two order parameters:  $P_1 = \langle \cos \theta \rangle$  and  $P_2 = \langle \frac{3}{2} \cos^2 \theta - \frac{1}{2} \rangle$ , where  $\theta$  is the angle between the C1-C5 vector and the surface normal. At the very edge of the film,  $P_2$  is negative, meaning the backbone tends to lie flat on the surface. Deeper into the film,  $P_2$  becomes positive, indicating the backbone tends to be vertical to the surface (parallel or antiparallel to  $z$ ). The peak value of  $P_2$  (0.25) corresponds to an average value of  $\theta = 45^\circ$ , slightly smaller than the magic angle of  $55^\circ$  for random orientation. Interestingly, for the C1-C5 vector,  $P_1$  is a negative peak at the top of the film and a positive peak at the bottom. This means the C1-C5 vector tends to point towards the vapor, that is, a surface molecule tends to have its C5 end up (close to the vapor phase) and C1 end down (buried

in the liquid phase). This tendency arises because the C1 and C5 ends are inequivalent. The C5 end has a bent CO group relative to the carbon chain and the molecule has lower energy if the C5 end is placed near the vapor phase, thus exposing the hydrophobic CH<sub>2</sub> group to the vapor phase and burying the polar CO group in the liquid to make hydrogen bonds, as observed for glycerol.<sup>18</sup> Together, the simulation results show that at the liquid/vapor interface, the molecules tend to be vertical with the polar CO and OH groups pointing downward (into the bulk) and with the C5 end pointing up (toward vapor). This structure maximizes the number of HBs per molecule, consistent with the nearly constant HB probability across the film (Figure 6a).

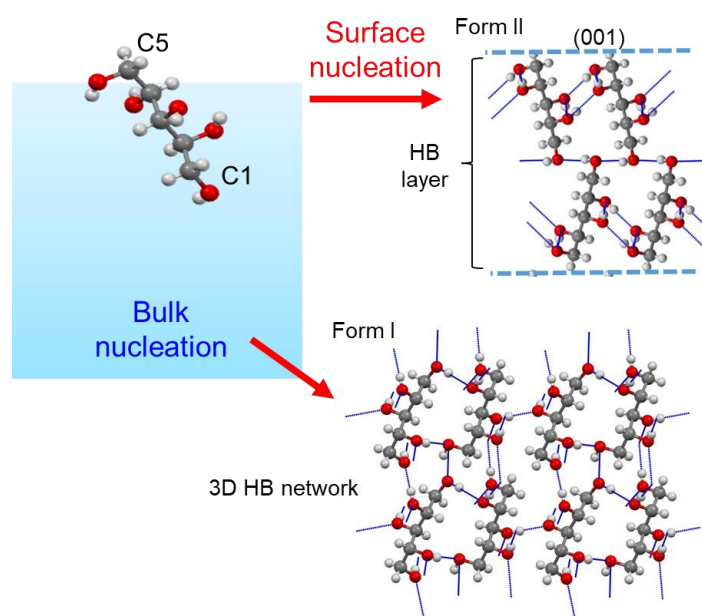


**Figure 7.** Surface-enhanced nucleation with polymorphic selection.

Based on the experimental and simulation results, we explain the fast, polymorph-selective nucleation at the liquid/vapor interface of D-arabitol as follows. Because surface molecules tend toward vertical orientation with the C5 end pointing up to maximize the number of HBs, the

local structure is similar to the layered HB structure in Form II, and dissimilar to the 3D HB network in Form I. As a result, the surface molecular packing promotes the nucleation of Form II but not Form I. This explanation is illustrated in Figure 7. Because the hydrogen-bonded layers are parallel to the (001) plane, our model immediately explains the preferred orientation of surface-nucleated crystals. Our model also explains the ability of a surface-active impurity (e.g., PVP; see Figure 5) to inhibit surface nucleation: the impurity is enriched in the surface layer, diluting the solvent molecules and modifying the local structure. This in turn disrupts the surface nucleation process. Because of mirror symmetry, the mechanism above applies equally to L-arabitol, thus explaining the same phenomenon observed for the enantiomer. We attribute the larger surface enhancement of nucleation with cooling (Figure 4b) to the increase of surface ordering. The rise of surface order with cooling is consistent with the literature results on the Lennard-Jones system<sup>21</sup> and liquid octane<sup>19</sup>, and with our simulation results conducted at 400 K and 500 K (Figure S3). As Figure 4b shows, Kuhn et al.'s result on water aerosols also indicates a rising  $J_s/J_v$  ratio with cooling. This suggests that surface nucleation might be more easily detected at low temperatures.

## 2.4. Conclusions

We have observed that crystal nucleation is vastly faster on the surface of the molecular liquid D-arabitol than in the bulk, by 12 orders of magnitude on the per-molecule basis. Surface nucleation selects a different polymorph (II) than bulk nucleation (I). To our knowledge, this is the first time surface and bulk nucleation rates have been independently measured in the same system, revealing a huge difference between the two. This phenomenon is a consequence of the similarity of the surface molecular packing to the structure of the surface-nucleating polymorph.

The mirror image of D-arabitol, L-arabitol, shows an identical phenomenon, strengthening our conclusion. We find that the surface enhancement effect intensifies with cooling.

Given the common occurrence of surface reconstruction, the surface effect on nucleation and polymorphism is potentially a general phenomenon. The phenomenon is expected if a slow-nucleating polymorph in the bulk has a structure that resembles the molecular organization at the liquid/vapor interface. The ability for surface nucleation to select a different polymorph from the bulk provides an intriguing avenue to expand the tools for polymorph discovery and control.<sup>28,40</sup> Besides arabitol, alkanes provide a possible example of polymorph selection by surface nucleation where the surface-frozen monolayer presumably nucleates the rotator phase in the bulk with little supercooling.<sup>12</sup> Even in bulk liquids and glasses, surface nucleation could play a role through free surfaces created by bubbles<sup>41</sup> and fractures.<sup>11, 42</sup> Surface nucleation might be more easily observed in systems of large surface-to-volume ratios (e.g., nano-droplets<sup>8,9</sup>) and at low temperatures, since the ratio  $J_s/J_v$  increases with cooling (Figure 4b). For liquids of multiple components, the surface layer can be enriched or depleted of certain components depending on surface tension. This effect will likely play a role in the surface crystallization of multi-component liquids.<sup>43-45</sup> It is of interest to learn whether the CNT provides a good foundation for understanding these phenomena.

## 2.5. Materials and Methods

D-arabitol and L-arabitol were purchased from Sigma-Aldrich and used either as received or after recrystallization, with no significant difference observed between as-received and recrystallized materials. For recrystallization, the material was dissolved in ethanol-water (15:1)

at 350 K and the hot solution was filtered. The solution was cooled to room temperature and seeded with D- or L-arabitol crystals. After complete crystallization, the mother liquor was decanted, and the crystals were washed three times with the solvent and dried under vacuum.

To investigate surface crystallization, a liquid film with an open surface was prepared by spreading a liquid of D-arabitol at 403 K on a heat-treated coverslip that facilitates spreading.<sup>46</sup> For comparison, bulk crystallization was investigated using a liquid film sandwiched between two coverslips. Briefly, in the one-stage method, crystals were allowed to form in a sample and the birth time of each crystal was calculated from the current time and the growth rate. This method was used for temperatures at which crystal growth was relatively fast. If crystal growth was slow, a two-stage method was used in which a sample was held at a low temperature for different times and heated to a high temperature to allow the nuclei to grow and be counted. For each measurement, an open-surface sample was kept in the nitrogen-purged chamber of a temperature-controlled microscope stage (Linkam THMS).

X-ray Photoelectron Spectroscopy (XPS) was performed using a Thermo Scientific K-Alpha X-ray Photoelectron Spectrometer with a monochromatic Al K $\alpha$  (1486.6 eV) source. Samples of D-arabitol doped with PVP K30 were prepared by melting the material, degassing at 403 K, and quenching to room temperature. XPS data were collected at 297 K in vacuum ( $10^{-5}$  Pa). The surfaces of the non-conductive samples were neutralized using an electron flood gun. The beam size was 400  $\mu\text{m}$ . A survey scan was performed for multiple elements at a step size of 1 eV and passing energy of 200 eV. High-resolution scans for the elements of interest (C, N, O) were performed at a step size of 0.1 eV and passing energy of 50 eV. The binding energy was

calibrated by shifting the observed carbon peak (C 1s) to 285.0 eV. The baseline for peak area integration was obtained using a smart baseline function in Avantage Data System. The peak areas of N and O were used to calculate the surface weight percent of PVP K30 ( $w_p$ ) as follows:

$$w_p = \frac{5R_{N/O} \times M_p}{5R_{N/O} \times M_p + (1 - R_{N/O})M_a} \times 100\%$$

where  $R_{N/O}$  is the observed N/O atomic ratio after normalizing each peak area with the Relative Sensitivity Factor,  $M_a$  is the molecular weight of D-arabitol, and  $M_p$  is the monomer molecular weight of PVP K30. This method has been validated against chemically pure compounds<sup>38</sup> and against PVP K30, for which the measured N/O ratio is 1.017 (0.038) in agreement with the theoretical value (1).

Differential Scanning Calorimetry (DSC) was performed with a TA Q2000 under 50 mL/min N<sub>2</sub> purge. Each sample was 2-10 mg placed in an aluminum pan. Single Crystal X-Ray Diffraction was used to solve the structure of D-arabitol Form II. A single crystal of Form II was grown as follows: melt the as-purchased crystals on a coverslip to form isolated droplets, cool the droplets to 303 K, nucleate the sample at 303 K for several seconds, crystallize the droplets at 343 K in 2 min (some of which contained Form II, identifiable on sight), select a Form II polycrystalline assembly, raise the temperature to melt all but one crystal as a seed, and grow the seed at 343 K to a single crystal, consuming all the liquid in the droplet. The process may be repeated to improve crystal quality. The resulting crystal has adequate size and quality for structural solution X-ray diffraction (Bruker APEXII diffractometer; see Supporting Information and deposited cif file for details).

Molecular dynamics (MD) simulations of D-arabitol were performed at 400 K and 0.1 MPa. The force field (FF) was modified AMBER BCFF (Table S3 and S4). BCFF has performed well for glycerol (a smaller polyol)<sup>34</sup> and we have modified it to ensure that the molecular conformations in the liquid state approximately match those observed in crystals (see below). As a validation of the FF, we tested the stability of the experimental crystal structures and found that the experimental structures were reproduced by the MD simulation (Table S5). For bulk-liquid simulations, a cubic box containing 800 molecules was used with periodic boundary conditions. To study a liquid with free surfaces, a box containing an equilibrated bulk system with 1600 molecules was extended in the z-direction to create a vacuum above and below the liquid film. The box size with 1600 molecules yielded a film thick enough to avoid any thin film effect; this was confirmed by (1) surface energy convergence tests and (2) comparing the structure with a film half as thick (with 800 molecules) and finding no significant difference (Figure S4). All simulations were performed using the GROMACS package<sup>47, 48</sup> on a high-performance computing cluster.<sup>49</sup> A timestep of 2 fs was used.<sup>50</sup> The simulation was conducted for 140 ns for both the bulk system and the free-standing film so that the mean square displacement of the molecules exceeded twice the molecular size and that the energy equilibrium was achieved. The temperature was controlled with a V-rescale style thermostat<sup>51</sup> and the pressure with a Berendsen barostat. The coupling time was 0.1 ps for the thermostat and 1 ps for the barostat. The following criteria were used for hydrogen bonds: O...O distance is between 2.5-3.5 Å and the H-O...O angle is less than 30°.



## 2.6. Acknowledgements

We thank AbbVie Inc. and the Wisconsin - Puerto Rico Partnership for Research and Education in Materials (NSF DMR-1827894) for supporting this work. BW and QL thank the support from the National Science Foundation through the University of Wisconsin Materials Research Science and Engineering Center (NSF DMR-1720415). The Bruker SMART APEX2 was purchased by the UW–Madison Department of Chemistry with a portion of a generous gift from Paul J. and Margaret M. Bender. We thank Ilia A. Guzei for his support on the single-crystal X-ray diffraction study.

## 2.7. Supporting Information

**Table S1.** Structural parameters of arabitol crystals.

Form	D-arabitol Form I	D-arabitol Form II	L-arabitol Form I	DL-arabitol
Stereoisomer	D	D	L	Racemate
CSD ref. code	VOZMAY	This work	MECRAP	ARABOL
<i>T</i> , K	283-303	105	283-303	283-303
<i>a</i> , Å	4.823	4.838	4.829	4.855
<i>b</i> , Å	7.675	4.930	7.680	9.213
<i>c</i> , Å	9.705	14.382	9.717	15.490
$\alpha$ , deg	96.13	90	96.09	90
$\beta$ , deg	96.04	96.15	96.04	90
$\gamma$ , deg	106.82	90	106.81	90
<i>V</i> , Å <sup>3</sup>	338.4	341.0	339.5	692.9
space group	P1	P2 <sub>1</sub>	P1	Pna2 <sub>1</sub>
$\rho$ , g/cm <sup>3</sup>	1.493	1.482	1.488	1.459
<i>Z</i>	2	2	2	4
<i>Z'</i>	2	1	1	1
R-factor %	2.8	4.3	2.9	3.7

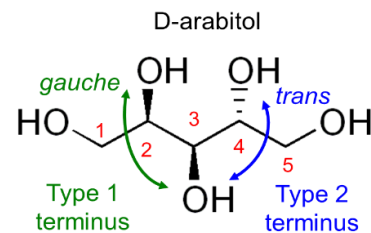
**Table S2.** Terminal CO orientations of linear polyols based on survey of the Cambridge Structural Database (CSD).<sup>a</sup>Type 1 terminus (D-arabitol C1; two nearest COs are *gauche*)

<i>nc</i>	Polyol, terminus	CSD ref. code	Terminal CO orientation
4	D-Threitol, terminus C1	PAGDEG	bent
4	D-Threitol, terminus C4	PAGDEG	bent
5	D-Arabitol Form I, molecule 1 terminus C1	VOZMAY	bent
5	D-Arabitol Form I, molecule 2 terminus C1	VOZMAY	extended
5	D-Arabitol Form II, terminus C1	This work	extended
5	DL-Arabitol (racemate), terminus C1	ARABOL	bent
5	Xylitol, terminus C1	XYLTOL	extended
6	L-Iditol, terminus C1	IDITOL	extended
6	L-Iditol, terminus C6	IDITOL	extended
6	Dulcitol, terminus C1	GALACT	extended
6	Dulcitol, terminus C6	GALACT	extended
6	D-Sorbitol epsilon, molecule 2 terminus C1	GLUCIT02	extended
6	D-Altritol, terminus C1	JOJZOX	extended
7	D-Perseitol, molecule 1, terminus C1	KAYNAZ	bent
7	D-Perseitol, molecule 2, terminus C1	KAYNAZ	bent
7	DL-Perseitol (racemate), terminus C1	TEBCUY	bent

Type 2 terminus (D-arabitol C5; two nearest COs are *trans*)

4	Erythritol, terminus C4	MERYOL	bent
4	Erythritol, terminus C1	MERYOL	bent
5	Ribitol, terminus C1	RIBTOL	bent
5	D-arabitol Form I, molecule 1 terminus C5	VOZMAY	bent
5	D-arabitol Form I, molecule 2 terminus C5	VOZMAY	bent
5	D-arabitol Form II, terminus C5	This work	bent
5	DL-Arabitol (racemate), terminus C5	ARABOL	bent
6	D-Mannitol alpha, terminus C1	DMANTL01	bent
6	D-Mannitol alpha, terminus C6	DMANTL01	bent
6	D-Mannitol beta, terminus C1	DMANTL	bent
6	D-Mannitol beta, terminus C6	DMANTL	bent
6	D-Mannitol delta, terminus C1	DMANTL10	bent
6	D-Mannitol delta, terminus C6	DMANTL10	bent
6	DL-Mannitol (racemate), terminus C1	DLMANT	bent
6	DL-Mannitol (racemate), terminus C6	DLMANT	bent
6	D-Sorbitol epsilon, molecule 1 terminus C6	GLUCIT02	bent
6	D-Sorbitol epsilon, molecule 2 terminus C6	GLUCIT02	bent
6	D-Sorbitol gamma, terminus C6	GLUCIT03	bent
6	D-Sorbitol alpha, terminus C6	GLUCIT	extended
7	D-Volemitol, terminus C1	VOXXOV	bent
7	D-Perseitol, molecule 1, terminus C7	KAYNAZ	bent
7	D-Perseitol, molecule 2, terminus C7	KAYNAZ	bent
7	DL-Perseitol (racemate), terminus C7	TEBCUY	bent

<sup>a</sup> A terminus is Type 1 if the two nearest COs are *gauche* to each other and Type 2 if they are *trans* (see Scheme S1). The CO orientation is overwhelmingly bent for a Type 2 terminus (21:1) and either bent or extended for a Type 1 terminus (8:9). The D-arabitol conformations agree with these statistics. The preference for a bent CO orientation at a Type 2 terminus can be explained by the gain of a weak hydrogen bond between a CH group and an OH group on alternate carbons (“1,3 attraction”) if the terminal CO changes from extended to bent orientation, without losing any stabilizing *gauche* contact.<sup>1,2</sup>



**Scheme S1.** Definitions of the terminus types using D-arabitol as example.

(a) Crystals observed after  $t_n$  at 288 K and 1 min at 323 K

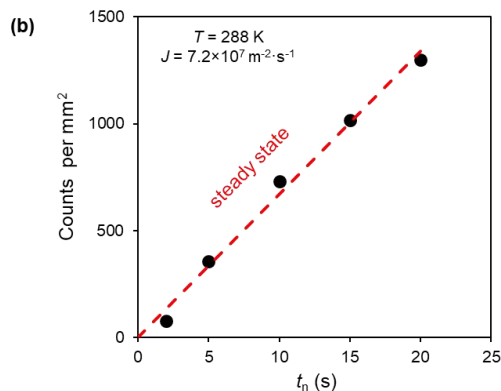
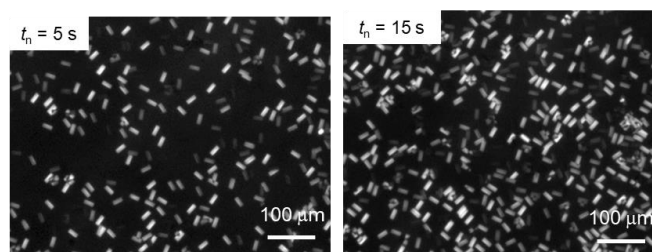


**Figure S1.** Illustration of nucleation rate measurement using the development method. (a) Photos of a surface sample that spent different times  $t_n$  at the nucleation temperature (288 K) and 1 min at the growth temperature (323 K). (b) Nuclei number vs.  $t_n$ . The slope is the nucleation rate. The nucleation process was found to occur at the surface by varying the thickness  $h$  of the liquid film. For example, increasing  $h$  from 30  $\mu\text{m}$  to 240  $\mu\text{m}$  had no significant effect on the number of crystals per unit area.

<sup>1</sup> O'Hagan, D., 2008. Understanding organofluorine chemistry. An introduction to the C–F bond. Chemical Society Reviews, 37(2), pp.308-319.

<sup>2</sup> Díaz, N., Jiménez-Grávalos, F., Suárez, D., Francisco, E. and Martín-Pendás, Á., 2019. Fluorine conformational effects characterized by energy decomposition analysis. Physical Chemistry Chemical Physics, 21(45), pp.25258-25275.

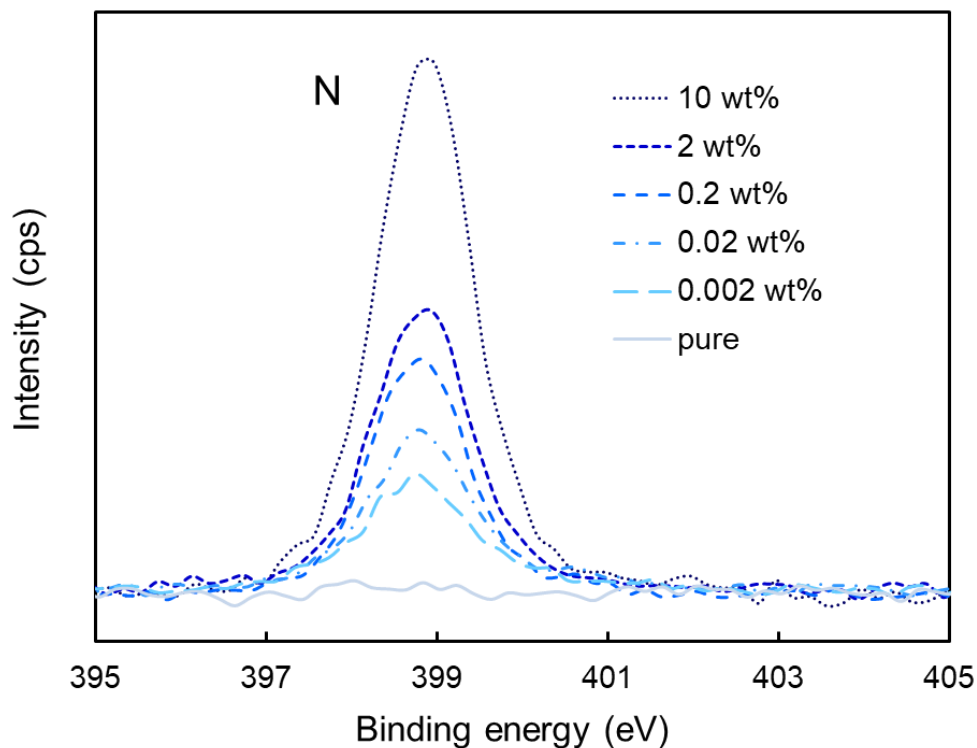


**Figure S2.** XPS scans of the nitrogen peak for D-arabitol samples containing PVP K30 at specified concentrations. The intensity has been normalized by the oxygen peak. Larger peak indicates higher surface concentration of PVP.

**Table S3.** Parameters for bonded (intramolecular) energies. The bonded energy is the sum of three terms corresponding to bond lengths  $V_b(r_{ij}) = \frac{1}{2}k_b(r_{ij} - b_0)^2$ , bond angles  $V_a(\theta_{ijk}) = \frac{1}{2}k_\theta(\theta_{ijk} - \theta_0)^2$ , and dihedral angles  $V_d(\phi_{ijkl}) = k_\phi(1 + \cos(n\phi_{ijkl} - \phi_s))$ . Atom labels and types are defined below the tables.

bond type	$b_0$ (nm)	$K_b$ (kJ/mol/nm <sup>2</sup> )
O-C	0.1410	267776
O-HO	0.0960	418400
HA-C	0.1090	251040
C-C	0.1526	259408

angle type	$\theta_0$ (deg)	$k_\theta$ (kJ/mol/rad <sup>2</sup> )
HO-O-C	108.5	460.24
O-C-HA	109.5	418.40
O-C-C	109.5	418.40
C-C-C	109.5	334.72
C-C-HA	109.5	418.40
HA-C-HA	109.5	292.88

atom 1	dihedral type			phase $\phi_s$ (deg)	$k_\phi$ (kJ/mol/rad <sup>2</sup> )	period $n$
	atom 2	atom 3	atom 4			
C	C	C	C	0	7.5	1
O	C3	C4	O	0	0.65103	3
O	C4	C5	O	120	12.0	1
O	C2	C3	O	0	0.65103	3
O	C1	C2	O	320	8.0	1
O	C5	C4	C3	0	0.65103	1
O	C2	C3	C4	0	0.65103	3
O	C3	C2	C1	0	0.65103	3
O	C3	C4	C5	0	0.65103	3
O	C4	C3	C2	0	0.65103	3
O	C1	C2	C3	0	0.65103	3
HA	C	C	C	0	0.65103	3
HA	C	C	HA	0	0.65103	3
O	C	C	HA	0	0.65103	3
HA	C	O	HO	0	0.4	3
C	C	O	HO	0	0.4	3

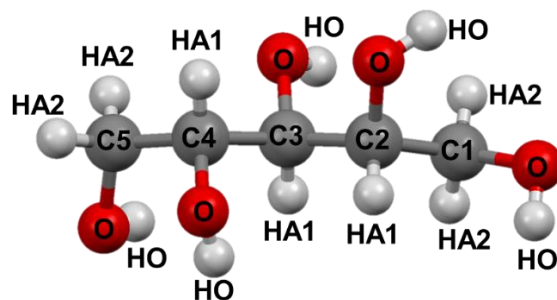


**Table S4.** Parameters for nonbonded (intermolecular) pair energies. Each pair energy is the sum of a Lennard-Jones term  $V_{LJ}(r_{ij}) = 4\epsilon_{ij}((\frac{\sigma_{ij}}{r_{ij}})^{12} - (\frac{\sigma_{ij}}{r_{ij}})^6)$  with the combination rules  $\sigma_{ij} = \frac{1}{2}(\sigma_{ii} + \sigma_{jj})$  and  $\epsilon_{ij} = (\epsilon_{ii}\epsilon_{jj})^{1/2}$  and a Columbic term  $V_c(r_{ij}) = \frac{q_i q_j}{4\pi\epsilon_0 r_{ij}}$ . Nonbonded interactions between bonded atoms separated by 3 bonds or less are excluded from the total energy (interactions between these atoms are given by bonded energies defined in Table S1). Atom types and numbers are defined below Table S1.<sup>a</sup>

atom type	$q$ (e)	$\epsilon$ (kJ/mol)	$\sigma$ (nm)
HA2	0.060	0.0656888	0.27740
HO	0.418	0.2083632	0.14254
C1 and C5	0.145	0.4577296	0.38160
O	-0.683	0.6656744	0.28508
C2-4	0.205	0.4577296	0.38160
HA1	0.060	0.0656888	0.27740

<sup>a</sup>The Lennard-Jones potential had a cutoff of 10 Å and then was brought to zero smoothly at 11 Å using a potential-switch function. The cutoff of Coulombic interactions was at 15 Å and the long-range electrostatic interactions were calculated using a Particle-Particle Particle-Mesh (P3M-AD) algorithm with an accuracy value of  $10^{-4}$ .

**Table S5.** Comparison of the unit-cell parameters of D-arabitol polymorphs from X-ray diffraction and MD simulations.

	Form I			Form II		
	expt	MD	deviation	expt	MD	deviation
$T$ (K)	300	300		105	105	
$a$ (Å)	4.823	4.918	1.97%	4.838	4.883	0.93%
$b$ (Å)	7.675	7.827	1.98%	4.930	4.976	0.93%
$c$ (Å)	9.705	9.896	1.97%	14.382	14.516	0.93%
$\alpha$ (deg)	96.13	96.13	0.00%	90.00	90.00	0.00%
$\beta$ (deg)	96.04	96.57	0.55%	96.15	96.15	0.00%
$\gamma$ (deg)	106.82	106.84	0.02%	90.00	90.00	0.00%

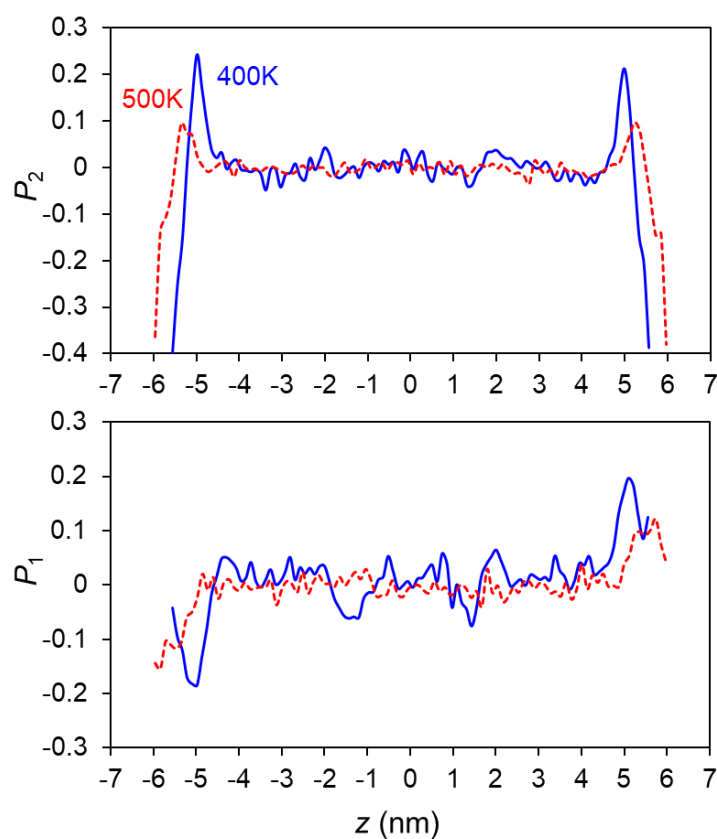


**Figure S3.**  $P_1$  and  $P_2$  order parameters of the C1C5 vector at temperatures at 500 K (red curves), and 400 K (blue solid curves). With cooling from 500 K to 400 K, both  $P_1$  and  $P_2$  show more order in the surface region.

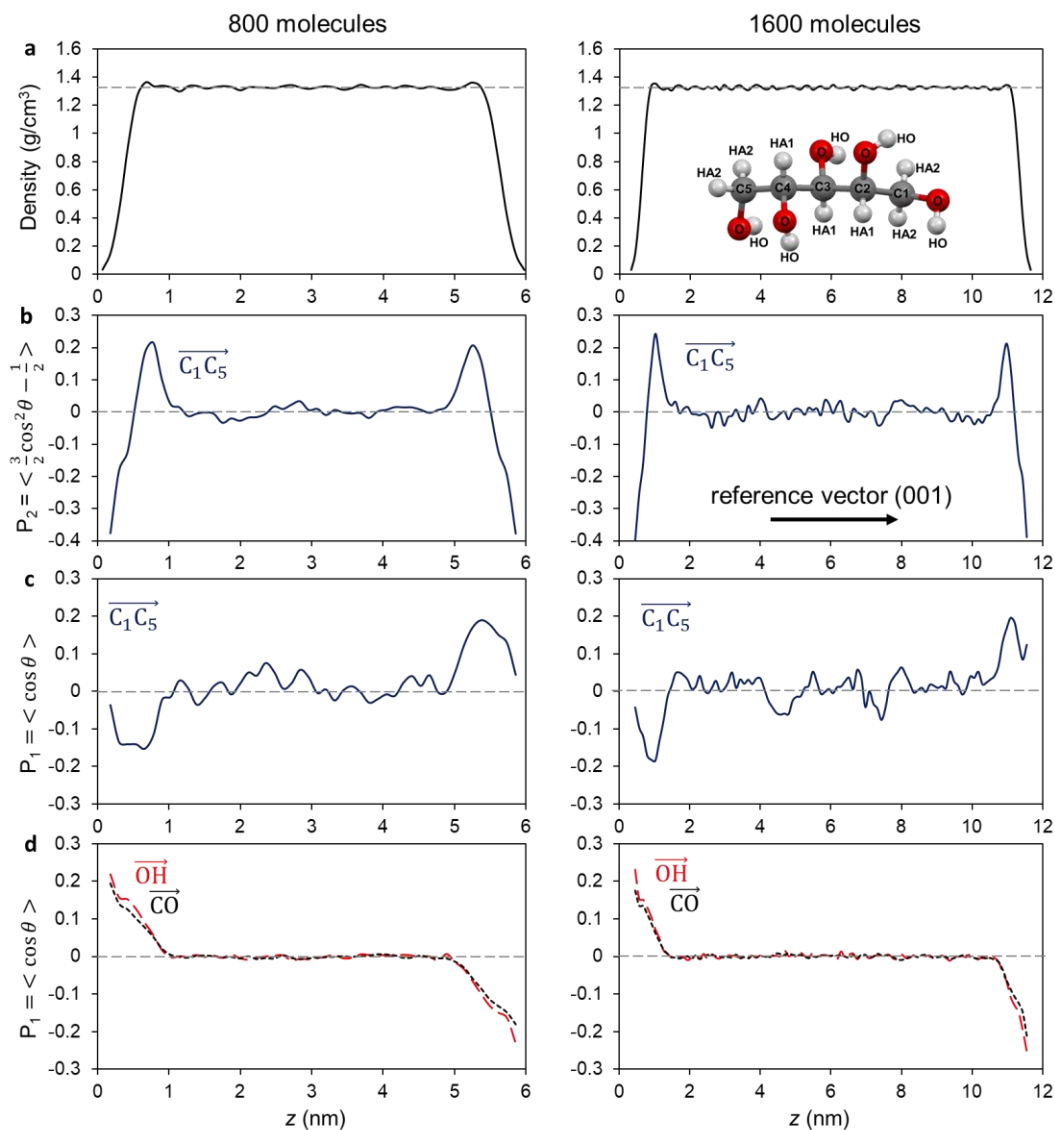


**Figure S4.** Comparison of simulation results with different box sizes. The left column is the results from a box of 800 molecules; the right column is the results from a box of 1600 molecules. No significant size effect is observed.

## 2.8. References

1. Nielsen, M. H.; Aloni, S.; De Yoreo, J. J., In situ TEM imaging of CaCO<sub>3</sub> nucleation reveals coexistence of direct and indirect pathways. *Science* **2014**, *345* (6201), 1158-1162.
2. Van Driessche, A. E.; Van Gerven, N.; Bomans, P. H.; Joosten, R. R.; Friedrich, H.; Gil-Carton, D.; Sommerdijk, N. A.; Sleutel, M., Molecular nucleation mechanisms and control strategies for crystal polymorph selection. *Nature* **2018**, *556* (7699), 89-94.



3. Walsh, M. R.; Koh, C. A.; Sloan, E. D.; Sum, A. K.; Wu, D. T., Microsecond simulations of spontaneous methane hydrate nucleation and growth. *Science* **2009**, *326* (5956), 1095-1098.
4. Zhou, J.; Yang, Y.; Yang, Y.; Kim, D. S.; Yuan, A.; Tian, X.; Ophus, C.; Sun, F.; Schmid, A. K.; Nathanson, M., Observing crystal nucleation in four dimensions using atomic electron tomography. *Nature* **2019**, *570* (7762), 500-503.
5. DeMott, P. J.; Prenni, A. J.; Liu, X.; Kreidenweis, S. M.; Petters, M. D.; Twohy, C. H.; Richardson, M.; Eidhammer, T.; Rogers, D., Predicting global atmospheric ice nuclei distributions and their impacts on climate. *Proceedings of the National Academy of Sciences* **2010**, *107* (25), 11217-11222.
6. Sosso, G. C.; Chen, J.; Cox, S. J.; Fitzner, M.; Pedevilla, P.; Zen, A.; Michaelides, A., Crystal nucleation in liquids: Open questions and future challenges in molecular dynamics simulations. *Chemical reviews* **2016**, *116* (12), 7078-7116.
7. Bartels-Rausch, T., Ten things we need to know about ice and snow. *Nature* **2013**, *494* (7435), 27-29.
8. Nam, H.-S.; Hwang, N. M.; Yu, B.; Yoon, J.-K., Formation of an icosahedral structure during the freezing of gold nanoclusters: surface-induced mechanism. *Physical review letters* **2002**, *89* (27), 275502.
9. Mendez-Villuendas, E.; Bowles, R. K., Surface nucleation in the freezing of gold nanoparticles. *Physical Review Letters* **2007**, *98* (18), 185503.
10. Li, T.; Donadio, D.; Ghiringhelli, L. M.; Galli, G., Surface-induced crystallization in supercooled tetrahedral liquids. *Nature materials* **2009**, *8* (9), 726-730.
11. Descamps, M.; Dudognon, E., Crystallization from the amorphous state: nucleation–growth decoupling, polymorphism interplay, and the role of interfaces. *Journal of pharmaceutical sciences* **2014**, *103* (9), 2615-2628.
12. Sirota, E., Supercooling, nucleation, rotator phases, and surface crystallization of n-alkane melts. *Langmuir* **1998**, *14* (11), 3133-3136.
13. Last, J. A.; Hooks, D. E.; Hillier, A. C.; Ward, M. D., The physicochemical origins of coincident epitaxy in molecular overlayers: Lattice modeling vs potential energy calculations. *The Journal of Physical Chemistry B* **1999**, *103* (32), 6723-6733.
14. Weissbuch, I.; Lahav, M.; Leiserowitz, L., Toward stereochemical control, monitoring, and understanding of crystal nucleation. *Crystal growth & design* **2003**, *3* (2), 125-150.
15. Mitchell, C. A.; Yu, L.; Ward, M. D., Selective nucleation and discovery of organic polymorphs through epitaxy with single crystal substrates. *Journal of the American Chemical Society* **2001**, *123* (44), 10830-10839.
16. Magnussen, O.; Ocko, B.; Regan, M.; Penanen, K.; Pershan, P. S.; Deutsch, M., X-ray reflectivity measurements of surface layering in liquid mercury. *Physical review letters* **1995**, *74* (22), 4444.
17. Regan, M.; Kawamoto, E.; Lee, S.; Pershan, P. S.; Maskil, N.; Deutsch, M.; Magnussen, O.; Ocko, B.; Berman, L., Surface layering in liquid gallium: An X-ray reflectivity study. *Physical review letters* **1995**, *75* (13), 2498.
18. Oh-e, M.; Yokoyama, H.; Baldelli, S., Structure of the glycerol liquid/vapor interface studied by sum-frequency vibrational spectroscopy. *Applied physics letters* **2004**, *84* (24), 4965-4967.
19. Haji-Akbari, A.; Debenedetti, P. G., Thermodynamic and kinetic anisotropies in octane thin films. *The Journal of chemical physics* **2015**, *143* (21), 214501.

20. Bishop, C.; Thelen, J. L.; Gann, E.; Toney, M. F.; Yu, L.; DeLongchamp, D. M.; Ediger, M. D., Vapor deposition of a nonmesogen prepares highly structured organic glasses. *Proceedings of the National Academy of Sciences* **2019**, *116* (43), 21421-21426.
21. Haji-Akbari, A.; Debenedetti, P. G., The effect of substrate on thermodynamic and kinetic anisotropies in atomic thin films. *The Journal of chemical physics* **2014**, *141* (2), 024506.
22. Zhu, L.; Brian, C.; Swallen, S.; Straus, P.; Ediger, M.; Yu, L., Surface self-diffusion of an organic glass. *Physical Review Letters* **2011**, *106* (25), 256103.
23. Turnbull, D., Kinetics of heterogeneous nucleation. *The Journal of Chemical Physics* **1950**, *18* (2), 198-203.
24. Vrbka, L.; Jungwirth, P., Homogeneous freezing of water starts in the subsurface. *The Journal of Physical Chemistry B* **2006**, *110* (37), 18126-18129.
25. Haji-Akbari, A.; DeFever, R. S.; Sarupria, S.; Debenedetti, P. G., Suppression of sub-surface freezing in free-standing thin films of a coarse-grained model of water. *Physical Chemistry Chemical Physics* **2014**, *16* (47), 25916-25927.
26. Haji-Akbari, A.; Debenedetti, P. G., Computational investigation of surface freezing in a molecular model of water. *Proceedings of the National Academy of Sciences* **2017**, *114* (13), 3316-3321.
27. Haji-Akbari, A.; Debenedetti, P. G., Perspective: Surface freezing in water: A nexus of experiments and simulations. *The Journal of chemical physics* **2017**, *147* (6), 060901.
28. Bernstein, J., *Polymorphism in Molecular Crystals 2e*. International Union of Crystal: 2020; Vol. 30.
29. Lewis, D.; Smith, D., Sugar alcohols (polyols) in fungi and green plants. I. Distribution, physiology and metabolism. *The New Phytologist* **1967**, *66* (2), 143-184.
30. Back, J. F.; Oakenfull, D.; Smith, M. B., Increased thermal stability of proteins in the presence of sugars and polyols. *Biochemistry* **1979**, *18* (23), 5191-5196.
31. Gunasekara, S. N.; Pan, R.; Chiu, J. N.; Martin, V., Polyols as phase change materials for surplus thermal energy storage. *Applied Energy* **2016**, *162*, 1439-1452.
32. Kopf, J.; Morf, M.; Zimmer, B.; Köll, P., Kristall- und molekülstruktur von d-arabinitol. *Carbohydrate research* **1991**, *218*, 9-13.
33. Jeffrey, G.; Kim, H., Conformations of the alditols. *Carbohydrate Research* **1970**, *14* (2), 207-216.
34. Huang, C.; Chen, Z.; Gui, Y.; Shi, C.; Zhang, G. G.; Yu, L., Crystal nucleation rates in glass-forming molecular liquids: D-sorbitol, D-arabitol, D-xylitol, and glycerol. *The Journal of chemical physics* **2018**, *149* (5), 054503.
35. Duft, D.; Leisner, T., Laboratory evidence for volume-dominated nucleation of ice in supercooled water microdroplets. *Atmospheric Chemistry and Physics* **2004**, *4* (7), 1997-2000.
36. Kuhn, T.; Earle, M.; Khalizov, A.; Sloan, J., Size dependence of volume and surface nucleation rates for homogeneous freezing of supercooled water droplets. *Atmospheric Chemistry and Physics* **2011**, *11* (6), 2853-2861.
37. Yao, X.; Huang, C.; Benson, E. G.; Shi, C.; Zhang, G. G.; Yu, L., Effect of polymers on crystallization in glass-forming molecular liquids: equal suppression of nucleation and growth and master curve for prediction. *Crystal Growth & Design* **2019**, *20* (1), 237-244.

38. Yu, J.; Li, Y.; Yao, X.; Que, C.; Huang, L.; Hui, H.-W.; Gong, Y. G.; Yu, L., Surface Enrichment of Surfactants in Amorphous Drugs: An X-Ray Photoelectron Spectroscopy Study. *Molecular pharmaceutics* **2022**, *19* (2), 654-660.
39. Jahn, D. A.; Akinkunmi, F. O.; Giovambattista, N., Effects of temperature on the properties of glycerol: A computer simulation study of five different force fields. *The Journal of Physical Chemistry B* **2014**, *118* (38), 11284-11294.
40. Bauer, J.; Spanton, S.; Henry, R.; Quick, J.; Dziki, W.; Porter, W.; Morris, J., Ritonavir: an extraordinary example of conformational polymorphism. *Pharmaceutical research* **2001**, *18* (6), 859-866.
41. Wohlgemuth, K.; Kordylla, A.; Ruether, F.; Schembecker, G., Experimental study of the effect of bubbles on nucleation during batch cooling crystallization. *Chemical Engineering Science* **2009**, *64* (19), 4155-4163.
42. Su, Y.; Yu, L.; Cai, T., Enhanced crystal nucleation in glass-forming liquids by tensile fracture in the glassy state. *Crystal Growth & Design* **2018**, *19* (1), 40-44.
43. Shpyrko, O. G.; Streitel, R.; Balagurusamy, V. S.; Grigoriev, A. Y.; Deutsch, M.; Ocko, B. M.; Meron, M.; Lin, B.; Pershan, P. S., Surface crystallization in a liquid AuSi alloy. *Science* **2006**, *313* (5783), 77-80.
44. Sutter, P. W.; Sutter, E. A., Dispensing and surface-induced crystallization of zeptolitre liquid metal-alloy drops. *Nature materials* **2007**, *6* (5), 363-366.
45. Lü, Y.; Chen, M., Surface layering-induced crystallization of Ni-Si alloy drops. *Acta materialia* **2012**, *60* (11), 4636-4645.
46. Zhang, D.; Gao, N.; Yan, W.; Luo, W.; Zhang, L.; Zhao, C.; Zhang, W.; Liu, D., Heat induced superhydrophilic glass surface. *Materials Letters* **2018**, *223*, 1-4.
47. Berendsen, H. J.; van der Spoel, D.; van Drunen, R., GROMACS: a message-passing parallel molecular dynamics implementation. *Computer physics communications* **1995**, *91* (1-3), 43-56.
48. Abraham, M. J.; Murtola, T.; Schulz, R.; Páll, S.; Smith, J. C.; Hess, B.; Lindahl, E., GROMACS: High performance molecular simulations through multi-level parallelism from laptops to supercomputers. *SoftwareX* **2015**, *1*, 19-25.
49. This research was performed using the compute resources and assistance of the UW-Madison Center For High Throughput Computing (CHTC) in the Department of Computer Sciences. The CHTC is supported by UW-Madison, the Advanced Computing Initiative, the Wisconsin Alumni Research Foundation, the Wisconsin Institutes for Discovery, and the National Science Foundation, and is an active member of the Open Science Grid, which is supported by the National Science Foundation and the U.S. Department of Energy's Office of Science.
50. Hess, B., P-LINCS: A parallel linear constraint solver for molecular simulation. *Journal of chemical theory and computation* **2008**, *4* (1), 116-122.
51. Bussi, G.; Donadio, D.; Parrinello, M., Canonical sampling through velocity rescaling. *The Journal of chemical physics* **2007**, *126* (1), 014101.

## **Chapter 3. Surface-Enhanced Crystal Nucleation and Polymorph Selection in Amorphous Posaconazole**

Xin Yao<sup>1</sup>, Kennedy A. Borchardt<sup>1</sup>, Yue Gui<sup>1,3</sup>, Ilia A. Guzei<sup>2</sup>, Geoff G. Z. Zhang<sup>4,\*</sup>, Lian Yu<sup>1,2,\*</sup>

<sup>1</sup> School of Pharmacy, <sup>2</sup> Department of Chemistry, University of Wisconsin-Madison, Madison, WI, 53705, USA

<sup>3</sup> Process Research and Development, <sup>4</sup>Drug Product Development, Research and Development, AbbVie Inc., North Chicago, IL, 60064, USA

To be submitted for publication in *The Journal of Chemical Physics*

### 3.1. Abstract

Molecules at a liquid/vapor interface have different organization and mobility from those in the bulk. These differences potentially influence the rate of crystal nucleation, but the effect remains imperfectly understood. We have measured the crystal nucleation rates at the surface and in the bulk of amorphous posaconazole and observed that surface nucleation is vastly enhanced over bulk nucleation, by approximately 9 orders of magnitude, and selects a different polymorph (II) from the bulk (I). This phenomenon mirrors the recently reported case of D-arabitol and results from the anisotropic molecular packing at the surface and its similarity to the structure of the surface-nucleating polymorph. In contrast to these two systems, the surface enhancement of nucleation is weaker (though still significant) in acetaminophen and in water, without polymorph switch. The systems investigated to date all feature surface enhancement, not suppression, of crystal nucleation, and the systems showing polymorphic switch feature (1) structural reconstruction at the surface relative to the bulk and (2) existence of a different polymorph that can take advantage of the surface environment to nucleate. These results help predict the effect of a liquid/vapor interface on crystal nucleation and polymorph selection, especially in systems with large surface/volume ratio such as atmospheric water and amorphous particles.

**Keywords:** liquid/vapor interface, surface, crystal nucleation, polymorph, anisotropic molecular packing, posaconazole.

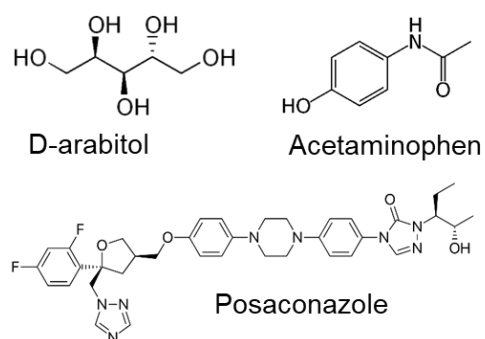
### 3.2. Introduction

Crystal nucleation is an important process in science and nature.<sup>1-6</sup> Together with crystal growth, nucleation defines the microstructure and the polymorphic outcome of a crystalline material. Despite this importance, many essential questions about nucleation remain unanswered.<sup>5, 7</sup> One of these questions concerns the effect of a liquid/vapor interface on crystal nucleation. This question arises whenever a free surface is present when a liquid crystallizes, notably atmospheric water,<sup>8</sup> metallic nano-droplets,<sup>9, 10</sup> alkanes,<sup>11</sup> and amorphous drugs.<sup>12, 13</sup>

At a liquid/vapor interface, molecules are organized differently from those in the bulk, showing layering<sup>14, 15</sup> and preferred orientation,<sup>16-18</sup> and can have enhanced mobility.<sup>19, 20</sup> For a multi-component system, the surface composition can differ from the bulk composition.<sup>21, 22</sup> Do these differences promote or inhibit crystal nucleation? For a polymorphic system,<sup>23</sup> do certain structures nucleate faster at the surface than in the bulk? At present, these questions have no satisfactory answers. In the case of water, the surface effect on nucleation has received much attention, but controversies persist.<sup>24</sup> The Classical Nucleation Theory (CNT)<sup>25</sup> anticipates a potential surface enhancement of nucleation,<sup>2, 26, 27</sup> but cannot be relied upon to predict quantitative nucleation rates due to the unknown model parameters. Molecular dynamics (MD) simulations have observed surface-enhanced nucleation,<sup>3, 9, 10</sup> but the results are often sensitive to the force fields used<sup>28-30</sup> and correspond to conditions far removed from those of practical interest.

Recently Yao et al. reported an unambiguous example of surface-enhanced nucleation in the glass-forming molecular liquid D-arabitol (Scheme 1).<sup>22</sup> In this viscous liquid, the timescales for

bulk and surface nucleation are well separated, allowing their rates to be independently measured. They found surface nucleation to be substantially faster than bulk nucleation, by 12 orders of magnitude when compared on a per-molecule basis. Remarkably, surface nucleation was observed to select a different polymorph from bulk nucleation. The strong surface effect on nucleation arises from the anisotropic molecular packing in the surface region, which templates



**Scheme 1.** Molecular structures of D-arabitol, acetaminophen, and posaconazole.

the surface-nucleating polymorph. Yao et al. compared their result on D-arabitol with that of Kuhn et al. on water<sup>31</sup> and noted a more modest surface enhancement of nucleation in water, with an enhancement factor of  $10^4$  on a per-molecule basis and without polymorphic change. More recently, Wu et al. investigated the surface nucleation in amorphous acetaminophen<sup>32</sup> and observed an enhancement factor of  $10^5$ , also without polymorphic change. At present, the wide range of effects observed are poorly understood and provide the motivation for this work.

In this work, we adopt the approach of Yao et al. to investigate the surface nucleation and polymorph selection in the glass-forming molecular liquid posaconazole (Scheme 1). This system is a model for the study of the structure and stability of amorphous drugs.<sup>33-35,36</sup> Unlike D-arabitol, posaconazole does not form extensive hydrogen bonds (HBs) and interacts with other

molecules mainly through van der Waals forces. Posaconazole is a rod-like molecule and its analogs itraconazole<sup>37, 38</sup> and saperconazole<sup>39</sup> are known to form nematic and smectic liquid crystals (LCs). Interestingly, posaconazole itself has no reported LC phases. Despite this, by physical vapor deposition (PVD), Bishop et al. were able to prepare glass films of posaconazole that have strong smectic order with a smectic-layer spacing of 3 nm (approximately the length of the molecule).<sup>18</sup> This suggests a layered organization of molecules at the liquid/vapor interface that gets propagated by PVD. Using near-edge X-ray absorption fine structure (NEXAFS) spectroscopy, Bishop et al. showed that the rod-like posaconazole molecules tend to be vertically oriented at the vapor interface, with an average angle between the long axis of the molecule and the surface normal of 33°. It is noteworthy that one end of posaconazole is fluorinated while the other end has a polar hydroxyl group (Scheme 1). Molecules with fluorinated end groups are known to orient themselves at a liquid/vapor interface so that the fluorinated end is exposed to the vapor, creating polar order.<sup>40-42</sup> This is a result of the low surface energies of fluorinated groups.<sup>43</sup> For posaconazole, this orientation would gain a further driving force since the OH group would be buried in the bulk, allowing it to form HBs. We investigate how such the anisotropic surface structure of posaconazole influences its crystal nucleation and polymorphism.

We find that the surface nucleation of posaconazole is vastly promoted, by approximately 9 orders of magnitude on a per-molecule basis, and selects a different polymorph (II) from the bulk (I). This effect arises from the preferred orientation and layering of surface molecules that resemble the structure of the surface-nucleating polymorph. This picture is similar to that of D-arabitol despite the difference in the extent of HBs and mechanism of surface ordering. In both systems, the surface effect on nucleation is large and favors a different polymorph. These



systems are in contrast to acetaminophen and water where the surface effect is smaller and causes no polymorphic change. We discuss these results in terms of the degree to which physical conditions are changed from the bulk to the surface and the availability of polymorphs that can take advantage the surface environment to nucleate.

### 3.3. Materials and Methods

Posaconazole was purchased from AstaTech and used either as received or after recrystallization, with no significant differences noted. For recrystallization, 920 mg of posaconazole was dissolved in 60 mL of ethanol at 350 K and the hot solution was filtered (0.45  $\mu\text{m}$  syringe filter). The solution was cooled to room temperature and seeded with Form I crystals. After 2 days, the mother liquor was decanted, and the crystals were washed three times with ethanol and dried under vacuum (50 % yield).

The details of measuring surface and bulk nucleation rates have been described previously.<sup>22, 26, 27</sup> Briefly, bulk nucleation was measured with a liquid film that was sandwiched between two coverslips and surface nucleation with a film supported on one coverslip exposing an open surface (see Figures 3a and 3b for illustrations). To facilitate spreading of a melt, a heat-treated coverslip was used.<sup>43</sup> To commence a rate measurement, the liquid film was cooled to the temperature of interest without accessing a lower temperature (at which nucleation could be faster). Nucleation rates were measured using the one-stage method at temperatures at which crystal growth was relatively fast and the two-stage method otherwise.<sup>26</sup> To eliminate ambient

moisture, each sample was stored in the nitrogen-purged chamber of a temperature-controlled microscope stage (Linkam THMS) or a nitrogen-purged mini-oven of custom construction.

Differential Scanning Calorimetry (DSC) was performed with a TA Q2000 under 50 mL/min N<sub>2</sub> purge. Each sample was 2-10 mg placed in an aluminum pan. The heating and cooling rates are 10 K/min. Powder X-ray Diffraction (PXRD) was performed with a Bruker D8 Advance X-ray diffractometer with a Cu K $\alpha$  source ( $\lambda = 1.54056 \text{ \AA}$ ) operating at a tube load of 40 kV and 40 mA. A powder sample ~10 mg in mass was spread and flattened on a Si (510) zero-background holder and scanned between 3° and 40° (2 $\theta$ ) at a step size of 0.02° and a maximum scan rate of 1 s/step.

The crystal structure of Form II was solved by single-crystal diffractometry. A single crystal of Form II was grown using the method of micro-droplet.<sup>44</sup> Small droplets were formed on a microscope coverslip, seeded with Form II at 442 K (Form II seeds were obtained by heating the methanol solvate of posaconazole at 403 K), and crystallized at 440 K. At this point, each droplet transformed to a cluster of crystals not suitable for structural solution. To improve crystal quality, the cluster was partially melted until only one small seed remained and the seed was allowed to grow at 440 K to consume the entire droplet. Repeating this process yielded a single crystal of high quality for structural solution. The entire process was performed under nitrogen purge. The details of data collection and structural solution are given in the Supporting Information and the Crystallographic Information File.

### 3.4. Results and Discussion

**Polymorphs of Posaconazole.** Two polymorphs of posaconazole are known at present: I (Ref. <sup>45</sup>, CSD reference code YIMVUO) and II (structure solved in this work, see the deposited CIF file).

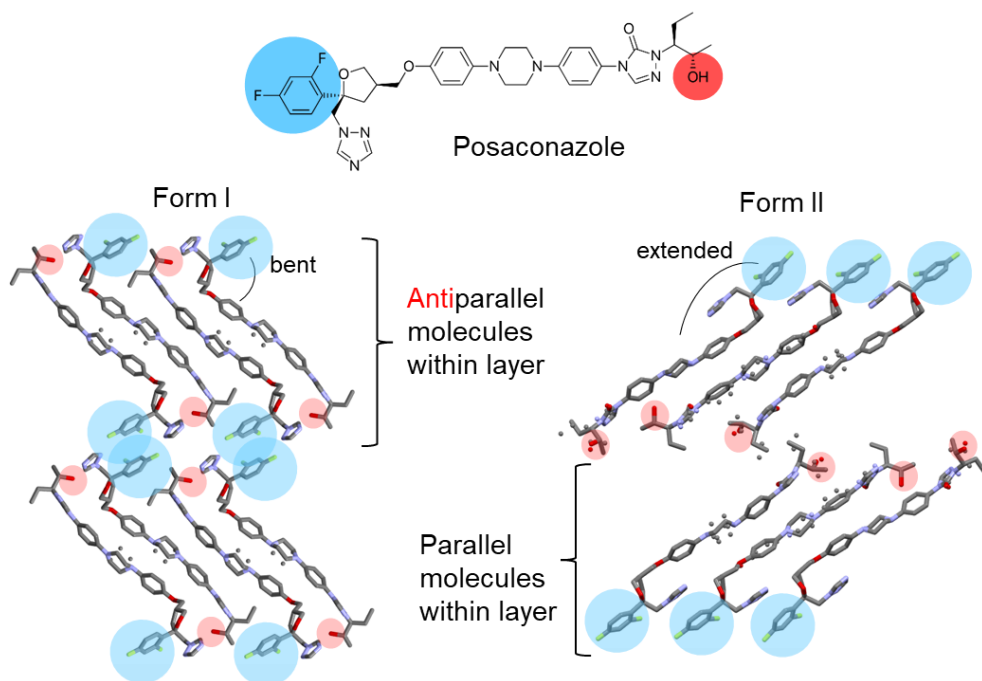


**Figure 1.** Crystal structures of posaconazole polymorphs. Overall the molecules have a rod-like shape while their detailed conformations differ. The difluorophenyl ring is bent relative to the long axis in Form I and extended in Form II. In each layer, the molecules are antiparallel in Form I and parallel in Form II. The unconnected atoms indicate positional disorder.

Table 1 summarizes their structural parameters. Based on powder diffraction patterns, Form II appears to match Form Y of Wieser et al.,<sup>46</sup> who did not solve its structure. Below we describe the key differences between the structures of the two polymorphs.

(1) Form I has one symmetry-independent molecule and Form II three. Overall, these molecules have an elongated, rod-like shape, but they differ in conformation and positional disorder. The

difluorophenyl ring is bent relative to the long axis of posaconazole in Form I and extended in Form II (see Figure 1). In Form I, the carbon atoms of the central piperazine ring are disordered. In Form II, there are more disordered sites, both in the central portion of the molecule and in the terminal groups (see SI and the CIF file for details).

(2) In both polymorphs, the molecules are organized into layers (Figure 1), with each approximately 2 nm thick. Posaconazole has two distinct ends, designated as the OH end and the F end. In Form I, the adjacent molecules are anti-parallel within each layer, whereas in Form II, they are parallel.

(3) With respect to hydrogen bonds (HB), posaconazole has a single donor (OH) and multiple acceptors. In Form II, all HBs occur on one side of a molecular layer, as dictated by the parallel arrangement of molecules, whereas in Form I, they occur on both sides of the layer, a consequence of the anti-parallel arrangement. Later, these structural differences between the two polymorphs will be used to investigate the polymorph selection of bulk and surface nucleation.

**Table 1.** Structural parameters of posaconazole polymorphs.

Form	Form I	Form II
CSD	YIMVUO	This work
$T$ , K	100	100
$a$ (Å)	12.246	23.433

$b$ (Å)	6.3485	6.0436
$c$ (Å)	22.796	36.550
$\alpha$ , deg	90	90
$\beta$ , deg	96.138	92.998
$\gamma$ , deg	90	90
$V$ , Å <sup>3</sup>	1762.1	5169.1
space group	P2 <sub>1</sub>	P2 <sub>1</sub>
$\rho$ , g/cm <sup>3</sup>	1.321	1.351
$Z$	2	6
$Z'$	1	3
R-factor %	3.42	3.65

---

The thermodynamic relations of the posaconazole polymorphs have been determined by DSC. Figure 2a shows the DSC traces of the polymorphs; Table 2 collects the temperatures and enthalpies of the phase transitions. Form I undergoes a reversible phase transition near 405 K.<sup>47</sup> We name the high-temperature form Form I'. Figure 2b shows the relative free energies of the polymorphs calculated from the constants in Table 2.<sup>48</sup> It is worth noting that Form I has lower density *and* lower enthalpy than Form II. This is atypical of most phase transitions where lower density usually goes with higher enthalpy, but is a known behavior of hydrogen-bonded systems such as water and nicotinamide cocrystals.<sup>49</sup> In the temperature range of our nucleation study (indicated by the double-sided arrow), both polymorphs are driven to crystallize from the liquid phase and Form I is more stable than Form II.

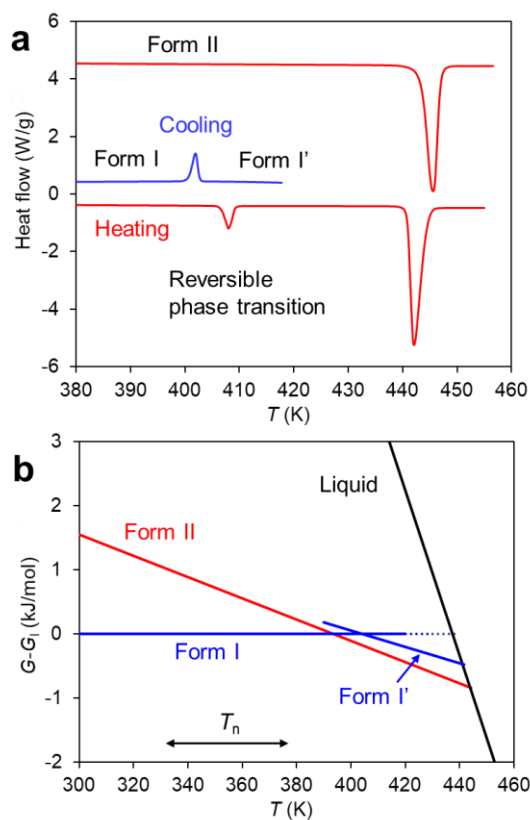


**Figure 2.** (a) DSC traces of posaconazole polymorphs. Form I has reversible phase transition, while Form II does not. (b) Relative free energies of posaconazole polymorphs. The two-sided arrow indicates the temperature range of nucleation measurements in which Forms I and II are both thermodynamically driven to crystallize.

**Table 2.** Temperatures and enthalpies of phase transitions in posaconazole

Form	I	II
$T_{t \text{ I} \rightarrow \text{I}'}$ (K) <sup>a</sup>	405	-
$\Delta H_t$ (kJ/mol)	5.2	-
$T_m$ (K)	441	443
$\Delta H_m$ (kJ/mol)	51.3	49.9

<sup>a</sup> Average of the onset temperatures during cooling (402 K) and heating (407 K)

**Surface Nucleation of Posaconazole and Polymorph Selection.** Figures 3a and 3b illustrate the experiments to measure bulk and surface nucleation. In a bulk experiment, a liquid film is sandwiched between two glass coverslips with no free surface in the region of observation. In a surface experiment, the liquid film is supported on one coverslip and has an exposed free surface. Figures 3c and 3d show the typical difference between the outcomes of bulk and surface nucleation. In this example, both samples were nucleated at 353 K and heated to 403 K for 1 min to grow the nuclei to a visible size. The surface sample nucleated more crystals in a shorter time (103 min) than the bulk sample in a longer time (1368 min). No crystals were observed without the heating step or only with the heating step (no nucleation step), indicating that nucleation occurred at 353 K and that the surface sample created more nuclei than the bulk sample.

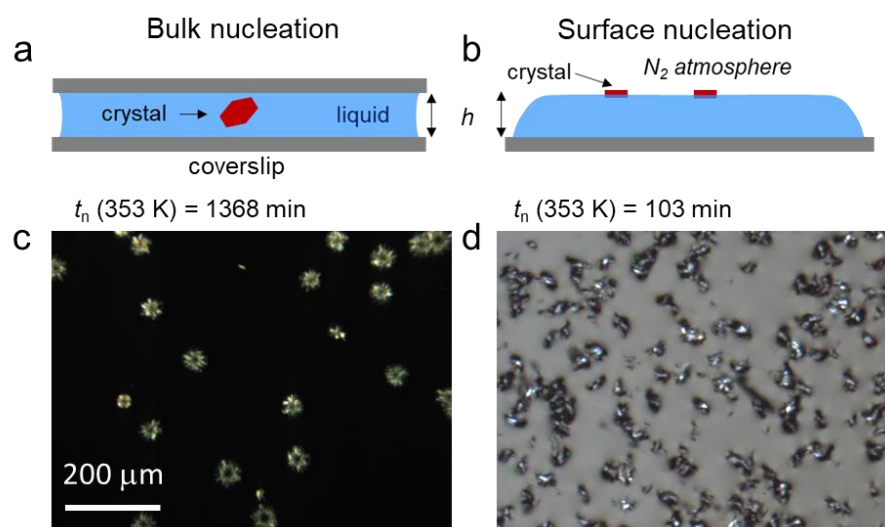


**Figure 3.** (a, b) Bulk- and surface-nucleation experiments. The thickness of the liquid film  $h$  is nominally 50  $\mu\text{m}$ . (c, d) Comparison of the densities of bulk- and surface-nucleated posaconazole crystals at 353 K. After nucleation at 353 K, both samples spent 1 min at 403 K for the nuclei to grow to visible size. Surface nucleation created more crystals in 103 min than bulk nucleation in 1368 min. Furthermore, surface nucleation yielded mainly Form II while bulk nucleation mainly Form I.

To confirm that the nucleation mechanisms, the thickness of the liquid film  $h$  was varied and the effect on the number of crystals per lateral viewing area  $n_A$  was observed. For a surface nucleation process,  $n_A$  should not depend on  $h$ , whereas for a bulk nucleation process, it should be proportional to  $h$ . This was indeed observed. For example, increasing  $h$  from 20 to 120 mm (a factor of 6) increased  $n_A$  by a factor of 5 for films nucleated under the bulk condition for 28 h at 343 K, and by 30 % for films nucleated under the surface condition for 190 min at 343 K. These thickness tests confirm the two mechanisms of nucleation.

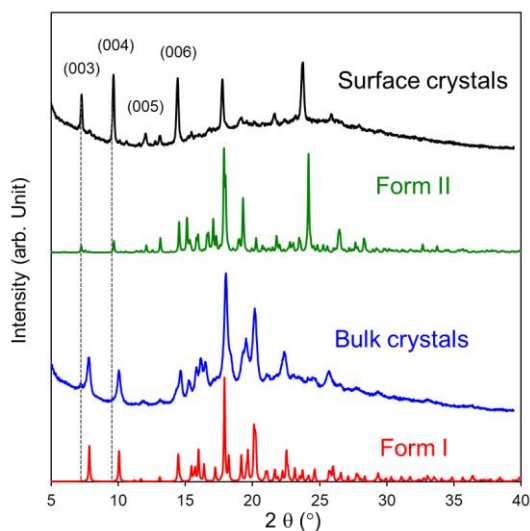


**Figure 4.** X-ray diffraction patterns of posaconazole crystals produced by surface and bulk nucleation. Comparison with the reference patterns indicates that surface nucleation produced Form II and bulk nucleation Form I.

It is significant that the surface nucleation of posaconazole selects a different polymorph from the bulk nucleation. Figure 4 shows the X-ray diffraction patterns of bulk- and surface-nucleated crystals. These results show that bulk nucleation produced Form I and surface nucleation Form II. Given the detection limit of this technique (several percent), we cannot rule out minute phase impurity but the major difference in polymorphic preference is evident. The diffraction peaks of



the surface-nucleated crystals, measured in the Bragg-Brentano mode, show significantly stronger (001) reflections than those in the calculated powder pattern. These enhanced reflections are labeled in Figure 4 and indicate a preferred orientation of the surface crystals with the (001) plane being parallel to the liquid surface. In contrast, the bulk-nucleated crystals do not show significant preferred orientation. As discussed later, the preferred orientation of the surface-nucleated crystals is consistent with the proposed surface-nucleation mechanism.

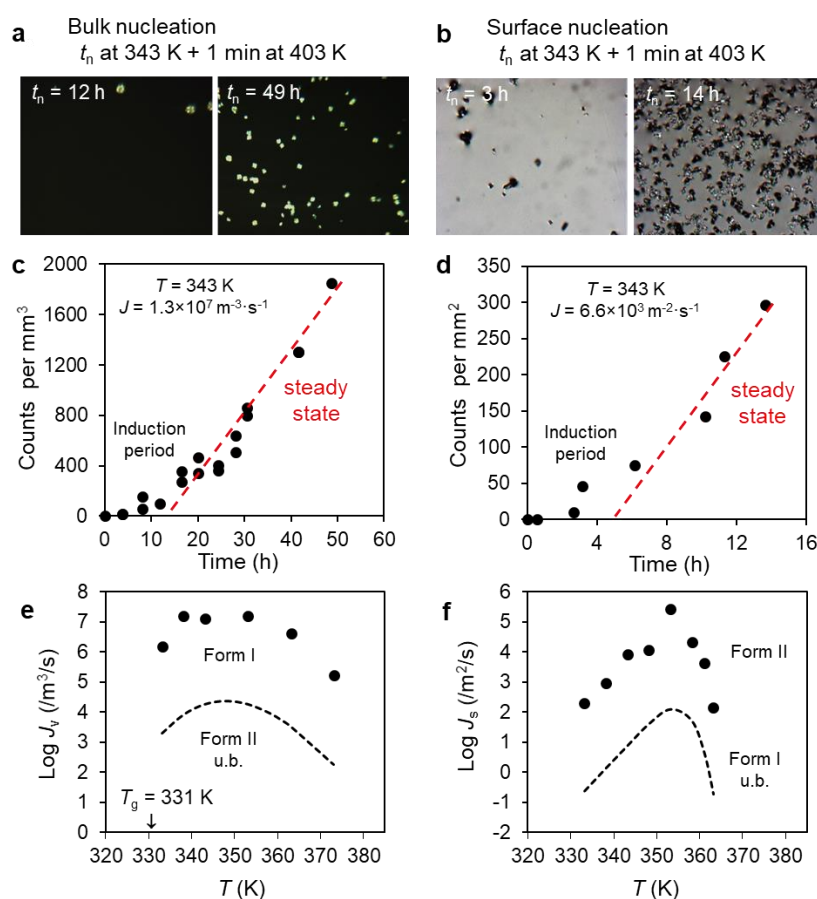


**Figure 5.** Nucleation rate measurements in the bulk (left column) and at the surface (right column). (a) and (b) Photos of a sample that spent different times  $t_n$  at the nucleation temperature (343 K) and 1 min at the growth temperature (403 K). (c) and (d) Volumetric and areal density of nuclei vs.  $t_n$ . The slope at steady state is the nucleation rate. (e) and (f) Nucleation rates vs temperature. u.b.: upper bound.

Figure 5 shows the measurements of the nucleation rates in the bulk and at the surface of posaconazole. Figures 5a and 5b show the representative images recorded for this purpose. Bulk and surface samples were nucleated at a chosen temperature (343 K in this example) for different times  $t_n$  and the nuclei were allowed to grow the same time at a higher temperature (1 min at 403 K) to visible size to be counted. For each sample, longer  $t_n$  yielded more crystals. Figures 5b and 5c plot the volumetric and areal densities of nuclei as a function of time. After an initial induction time, a steady state was reached and the slope of the plot at the steady state is the nucleation rate.

Figures 5e and 5f show the rates of nucleation in the bulk and at the surface of posaconazole. Both rates show a maximum slightly above  $T_g$ , consistent with results on other glass-forming molecular liquids.<sup>26</sup> The curves in these figures are the estimated upper bounds (u.b.) for the

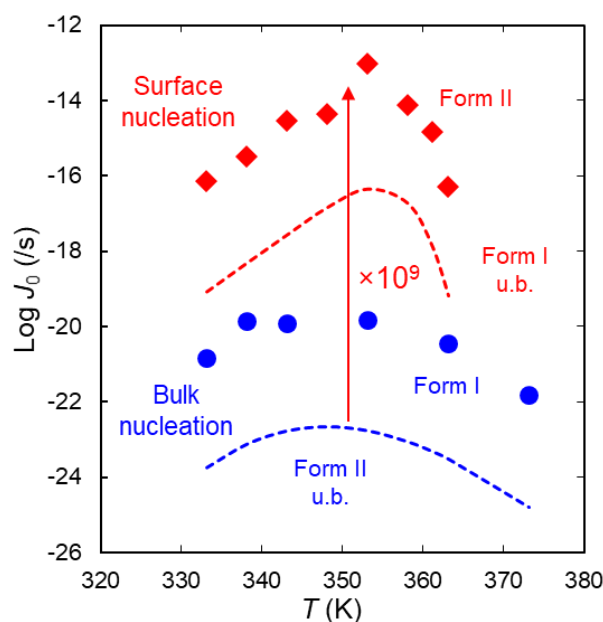


**Figure 6.** Per-molecule rates of surface and bulk nucleation in posaconazole. The surface nucleation of Form II is enhanced by a factor of  $10^9$  relative to the bulk nucleation while the difference is smaller for Form I. u.b.: upper bound.

nucleation rates of the polymorphs that were not observed in the bulk (Form II) and at the surface (Form I). To calculate these bounds, we assume fewer than one nucleus in the entire time of observation in all the samples measured. The upper bounds are estimated to be 1000 times smaller than the observed rates.

As presented in Figures 5e and 5f, the rates of bulk and surface nucleation in posaconazole cannot be compared directly. This is because the two rates have different units:  $J_v$  in  $1/\text{m}^3/\text{s}$  and  $J_s$  in  $1/\text{m}^2/\text{s}$ . To compare them, we convert each rate to the per-molecule value:  $J_{v0} = J_v \Omega_0$  and  $J_{s0} = J_s A_0$ , where  $\Omega_0$  and  $A_0$  are the volume and surface area occupied by one molecule, respectively.  $J_{v0}$  ( $J_{s0}$ ) is the number of nucleation events per second in the volume (surface area) occupied by one molecule. (Equivalently, we can define  $J_{v0}$  ( $J_{s0}$ ) as the number of nucleation events per second per molar volume (molar surface area), by multiplying each rate by

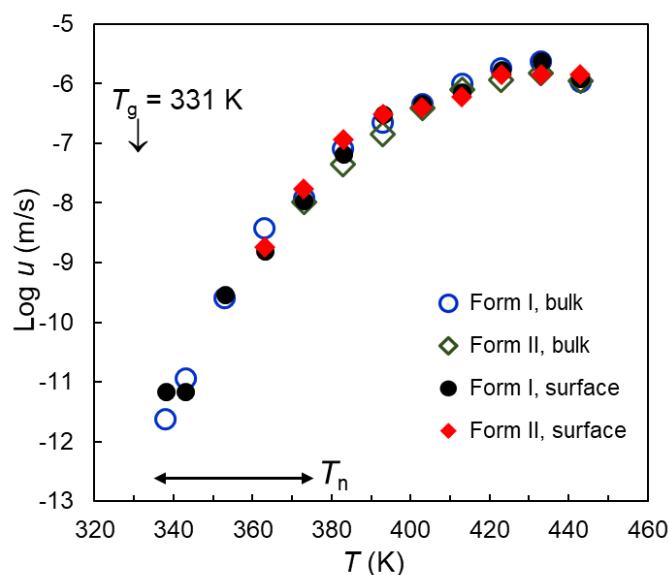


**Figure 7.** Crystal growth rates of posaconazole polymorphs at the surface and in the bulk. No significant difference is seen in the temperature range of nucleation study for either polymorph. The two-sided arrow indicates the temperature range of nucleation measurement.

Avogadro's number.) For posaconazole,  $\Omega_0 = 0.92 \text{ nm}^3$  calculated from its bulk density, and  $A_0 = \Omega_0/L \approx 0.35 \text{ nm}^2$ , where  $L = 2.8 \text{ nm}$  is the length of the rod-like molecule.<sup>36</sup> In Figure 6, the  $J_{v0}$  and  $J_{s0}$  values are plotted against temperature. The curves are the estimated upper bounds for the unobserved polymorphs. These results quantify the surface enhancement effect for the nucleation of the two polymorphs. For Form II at 343 K (arrow), the enhancement factor  $J_{s0}/J_{v0}$  is approximately  $10^9$  near the peak temperature for nucleation rate ( $T_{\text{max}} \approx 350 \text{ K}$ ), meaning that surface molecules nucleate Form II faster than bulk molecules by 9 orders of magnitude. In contrast,  $J_{s0}/J_{v0} \approx 10^4$  for Form I near  $T_{\text{max}}$ . This quantifies the strong polymorphic preference of surface nucleation.

**Surface Effect on Crystal Growth Rates of Posaconazole Polymorphs.** Given the large surface effect on crystal nucleation and polymorphism, we now consider whether a similar effect exists on crystal growth. Figure 7 shows the crystal growth rates of posaconazole polymorphs in the bulk and at the surface as a function of temperature. Within experimental error, we observe

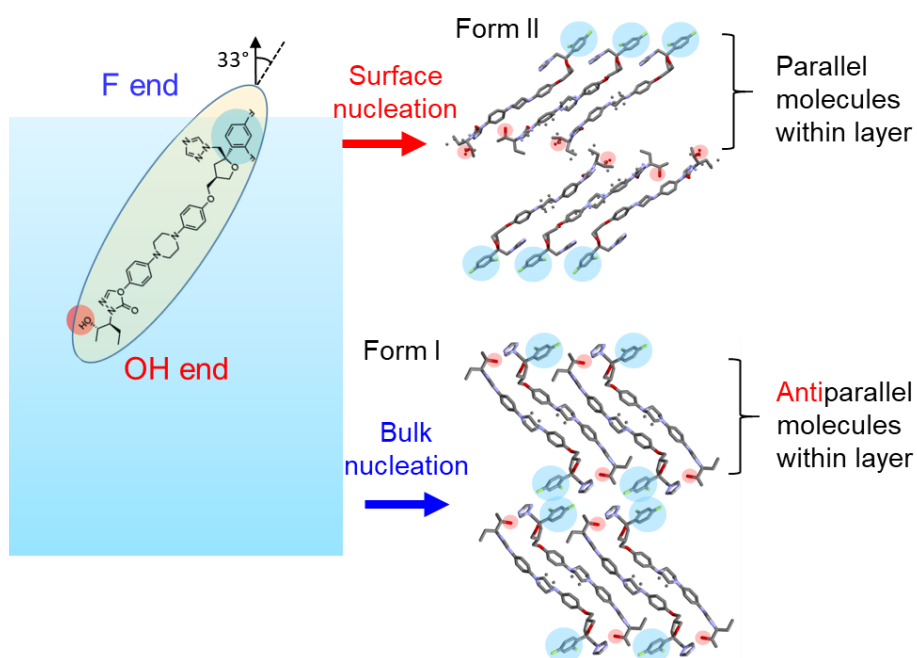


**Figure 8.** Surface-enhanced nucleation of posaconazole with polymorphic selection.

no significant dependence of the crystal growth rate on the physical environment (bulk or surface) or on the polymorph (I or II) in the temperature range investigated. (Form II growth rates could not be measured below 363 K because Form I cross-nucleated on Form II.) These results are attributed to the fact that as temperature approaches  $T_g$ , the crystal growth rate is mainly limited by molecular mobility, that is, by how fast molecules can join a crystal.<sup>50</sup> This explains why different polymorphs show similar diffusion-controlled growth rates.<sup>51</sup> Extending this line of reasoning, the similar crystal growth rates in the bulk and at the surface indicate that the two regions have similar molecular mobility that support crystal growth and presumably the enlargement to a nucleus. Thus, the faster nucleation rate in the surface region is not caused by their higher mobility. If this were the case, the two polymorphs should show a similar enhancement factor for their nucleation rates, rather than very different factors (Figure 6).

Having eliminated kinetics as the cause for the surface enhancement of nucleation, we now consider surface structure as a possible cause. Using X-ray scattering, Bishop et al. observed strong smectic order in the glass films of posaconazole prepared by physical vapor deposition (PVD) with a smectic-layer spacing of 3 nm,<sup>18</sup> approximately the molecular length. This suggests a layered organization of the rod-like molecules at the liquid/vapor interface, which is propagated by PVD. Using NEXAFS, Bishop et al. showed that posaconazole molecules tend to be vertically oriented at the surface with the average angle between the long axis of the molecule and the surface normal being  $\sim 33^\circ$ .<sup>18</sup> This angle is significantly smaller than the magic angle of  $54^\circ$  for random orientation. In addition, based on the observation that molecules with fluorinated end groups tend to be oriented at a liquid/vapor interface with the fluorinated end pointing to the vapor phase,<sup>40-42</sup> we expect posaconazole to have the same orientation on the surface. This

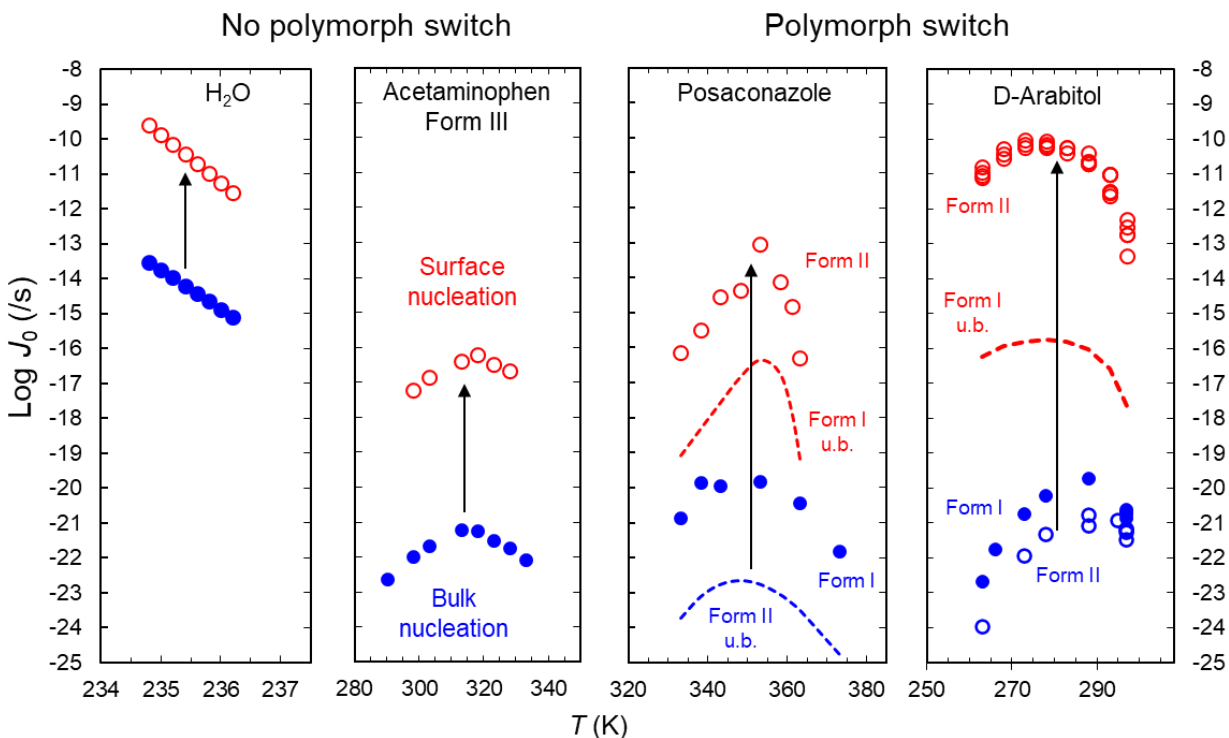


**Figure 9.** Per-molecule surface and bulk nucleation rates of water, D-arabitol, acetaminophen, and posaconazole. Surface nucleation causes a polymorph switch in D-arabitol and posaconazole and no such switch in water and acetaminophen. The vertical arrow indicates the surface enhancement effect on nucleation (for the surface-nucleating polymorphs in the cases of D-arabitol and posaconazole). u.b.: upper bound.

orientation exposes the low-surface-energy fluorinated group<sup>43</sup> and buries the high-surface-energy OH group. Apart from this surface-energy consideration, the orientation with fluorine up and OH down orientation facilitates the formation of HBs. We depict this surface structure in Figure 8 and use it to explain the surface effect on nucleation. The presence of a smooth vapor interface and the near-vertical orientation of molecules means a smectic-like surface layer. In this layer, the molecules tend to be parallel with each other, expose their F ends, and bury their OH ends. This surface structure resembles that of Form II and is unlike that of Form I, in which the molecules are antiparallel within a layer. As a result, surface nucleation favors Form II over Form I. In the bulk, the driving force described above for layering and polar order is absent and

the molecules are expected to be randomly oriented. Using ssNMR, Lu et al. showed that posaconazole molecules form “head-to-tail” interactions in the amorphous phase,<sup>34</sup> consistent with the absence of parallel packing. As a result, bulk nucleation favors Form I over Form II.

To date the surface and bulk nucleation rates have been reported for four systems: water,<sup>31</sup> D-arabitol,<sup>22</sup> acetaminophen,<sup>32</sup> and posaconazole (this work). For water, the surface and bulk rates were inferred from the dependence of the total nucleation rate on the droplet size, whereas for the latter three systems, the two rates were independently measured. In Figure 9, we compare the per-molecule nucleation rates at the surface (red color) and in the bulk (blue color) for the four systems on a common scale. Water was investigated in a narrow temperature range that lies above the temperature of maximal nucleation rate  $T_{\max}$ , whereas the other three systems at temperatures that cover  $T_{\max}$ . For the three organic liquids, the bulk nucleation rates are comparable, while the surface nucleation rates show greater variation. Of the four systems, D-arabitol and posaconazole fall in one group for which surface nucleation selects a different polymorph (II) from bulk nucleation (I). For the surface-nucleating polymorph, the enhancement factor for nucleation rate near  $T_{\max}$  is  $J_{s0}/J_{v0} = 10^{12}$  for D-arabitol Form II and  $10^9$  for posaconazole Form II, and for the bulk-nucleating polymorph,  $J_{s0}/J_{v0} \approx 10^5$  for D-arabitol Form I and  $10^4$  for posaconazole Form I. For the other two systems, water and acetaminophen, surface nucleation does not select a different polymorph with  $J_{s0}/J_{v0} \approx 10^4$  and  $10^5$ , respectively.

The available data (Figure 9) gives the impression that *if no polymorph switch occurs*, all four systems would show a similar surface enhancement factor of nucleation:  $J_{s0}/J_{v0} \approx 10^5$ . For water and acetaminophen (no polymorph switch), this is simply the factor observed; for D-arabitol and

posaconazole (polymorph switch), it is the factor estimated for the bulk-nucleating polymorph that is unobserved in surface nucleation. This seemingly common factor in the absence of polymorph switch might be a fortuitous result since situations might exist where a bulk-nucleating polymorph receives a strong boost by the surface environment ( $J_{s0}/J_{v0} \gg 10^5$ ) while no other polymorphs exist that can take advantage of the surface environment to nucleate even faster. The study of additional systems may shed light on this point.

A surface-induced polymorph switch is a strong indication of the surface effect on nucleation: a hidden polymorph in bulk nucleation receives such a large enhancement that it goes from disfavored in the bulk to favored on the surface. In the two systems where such polymorph switch is observed, D-arabitol and posaconazole, there is evidence for a major reconstruction of structure in the surface region relative to the bulk and for a greater similarity of the surface structure to the surface-nucleating polymorph than to the bulk-nucleating polymorph. We speculate that this is general condition for a surface-induced polymorph switch, namely, (1) the surface structure is reconstructed relative to the bulk and (2) another polymorph exists that can take advantage of the surface environment to nucleate at a faster rate than the bulk-favored polymorph. Had there been no change of the surface environment relative to the bulk, we would expect the bulk-favored polymorph to nucleate in the surface region. In D-arabitol and posaconazole, the surface-nucleating polymorph has a polar layered structure, with each layer containing molecules in parallel, rather than antiparallel, arrangement. This result is sensible given that a liquid/vapor interface can induce layering<sup>14, 15</sup> and polar order.<sup>16, 40-42</sup> Whether these features characterize surface-nucleating polymorphs in general deserves future studies. By this line of thinking, the lack of polymorph switch in water and acetaminophen could originate from



a smaller degree of surface reconstruction in these systems, the lack of a polymorph that can utilize the surface environment to nucleate, or both.

### 3.5. Conclusions

We have investigated the surface effect on the crystal nucleation in amorphous posaconazole. As in the case of D-arabitol,<sup>22</sup> experiments were performed under conditions that cleanly separate the timescales for surface and bulk nucleation. In posaconazole, crystal nucleation at the surface is vastly faster than in the bulk, by approximately 9 orders of magnitude on the per-molecule basis, and selects a different polymorph (II) from bulk nucleation (I). This phenomenon is attributed to the similarity of the anisotropic molecular packing at the surface to the structure of the surface-nucleating polymorph.

To date, all the cases investigated feature surface enhancement, not suppression, of crystal nucleation. Of these systems, D-arabitol and posaconazole fall in one group with polymorph switch, while water and acetaminophen fall in another group with no polymorph switch. Interestingly, if the surface-nucleating polymorphs are excluded, the four systems investigated to date feature a similar surface enhancement factor of  $J_{s0}/J_{v0} \approx 10^5$ . Relative to this, the surface-selected polymorph has a significantly larger enhancement factor:  $J_{s0}/J_{v0} \approx 10^{12}$  for D-arabitol and 109 for posaconazole. Future work is warranted to understand and predict this wide range of behaviors. For D-arabitol and posaconazole, there is evidence for major structural reconstruction at the surface, which facilitates the nucleation of a new polymorph that is disfavored in the bulk. In both systems, the surface-nucleating polymorph has a layered structure, with each layer

containing molecules in parallel arrangement. For systems like D-arabitol and posaconazole, surface nucleation provides a new avenue for polymorph discovery and control.<sup>23, 52</sup> Crystallization and polymorph selection in such systems are expected to be sensitive to the presence of free surfaces, bubbles,<sup>53</sup> and fractures.<sup>12, 54</sup>

Our discussion has focused on structure in understanding surface nucleation. It is conceivable that the potentially higher mobility of molecules in the surface layer could also facilitate nucleation. Fast surface diffusion in molecular glasses is known to cause fast surface crystal growth<sup>13</sup> but its role in surface nucleation is less well understood. For posaconazole, the similar crystal growth rates in the bulk and at the surface (Figure 7) indicate that surface dynamics is not the main effect in the fast surface nucleation observed. The same conclusion has been reached for D-arabitol<sup>22</sup> and for acetaminophen.<sup>32</sup> Given that the relative rate of surface diffusion to bulk diffusion increases with cooling, surface dynamics could play a larger role at lower temperatures.

### **3.6. Acknowledgements**

We thank AbbVie Inc. and the Wisconsin - Puerto Rico Partnership for Research and Education in Materials (NSF DMR-1827894) for supporting this work. The purchase of the Bruker D8 VENTURE Photon III X-ray diffractometer was partially funded by NSF Award #CHE-1919350 to the UW–Madison Department of Chemistry.

### **3.7. Supporting Information**

**Structural Solution by Single-Crystal X-ray Diffraction**

A yellow crystal with approximate dimensions  $0.1 \times 0.1 \times 0.05 \text{ mm}^3$  was selected under oil under ambient conditions and attached to the tip of a MiTeGen MicroMount<sup>®</sup>. The crystal was mounted in a stream of cold nitrogen at 100(1) K and centered in the X-ray beam by using a video camera. The crystal evaluation and data collection were performed on a Bruker D8 VENTURE PhotonIII four-circle diffractometer with Cu K $\alpha$  ( $\lambda = 1.54178 \text{ \AA}$ ) radiation and the detector to crystal distance of 4.0 cm.

The initial cell constants were obtained from a  $180^\circ \phi$  scan conducted at a  $2\theta = 50^\circ$  angle with the exposure time of 3 second per frame. The reflections were successfully indexed by an automated indexing routine built in the APEX3 program. The final cell constants were calculated from a set of 9468 strong reflections from the actual data collection.

The data were collected using the full sphere data collection routine to survey the reciprocal space to the extent of a full sphere to a resolution of  $0.8 \text{ \AA}$ . A total of 22130 data were harvested by collecting 24 sets of frames with  $0.6^\circ$  scans in  $\omega$  and  $\phi$  with an exposure time 1-15 sec per frame. These highly redundant datasets were corrected for Lorentz and polarization effects. The absorption correction was based on fitting a function to the empirical transmission surface as sampled by multiple equivalent measurements.

The systematic absences in the diffraction data were consistent for the space groups  $P2_1$  and  $P2_1/m$ . The  $E$ -statistics strongly suggested the non-centrosymmetric space group  $P2_1$  that yielded chemically reasonable and computationally stable results of refinement.

A successful solution by the direct methods provided most non-hydrogen atoms from the  $E$ -map. The remaining non-hydrogen atoms were located in an alternating series of least-squares cycles and difference Fourier maps. All non-hydrogen atoms were refined with anisotropic displacement coefficients unless specified otherwise. All hydrogen atoms were included in the structure factor calculation at idealized positions and were allowed to ride on the neighboring atoms with relative isotropic displacement coefficients.

There are three symmetry-independent molecules per unit cell. There is positional disorder in each molecule as described below:

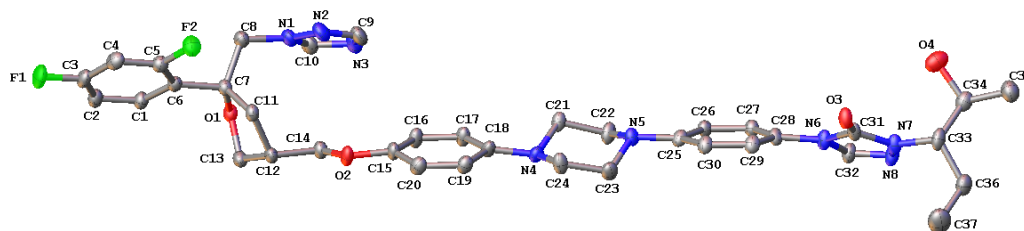
Molecule 1. The four-ring chain between atoms C14 and C33 is disordered over two positions with the major component contribution of 0.539(4), see Figure S1.

Molecule 2: The piperazine ring is disordered over two positions with the minor component contribution of 0.093(3). The four carbon atoms in the minor component were refined isotropically. The major component has occupancy of 0.907(3). One side of the major component (C58, C59) is further disordered over two positions with contributions of 0.469(4) and 0.438(4). There substituent at N15 is also disordered over two positions with the major component contribution of 0.539(4), see Figure S2.

Molecule 3: The substituent at C102 is disordered over two positions with the major component contribution of 0.505(4), see Figure S3. The disordered fragments were refined with restraints and constraints.

The absolute structure was unequivocally established by anomalous dispersion. It is possible there is 8(3) % of the inverted twin component present. The absolute configuration of the chiral centers is *S* for atoms C7, C12, C44, C49, C81, and C86 and *R* for atoms C33, C34, C70, C71(C71a), C107(C7b), and C108(C8b).

The final least-squares refinement of 1755 parameters against 22102 data resulted in residuals *R* (based on  $F^2$  for  $I \geq 2\sigma$ ) and  $wR$  (based on  $F^2$  for all data) of 0.0365 and 0.0912, respectively. The final difference Fourier map was featureless.



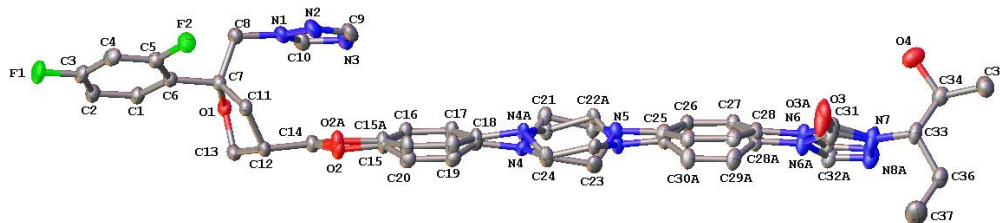


Figure S1. The structure of the first symmetry-independent molecule (“Molecule 1”) in posaconazole Form II shown with 50% probability ellipsoids. Top: All H atoms and minor disorder components are omitted. Bottom: All H atoms are omitted but all minor disorder components are shown.

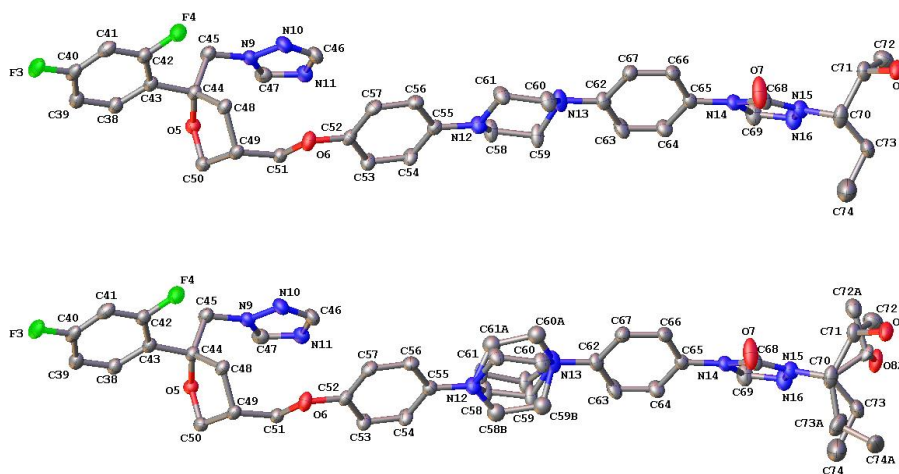
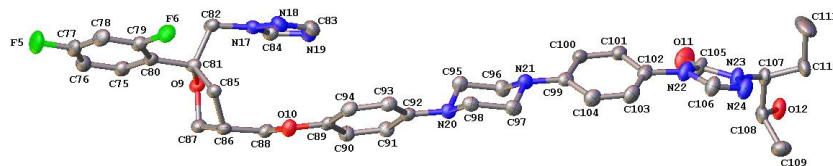


Figure S2. The structure of the second symmetry-independent molecule (“Molecule 2”) in posaconazole Form II shown with 50% probability ellipsoids. Top: All H atoms and minor disorder components are omitted. Bottom: All H atoms are omitted but all minor disorder components are shown.



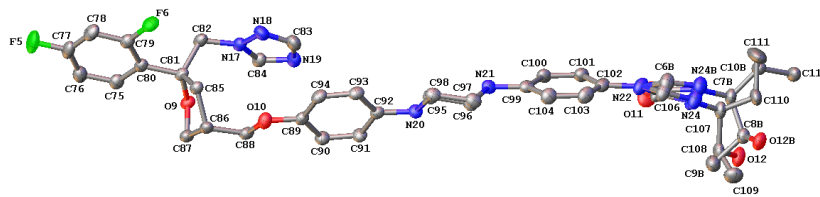


Figure S3. The structure of the third symmetry-independent molecule (“Molecule 3”) in posaconazole Form II shown with 50% probability ellipsoids. Top: All H atoms and minor disorder components are omitted. Bottom: All H atoms are omitted but all minor disorder components are shown.

**Table S1.** Data collection and structure refinement parameters for posaconazole Form II.

Empirical formula	$C_{37}H_{42}F_2N_8O_4$
Formula weight	700.78
Temperature/K	100.0
Crystal system	monoclinic
Space group	$P2_1$
$a/\text{\AA}$	23.433(2)
$b/\text{\AA}$	6.0436(7)
$c/\text{\AA}$	36.550(3)
$\alpha/^\circ$	90
$\beta/^\circ$	92.998(6)
$\gamma/^\circ$	90
Volume/ $\text{\AA}^3$	5169.1(9)
Z	6
$\rho_{\text{calc}}/\text{g/cm}^3$	1.351
$\mu/\text{mm}^{-1}$	0.807
F(000)	2220.0
Crystal size/ $\text{mm}^3$	$0.1 \times 0.1 \times 0.05$
Radiation	$\text{CuK}\alpha$ ( $\lambda = 1.54178$ )
$2\theta$ range for data collection/ $^\circ$	3.776 to 159.87
Index ranges	$-29 \leq h \leq 29, -7 \leq k \leq 7, -46 \leq l \leq 46$
Reflections collected	166361
Independent reflections	22102 [ $R_{\text{int}} = 0.0406, R_{\text{sigma}} = 0.0253$ ]
Data/restraints/parameters	22102/1788/1755
Goodness-of-fit on $F^2$	1.041
Final R indexes [ $I \geq 2\sigma(I)$ ]	$R_1 = 0.0365, wR_2 = 0.0900$
Final R indexes [all data]	$R_1 = 0.0382, wR_2 = 0.0912$
Largest diff. peak/hole / $e \text{\AA}^{-3}$	0.29/-0.41
Flack parameter	0.08(3)

### 3.8. References

1. Herlach, D. M.; Palberg, T.; Klassen, I.; Klein, S.; Kobold, R., Overview: Experimental studies of crystal nucleation: Metals and colloids. *The Journal of chemical physics* **2016**, *145* (21), 211703.
2. Fokin, V. M.; Zanutto, E. D.; Yuritsyn, N. S.; Schmelzer, J. W., Homogeneous crystal nucleation in silicate glasses: A 40 years perspective. *Journal of Non-Crystalline Solids* **2006**, *352* (26-27), 2681-2714.
3. Li, T.; Donadio, D.; Ghiringhelli, L. M.; Galli, G., Surface-induced crystallization in supercooled tetrahedral liquids. *Nature materials* **2009**, *8* (9), 726-730.
4. Chen, J.; Sarma, B.; Evans, J. M.; Myerson, A. S., Pharmaceutical crystallization. *Crystal growth & design* **2011**, *11* (4), 887-895.
5. Sosso, G. C.; Chen, J.; Cox, S. J.; Fitzner, M.; Pedevilla, P.; Zen, A.; Michaelides, A., Crystal nucleation in liquids: Open questions and future challenges in molecular dynamics simulations. *Chemical reviews* **2016**, *116* (12), 7078-7116.
6. Weissbuch, I.; Lahav, M.; Leiserowitz, L., Toward stereochemical control, monitoring, and understanding of crystal nucleation. *Crystal growth & design* **2003**, *3* (2), 125-150.
7. Desiraju, G. R., Crystal engineering: from molecule to crystal. *Journal of the American Chemical Society* **2013**, *135* (27), 9952-9967.
8. Bartels-Rausch, T., Ten things we need to know about ice and snow. *Nature* **2013**, *494* (7435), 27-29.
9. Nam, H.-S.; Hwang, N. M.; Yu, B.; Yoon, J.-K., Formation of an icosahedral structure during the freezing of gold nanoclusters: surface-induced mechanism. *Physical review letters* **2002**, *89* (27), 275502.
10. Mendez-Villuendas, E.; Bowles, R. K., Surface nucleation in the freezing of gold nanoparticles. *Physical Review Letters* **2007**, *98* (18), 185503.
11. Sirota, E., Supercooling, nucleation, rotator phases, and surface crystallization of n-alkane melts. *Langmuir* **1998**, *14* (11), 3133-3136.
12. Descamps, M.; Dudognon, E., Crystallization from the amorphous state: nucleation–growth decoupling, polymorphism interplay, and the role of interfaces. *Journal of pharmaceutical sciences* **2014**, *103* (9), 2615-2628.
13. Huang, C.; Ruan, S.; Cai, T.; Yu, L., Fast surface diffusion and crystallization of amorphous griseofulvin. *The Journal of Physical Chemistry B* **2017**, *121* (40), 9463-9468.
14. Magnussen, O.; Ocko, B.; Regan, M.; Penanen, K.; Pershan, P. S.; Deutsch, M., X-ray reflectivity measurements of surface layering in liquid mercury. *Physical review letters* **1995**, *74* (22), 4444.
15. Regan, M.; Kawamoto, E.; Lee, S.; Pershan, P. S.; Maskil, N.; Deutsch, M.; Magnussen, O.; Ocko, B.; Berman, L., Surface layering in liquid gallium: An X-ray reflectivity study. *Physical review letters* **1995**, *75* (13), 2498.
16. Oh-e, M.; Yokoyama, H.; Baldelli, S., Structure of the glycerol liquid/vapor interface studied by sum-frequency vibrational spectroscopy. *Applied physics letters* **2004**, *84* (24), 4965-4967.
17. Haji-Akbari, A.; Debenedetti, P. G., Thermodynamic and kinetic anisotropies in octane thin films. *The Journal of chemical physics* **2015**, *143* (21), 214501.

18. Bishop, C.; Thelen, J. L.; Gann, E.; Toney, M. F.; Yu, L.; DeLongchamp, D. M.; Ediger, M. D., Vapor deposition of a nonmesogen prepares highly structured organic glasses. *Proceedings of the National Academy of Sciences* **2019**, *116* (43), 21421-21426.
19. Haji-Akbari, A.; Debenedetti, P. G., The effect of substrate on thermodynamic and kinetic anisotropies in atomic thin films. *The Journal of chemical physics* **2014**, *141* (2), 024506.
20. Zhu, L.; Brian, C.; Swallen, S.; Straus, P.; Ediger, M.; Yu, L., Surface self-diffusion of an organic glass. *Physical Review Letters* **2011**, *106* (25), 256103.
21. Yu, J.; Li, Y.; Yao, X.; Que, C.; Huang, L.; Hui, H.-W.; Gong, Y. G.; Yu, L., Surface Enrichment of Surfactants in Amorphous Drugs: An X-Ray Photoelectron Spectroscopy Study. *Molecular pharmaceutics* **2022**, *19* (2), 654-660.
22. Yao, X.; Liu, Q.; Wang, B.; Yu, J.; Aristov, M. M.; Shi, C.; Zhang, G. Z. G.; Yu, L., Anisotropic Molecular Organization at a Liquid/Vapor Interface Promotes Crystal Nucleation with Polymorph Selection. *Journal of the American Chemical Society* **2022**.
23. Bernstein, J., *Polymorphism in Molecular Crystals 2e*. International Union of Crystal: 2020; Vol. 30.
24. Haji-Akbari, A.; Debenedetti, P. G., Perspective: Surface freezing in water: A nexus of experiments and simulations. *The Journal of chemical physics* **2017**, *147* (6), 060901.
25. Turnbull, D., Kinetics of heterogeneous nucleation. *The Journal of Chemical Physics* **1950**, *18* (2), 198-203.
26. Huang, C.; Chen, Z.; Gui, Y.; Shi, C.; Zhang, G. G.; Yu, L., Crystal nucleation rates in glass-forming molecular liquids: D-sorbitol, D-arabitol, D-xylitol, and glycerol. *The Journal of chemical physics* **2018**, *149* (5), 054503.
27. Gui, Y.; Huang, C.; Shi, C.; Zhang, G. G. Z.; Yu, L., Polymorphic Selection in Crystal Nucleation. *The Journal of chemical physics* **2022**, doi: 10.1063/5.0086308.
28. Vrbka, L.; Jungwirth, P., Homogeneous freezing of water starts in the subsurface. *The Journal of Physical Chemistry B* **2006**, *110* (37), 18126-18129.
29. Haji-Akbari, A.; DeFever, R. S.; Sarupria, S.; Debenedetti, P. G., Suppression of sub-surface freezing in free-standing thin films of a coarse-grained model of water. *Physical Chemistry Chemical Physics* **2014**, *16* (47), 25916-25927.
30. Haji-Akbari, A.; Debenedetti, P. G., Computational investigation of surface freezing in a molecular model of water. *Proceedings of the National Academy of Sciences* **2017**, *114* (13), 3316-3321.
31. Kuhn, T.; Earle, M.; Khalizov, A.; Sloan, J., Size dependence of volume and surface nucleation rates for homogeneous freezing of supercooled water droplets. *Atmospheric Chemistry and Physics* **2011**, *11* (6), 2853-2861.
32. Wu, H.; Yao, X.; Gui, Y.; Hao, H.; Yu, L., Surface Enhancement of Crystal Nucleation in Amorphous Acetaminophen. *Crystal Growth & Design* **2022**, *In review*.
33. Din, S. U.; Hughes, H.; O'Reilly, N. J.; Cathcart, H.; O'Ceallaigh, T.; Ndzie, E.; McLoughlin, P., Investigation into the stability, crystallization kinetics, and heating rate dependent crystallization of amorphous posaconazole. *Crystal Growth & Design* **2020**, *20* (8), 5129-5142.
34. Lu, X.; Huang, C.; Li, M.; Skomski, D.; Xu, W.; Yu, L.; Byrn, S. R.; Templeton, A. C.; Su, Y., Molecular mechanism of crystalline-to-amorphous conversion of pharmaceutical solids from 19F magic angle spinning NMR. *The Journal of Physical Chemistry B* **2020**, *124* (25), 5271-5283.



35. Lu, X.; Li, M.; Huang, C.; Lowinger, M. B.; Xu, W.; Yu, L.; Byrn, S. R.; Templeton, A. C.; Su, Y., Atomic-level drug substance and polymer interaction in posaconazole amorphous solid dispersion from solid-state NMR. *Molecular pharmaceutics* **2020**, *17* (7), 2585-2598.
36. Li, Y.; Zhang, W.; Bishop, C.; Huang, C.; Ediger, M.; Yu, L., Surface diffusion in glasses of rod-like molecules posaconazole and itraconazole: Effect of interfacial molecular alignment and bulk penetration. *Soft Matter* **2020**, *16* (21), 5062-5070.
37. Tarnacka, M.; Adrjanowicz, K.; Kaminska, E.; Kaminski, K.; Grzybowska, K.; Kolodziejczyk, K.; Wlodarczyk, P.; Hawelek, L.; Garbacz, G.; Kocot, A., Molecular dynamics of itraconazole at ambient and high pressure. *Physical Chemistry Chemical Physics* **2013**, *15* (47), 20742-20752.
38. Teerakapibal, R.; Huang, C.; Gujral, A.; Ediger, M. D.; Yu, L., Organic glasses with tunable liquid-crystalline order. *Physical review letters* **2018**, *120* (5), 055502.
39. Chen, Z.; Yu, J.; Teerakapibal, R.; Meerpoel, L.; Richert, R.; Yu, L., Organic glasses with tunable liquid-crystalline order through kinetic arrest of end-over-end rotation: the case of saperconazole. *Soft Matter* **2020**, *16* (8), 2025-2030.
40. Hunt Jr, M.; Belu, A.; Linton, R.; DeSimone, J., End-functionalized polymers. 1. Synthesis and characterization of perfluoroalkyl-terminated polymers via chlorosilane derivatives. *Macromolecules* **1993**, *26* (18), 4854-4859.
41. Tanaka, K.; Kawaguchi, D.; Yokoe, Y.; Kajiyama, T.; Takahara, A.; Tasaki, S., Surface segregation of chain ends in  $\alpha$ ,  $\omega$ -fluoroalkyl-terminated polystyrenes films. *Polymer* **2003**, *44* (15), 4171-4177.
42. Even, M. A.; Lee, S.-H.; Wang, J.; Chen, Z., Detection and spectral analysis of trifluoromethyl groups at a surface by sum frequency generation vibrational spectroscopy. *The Journal of Physical Chemistry B* **2006**, *110* (51), 26089-26097.
43. Kunieda, H.; Shinoda, K., Krafft points, critical micelle concentrations, surface tension, and solubilizing power of aqueous solutions of fluorinated surfactants. *The Journal of Physical Chemistry* **1976**, *80* (22), 2468-2470.
44. Ou, X.; Li, X.; Rong, H.; Yu, L.; Lu, M., A general method for cultivating single crystals from melt microdroplets. *Chemical Communications* **2020**, *56* (69), 9950-9953.
45. McQuiston, D. K.; Mucalo, M. R.; Saunders, G. C., The structure of posaconazole and its solvates with methanol, and dioxane and water: Difluorophenyl as a hydrogen bond donor. *Journal of Molecular Structure* **2019**, *1179*, 477-486.
46. Wieser, J.; Pichler, A.; Hotter, A.; Griesser, U.; Langes, C.; Laschober, C., Pharmaceutical compositions containing a crystalline form of posaconazole. Google Patents: 2013.
47. Adrjanowicz, K.; Kaminski, K.; Wlodarczyk, P.; Grzybowska, K.; Tarnacka, M.; Zakowiecki, D.; Garbacz, G.; Paluch, M.; Jurga, S., Molecular dynamics of the supercooled pharmaceutical agent posaconazole studied via differential scanning calorimetry and dielectric and mechanical spectroscopies. *Molecular Pharmaceutics* **2013**, *10* (10), 3934-3945.
48. Yu, L., Inferring thermodynamic stability relationship of polymorphs from melting data. *Journal of pharmaceutical sciences* **1995**, *84* (8), 966-974.
49. Zhang, S.-W.; Harasimowicz, M. T.; de Villiers, M. M.; Yu, L., Cocrystals of nicotinamide and (R)-mandelic acid in many ratios with anomalous formation properties. *Journal of the American Chemical Society* **2013**, *135* (50), 18981-18989.

50. Ediger, M. D.; Harrowell, P.; Yu, L., Crystal growth kinetics exhibit a fragility-dependent decoupling from viscosity. *The Journal of chemical physics* **2008**, *128* (3), 034709.
51. Wu, T.; Yu, L., Origin of enhanced crystal growth kinetics near  $T_g$  probed with indomethacin polymorphs. *The Journal of Physical Chemistry B* **2006**, *110* (32), 15694-15699.
52. Bauer, J.; Spanton, S.; Henry, R.; Quick, J.; Dziki, W.; Porter, W.; Morris, J., Ritonavir: an extraordinary example of conformational polymorphism. *Pharmaceutical research* **2001**, *18* (6), 859-866.
53. Wohlgemuth, K.; Kordylla, A.; Ruether, F.; Schembecker, G., Experimental study of the effect of bubbles on nucleation during batch cooling crystallization. *Chemical Engineering Science* **2009**, *64* (19), 4155-4163.
54. Su, Y.; Yu, L.; Cai, T., Enhanced crystal nucleation in glass-forming liquids by tensile fracture in the glassy state. *Crystal Growth & Design* **2018**, *19* (1), 40-44.

**Chapter 4. Effect of Polymers on Crystallization in Glass-Forming  
Molecular Liquids: Equal Suppression of Nucleation and Growth  
and Master Curve for Prediction**

Xin Yao, Chengbin Huang, Emily G. Benson, Chenyang Shi, Geoff G. Z. Zhang, Lian Yu

As published in:

*Crystal Growth & Design* **2020** 20 (1), 237-244

DOI: 10.1021/acs.cgd.9b01095

#### **4.1. Abstract**

Crystal nucleation plays a critical role in the stability of supercooled liquids and glasses and is often controlled through addition of polymers. A dissolved polymer alters both the thermodynamics and the kinetics of nucleation, but the current understanding of these effects is limited. The rate of crystal nucleation has been measured in two molecular liquids, D-sorbitol and D-arabitol, containing polyvinylpyrrolidone (PVP) at different concentrations (0 – 15 wt %) and molecular weights (224 g/mole for the dimer up to 2 Mg/mole). We observe a significant inhibitory effect of PVP on crystal nucleation. Near the peak temperature for nucleation rate (~ 20 K above the glass transition temperature), 10 wt % PVP can slow down nucleation by approximately one order of magnitude, and the effect increases with polymer concentration exponentially and with molecular weight. Remarkably, the polymer effect on nucleation rate is nearly the same as that on crystal growth rate so that the ratio of the two rates is nearly constant at a given temperature independent of polymer concentration and molecular weight. This “master curve” behavior can be used to predict nucleation rates in multi-component systems from more easily measured growth rates. It argues that nucleation and growth in these viscous liquids are both mobility-limited and that a polymer solute functions mainly as a mobility modifier, suppressing nucleation and growth by a similar degree.

#### **4.2. Introduction**

Glasses are important materials that combine the spatial uniformity of liquids and the mechanical strength of crystals, with applications in numerous technologies. If crystallization is prevented, a liquid under cooling eventually solidifies to a glass. A glass inherits the spatial uniformity of its precursor liquid, useful as windows and optics. A glass can more easily incorporate multiple

chemical components than a crystal, providing compositional flexibility in materials design. A glass can be shaped, extruded, and drawn into fibers in the molten state. Pharmaceutical scientists take advantage of the higher solubility of glasses over crystals to deliver poorly soluble drugs.

Crystallization plays an important role in glass science. The very existence of glasses requires avoidance of crystallization, and crystallization during storage can compromise the performance of amorphous materials. On the other hand, controlled crystallization can be exploited to produce glass ceramics – materials with crystallized domains embedded in a glassy matrix, offering useful properties such as ultra-low thermal expansion.

Crystallization consists of nucleation and growth, and each step has its own unique kinetics. At present, the growth process in glass-forming liquids is better understood than the nucleation process. Crystal growth rates have been measured in many systems, enabling mining of systematic trends for prediction;<sup>1,2</sup> new mechanisms of crystal growth have been identified that are active in the glassy state, but absent in the fluid state.<sup>3,4</sup> In contrast, the literature is scant on quantitative nucleation rates,<sup>5-9</sup> especially for organic glasses, preventing a systematic analysis. It is difficult at present to make an order-of-magnitude prediction of nucleation rates on theoretical or empirical grounds, while such predictions are becoming realistic for crystal growth.<sup>1,2</sup>

Amorphous materials are often fabricated to contain multiple components in a single phase, and for these systems, a central question is how the additional components influence the crystallization process. Amorphous pharmaceuticals are usually formulated with polymers to

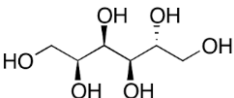
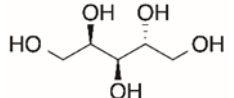
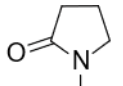
improve stability and dissolution,<sup>10-12</sup> prompting extensive research on the polymer effect on drug crystallization.<sup>13-17</sup> Here, again, the polymer effect is better understood on crystal growth than on nucleation. It has been shown that even at a low concentration of 1 wt %, a polymer can strongly influence the rate of crystal growth, from a 10-fold increase to a 10-fold decrease, depending on the polymer's segmental mobility relative to the host molecules.<sup>18-20</sup> In contrast to this detailed understanding, a comparable progress is yet to be made on crystal nucleation.

The goal of this work is to study the effect of a polymer solute on crystal nucleation in glass-forming molecular liquids. The rate of nucleation has been measured in D-sorbitol and D-arabitol containing polyvinylpyrrolidone (PVP). At present, these two polyalcohols are the only molecular glass-formers for which quantitative nucleation rates are reported.<sup>9</sup> PVP is a commonly used pharmaceutical polymer that is melt-miscible with the two host materials. We observe a significant inhibitory effect of PVP on crystal nucleation. Near the peak temperature for nucleation rate ( $\sim 20$  K above the glass transition temperature  $T_g$ ), 10 wt % PVP can slow crystal nucleation by approximately one order of magnitude, and the effect increases with polymer concentration and molecular weight. Interestingly, the polymer has very similar effects on the nucleation rate and the growth rate so that the ratio of the two rates is nearly constant at a given temperature, independent of polymer concentration and molecular weight. This argues that in these viscous liquids, crystal nucleation and growth are both mobility-limited and the polymer solute acts mainly as a mobility modifier, suppressing nucleation and growth to a similar extent. Our finding is relevant for the selection of polymers for amorphous formulations and the prediction of their performance.

### 4.3. Materials and Methods

**Materials.** D-sorbitol and D-arabitol (both  $\geq 99\%$  pure) were purchased from Sigma-Aldrich. The dimer of vinyl pyrrolidone (“VP dimer”) was obtained from AbbVie Inc. Polyvinylpyrrolidone (PVP) of different molecular weights was purchased from commercial sources: PVP K12 (Kollidon 12PF) and PVP K30 (Kollidon 30) from BASF; PVP K15 from ISP Technologies; PVP K90 from GAF Chemicals. All the materials were used as received. Table 1 shows the molecular structures of the materials and some of their physical properties.

**Table 1.** Molecular structures and properties of the materials used.

	Molecular structure	$M_w$ (g/mol)	$T_g$ (K)
D-sorbitol		182.2	269
D-arabitol		152.1	260
VP dimer		224	217
PVP K12		2000-3000	375
PVP K15		8000	393
PVP K30	$\text{-(CH}_2\text{-CH)}_n\text{-}$	44-54 K	437
PVP K90		1-2 M	449

**Sample Preparation.** PVP was dissolved in a host material by cryomilling (SPEX CertiPrep 6750 with liquid nitrogen as coolant) followed by melting. One gram of D-sorbitol or D-arabitol containing 10 or 15 wt % PVP was cryomilled, and the resulting mixture was diluted by further cryomilling as needed. Cryomilling was performed at 10 Hz for five 2-min cycles, each followed by a 2-min cool down. Before measuring its crystallization, a sample was held in the molten state

(12 h at 413 K for D-sorbitol/PVP, 6 h at 403 K for D-arabitol/PVP) to remove air bubbles. A coverslip was then placed over the melt to produce a sandwiched liquid film ~ 40  $\mu\text{m}$  thick. The film thickness was confirmed not to affect the observed rate of nucleation (see below).

**Nucleation Rate.** To measure nucleation rates, each film sample was stored in a desiccator at a chosen temperature maintained within  $\pm 1$  K by different devices: 288 and 278 K using commercial refrigerators, 273 K using the coolant chamber of a circulating cooler, 295 K using an air-conditioned room, and higher temperatures using custom-built mini-ovens. Crystals were observed and counted through a polarized light microscope (Olympus BX53) equipped with a digital camera. The calculation of nucleation rate is described in the Results section.

**Crystal Growth Rate.** Crystal growth rate was measured by tracking the advance of a growth front over time; each reported rate was the average of 9-12 measurements in three separate samples. The measurement time intervals were chosen so that the total advance distance of the growth front was at least 30  $\mu\text{m}$  and there were at least equally spaced time points to evaluate the constancy of growth rates (see Figure S3 for an example). Crystal growth rates were found to be constant over time.

**Differential Scanning Calorimetry (DSC).** DSC was performed with a TA Q2000 differential scanning calorimeter under 50 ml/min  $\text{N}_2$  purge. Each sample was 5-10 mg placed in a crimped aluminum pan. The glass transition temperature  $T_g$  was measured during heating at 10 K/min after cooling at 10 K/min and the onset temperature is reported. Melting-point depression by PVP was evaluated by heating at 1 K/min and monitoring the change of the melting endpoint.



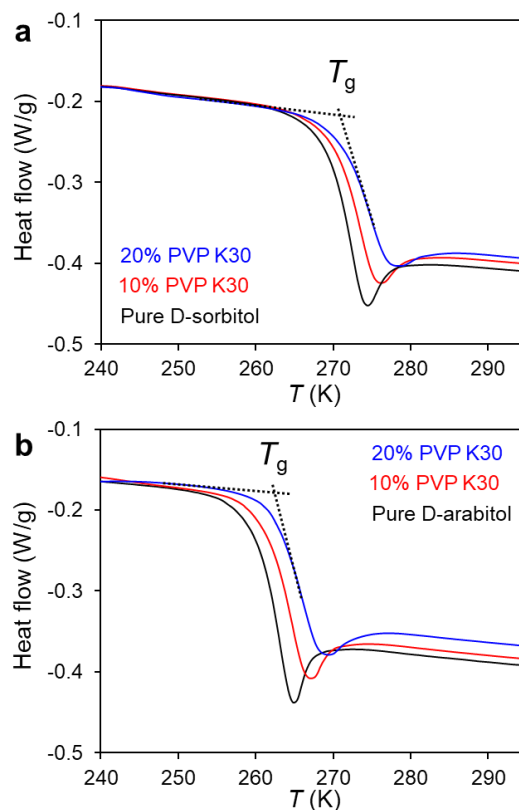


**Figure 1.** DSC heating traces of the glass transition in (a) D-sorbitol/PVP K30 and (b) D-arabitol/PVP K30. Each glass was prepared by cooling at 10 K/min and the subsequent heating scan at 10 K/min is shown. The increase of  $T_g$  with PVP concentration indicates miscibility of components.

#### 4.4. Results

**Polymer-Host Miscibility.** To interpret a polymer's effect on crystallization, it is necessary to determine whether the polymer is dissolved in or phase separated from the host material. For this purpose, the glass transition temperature  $T_g$  was measured as a function of polymer concentration. Given the higher  $T_g$  of PVP than the host material (Table 1), miscibility implies an increase of  $T_g$  with PVP concentration. This is indeed the case, as illustrated in Figure 1 for PVP K30. In this test, the range of polymer concentration was 0–20 wt %, encompassing the 0–15 wt

% range for the crystallization studies and ensuring miscibility in all our experiments. In addition, the  $T_g$  of a polymer-doped material is unchanged during prolonged annealing at nucleation temperatures (see Figure S2 for an example), indicating no phase separation. The miscibility of PVP with the two polyalcohols of this study is consistent with its miscibility with D-mannitol, a stereoisomer of D-sorbitol.<sup>21</sup>

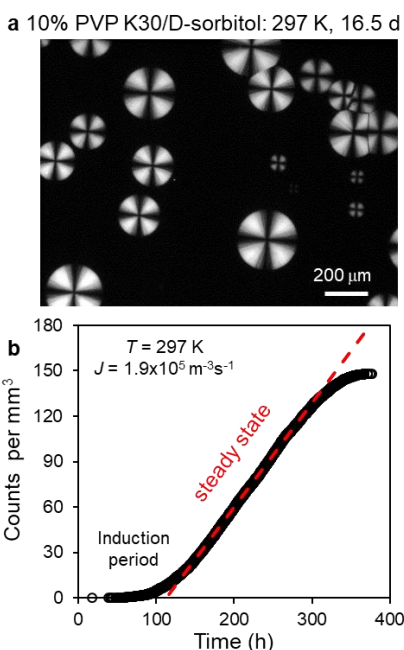


**Figure 2.** One-stage method for measuring crystal nucleation rate in D-sorbitol/PVP. (a) A sample of D-sorbitol containing 10 wt % PVP K30 after 16.5 days at 297 K. A range of crystal size is seen, from which the birth time of each crystal can be calculated (eq. 1). (b) Density of crystal nuclei vs. time. The slope of this plot at the steady state is the nucleation

**D-sorbitol/PVP.** Figure 2 shows the typical data collected for measuring the rate of nucleation in D-sorbitol/PVP using the “one-stage” method.<sup>9</sup> In this method, a supercooled liquid is allowed to crystallize for some time  $t_0$  at which individual crystals are observable (Figure 2a). The birth time  $t$  of each crystal is calculated from its current size (radius  $r$ ) and its growth rate ( $u$ ):

$$t = t_0 - r/u \quad (1)$$

From the birth time of each crystal, the number of nucleation events per unit volume can be obtained as a function of time (Figure 2b). Following an induction period, a steady state is reached where nuclei appear at a constant rate. The steady-state nucleation rate  $J$  is the slope indicated in Figure 2b. After the steady-state period, nucleation rate is seen to decrease, which is caused by the reduction of liquid volume available for nucleation.

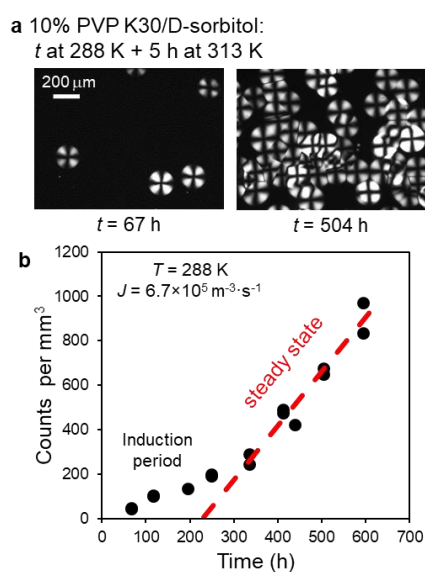


**Figure 3.** Two-stage method for measuring crystal nucleation rates in D-sorbitol/PVP. (a) Crystals observed after D-sorbitol containing 10 wt % PVP K30 spent 67 or 504 h at 288 K followed by 5 h at 313 K. More crystals are observed after longer time at 288 K. (b) Crystal density vs. nucleation time at 288 K. The slope of this plot at the steady state is the nucleation rate  $J$ .

The one-stage method above is useful when crystal growth is relatively fast but not otherwise. In the latter case, a “two-stage” method<sup>22</sup> was used, and Figure 3 shows the typical result for D-sorbitol/PVP. In this method, a supercooled liquid is nucleated at a low temperature without visible growth and then heated to a high temperature to allow growth of the nuclei to visible size

to be counted. The growth temperature is so chosen that nuclei formed at the low temperature can grow quickly but no new nuclei appear during the time of growth. In the example shown, D-sorbitol containing 10 wt % PVP K30 spent different times at 288 K but the same time (5 h) at 313 K. The sample that spent longer time at 288 K nucleated more crystals than the sample that spent shorter time. Note that after development, both samples contained crystals of similar size, indicating the crystals were indeed nucleated at the low temperature without significant growth. This latter conclusion has further support from the fact that no crystals were observed at 313 K up to 10 h if the sample was not previously stored at 288 K. Figure 3b shows the density of nuclei developed at 288 K as a function of nucleation time. As in Figure 2b, an induction period is seen in Figure 3b, followed by a steady state of nuclei production; the nucleation rate  $J$  corresponds to the slope of the plot in the steady state.

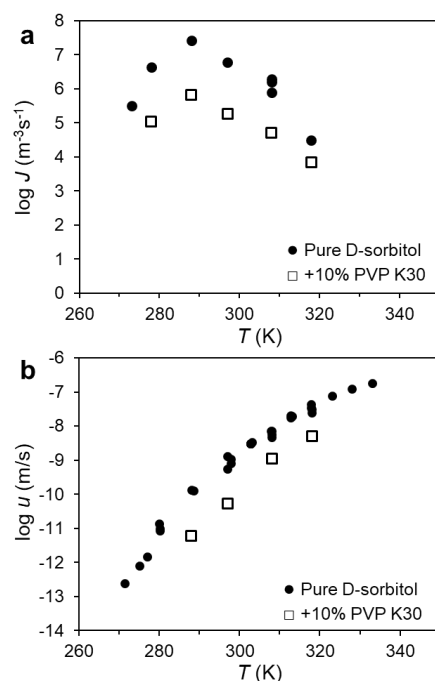


**Figure 4.** Effect of 10 wt % PVP K30 on the rate of nucleation (a) and growth (b) in D-sorbitol.

Figure 4a compares the rates of nucleation  $J$  in pure D-sorbitol<sup>9</sup> and D-sorbitol containing 10 wt % PVP. For clarity, the results are shown only for PVP K30; the results on other PVP molecular weights are collected in Table 2. In the pure liquid,  $J$  reaches a maximum near 290 K ( $T_{\max}$ ), and all our measurement of the polymer effect was near that temperature. At all the temperatures investigated, PVP decreases the nucleation rate, by an average factor of 30 for the sample shown. It is worth noting that the effect of PVP on crystal nucleation (Figure 4a) is similar to that on crystal growth (Figure 4b), despite the different temperature dependence of the two processes.

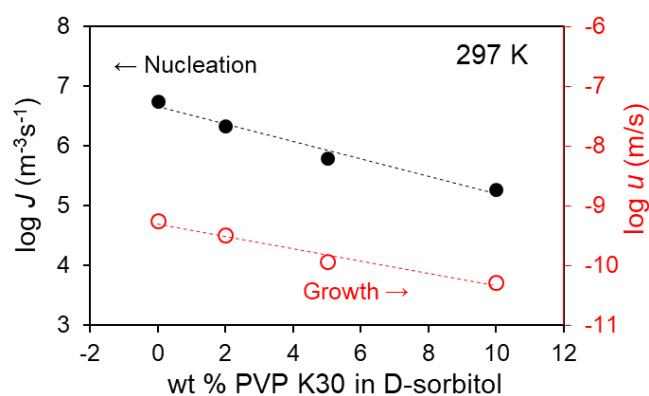


**Figure 5.** Effect of PVP K30 concentration on the rates of crystal nucleation  $J$  and growth  $u$  in D-sorbitol at 297 K.

Figure 5 shows the effects of PVP concentration on the nucleation rate  $J$  and the growth rate  $u$  in D-sorbitol at 297 K. For this comparison, the PVP molecular weight grade was fixed at K30. As the polymer concentration increases, both  $J$  and  $u$  decrease and do so at similar rates. To a good approximation, both nucleation and growth rates decrease *exponentially* with the polymer concentration; that is, the log (rate) vs concentration plot is approximately linear.

In addition to PVP K30, other PVP molecular-weight grades were studied to assess the effect of polymer molecular weight on crystallization in D-sorbitol. These results are found in Table 2.

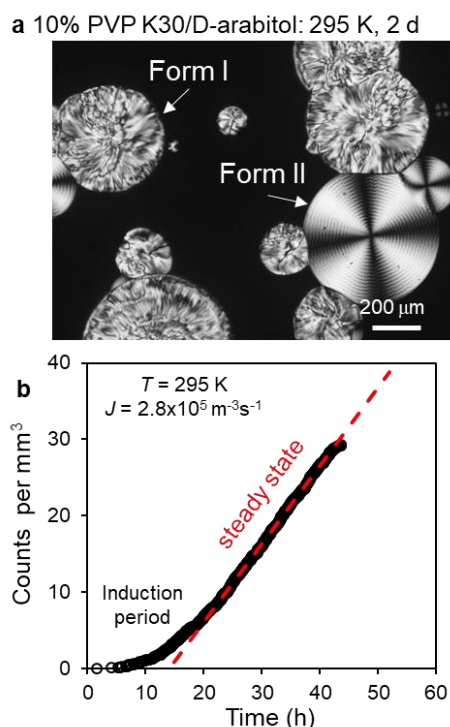
Altogether, the PVP molecular weights cover the range 224 g/mole (VP dimer) to 2 Mg/mole (K90). For each PVP grade tested, we observe qualitatively similar effect as described for PVP K30 (Figures 4 and 5), but the magnitude of the effect increases with increasing molecular weight. This is seen by comparing the entries in Table 2 for different PVP molecular weights at the same concentration (10 wt %) and temperature. In general, the higher the molecular weight, the stronger the polymer's inhibitory effect on nucleation and growth. Furthermore, as we discuss below, the quantitative effect of the polymer molecular weight on the nucleation rate is similar to that on the growth rate. These results argue that the polymer effect on crystallization rate is mainly kinetic – through its modification of molecular mobility. We shall return to this point in the Discussion section.

Table 2. Effects of PVP on the rates of nucleation and growth in D-sorbitol.<sup>a</sup>

Polymer (concentration)	$T$ (K)	$\log u$ (m/s)	$\log J$ ( $\text{m}^{-3}\text{s}^{-1}$ )	$\log J/u$ ( $\text{m}^{-4}$ )
None (pure D-sorbitol) <sup>b</sup>	273	-12.3	5.5	17.8
	278	-11.4	6.6	18.1
	288	-10.0	7.4	17.4
	297	-9.0	6.8	15.8
	308	-8.1	6.1	14.3
	318	-7.5	4.5	12.0
VP dimer (10 wt %)	297	-9.3	6.5	15.8
	308	-8.3	6.1	14.4
	318	-7.7	4.6	12.3
PVP K12 (10 wt %)	297	-9.7	5.9	15.5

	308	-8.7	5.2	14.0
	318	-8.1	4.2	12.3
	297	-9.9	5.6	15.5
PVP K15 (10 wt %)	308	-8.9	5.1	14.0
	318	-8.2	4.0	12.3
PVP K30 (2 wt %)	297	-9.5	6.3	15.8
PVP K30 (5 wt %)	297	-9.9	5.8	15.7
	278	-12.6 <sup>c</sup>	5.0	17.7
	288	-11.2	5.8	17.0
PVP K30 (10 wt %)	297	-10.3	5.3	15.5
	308	-9.0	4.7	13.7
	318	-8.3	3.8	12.1
	297	-10.6	4.9	15.5
PVP K90 (10 wt %)	308	-9.2	4.5	13.7
	318	-8.4	3.6	12.0

Notes: <sup>a</sup>The error is  $\pm 0.2$  for each reported value of  $\log u$  or  $\log J$ . <sup>b</sup>The  $\log u$  values for pure D-sorbitol are obtained from a polynomial fit ( $n = 3$ ) of the data in Figure 4b. <sup>c</sup>Obtained by extrapolation of the data in Figure 4b to lower temperature.



**Figure 6.** One-stage method for measuring crystal nucleation rates in D-arabitol/PVP K30. (a) A sample of D-arabitol containing 10 wt % PVP K30 after 2 d at 295 K. Two polymorphs can be observed (I and II). A range of crystal size is seen, from which the birth time of each crystal can be calculated (eq. 1). (b) Density of crystal nuclei vs. time. The slope of this plot in the steady state is the nucleation rate  $J$ .

**D-arabitol/PVP.** The same methods described above were applied to measure crystal nucleation rates in D-arabitol/PVP, with the exception that only one molecular-weight grade (K30) was used. Figures 6 and 7 show the typical data on this system; Table 3 collects the numerical results. As reported previously for pure D-arabitol,<sup>9</sup> two different polymorphs (I and II) can crystallize simultaneously, and this is also seen in the presence of PVP. The two polymorphs are distinguishable by their melting points (375 K for Form I, 355 K for Form II), by Raman spectroscopy, and by X-ray diffraction.<sup>9</sup> In this work, we focus on the faster-nucleating Form I and the effect of PVP on its nucleation.



Figure 6 illustrates how the one-stage method was used to measure the rate of nucleation in D-arabitol/PVP. As explained above, from the different sizes of the crystals (Figure 6a), their birth times are calculated using eq. 1 and this yields a plot of nuclei density vs. time (Figure 6b). The slope of this plot at the steady state is the rate of nucleation  $J$ .

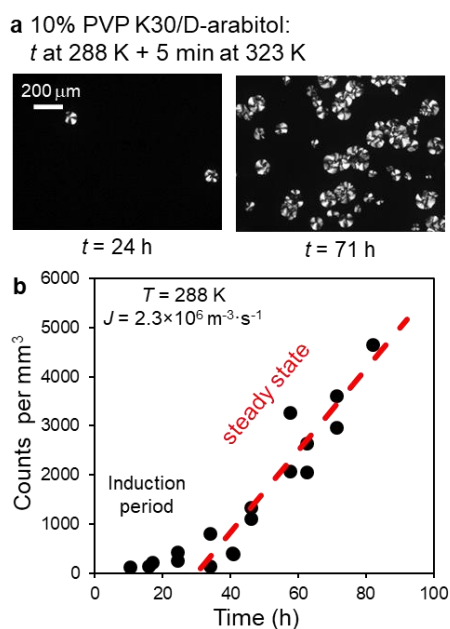


**Figure 7.** Two-stage method for measuring nucleation rates in D-arabitol/PVP K30. (a) Crystals observed after a sample spent 24 or 71 h at 288 K followed by 5 h at 323 K. (b) Crystal density vs. nucleation time at 288 K. The slope of this plot at the steady state is the nucleation rate  $J$ .

Figure 7 shows the typical data collected using the two-stage method for D-arabitol/PVP. This sample was nucleated at 288 K for different length of time and the nuclei were allowed to grow at 323 K. A longer time at 288 K yielded more crystals observed at the growth temperature (Figure 7a), and from the increase of crystal density with nucleation time, we obtain the steady-state nucleation rate  $J$  (Figure 7b).

Table 3. Effects of PVP on the rates of nucleation and growth in D-arabitol.<sup>a</sup>

Polymer (concentration)	$T$ (K)	$\log u$ (m/s)	$\log J$ ( $\text{m}^{-3}\text{s}^{-1}$ )	$\log J/u$ ( $\text{m}^{-4}$ )
None (Pure D-arabitol) <sup>b</sup>	263	-13.0	5.1	18.0
	266	-12.2	6.0	18.2
	273	-10.8	7.0	17.8
	278	-9.9	7.6	17.5
	288	-8.7	8.0	16.7
	295	-8.1	7.0	15.2
PVP K30 (5 wt %)	288	-9.3	7.6	16.8
PVP K30 (10 wt %)	266	-12.8 <sup>c</sup>	5.2	18.0
	273	-11.5	6.2	17.7
	278	-10.9	7.1	18.0
	288	-9.5	7.4	16.9
	295	-8.8	5.5	14.3
PVP K30 (15 wt %)	288	-9.8	6.8	16.6

Notes: <sup>a</sup>The error is  $\pm 0.2$  for each reported value of  $\log u$  or  $\log J$ . <sup>b</sup>The  $\log u$  values for pure D-arabitol are obtained from a polynomial fit ( $n = 3$ ) of the data in Figure 8b. <sup>c</sup>Obtained by extrapolation of the data in Figure 8b to lower temperature.

Figure 8a compares the rates of nucleation in pure D-arabitol<sup>9</sup> and D-arabitol containing 10 wt % PVP K30. In the temperature range investigated (near the temperature of the fastest nucleation in the pure liquid), PVP decreases the nucleation rate by approximately 10 times. A similar effect is seen on the rate of crystal growth in D-arabitol (Figure 8b), which is also reduced by the polymer by approximately a factor of 10 in the same temperature range. Thus, in both host materials, D-

sorbitol and D-arabitol, the polymer has similar effects on the rates of nucleation and growth, reducing both by a similar factor.

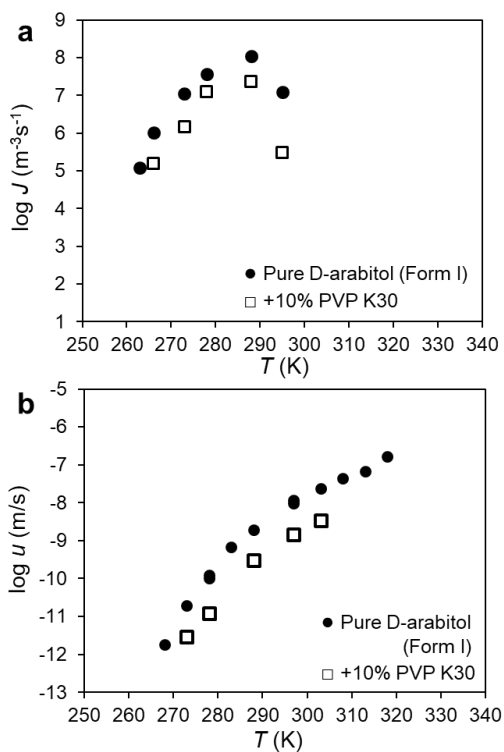


**Figure 8.** Effect of 10 wt % PVP K30 on the rate of nucleation (a) and growth (b) in D-arabitol.

Figure 9 compares the effects of PVP concentration on the nucleation rate  $J$  and the growth rate  $u$  in D-arabitol at 297 K. Both rates decrease with increasing polymer concentration and the effects

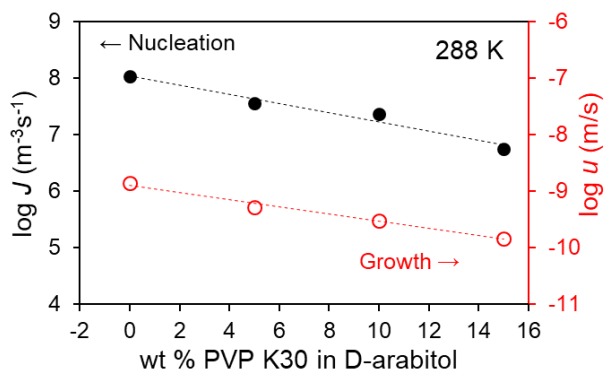


**Figure 9.** Effect of PVP concentration on the rates of crystal nucleation  $J$  and growth  $u$  in D-arabitol.

are approximately exponential [ $\log(\text{rate})$  is approximately linear on polymer concentration]. As in the case of D-sorbitol (Figure 5), we observe a similar dependence of the nucleation rate and the growth rate in D-arabitol on PVP concentration.

**Homogeneous Nucleation.** For any nucleation process, a fundamental question is whether the process is homogeneous or heterogeneous. Homogeneous nucleation is stochastic, occurring in the volume of the material, whereas heterogeneous nucleation occurs at active sites catalyzed by foreign particles and interfaces. In this work, the nucleation process observed exhibits a steady state (Figures 2, 3, 6, and 7) and this is suggestive of homogeneous nucleation, for a heterogeneous process is expected to rapidly reach a saturation crystal density corresponding to the available active sites. To further evaluate the nature of the nucleation process, the thickness of the liquid films was varied and the effect on the nucleation rate was evaluated. For a homogeneous process, the number of nuclei per unit volume should be independent of the film thickness, whereas for a heterogeneous process facilitated by the substrate, the apparent number of nuclei per unit volume should decrease with increasing film thickness. By this test, previous work reached the conclusion that nucleation in pure D-sorbitol and D-arabitol is homogeneous.<sup>9</sup> In this work, the test was repeated for polymer-doped materials and reached the same conclusion. For example, D-arabitol with 10 wt % PVP K30 was prepared at two thicknesses (10 and 140  $\mu\text{m}$ ). After crystallizing under the same condition (23 h at 288 K followed by 5 min at 323 K), the thicker sample showed 150 crystals per  $\text{mm}^3$  and the thinner sample 160 per  $\text{mm}^3$ . This shows that the observed nucleation process is a true volume process, unaffected by the presence of interfaces, as expected for homogeneous nucleation.

#### 4.5. Discussion

This study has examined the effect of a polymer solute on crystal nucleation and growth in two glass-forming molecular liquids: D-sorbitol and D-arabitol. The PVP solute strongly inhibits nucleation and growth in the two systems and under the conditions of this study, the effects are quite similar on the two processes. This similarity might come as a surprise given the different kinetics of nucleation and growth. Here we discuss this result and argue that it arises from the similar kinetic barriers of the two processes.

According to classical theories,<sup>8,23-26</sup> the rates of nucleation and growth in a pure liquid can be written as a product of thermodynamic and kinetic factors:

$$J = k_J F_J \quad (2)$$

$$u = k_u F_u \quad (3)$$

In these equations,  $k$  is a kinetic factor specifying the frequency at which attempts are made to grow a small nucleus ( $k_J$ ) or a macroscopic crystal ( $k_u$ ), and  $F$  is a thermodynamic factor appropriate for nucleation ( $F_J$ ) or growth ( $F_u$ ). For pure D-sorbitol and D-arabitol, previous work has shown that  $k_J$  and  $k_u$  have a similar temperature dependence<sup>5</sup> so that  $k_J/k_u$  is approximately constant. Under this assumption, the nucleation rates in the two liquids are well described by the Classical Nucleation Theory (CNT) using reasonable nucleus/liquid interfacial energies.

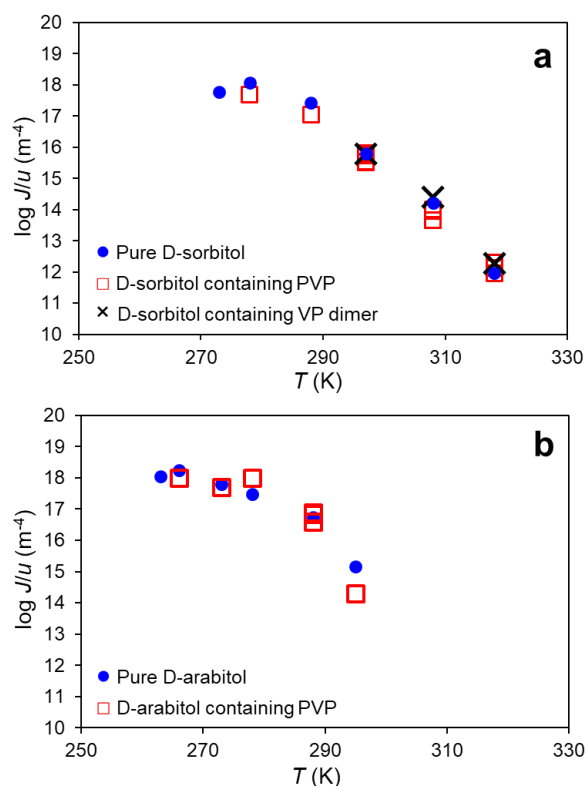


**Figure 10.** The logarithm of the ratio  $J/u$  as a function of temperature for (a) D-sorbitol and (b) D-arabitol. Data are plotted for the pure liquids and the PVP-doped liquids. The open squares correspond to doped systems (see Tables 2 and 3) without distinguishing the polymer's molecular weights and concentrations. For D-sorbitol, the PVP used had different molecular weights (VP dimer, K12, K15, K30, and K90; see Table 1) and concentrations (0 – 10 wt %). For D-arabitol, the PVP used was PVP K30 and its concentration was 0-15 wt % . The collapse of data points indicates that under the conditions studied, the polymer has similar effects on nucleation and growth.

The presence of a polymer solute alters both the kinetic factors and the thermodynamic factors for nucleation and growth. To evaluate these effects, we plot the ratio  $J/u$  as a function of temperature for the systems studied (Figure 10). Assuming nucleation and growth share a similar kinetic barrier, this plot is expected to show a plateau at low temperatures at which both processes are limited by kinetics, as well as a decrease at high temperatures resulting from the

larger thermodynamic barrier for nucleation than for growth. This pattern is indeed observed. Furthermore, the data points for the pure liquids (solid circles) coincide with those for PVP-doped liquids (open squares) within experimental error. This is a remarkable collapse of data points given the wide-ranging effects observed at different temperatures, different polymer concentrations, and in the case of D-sorbitol, different polymer molecular weights. Even the data on the VP dimer as dopant (crosses in Figure 10a) fall on the master curve for D-sorbitol.

We interpret the “master curve” behavior on the basis of eqs. (2) and (3). According to these equations, the ratio  $J/u$  is given by

$$J/u = (k_J/k_u) (F_J/F_u) \quad (4)$$

Given the low polymer concentrations used (0 – 10 wt % in D-sorbitol and 0-15 wt % in D-arabitol), we expect a relatively small effect on the thermodynamic factors  $F_J$  and  $F_u$  and hence their ratio. This is supported by the small melting-point depression by the polymer (~1 K at 10 wt % PVP K30, see Figure S1 for the result on D-arabitol) relative to the much larger supercooling for our crystallization experiments (50 K on average for D-sorbitol; 90 K on average for D-arabitol). On the other hand, we expect a large decrease of the kinetic factors  $k_J$  and  $k_u$  by the polymer as a result of reduced molecular mobility. This is evident from the increase of the  $T_g$  of the host material by the polymer (Figure 1), and expected from the fact that low-concentration polymers can greatly increase viscosity<sup>27</sup> and reduce mobility.<sup>19</sup> Huang et al. showed that even at 1 wt %, a polymer can reduce crystal growth rate by a factor of 10, with the effect correlating with the polymer’s segmental mobility.<sup>20</sup> Building on these observations, we explain the master curve behavior in Figure 10 as follows: Nucleation and growth share a similar kinetic barrier and involve similar molecular motions.<sup>9</sup> A polymer solute hinders these motions,

slowing down both processes by a similar degree. As a result, the ratio  $J/u$  remains largely unchanged leading to the master curves.

In the development of amorphous formulations, the master curves in Figure 10 can be used to predict nucleation rates in a multi-component system. If the rates of nucleation and growth,  $J_0$  and  $u_0$ , are known in a pure liquid at temperature  $T$ , the master curve behavior implies that the nucleation rate in a multi-component system at the same temperature is given by

$$J = (J_0/u_0) u \quad (5)$$

where  $u$  is the rate of crystal growth in the multi-component system at  $T$ . Since it is more time-consuming to measure nucleation rates than growth rates, this method provides a quick evaluation of the nucleation rate. Figure 11 presents a test of this method using data from the present study (Tables 2 and 3). Here the predicted  $J$  values using eq. (5) are plotted against the observed values and the diagonal line indicates perfect prediction. We note that all the points in Figure 11 cluster around the diagonal line. Together the observed nucleation rates cover 4 orders

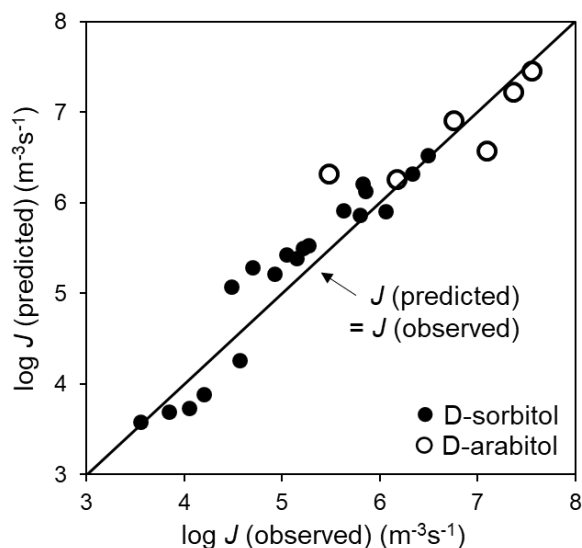


**Figure 11.** Predicted vs. observed nucleation rates in PVP-doped D-sorbitol and D-arabitol.



of magnitude, and the prediction can reproduce these rates without systematic error and with an average absolute error of 0.27 on the log scale, which is comparable to the experimental error.

#### 4.6. Conclusions

We have measured the rates of crystal nucleation and growth in two glass-forming molecular liquids (D-sorbitol and in D-arabitol) in the presence of a dissolved polymer (PVP). At a relatively low concentration ( $\leq 15$  wt %), PVP can significantly slow down both nucleation and growth, with its effect increasing with concentration and molecular weight. Interestingly, the PVP effect on nucleation rate is quite similar to that on growth rate, so that their ratio is nearly a constant independent of polymer concentration and molecular weight. This supports the view that in these viscous liquids, nucleation and growth are both mobility-limited, and a dissolved polymer mainly functions as a mobility modifier, slowing the two processes by a similar factor. This result is relevant for the selection of polymers for stabilizing amorphous formulations and for the prediction of their performance. For example, our result indicates that the nucleation rate in a multi-component system can be predicted from the rate of crystal growth and the crystallization kinetics of the pure system (Figure 11). This would avoid the laborious measurements of nucleation rates. The knowledge of both nucleation and growth rates will enable prediction of the overall rate of crystallization and the shelf life of multi-component amorphous formulations. Further progress in this area will benefit from a broader test of the master curve behavior (Figure 10), including systems in which the second component is a high-mobility small molecule (e.g., surfactants commonly introduced in amorphous pharmaceutical formulations) and increases the rate of crystallization.

#### 4.8. Supporting Information

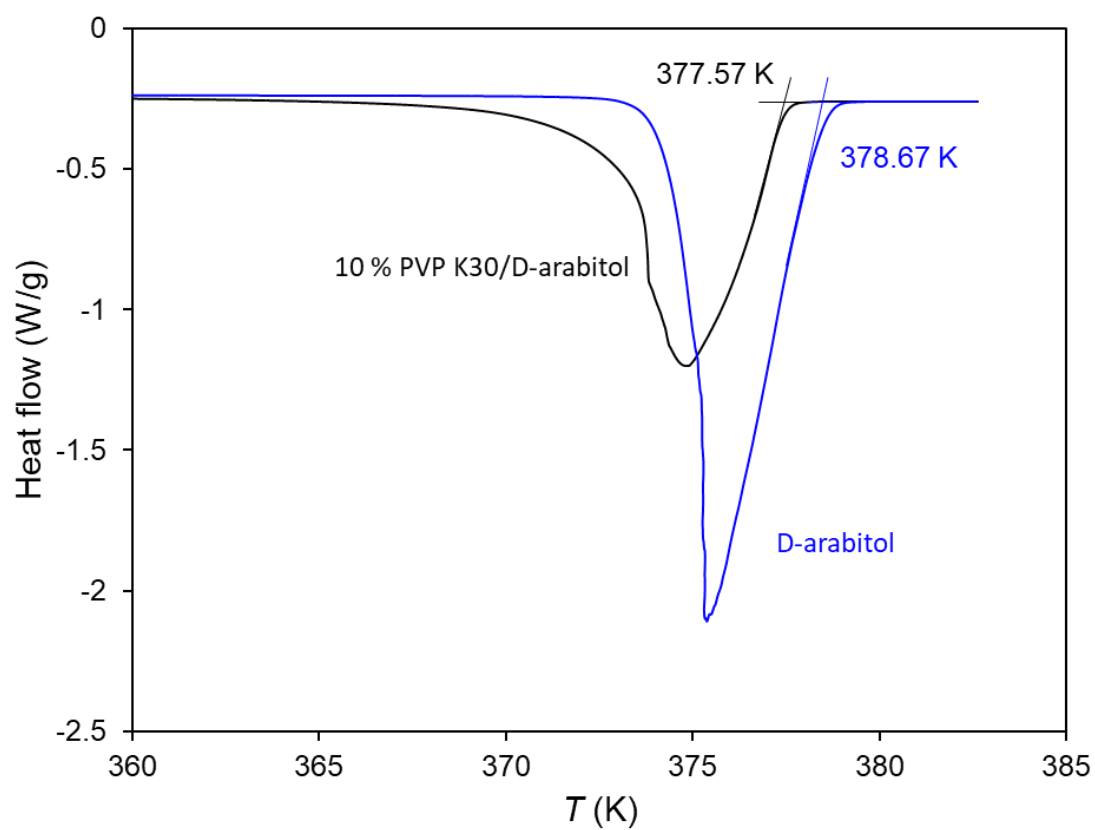


**Figure S1.** Effect of 10 wt % PVP K30 on the melting point of D-arabitol Form I. Each DSC trace was recorded at a heating rate of 1 K/min in the temperature range shown. The endpoint of melting is depressed by approximately 1 K by 10 wt % PVP K30.

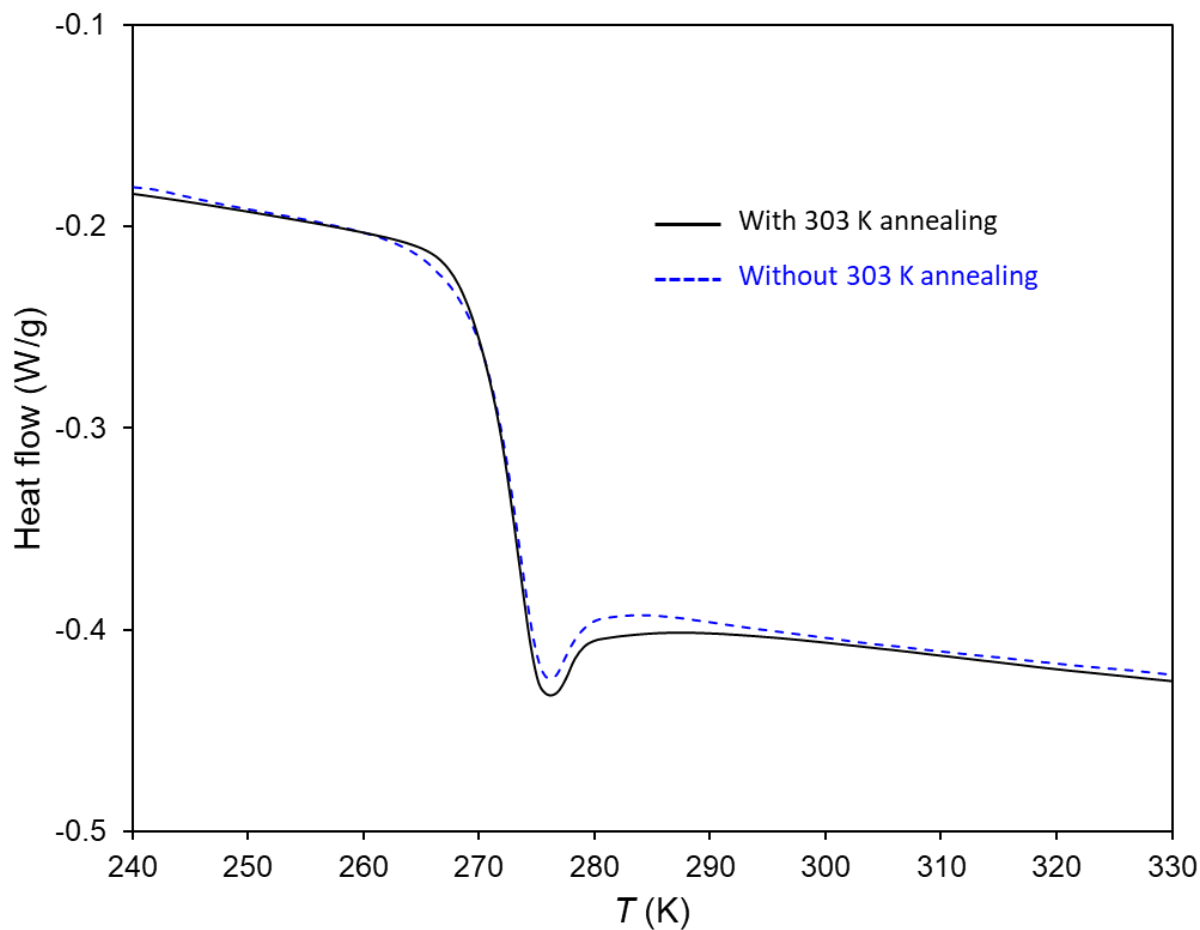


**Figure S2.** Effect of annealing on the glass transition temperature  $T_g$  of D-sorbitol containing 10 wt % PVP K30. Both DSC traces were recorded during heating at 10 K/min, one for the freshly prepared material and the other after annealing at 303 K for 120 min. There is no significant change of  $T_g$  as a result of annealing, indicating no phase separation.

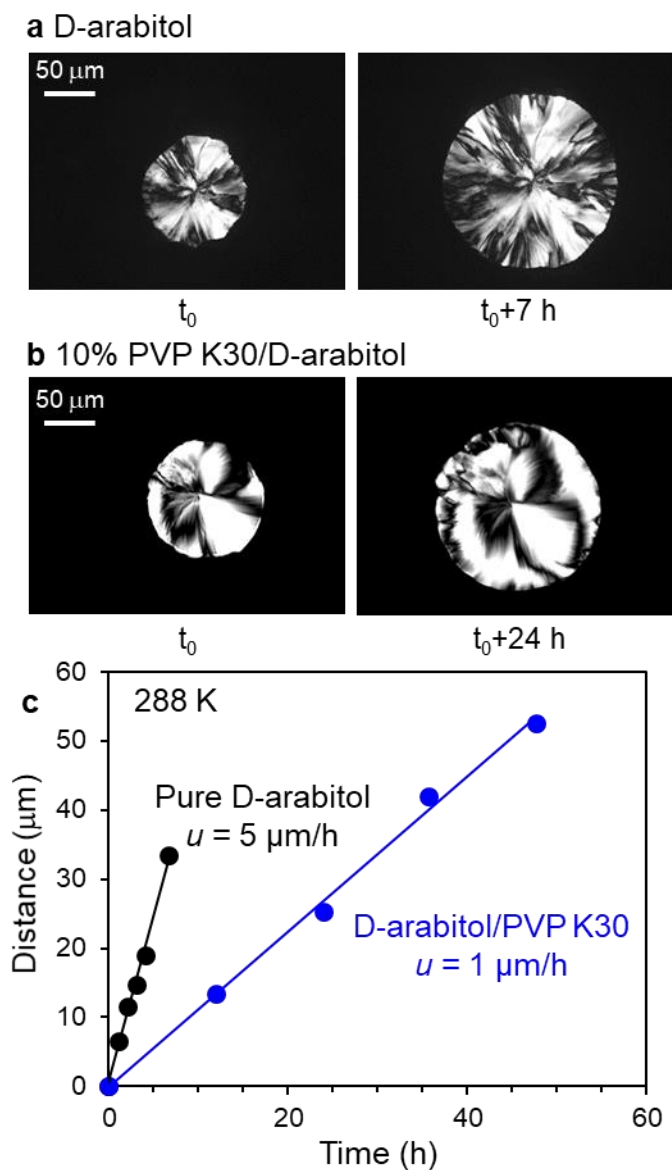


**Figure S3.** The measurement of crystal growth rate in D-arabitol and D-arabitol containing 10% PVP K30 at 288 K. (a) and (b): Light microscopy images of growing crystals. (c) Distance of growth vs. time at 288 K. The slope of each plot is the crystal growth rate.

## 4.7. Acknowledgements

We thank AbbVie Inc. and the Wisconsin - Puerto Rico Partnership for Research and Education in Materials supporting (NSF DMR-1827894) for supporting this work. We dedicate this work to the memory of Joel Bernstein.

## 4.9. References

1. Ediger, M. D.; Harrowell, P.; Yu, L., Crystal growth kinetics exhibit a fragility-dependent decoupling from viscosity. *The Journal of chemical physics* **2008**, *128* (3), 034709.
2. Orava, J.; Greer, A. á., Fast and slow crystal growth kinetics in glass-forming melts. *The Journal of chemical physics* **2014**, *140* (21), 214504.
3. Hikima, T.; Adachi, Y.; Hanaya, M.; Oguni, M., Determination of potentially homogeneous-nucleation-based crystallization in o-terphenyl and an interpretation of the nucleation-enhancement mechanism. *Physical Review B* **1995**, *52* (6), 3900.
4. Sun, Y.; Zhu, L.; Kearns, K. L.; Ediger, M. D.; Yu, L., Glasses crystallize rapidly at free surfaces by growing crystals upward. *Proceedings of the National Academy of Sciences* **2011**, *108* (15), 5990-5995.
5. Bokeloh, J.; Rozas, R. E.; Horbach, J.; Wilde, G., Nucleation barriers for the liquid-to-crystal transition in Ni: experiment and simulation. *Physical review letters* **2011**, *107* (14), 145701.
6. Sosso, G. C.; Chen, J.; Cox, S. J.; Fitzner, M.; Pedevilla, P.; Zen, A.; Michaelides, A., Crystal nucleation in liquids: Open questions and future challenges in molecular dynamics simulations. *Chemical reviews* **2016**, *116* (12), 7078-7116.
7. Laksmono, H.; McQueen, T. A.; Sellberg, J. A.; Loh, N. D.; Huang, C.; Schlesinger, D.; Sierra, R. G.; Hampton, C. Y.; Nordlund, D.; Beye, M., Anomalous behavior of the homogeneous ice nucleation rate in “no-man’s land”. *The journal of physical chemistry letters* **2015**, *6* (14), 2826-2832.
8. Fokin, V. M.; Zanutto, E. D.; Yuritsyn, N. S.; Schmelzer, J. W., Homogeneous crystal nucleation in silicate glasses: A 40 years perspective. *Journal of Non-Crystalline Solids* **2006**, *352* (26-27), 2681-2714.
9. Huang, C.; Chen, Z.; Gui, Y.; Shi, C.; Zhang, G. G.; Yu, L., Crystal nucleation rates in glass-forming molecular liquids: D-sorbitol, D-arabitol, D-xylitol, and glycerol. *The Journal of chemical physics* **2018**, *149* (5), 054503.
10. Gupta, P.; Kakumanu, V. K.; Bansal, A. K., Stability and solubility of celecoxib-PVP amorphous dispersions: a molecular perspective. *Pharmaceutical research* **2004**, *21* (10), 1762-1769.
11. Konno, H.; Handa, T.; Alonzo, D. E.; Taylor, L. S., Effect of polymer type on the dissolution profile of amorphous solid dispersions containing felodipine. *European journal of pharmaceuticals and biopharmaceutics* **2008**, *70* (2), 493-499.
12. Li, Y.; Yu, J.; Hu, S.; Chen, Z.; Sacchetti, M.; Sun, C. C.; Yu, L., Polymer nanocoating of amorphous drugs for improving stability, dissolution, powder flow, and tabletability: The case of chitosan-coated indomethacin. *Molecular pharmaceutics* **2019**, *16* (3), 1305-1311.

13. Matsumoto, T.; Zografi, G., Physical properties of solid molecular dispersions of indomethacin with poly (vinylpyrrolidone) and poly (vinylpyrrolidone-co-vinyl-acetate) in relation to indomethacin crystallization. *Pharmaceutical research* **1999**, *16* (11), 1722-1728.
14. Miyazaki, T.; Yoshioka, S.; Aso, Y.; Kojima, S., Ability of polyvinylpyrrolidone and polyacrylic acid to inhibit the crystallization of amorphous acetaminophen. *Journal of pharmaceutical sciences* **2004**, *93* (11), 2710-2717.
15. Pajula, K.; Taskinen, M.; Lehto, V.-P.; Ketolainen, J.; Korhonen, O., Predicting the formation and stability of amorphous small molecule binary mixtures from computationally determined Flory– Huggins interaction parameter and phase diagram. *Molecular pharmaceutics* **2010**, *7* (3), 795-804.
16. Shi, Q.; Zhang, C.; Su, Y.; Zhang, J.; Zhou, D.; Cai, T., Acceleration of crystal growth of amorphous griseofulvin by low-concentration poly (ethylene oxide): aspects of crystallization kinetics and molecular mobility. *Molecular pharmaceutics* **2017**, *14* (7), 2262-2272.
17. Cai, T.; Zhu, L.; Yu, L., Crystallization of organic glasses: effects of polymer additives on bulk and surface crystal growth in amorphous nifedipine. *Pharmaceutical research* **2011**, *28* (10), 2458-2466.
18. Kestur, U. S.; Taylor, L. S., Role of polymer chemistry in influencing crystal growth rates from amorphous felodipine. *CrystEngComm* **2010**, *12* (8), 2390-2397.
19. Kothari, K.; Ragoonanan, V.; Suryanarayanan, R., The role of drug–polymer hydrogen bonding interactions on the molecular mobility and physical stability of nifedipine solid dispersions. *Molecular pharmaceutics* **2015**, *12* (1), 162-170.
20. Huang, C.; Powell, C. T.; Sun, Y.; Cai, T.; Yu, L., Effect of low-concentration polymers on crystal growth in molecular glasses: a controlling role for polymer segmental mobility relative to host dynamics. *The Journal of Physical Chemistry B* **2017**, *121* (8), 1963-1971.
21. Sun, Y.; Tao, J.; Zhang, G. G.; Yu, L., Solubilities of crystalline drugs in polymers: an improved analytical method and comparison of solubilities of indomethacin and nifedipine in PVP, PVP/VA, and PVAc. *Journal of pharmaceutical sciences* **2010**, *99* (9), 4023-4031.
22. Tammann, G.; Jenckel, E., Die Kristallisationsgeschwindigkeit und die Kernzahl des Glycerins in Abhängigkeit von der Temperatur. *Zeitschrift für anorganische und allgemeine Chemie* **1930**, *193* (1), 76-80.
23. Turnbull, D.; Fisher, J. C., Rate of nucleation in condensed systems. *The Journal of chemical physics* **1949**, *17* (1), 71-73.
24. Kelton, K. F., Crystal nucleation in liquids and glasses. In *Solid state physics*, Elsevier: 1991; Vol. 45, pp 75-177.
25. Weinberg, M. C., *Nucleation and crystallization in liquids and glasses*. Amer Ceramic Society: 1993; Vol. 30.
26. Jackson, K.; Uhlmann, D. R.; Hunt, J., On the nature of crystal growth from the melt. *Journal of Crystal Growth* **1967**, *1* (1), 1-36.
27. Hiemenz, P. C.; Lodge, T. P., *Polymer chemistry*. CRC press: 2007.

**Chapter 5. Surfactants Accelerate Crystallization of Amorphous  
Nifedipine by Similar Enhancement of Nucleation and Growth  
Independent of Hydrophilic-Lipophilic Balance**

Xin Yao, Emily G. Benson, Yue Gui, Torsten Stelzer, Geoff G. Z. Zhang, Lian Yu

As published in:

*Molecular Pharmaceutics* **2022** 19 (7), 2343-2350

DOI: 10.1021/acs.molpharmaceut.2c00156

## 5.1. Abstract

Amorphous formulations, increasingly employed to deliver poorly soluble drugs, generally contain surfactants to improve wetting and dissolution. These surfactants are often liquids and can potentially increase the mobility of the drug and reduce its stability, but little is known about this effect. Here we investigate the effect of 4 common non-ionic surfactants (Tween 80, Span 80, Triton X-100, and poloxamer 407) on crystallization in amorphous nifedipine (NIF). We find that the surfactants significantly enhance the rates of crystal nucleation and growth even at low concentrations, by up to 2 orders of magnitude at 10 wt %. The surfactants tested show similar enhancement effects independent of their structural details and hydrophilic-lipophilic balance (HLB), suggesting that surfactant adsorption at solid/liquid interfaces does not play a major role in crystal nucleation and growth. Importantly, the surfactants accelerate crystal nucleation and growth by a similar factor. This result mirrors the previous finding that a polymer dopant causes similar slowdown of nucleation and growth. These results indicate that nucleation and growth in a deeply supercooled liquid are both mobility-limited, and a dopant mainly functions as a mobility modifier (enhancer or suppressor depending on the dopant). The common surfactants tested are all mobility enhancers and destabilize the amorphous drug and this negative effect must be managed using stabilizers such as polymers. The effect of surfactants on nucleation can be predicted from the rate of crystal growth and the crystallization kinetics of the pure system, using the same principle previously established for drug-polymer systems. We show how the independently measured nucleation and growth rates enable predictions of the overall crystallization rates.



**Keywords:** crystal nucleation, crystal growth, non-ionic surfactants, ASDs, amorphous, nifedipine, HLB, crystallization kinetics

## 5.2. Introduction

Amorphous solid dispersions (ASDs) are increasingly used to improve the solubility and bioavailability of poorly water-soluble drugs.<sup>1</sup> An ASD typically consists of an active pharmaceutical ingredient (API), a dispersion polymer, and a surfactant. The excipients in an ASD are essential for its performance and stability. A polymer can inhibit the crystallization of an amorphous drug,<sup>2</sup> improve its tableability,<sup>3</sup> and maintain high supersaturation during dissolution.<sup>4</sup> A surfactant is introduced to improve wetting and dissolution,<sup>5-7</sup> and to lower the processing temperature for melt-extruded formulations.<sup>8</sup> Table 1 lists several marketed ASDs and the polymers and surfactants therein.

**Table 1.** Examples of marketed ASDs containing surfactants.

API	Surfactant	Polymer	Product Name
Venetoclax	Tween 80	Kollidon VA 64	Venclexta <sup>®</sup>
Lopinavir/Ritonavir	Span 20	Kollidon VA 64	Kaletra <sup>®</sup>
Ritonavir	Span 20	Kollidon VA 64	Norvir <sup>®</sup>
Ivacaftor	SDS	HPMCAS	Kalydeco <sup>®</sup>
Telaprevir	SDS	HPMCAS	Incivek <sup>®</sup>

The design of ASDs requires an understanding of the effects of the excipients on the crystallization of the API. The crystallization of an amorphous drug would eliminate its solubility advantage over the corresponding crystalline drug. There has been extensive work on the effect of polymers on the crystallization of amorphous drugs.<sup>2, 9-11</sup> For example, at a common concentration of 1 wt %, different polymers dispersed in amorphous nifedipine can significantly decrease or increase the crystal growth rate in correlation with the polymer's segmental mobility.<sup>11, 12</sup> Recently, amorphous drug-polymer salts have been used to vastly improve the stability against crystallization under tropical conditions (high temperature and high humidity).<sup>13</sup> In contrast to the growing understanding of drug-polymer systems, less is known about the effect of surfactants on amorphous stability.<sup>14, 15</sup> Given that pharmaceutical surfactants are generally liquids at room temperature, their presence in ASDs could increase molecular mobility and accelerate crystallization. Besides their effect on mobility, surfactants are known to adsorb at solid/liquid interfaces<sup>16</sup> and could influence the kinetics of crystallization by modifying the interface. At present, a systematic understanding of these effects is lacking and is the motivation for the present work.

Crystallization has two elemental steps – nucleation and growth, with very different kinetics. In a pure supercooled liquid, for example, the peak temperature for nucleation is usually lower than that for growth.<sup>17-19</sup> This means that both nucleation and growth must be understood to predict the overall crystallization process. Previous work has investigated the effects of surfactants on the overall crystallization rate<sup>14</sup> and the crystal growth rate,<sup>15</sup> but there has been no systematic study to our knowledge of a surfactant's effect on both nucleation and growth. In this context, the recent work on drug-polymer systems offers further motivation.<sup>19, 20</sup> For drug-polymer

systems at low enough temperatures (near the glass transition temperature  $T_g$ ), the polymer solute has a similar effect on nucleation and growth, that is, altering their rates by a similar factor. This suggests that in a typical amorphous formulation, nucleation and growth are both limited by molecular mobility and a polymer solute serves as a mobility modifier. This conclusion has enabled prediction of the hard-to-measure nucleation rates from the easy-to-measure growth rates.<sup>19</sup> A goal of this work is to determine whether the same principle holds for surfactants in amorphous drugs. The general validity of this principle would allow prediction of the physical stability of realistic multi-component ASDs.

In this study, we investigated the effect of four non-ionic surfactants (Tween 80, Span 80, Triton X-100, and Poloxamer 407, Chart 1) on the crystal nucleation and growth of nifedipine (NIF). The surfactants have different structures and hydrophilic-lipophilic balance (HLB)<sup>21</sup> to assess the relative importance of mobility enhancement and interfacial adsorption. NIF is a model amorphous drug whose crystallization and polymorphism have been investigated.<sup>22, 23</sup>

We find that the surfactants significantly enhance crystal nucleation and growth in amorphous NIF. Near the peak temperature (343 K) for nucleation rate, 10% surfactant increased the rates of crystal nucleation and growth by approximately 30 times. Interestingly, the different surfactants have very similar effects on nucleation and growth, despite their different structures and HLB values. This indicates that the surfactants act mainly as mobility enhancers as opposed to interfacial modifiers. The surfactants decrease the  $T_g$  of NIF by a similar degree and cause a similar enhancement of nucleation and growth. This finding is in complete agreement with the

previous result on polymer dopants in amorphous drugs.<sup>19, 20</sup> In both cases, the dopant (polymer or surfactant) modifies the local mobility, thereby increasing or suppressing nucleation and growth by a similar factor. We discuss the relevance of our finding for the prediction of crystallization kinetics of ASDs.

### 5.3. Materials and Methods

**Materials.** Nifedipine (NIF, > 98% pure) and the surfactants [Tween 80 (Polysorbate 80), Span 80 (sorbitan monooleate), Triton X-100, and Poloxamer 407] were purchased from Sigma-Aldrich (St. Louis, MO). Poly(ethylene oxide) (PEO 10,000 g/mol) was from Alfa Aesar, and polyvinylpyrrolidone (PVP K30, Kollidon 30) from BASF. All materials were used as received.

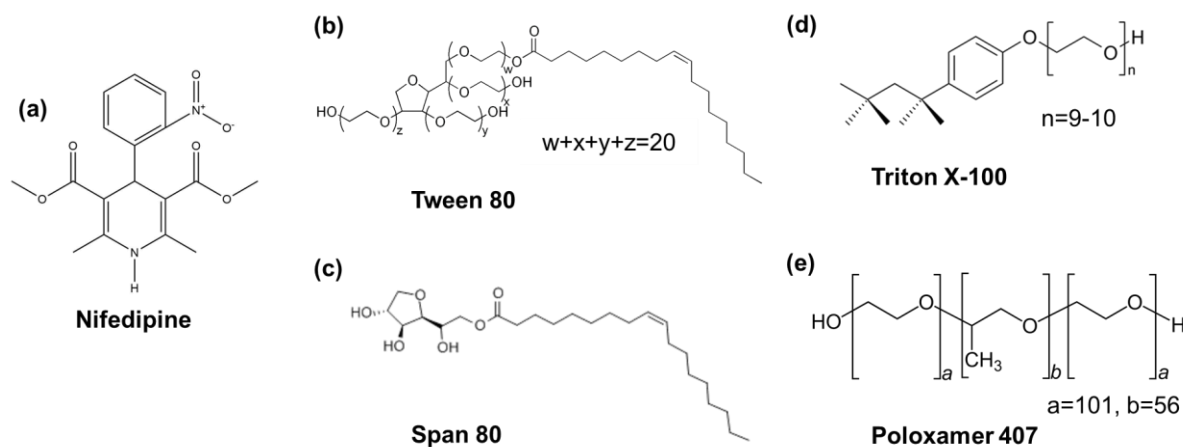


**Chart 1.** Chemical structures of the model drug nifedipine and the surfactants: Tween 80, Span 80, Triton X-100, and Poloxamer 407.

**Nucleation and Growth Rates.** A surfactant or polymer was mixed in NIF by cryomilling (SPEX CertiPrep 6750 Freezer/Mill with liquid nitrogen as coolant) followed by melting. Cryomilling was performed at 10 Hz for five 2-min cycles, each followed by a 2-min cool down. To measure nucleation and crystal growth, 3 – 20 mg of sample were melted at 450 K, and a

coverslip was placed over the melt producing a sandwiched liquid film. The film thickness was confirmed not to affect the observed rate of nucleation.<sup>24</sup> To determine nucleation rate, a liquid film was cooled directly to a target temperature (295 – 393 K) and held at that temperature until crystals appeared. Crystals were observed through a polarized light microscope (Olympus BX35) equipped with a digital camera. The data analysis to extract nucleation rate is described in the Results. The polymorphs were determined by Raman spectroscopy, X-ray diffraction and melting point as previously described.<sup>22</sup> Crystal growth rate was measured by tracking the advance of a growth front over time.<sup>25</sup> Each growth rate reported was the average of the data from at least 5 individual crystals, each measured at least 4 different time points.

**Differential Scanning Calorimetry (DSC).** DSC was performed with a TA Q2000 differential scanning calorimeter under 50 ml/min N<sub>2</sub> purge. Each sample was ~5 mg placed in a crimped aluminum pan. The glass transition temperature  $T_g$  was measured during heating at 10 K/min after cooling at 10 K/min and the onset temperature is reported. Modulated DSC (MDSC) was performed at 2 K/min heating and cooling with a modulation amplitude of  $\pm 0.5$  K and a period of 60 s.

## 5.4. Results

Before describing our results on the surfactant effect on crystallization, we summarize the relevant properties of the surfactants for interpreting their effects on nucleation and growth. As Table 2 shows, these surfactants have different HLB values, while their  $T_g$ s are similarly low relative to the host drug NIF ( $T_g = 315$  K).<sup>24, 25</sup> Furthermore, we established by DSC that all four surfactants are miscible with NIF at the concentrations studied. For this purpose, we used the effect of a surfactant on the  $T_g$  of NIF as a test for miscibility, with a single, concentration-

dependent  $T_g$  indicating a single phase.<sup>19, 26</sup> Figure 1a shows the typical DSC data for this purpose. In this example, NIF containing Tween 80 was tested. With increasing Tween 80 concentration, the  $T_g$  of NIF decreased steadily, indicating that the two components are miscible in the concentration range tested (0 – 25%).

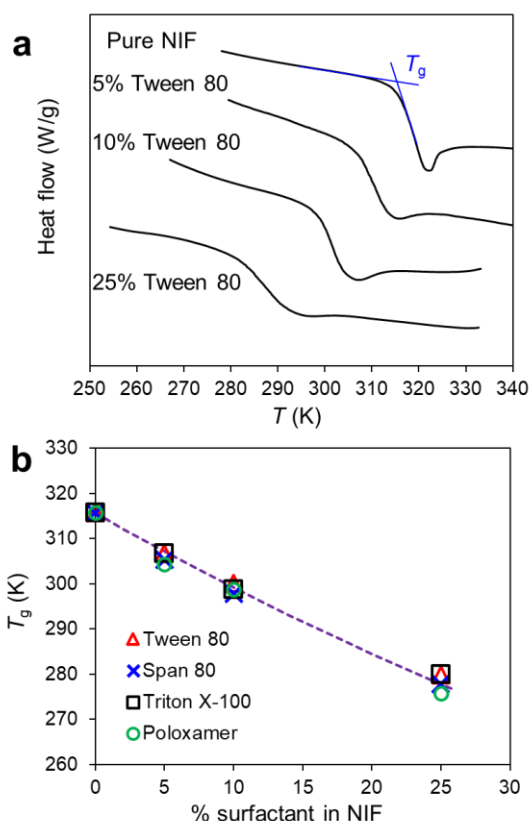


**Figure 1.** (a) DSC traces of NIF containing Tween 80 at different concentrations during heating. A single  $T_g$  is observed, and it decreases with increasing surfactant concentration. (b)  $T_g$  of NIF as a function of surfactant concentration. The different surfactants show similar effects. The curve indicates the average trend for all data points.

Figure 1b shows the  $T_g$  of NIF as a function of surfactant concentration for all the surfactants used. For each system, the  $T_g$  decreases with surfactant concentration up to at least 25%, indicating miscibility between NIF and the surfactant in the concentration range of our

crystallization experiments (0 – 10%). The different surfactants have similar effects on the  $T_g$  of NIF. This is consistent with the similar and low  $T_g$ s of the surfactants (Table 2) and indicates that the surfactants have similar strengths of interaction with NIF. The miscibility between NIF and the two polymers used in this work (PVP K30 and PEO) has been previously verified.<sup>10</sup>

**Table 2.** Physical properties of the surfactants used in this work.

	HLB <sup>a</sup>	$T_g$ , K <sup>b</sup>	$T_{g\ 10\%}$ , K <sup>c</sup>	$T_m$ , K
Span 80	4.3	212	297	Not observed
Triton X-100	13.5	210	301	251
Tween 80	15.0	201	300	249
Poloxamer 407	22	204	298	325
NIF	–	315	–	437

<sup>a</sup> From Ref. <sup>27</sup>

<sup>b</sup> See Figure S1 for MDSC data.

<sup>c</sup>  $T_{g\ 10\%}$  is the  $T_g$  of NIF containing 10% surfactant.

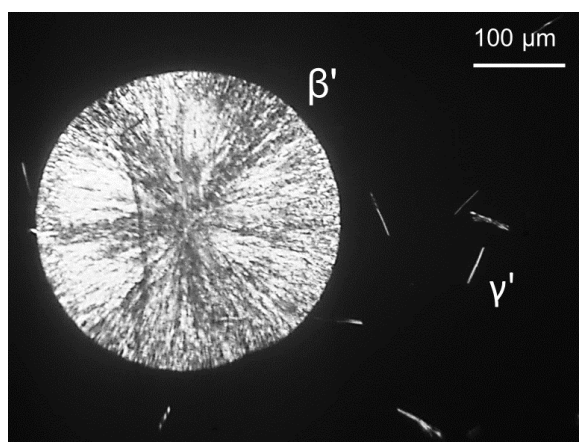


**Figure 2.** Spontaneously crystallized NIF containing 10% Tween 80 at 373 K in  $\beta'$  and  $\gamma'$  polymorphs as indicated.

**Nucleation and Growth Rates.** Two polymorphs of NIF,  $\beta'$  and  $\gamma'$ , spontaneously nucleate from its melt<sup>22, 24</sup>, and Gui et al. have measured their nucleation and growth rates in the pure melt.<sup>23</sup> In this work, we investigated the effect of the four surfactants in Scheme 1 on the crystallization of NIF. When the surfactants were present, we observed the same two polymorphs that crystallized in the pure melt. As an example, Figure 2 shows the  $\beta'$  and  $\gamma'$  polymorphs that crystallized from a melt of NIF containing 10% Tween 80 at 373 K. The faster-growing, larger spherulite is  $\beta'$  and the smaller needles are  $\gamma'$ .<sup>22</sup> In addition, these polymorphs can be distinguished by their Raman spectra.<sup>22</sup> To investigate the surfactant effect on crystallization, we focused on the response of the faster-crystallizing  $\beta'$  form.<sup>23, 25</sup> (It was difficult to observe the  $\gamma'$  polymorph below 353 K (see Figure 3a for example) because of its slow growth.<sup>23</sup>)

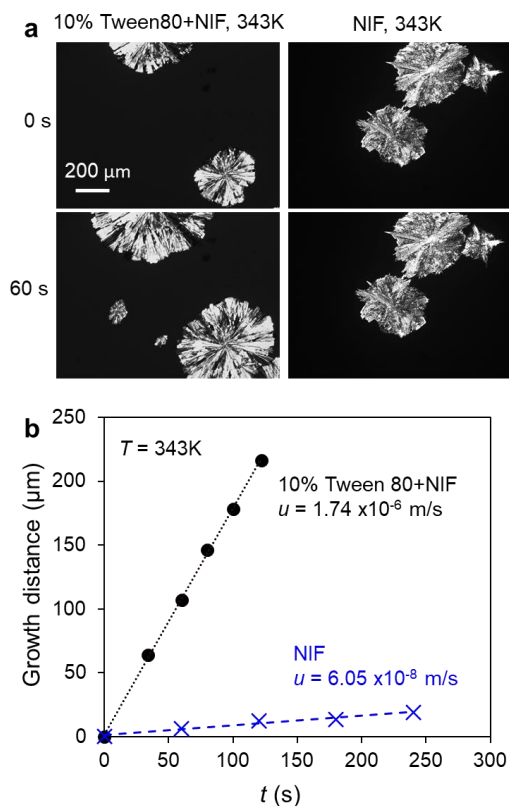


**Figure 3.** Example of growth rate measurements. (a) Crystals after different growth time at 343 K. (b) Crystal growth distance vs. time. The slope is the growth rate.



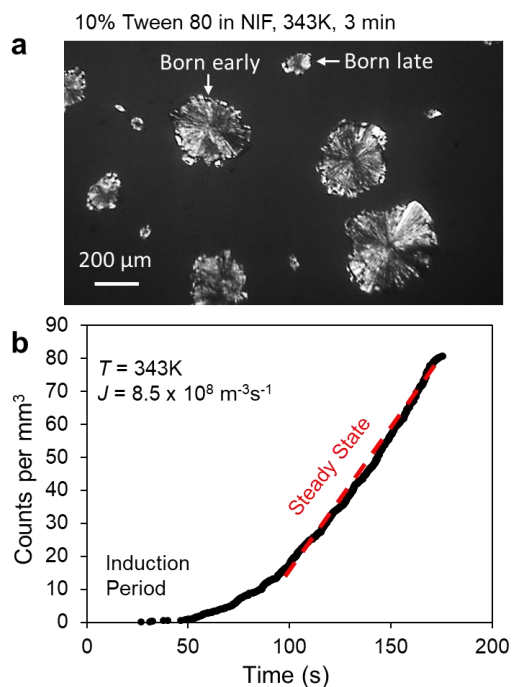


**Figure 4.** One-stage method for measuring crystal nucleation rate. (a) NIF containing 10% Tween 80 after 3 min at 343 K. A range of crystal size is seen, from which the birth time of each crystal can be calculated. (b) Nuclei density as a function of time. The slope at the steady state is the nucleation rate  $J$ .

Figure 3 shows the typical data collected to measure the crystal growth rate. Figure 3a shows the images of the crystals growing at 343 K in pure NIF and in NIF containing 10% Tween 80. Figure 3b shows the size of a crystal as a function of time. The linear increase of size with time indicates a constant growth rate. Note that crystal growth is much faster in the presence of the surfactant. These growth rates are used to calculate the birth time of crystals in the measurement of nucleation rates (see below).

Figure 4a shows the typical data collected to measure nucleation rates. The method has been described previously.<sup>17, 18</sup> In brief, the sample was allowed to crystallize spontaneously at a fixed

temperature for a certain time. The crystals of different sizes indicate they were nucleated at different times, with larger crystals being born at earlier times (thus having longer times to grow) than smaller crystals. The nucleation time of each crystal was calculated as follows:

$$t_n = t_0 - r/u \quad (1)$$

where  $t_n$  is the nucleation time,  $t_0$  the time of observation,  $r$  the size (radius) of the crystal, and  $u$  the growth rate. This yields the nucleation density (counts/mm<sup>3</sup>) as a function of time, as shown in Figure 4b. The data show that after an induction time, a steady state was reached where nucleation density increases linearly with time. The slope in the steady state is the nucleation rate  $J$  in the unit of number/m<sup>3</sup>/s.

Figure 5 shows the effect of the surfactants on the nucleation and growth rates in NIF. All the surfactants tested increase the rates of nucleation and growth. Interestingly, at the common concentration of 10%, there is no significant difference between the surfactants tested. Poloxamer 407 is a slight (but experimentally significant) outlier relative to the other surfactants, showing a larger enhancement of nucleation and a smaller enhancement of growth. Given their different structures and HLB values (Table 2), the similar effects of the surfactants suggest that interfacial adsorption plays a relatively minor role in the crystallization of NIF, and the plasticizing effect is more important. Consistent with this conclusion, we note that at 10%, the different surfactants reduce the  $T_g$  of NIF by a similar amount, ~20 K (Figure 1b). This implies a similar enhancement of mobility by the different surfactants.

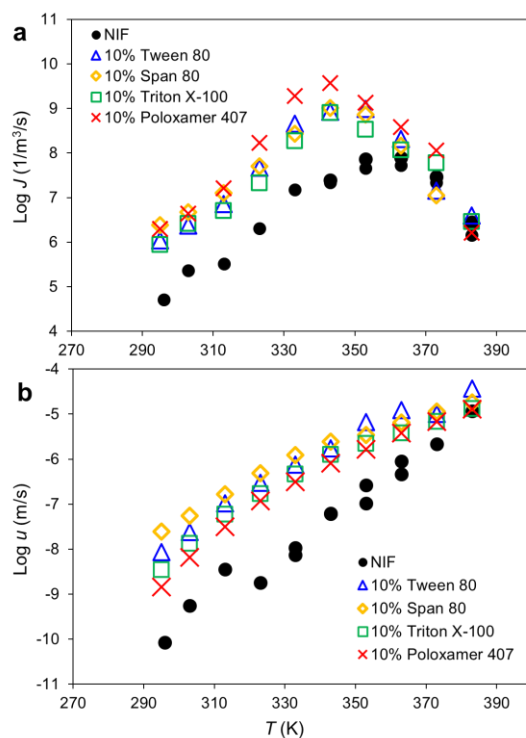


**Figure 5.** (a) Nucleation and (b) growth rates of pure NIF and NIF containing 10% surfactant as indicated. All surfactants tested accelerate crystal nucleation and growth and the effects are similar, regardless of their different structures and HLB values.

It is worth noting that in the presence of the surfactants, the peak temperature for nucleation shifts to lower temperatures relative to pure NIF (from 360 K to 340 K). This result is also consistent with the mobility control of the nucleation process. A peak temperature for nucleation is a result of two competing factors: (1) the driving force for nucleation increases with cooling and (2) the mobility needed for nucleation decreases with cooling. Assuming the smaller amount of the surfactant present does not alter the driving force significantly, the enhanced mobility by the surfactant would shift the peak temperature to lower value (larger supercooling is needed to bring down the nucleation rate).

## 5.5. Discussion

This study investigated the effects of four common surfactants on the crystal nucleation and growth in the amorphous drug nifedipine. The four surfactants tested (Scheme 1) have different structures, HLB values, and similar low  $T_g$ s (Table 1). Despite these differences, these four surfactants have very similar effects on the nucleation and growth of NIF. Furthermore, each surfactant enhances the rates of nucleation and growth by approximately the same factor. We now discuss these results and argue the surfactants act mainly as mobility enhancers, not as interface modifiers, in their effect on crystallization.

Given the ability of surfactants to adsorb onto interfaces,<sup>28</sup> one might expect that they could modify the crystal/liquid interface, thus altering the rates of nucleation and growth. Our results, however, provide no evidence for such an effect. If interfacial adsorption was important, the four surfactants with their different HLB values (4.3 to 22) would have different interfacial concentrations<sup>29</sup> and different effects on crystallization. The lack of differentiation among the surfactants could be a result of thermodynamics (no driving force for interfacial enrichment), kinetics (slow rate of interfacial adsorption relative to crystallization rate), or both.

We attribute the similar effect of the four surfactants on crystallization to their role as mobility enhancers, not interfacial modifiers. This conclusion is supported by the similar and low  $T_g$ s of the surfactants (Table 2). The low  $T_g$ s of the surfactants relative to NIF imply that their presence in NIF should increase molecular mobility. Indeed, all four surfactants depress the  $T_g$  of NIF (Figure 1b) and do so by a similar amount at the same concentration. This indicates that the four

surfactants enhance the molecular mobility to a similar degree, leading to a similar effect on nucleation and growth.

We now turn to the approximately equal enhancement of the nucleation and growth rates by each surfactant (Figure 5). According to these results, if a surfactant increases the rate of crystal growth by some factor, it increases the nucleation rate by approximately the same factor; that is,

$$J / J_0 = u / u_0 \quad (2)$$

where  $J_0$  and  $u_0$  are the nucleation and growth rates of pure NIF, and  $J$  and  $u$  the corresponding rates of the surfactant-doped NIF. This relation has been observed previously for D-arabitol and D-sorbitol doped with polyvinylpyrrolidone (PVP).<sup>19</sup> In the latter systems, PVP has an inhibitory effect on crystallization, and it reduces the rates of nucleation and growth by a similar factor, regardless of its molecular weight and concentration. The interpretation of Eq. 2 is that in a deeply supercooled liquid, nucleation and growth are both limited by mobility, and a dopant (surfactant or polymer) acts as a mobility modifier, altering both rates by the same factor.

One application of Eq. 2 is to predict the hard-to-measure nucleation rates from the easy-to-measure growth rates as follows:

$$J = J_0 (u/u_0) \quad (3)$$

Yao et al. have applied Eq. 3 to predict nucleation rates in PVP-doped D-sorbitol or D-arabitol,<sup>19</sup> and they observed a good agreement between the predicted and the observed rates. Recently Zhang et al. performed the same prediction on polymer-doped fluconazole (FCZ).<sup>20</sup> In Figure 6,

we summarize these previous results and incorporate the new results from this work. Here the predicted nucleation rate is plotted against the observed rate and the diagonal line corresponds to perfect prediction. Figure 6 shows that the data points cluster around the diagonal line, with an average deviation of 0.5 on the logarithmic scale, which is comparable to the experimental error of the nucleation rate. The systems plotted in Figure 6 include four host molecules and 7 dopants

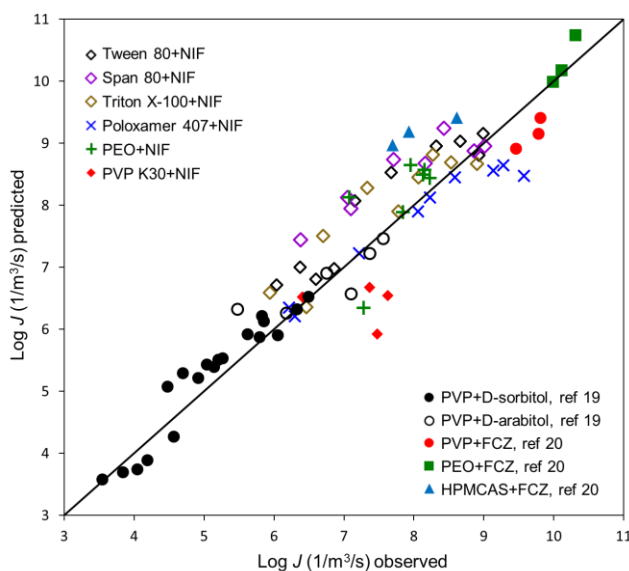


**Figure 6.** Predicted vs. observed nucleation rates in binary amorphous systems. In total, there are 4 host molecules and 7 dopants. To broaden the comparison for the NIF host, this work also measured the nucleation rates and growth rates of NIF containing PEO and PVP K30 (Figure S2).

and cover 7 orders of magnitude in nucleation rate. This performance provides a strong validation for the predictive model. The success of Eq. 3 for predicting nucleation rates also provides a self-consistency test for the understanding described above, that is, nucleation and growth are both controlled by mobility in deeply supercooled liquids and a dopant modifies the molecular mobility, thus similarly changing their rates. This method is a potential tool for predicting mobility-limited nucleation rates in multi-component systems.

Knowing a dopant's effect on the individual rates of nucleation and growth, one should be able to predict the total crystallization rate. Here we explore this possibility. For simplicity, we assume spherical crystalline domains forming in a 3-dimensional sample for which the fraction crystallized increases with time  $t$  following the Avrami equation:<sup>30</sup>

$$F(t) = 1 - \exp\left(-\frac{\pi}{3}Ju^3t^4\right) \quad (4)$$

Figure 7a shows the  $F(t)$  curves calculated from our experimental nucleation and growth rates,  $J$  and  $u$ , for pure and surfactant-doped NIF at 343 K. For pure NIF, our calculated curve (black)

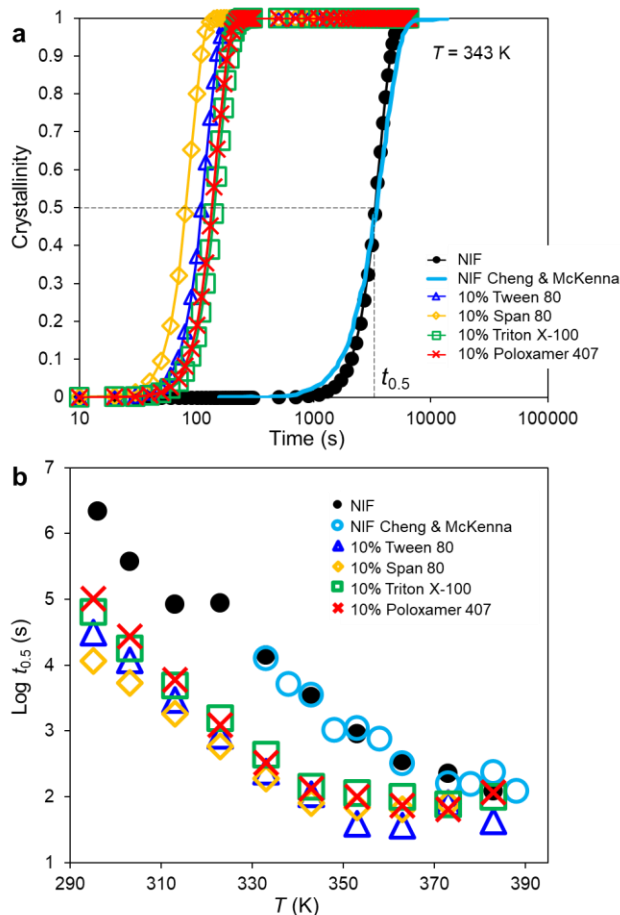


**Figure 7.** (a) Calculated fraction crystallized vs. time at 343 K. Surfactants decrease the  $t_{0.5}$  of NIF by  $\sim 30$  times at 343 K. For pure NIF, the experimental data of Cheng and McKenna is shown for comparison. (b) Half time of crystallization ( $t_{0.5}$ ) vs. temperature. For pure NIF, the experimental  $t_{0.5}$  from Cheng and McKenna is given for comparison.

agrees reasonably well with Cheng and McKenna's experimental curve (light blue) measured by DSC.<sup>31</sup> Relative to pure NIF, surfactant-doped NIF is predicted to crystallize much faster, with the half time of crystallization,  $t_{0.5}$ , shortened by approximately 30 times.

In Figure 7b, we plot the  $t_{0.5}$  as a function of temperature for the various systems. From eq. 4,  $t_{0.5}$  is given by

$$t_{0.5} = \sqrt[4]{3 \ln 2 / (\pi J u^3)} \quad (5)$$

Again, for pure NIF, the experimental data of Cheng and McKenna are shown and they agree well with the calculated values.<sup>23</sup> This validates the accuracy of the calculation. According to the calculation, the presence of the surfactants significantly shortens the  $t_{0.5}$  and the effect is stronger at lower temperatures, where  $t_{0.5}$  is shortened by ~30 times. The analysis above demonstrates the value of knowing the individual rates of nucleation and growth in predicting the overall rate of crystallization. While eq. 4 assumes 3-dimensional crystallization, the same  $J$  and  $u$  values can be used to calculate the crystallization kinetics in other sample geometries (e.g., thin films).

## 5.6. Conclusions

This work has investigated the effect of common pharmaceutical surfactants on the crystal nucleation and growth of an amorphous drug. At a relatively low concentration (10 wt %), the four surfactants tested can all significantly accelerate the crystallization of amorphous nifedipine and they do so in a similar manner, despite their different structures and hydrophilic-lipophilic balance. In addition, each surfactant increases the rates of nucleation and growth by a similar factor. This supports the view<sup>19, 20</sup> that nucleation and growth are both mobility-limited in a



deeply supercooled liquid and the surfactant mainly functions as a plasticizer, causing similar acceleration of the two processes. For the surfactants tested, interfacial adsorption does not play an important role in their effect on nucleation and growth. Although our conclusion has been reached for non-ionic surfactants, we expect it to hold for ionic surfactants doped in weakly ionizable drugs like nifedipine. Our new results on surfactants are in complete agreement with the previous result on polymer dopants.<sup>19</sup> This enables the prediction of the hard-to-measure nucleation rates from the easy-to-measure growth rates (Figure 6) in multi-component systems. The knowledge of the individual rates of nucleation and growth enables the prediction of the overall rate of crystallization (Figure 7b). Future work could explore the validity of this prediction for realistic ASDs each composed of a drug, a polymer, and a surfactant. Systems investigated to date are all melt-miscible and it is of interest to investigate systems in which components are only partially miscible (phase separated). This work has focused on a surfactant's effect on crystal nucleation *in the bulk*. Given that ASD components can be enriched or depleted at a free surface,<sup>29, 32</sup> it is of interest to determine whether a second component has different effects on crystal nucleation in the bulk and on the surface.

## 5.7. Acknowledgments

We thank AbbVie Inc. and the Wisconsin - Puerto Rico Partnership for Research and Education in Materials (NSF DMR-1827894) for supporting this work.

## 5.8. Supporting Information

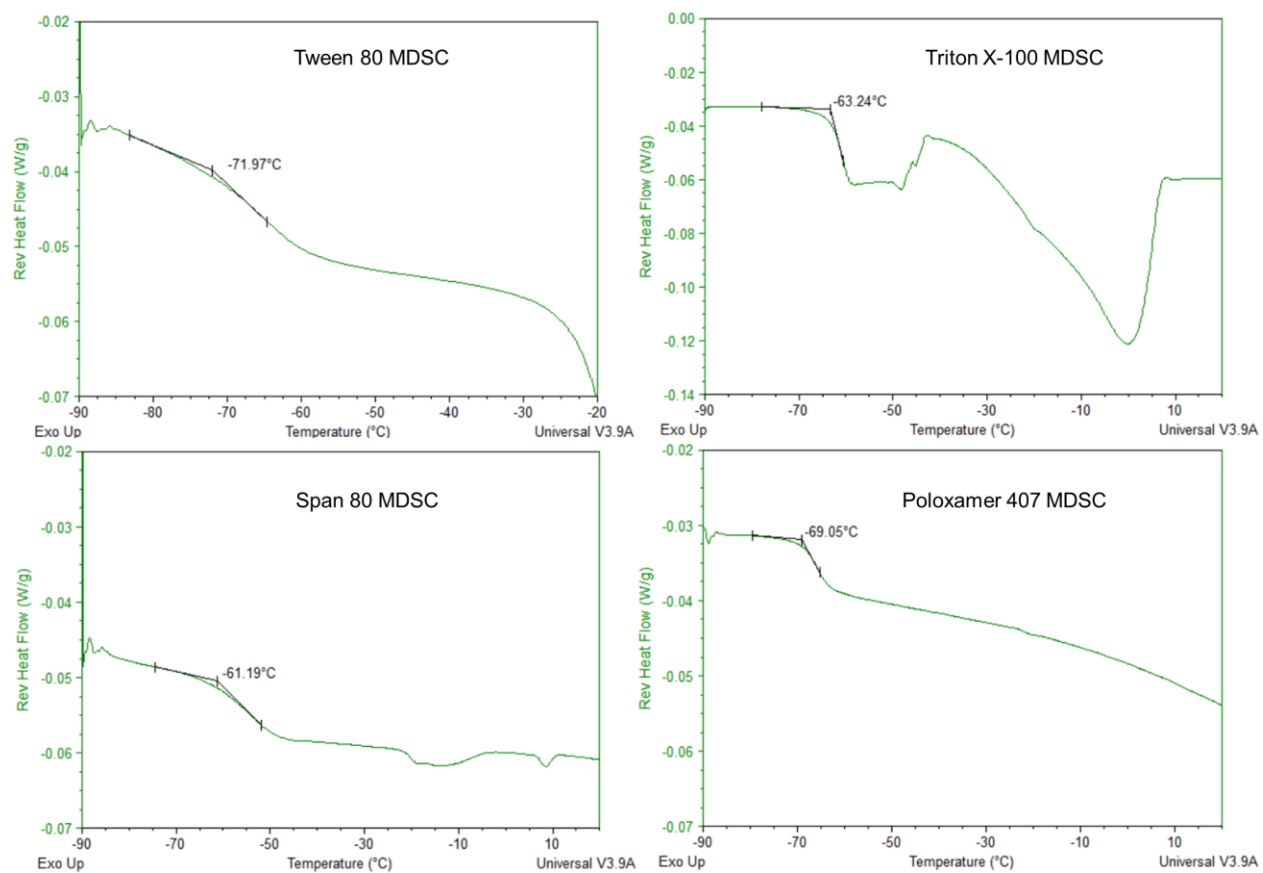


**Figure S1.** MDSC reversing heat flow traces of Tween 80, Span 80, Triton X-100, and Poloxamer 407 during heating at 2 K/min. The  $T_g$  onsets are indicated.

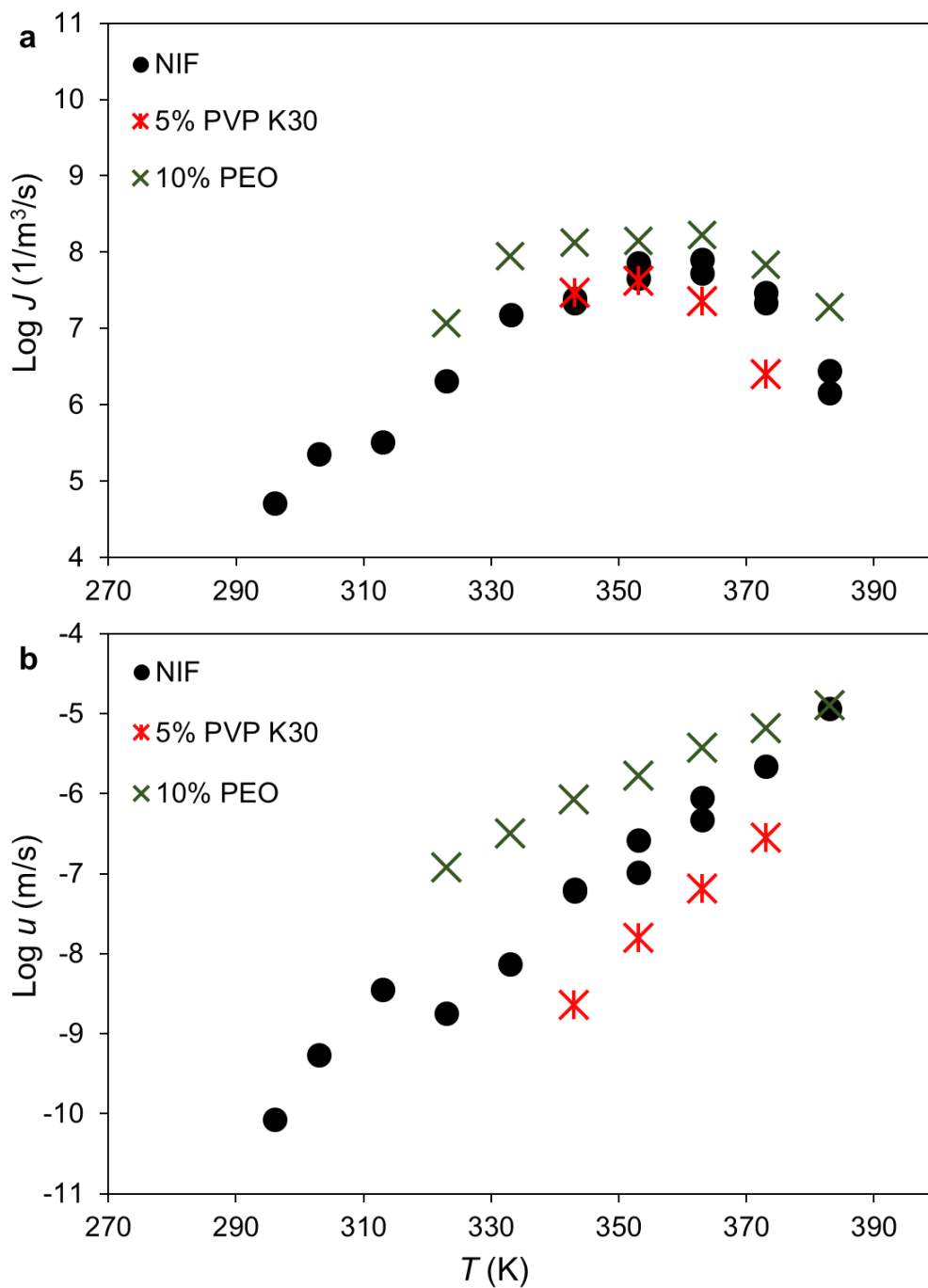


**Figure S2.** Rates of crystal nucleation (a) and growth (b) in pure NIF and NIF containing 10% PEO (10,000 g/mol) and 5% PVP K30.

## 5.9. References

1. Yu, L., Amorphous pharmaceutical solids: preparation, characterization and stabilization. *Advanced drug delivery reviews* **2001**, *48* (1), 27-42.
2. Nie, H.; Su, Y.; Zhang, M.; Song, Y.; Leone, A.; Taylor, L. S.; Marsac, P. J.; Li, T.; Byrn, S. R., Solid-state spectroscopic investigation of molecular interactions between clofazimine and hypromellose phthalate in amorphous solid dispersions. *Molecular pharmaceutics* **2016**, *13* (11), 3964-3975.
3. Flügel, K.; Schmidt, K.; Mareczek, L.; Gäbe, M.; Hennig, R.; Thommes, M., Impact of incorporated drugs on material properties of amorphous solid dispersions. *European Journal of Pharmaceutics and Biopharmaceutics* **2021**, *159*, 88-98.
4. Alonzo, D. E.; Zhang, G. G.; Zhou, D.; Gao, Y.; Taylor, L. S., Understanding the behavior of amorphous pharmaceutical systems during dissolution. *Pharmaceutical research* **2010**, *27* (4), 608-618.
5. Saboo, S.; Bapat, P.; Moseson, D. E.; Kestur, U. S.; Taylor, L. S., Exploring the Role of Surfactants in Enhancing Drug Release from Amorphous Solid Dispersions at Higher Drug Loadings. *Pharmaceutics* **2021**, *13* (5), 735.
6. Que, C.; Lou, X.; Zemlyanov, D. Y.; Mo, H.; Indulkar, A. S.; Gao, Y.; Zhang, G. G.; Taylor, L. S., Insights into the dissolution behavior of ledipasvir–copovidone amorphous solid dispersions: role of drug loading and intermolecular interactions. *Molecular pharmaceutics* **2019**, *16* (12), 5054-5067.
7. Indulkar, A. S.; Gao, Y.; Raina, S. A.; Zhang, G. G.; Taylor, L. S., Impact of monomeric versus micellar surfactant and surfactant–polymer interactions on nucleation–induction times of atazanavir from supersaturated solutions. *Crystal Growth & Design* **2019**, *20* (1), 62-72.
8. Ghebremeskel, A. N.; Vemavarapu, C.; Lodaya, M., Use of surfactants as plasticizers in preparing solid dispersions of poorly soluble API: selection of polymer–surfactant combinations using solubility parameters and testing the processability. *International journal of pharmaceutics* **2007**, *328* (2), 119-129.
9. Sahoo, A.; Suryanarayanan, R.; Siegel, R. A., Stabilization of Amorphous Drugs by Polymers: The Role of Overlap Concentration ( $C^*$ ). *Molecular pharmaceutics* **2020**, *17* (11), 4401-4406.
10. Huang, C.; Powell, C. T.; Sun, Y.; Cai, T.; Yu, L., Effect of low-concentration polymers on crystal growth in molecular glasses: a controlling role for polymer segmental mobility relative to host dynamics. *The Journal of Physical Chemistry B* **2017**, *121* (8), 1963-1971.
11. Kestur, U. S.; Lee, H.; Santiago, D.; Rinaldi, C.; Won, Y.-Y.; Taylor, L. S., Effects of the molecular weight and concentration of polymer additives, and temperature on the melt crystallization kinetics of a small drug molecule. *Crystal growth & design* **2010**, *10* (8), 3585-3595.
12. Powell, C. T.; Cai, T.; Hasebe, M.; Gunn, E. M.; Gao, P.; Zhang, G.; Gong, Y.; Yu, L., Low-concentration polymers inhibit and accelerate crystal growth in organic glasses in correlation with segmental mobility. *The Journal of Physical Chemistry B* **2013**, *117* (35), 10334-10341.
13. Yao, X.; Neusaenger, A. L.; Yu, L., Amorphous Drug-Polymer Salts. *Pharmaceutics* **2021**, *13* (8), 1271.
14. Ghebremeskel, A. N.; Vemavarapu, C.; Lodaya, M., Use of surfactants as plasticizers in preparing solid dispersions of poorly soluble API: stability testing of selected solid dispersions. *Pharmaceutical research* **2006**, *23* (8), 1928-1936.
15. Mosquera-Giraldo, L. I.; Trasi, N. S.; Taylor, L. S., Impact of surfactants on the crystal growth of amorphous celecoxib. *International journal of pharmaceutics* **2014**, *461* (1-2), 251-257.

16. Kovalchuk, N. M.; Simmons, M. J., Surfactant-mediated wetting and spreading: Recent advances and applications. *Current Opinion in Colloid & Interface Science* **2021**, *51*, 101375.
17. Huang, C.; Chen, Z.; Gui, Y.; Shi, C.; Zhang, G. G.; Yu, L., Crystal nucleation rates in glass-forming molecular liquids: D-sorbitol, D-arabitol, D-xylitol, and glycerol. *The Journal of chemical physics* **2018**, *149* (5), 054503.
18. Fokin, V. M.; Zanotto, E. D.; Yuritsyn, N. S.; Schmelzer, J. W., Homogeneous crystal nucleation in silicate glasses: A 40 years perspective. *Journal of Non-Crystalline Solids* **2006**, *352* (26-27), 2681-2714.
19. Yao, X.; Huang, C.; Benson, E. G.; Shi, C.; Zhang, G. G.; Yu, L., Effect of polymers on crystallization in glass-forming molecular liquids: equal suppression of nucleation and growth and master curve for prediction. *Crystal Growth & Design* **2019**, *20* (1), 237-244.
20. Zhang, J.; Liu, Z.; Wu, H.; Cai, T., Effect of polymeric excipients on nucleation and crystal growth kinetics of amorphous fluconazole. *Biomaterials Science* **2021**, *9* (12), 4308-4316.
21. Myers, D., *Surfactant science and technology*. John Wiley & Sons: 2020.
22. Gui, Y.; Yao, X.; Guzei, I. A.; Aristov, M. M.; Yu, J.; Yu, L., A Mechanism for Reversible Solid-State Transitions Involving Nitro Torsion. *Chemistry of Materials* **2020**, *32* (18), 7754-7765.
23. Gui, Y.; Huang, C.; Shi, C.; Zhang, G. G. Z.; Yu, L., Polymorphic Selection in Crystal Nucleation. *The Journal of chemical physics* **2022**, doi: 10.1063/5.0086308.
24. Gui, Y., *Phase Transitions in Molecular Solids: Understanding Polymorphic Transformation and Crystal Nucleation, and Engineering Amorphous Drugs for Global Health*. The University of Wisconsin-Madison: 2021.
25. Ishida, H.; Wu, T.; Yu, L., Sudden rise of crystal growth rate of nifedipine near T<sub>g</sub> without and with polyvinylpyrrolidone. *Journal of pharmaceutical sciences* **2007**, *96* (5), 1131-1138.
26. Sun, Y.; Tao, J.; Zhang, G. G.; Yu, L., Solubilities of crystalline drugs in polymers: an improved analytical method and comparison of solubilities of indomethacin and nifedipine in PVP, PVP/VA, and PVAc. *Journal of pharmaceutical sciences* **2010**, *99* (9), 4023-4031.
27. Ash, M.; Ash, I., *Handbook of industrial surfactants*. Synapse information resources: 2010.
28. Rosen, M. J.; Kunjappu, J. T., *Surfactants and interfacial phenomena*. John Wiley & Sons: 2012.
29. Yu, J.; Li, Y.; Yao, X.; Que, C.; Huang, L.; Hui, H.-W.; Gong, Y. G.; Yu, L., Surface Enrichment of Surfactants in Amorphous Drugs: An X-Ray Photoelectron Spectroscopy Study. *Molecular pharmaceuticals* **2022**, *19* (2), 654-660.
30. Fultz, B., *Phase transitions in materials*. Cambridge University Press: 2020.
31. Cheng, S.; McKenna, G. B., Isothermal Crystallization and Time-Temperature Transformation of Amorphous Nifedipine: A Case of Polymorphism Formation and Conversion. *Molecular Pharmaceuticals* **2021**, *18* (7), 2786-2802.
32. Chen, Z.; Yang, K.; Huang, C.; Zhu, A.; Yu, L.; Qian, F., Surface enrichment and depletion of the active ingredient in spray dried amorphous solid dispersions. *Pharmaceutical Research* **2018**, *35* (2), 1-11.

**Chapter 6. Amorphous Drug-Polymer Salt with High Stability  
under Tropical Conditions and Fast Dissolution: The Challenging  
Case of Lumefantrine-PAA**

Xin Yao, Soojin Kim, Yue Gui, Zhenxuan Chen, Junguang Yu, Karen J. Jones, Lian Yu

As published in:

*Journal of Pharmaceutical Sciences* **2021** 110(11), 3670-3677.

DOI: 10.1016/j.xphs.2021.07.018

## 6.1. Abstract

Lumefantrine (LMF), a high-mobility and easy-to-crystallize WHO drug for treating malaria, can form an amorphous salt with poly(acrylic acid) (PAA) that is remarkably stable against crystallization at high humidity and temperature and has fast dissolution rate. The amorphous salt up to 75 % drug loading was synthesized under a mild slurry condition easily implemented in basic facilities for global health. Salt formation was confirmed by IR spectroscopy and the much elevated glass transition temperature. At 50 % drug loading, the amorphous salt resists crystallization for at least 18 months under the highly stressful condition of 40 °C and 75 % RH. In contrast, the dispersion containing neutral LMF in PVP fully crystallized in 4 d and the dispersion in HPMCAS, a weak polyelectrolyte of lower charge density than PAA, crystallized by 50 % in 7 d. The amorphous salt at 50 % drug loading showed much faster dissolution than crystalline LMF: In SGF, the area under the curve (AUC) was 30 times larger within the gastric emptying time (4 h); in FaSSIF, the enhancement was even larger – by 200 times. Nanodroplets were detected during the dissolution in SGF, possibly accounting for the apparent enhancement of dissolution rate. The LMF-PAA example as a challenging case, along with the previously reported clofazimine-PAA, demonstrates the general utility of amorphous drug-polymer salts to achieve high stability under tropical conditions and enhanced dissolution and bioavailability.

**Keywords:** amorphous drug-polymer salt, lumefantrine, poly(acrylic acid), physical stability, tropical conditions, dissolution, nanodroplets

## 6.2. Introduction

Malaria is a global disease. In 2018 alone, 405 000 deaths were attributed to malaria, of which 67 % were children under 5.<sup>1</sup> Lumefantrine (LMF, Chart 1) is a WHO Essential Medicine for treating malaria and preventing its recurrence. LMF was combined with artemether as a fixed-dose treatment in 1992, offering high efficacy and low toxicity.<sup>2-4</sup> The combination is one of the WHO-approved first-line treatments<sup>5</sup> and has benefited over 750 million patients worldwide.<sup>6</sup>

Despite its advantages, there is an acknowledged need to improve the bioavailability of LMF.<sup>6</sup> With its low solubility in water, LMF falls into the BCS II or BCS IV category.<sup>7,8</sup> The issue of low exposure has been noted especially for children under 5 and those taking drugs like mefloquine, rifampicin and efavirenz during treatment,<sup>5</sup> and can lead to treatment failure and recurrence of malaria. Recent work has shown that co-administration with fatty food can improve the bioavailability of LMF by 2-16 times.<sup>2,9,10</sup> This motivates development of other formulation approaches to improve bioavailability.

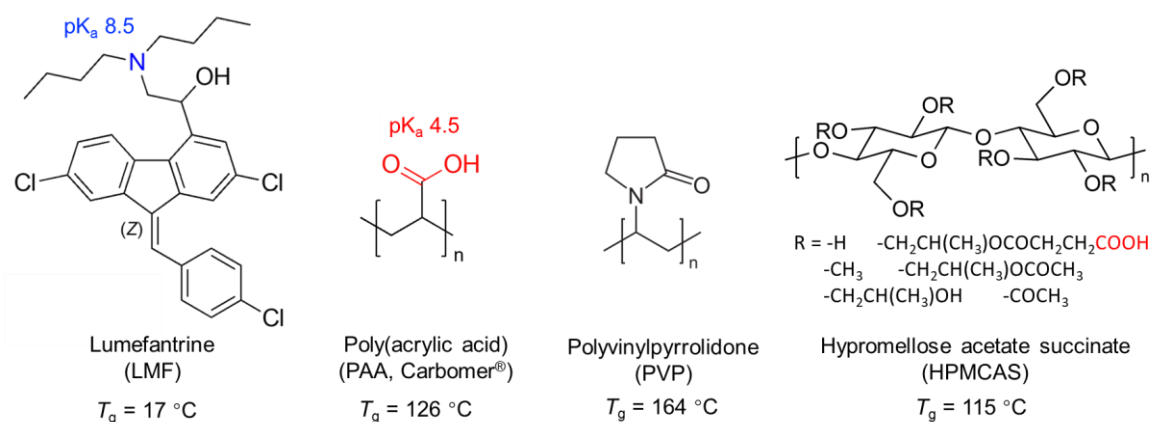


**Chart 1.** Chemical structures of lumefantrine (LMF), poly(acrylic acid) (PAA), polyvinylpyrrolidone (PVP), and hypromellose acetate succinate (HPMCAS).  $pK_a$  and  $T_g$  are given when relevant.



Amorphous formulations provide a general approach to improving solubility and bioavailability of drugs.<sup>11, 12</sup> While conventional formulations of LMF contain the crystalline drug, recent work by Novartis has shown that an amorphous solid dispersion (ASD) can significantly increase the bioavailability, by a factor of 24<sup>13</sup> (though few details were provided about the formulation). In this work, we investigate the use of amorphous drug-polymer salts to formulate LMF to achieve high physical stability and fast dissolution.

Given that malaria afflicts many developing countries in tropical and subtropical regions, medicines for treating malaria must be stable under the high-temperature, high-humidity conditions that often shorten shelf life. Under such conditions, amorphous drugs can crystallize rapidly, losing their advantages in dissolution rate and bioavailability. *This challenge is especially severe for a drug like LMF* for its low glass transition temperature ( $T_g = 17\text{ }^\circ\text{C}$ ). Under tropical conditions, the ambient temperature already exceeds the drug's  $T_g$ , leading to fast molecular motions and crystallization. The environmental moisture in tropical climates further exacerbates the problem by lowering the  $T_g$ .<sup>14, 15</sup> An ideal formulation for global health must be stable under tropical conditions without relying on costly environmental control.

In this work, we formulated LMF (a basic drug,  $pK_a = 8.5$ )<sup>16</sup> with an acidic polymer, poly(acrylic acid) (PAA,  $pK_a = 4.5$ ), into an amorphous salt to achieve high stability under tropical conditions. The polymer chosen for this study, PAA, has a high density of carboxylic acid groups, and its  $pK_a$  (4.5)<sup>16, 17</sup> is more than 2 units below that of LMF (8.5), enabling salt formation.<sup>18, 19</sup> A drug-polymer amorphous salt is expected to resist crystallization for several reasons. First, salt formation lowers the free energy to a greater extent than blending neutral components, a result of

the stronger ionic interactions. This in turn lowers the driving force for crystallization. Second, salt formation typically elevates a drug's  $T_g$  to a greater extent than mixing neutral components.<sup>17, 20-23</sup> This would decrease molecular mobility and slow crystallization. Finally, while crystalline salts are common between a drug and a small counter ion (inorganic or organic),<sup>24</sup> it is unlikely (perhaps impossible) for a drug-polymer salt to crystallize, because of the awkward packing required to co-crystallize a drug and a polymer. There has been limited previous work on amorphous drug-polymer salts to gain stability. For example, polymer coatings have been deposited on amorphous drugs by local salt formation to inhibit surface crystallization;<sup>25-28</sup> polymeric counterions are doped in amorphous drugs to suppress bulk crystallization.<sup>29-32</sup> Recently, the approach of amorphous drug-polymer salt has been applied to clofazimine (CFZ) to vastly improve physical stability under tropical conditions and to enhance dissolution,<sup>32</sup> but as noted above, LMF presents fresh new challenges because of its low  $T_g$  and high mobility and serves as a needed test for the generality of the approach.

We report that an amorphous salt can form between LMF and PAA at high drug loading (up to 75 % by weight) and the salt is exceptionally stable against crystallization under tropical conditions and shows fast dissolution in bio-relevant media. LMF-PAA salt was synthesized using a simple slurry method under mild conditions, suitable for thermally unstable materials such as PAA and for deployment in rudimentary facilities. Salt formation was demonstrated by IR spectroscopy and elevation of  $T_g$ . At 50 % drug loading, the LMF-PAA amorphous salt showed no crystallization for at least 18 months under the highly stressful condition of 40 °C and 75 % RH, while the dispersion containing neutral LMF in PVP fully crystallized in 4 d under the same condition and the dispersion in HPMCAS, a weak polyelectrolyte of lower charge density

than PAA, crystallized by 50 % in 7 d. Despite its high stability, the amorphous salt dissolved much faster than crystalline LMF. At 50 % drug loading, the enhancement of dissolution rate in SGF was a factor of 30 judging by the area under the curve (AUC) within the gastric emptying time (4 h), and a factor of 200 in FaSSIF. Dynamic light scattering (DLS) detected nanodroplets during the dissolution test in SGF, which potentially explains the high drug concentration.

### 6.3. Materials and Methods

**Materials.** Poly(acrylic acid) (PAA, Carbomer,  $M_w = 450\ 000$  g/mol) was purchased from Sigma-Aldrich (St. Louis, MO), lumefantrine (LMF) from Nanjing Bilatchem Industrial Co. (Nanjing, China), dichloromethane (ChromAR grade) from Thermo Fisher Scientific (Fair Lawn, NJ), ethanol from Decon Laboratories (King of Prussia, PA), biorelevant dissolution media (FaSSIF and SGF) from Biorelevant.Com (UK), hypromellose acetate succinate (HPMCAS-MF) from Shin-Etsu Chemical Co. (Tokyo, Japan), and polyvinylpyrrolidone (PVP K30; Kollidon 30) from BASF (Germany). All materials were used as received.

**Preparation of LMF-PAA Amorphous Salts.** LMF and PAA were mixed in a vial at 25, 50 or 75 % drug loading. A mixed solvent of dichloromethane and ethanol (1:1 v/v) was added to the powder at a solid/liquid ratio of 1:4 (w/w). Each batch contained 400 mg of LMF. This paste-like mixture was stirred magnetically for 5 min at 75 °C maintained with a sand bath, and dried under vacuum at room temperature for 1 day. The solid product was ground and sieved to obtain particles in the size range 45-75  $\mu\text{m}$ . Amorphous LMF-PVP and LMF-HPMCAS solid dispersion were prepared by melting a mixture of LMF and PVP or HPMCAS at 135 °C, and cooling to room temperature. Every batch was tested by powder X-ray diffraction (PXRD) to

verify its amorphous character. The sodium salt of PAA was prepared by mixing PAA and NaOH at 1:1 molar ratio in the presence of a small amount of water. The mixture was then dried in vacuum.

Infrared (IR) spectroscopy was performed in transmission using a Bruker Equinox 55. A solid sample was ground with KBr, dried under vacuum, and pressed into a tablet 6 mm in diameter under a pressure of 6000 lb (Carver Press Auto M 3890, Wabash, IN). IR spectra were collected in the range 400–4000  $\text{cm}^{-1}$  at 4  $\text{cm}^{-1}$  resolution. Pure nitrogen gas was purged through the detector chamber to minimize interference from moisture. Spectra were analyzed by OPUS software (Bruker, Ettlingen, Germany). Powder X-ray Diffraction (PXRD) was performed with a Bruker D8 Advance X-ray diffractometer with a Cu  $K\alpha$  source ( $\lambda = 1.54056 \text{ \AA}$ ) operating at a tube load of 40 kV and 40 mA. A powder sample ~10 mg in mass was spread and flattened on a Si (510) zero-background holder and scanned between 3° and 40° ( $2\theta$ ) at a step size of 0.02° and a maximum scan rate of 1 s/step. Differential scanning calorimetry (DSC) was conducted with a TA Instruments Q2000 at 10 °C/min with nitrogen purge (50 mL/min). Thermogravimetric analysis (TGA) was performed with a TA Instrument SDT Q600 at 10 °C/min with nitrogen purge (100 mL/min). Dynamic light scattering (DLS) was performed with a Malvern Zetasizer Nano-ZS (Malvern, U.K.). Each sample solution was scanned three times, with the solutions of pure LMF and SGF as controls.

**Crystallization Studies.** Physical stability was tested at 40 °C and 75 % relative humidity (RH). The temperature was maintained with an oven with a 1 °C precision; 75 % RH was maintained

by a saturated NaCl solution. A powder sample was stored in a loosely-capped vial in a controlled environment and its PXRD pattern was recorded periodically.

**Dissolution.** Dissolution rates were measured at 37 °C in two biorelevant media: Simulated Gastric Fluid (SGF) and Fasted State Simulated Intestinal Fluid (FaSSIF). See Table 1 for the compositions of the two media. SGF was prepared by dissolving its components in Milli-Q water; FaSSIF was prepared by dissolving a commercial powder (Biorelevant.com) in a pH 6.5 buffer following the product instruction. 25 mg of crystalline LMF or 50 mg of LMF-PAA amorphous salt (50 % drug loading) was added in a dry dissolution vessel (100 mL, USP II apparatus) at 37 °C; 100 mL of SGF or FaSSIF prewarmed to 37 °C was poured into the vessel. Each powder tested was in the 45–75 µm sieve cut. The mixture was stirred at a paddle speed of 100 rpm. The start of stirring was taken as time zero. At each time point, 3 mL of solution was withdrawn from the vessel and replaced by 3 mL of the dissolution medium at 37 °C. The withdrawn solution was filtered through a 0.45 µm syringe filter, and its concentration was determined by UV–vis spectrometry (8453, Agilent Technologies, Inc.) at 338 nm<sup>33</sup> against a standard curve obtained by measuring LMF solutions of known concentrations. The standard solutions of LMF were prepared by diluting a concentrated DMSO solution of LMF in the corresponding medium. Each dissolution profile reported (concentration versus time) was the average of at least 3 independent measurements.

Table 1. Compositions of SGF and FaSSIF.

SGF (pH = 2)	FaSSIF (pH = 6.5)
	NaCl (106 mM)
NaCl (43 mM)	NaH <sub>2</sub> PO <sub>4</sub> (29 mM)
HCl (10 mM)	NaOH (10 mM)
SDS (3.5 mM)	Sodium taurocholate (3 mM)
	Soybean lecithin (0.75 mM)

**Tabletability Assessment.** Approximately 100 mg of powder was filled into a 6, 8, or 10 mm diameter die, and compressed using flat-faced punches on a Caver Press. The diameter, thickness, and weight of each tablet were measured after relaxation under ambient condition for 24 h. The diametrical breaking force was measured using a Varian VK 200 tablet hardness tester (Varian, Inc., NC). Tablet tensile strength was calculated from the diametrical breaking force and tablet dimensions using  $\sigma = 2F/(\pi DT)$ , where  $\sigma$  is tensile strength,  $F$  the breaking force,  $D$  the tablet diameter, and  $T$  the tablet thickness.

## 6.4. Results

**Salt Formation.** Figure 1(A) illustrates the experimental setup used to prepare an amorphous salt of LMF and PAA under a mild slurry condition. Solid components were mixed and stirred in the presence of a solvent with mild heating (75 °C). Figure 1(B) shows the PXRD patterns of the solid products formed under various conditions and after drying. Under a suitable condition, namely, Condition (a), an amorphous product is obtained, while the success of the preparation

depends on the slurry solvent used, as discussed below. The amount of residual solvent was measured using TGA. The weight loss is ~1 % at 120 °C, see Figure S1.

Figure 1(B) shows that the slurry solvent plays a key role in forming an amorphous LMF-PAA salt. With water, ethanol, or dichloromethane as solvent, the product was not fully amorphous under the conditions used. With the mixed solvent of CH<sub>2</sub>Cl<sub>2</sub> and ethanol, however, a fully amorphous material was obtained after a slurry time of 5 min. In this preparation process, the solvent is a mass-transport aid, helping the initial solid materials to disintegrate and react. It is likely that the synthetic method can be further improved. In the remainder of this work, we focus on the interesting properties of the amorphous drug-polymer salt.

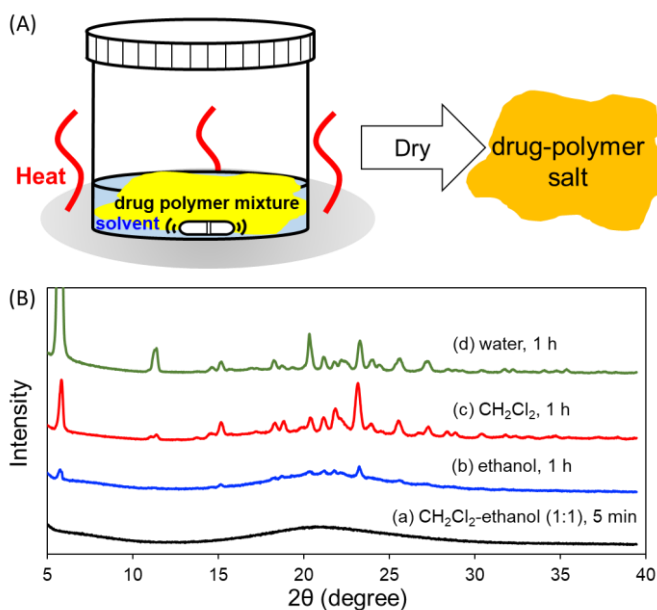


**Figure 1.** (A) Preparation of amorphous LMF-PAA salt. A drug-polymer mixture is stirred in the presence of a small amount of solvent with mild heating (75 °C). (B) PXRD patterns of reaction products formed under different conditions (slurry solvent and reaction time) as indicated. 50 % drug loading in all cases. The reaction was complete under Condition (a), producing a fully amorphous material, and incomplete under the other conditions.

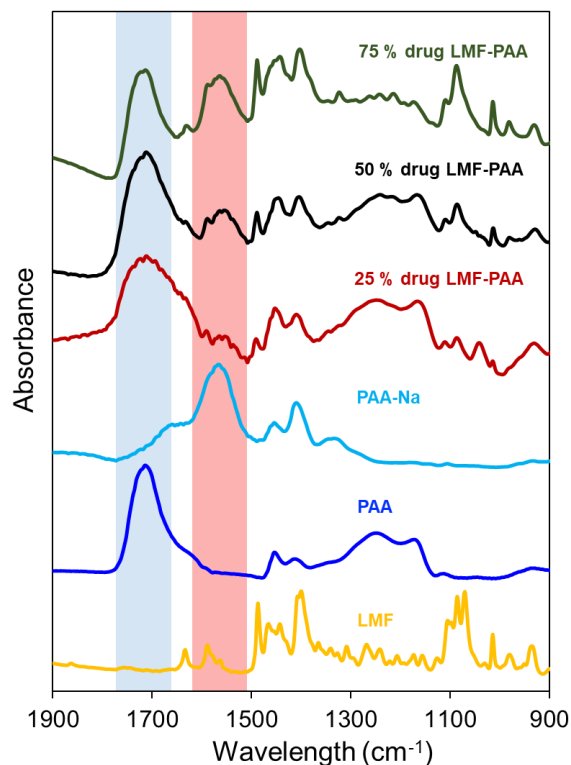


**Figure 2.** IR spectra of amorphous LMF-PAA salts and other materials for comparison. The peak at  $1700\text{ cm}^{-1}$  is due to C=O stretch of the  $-\text{COOH}$  group; the peak at  $1550\text{ cm}^{-1}$  is due to the antisymmetric stretch of the  $-\text{COO}^-$  ion. The ion peak increases with increase of drug loading, indicating the reaction between PAA and LMF and salt formation.

Salt formation between LMF and PAA was demonstrated by IR spectroscopy and elevated  $T_g$ . Figure 2 shows the IR spectra of the LMF-PAA reaction products prepared at different drug loading. Salt formation between a carboxylic acid and an amine is expected to produce a new peak at  $1550\text{ cm}^{-1}$  (antisymmetric stretch of  $-\text{COO}^-$ , as seen in the spectrum of the sodium salt of PAA, third spectrum from the bottom).<sup>34</sup> This peak is absent in the spectra of PAA and LMF, but present in their reaction product, indicating salt formation. The peak at  $1700\text{ cm}^{-1}$  is the C=O stretch of the  $-\text{COOH}$  group in PAA, and salt formation is expected to increase the ratio of the



1550  $\text{cm}^{-1}$  peak to the 1700  $\text{cm}^{-1}$  peak with increasing drug loading. This is also observed, further confirming salt formation.

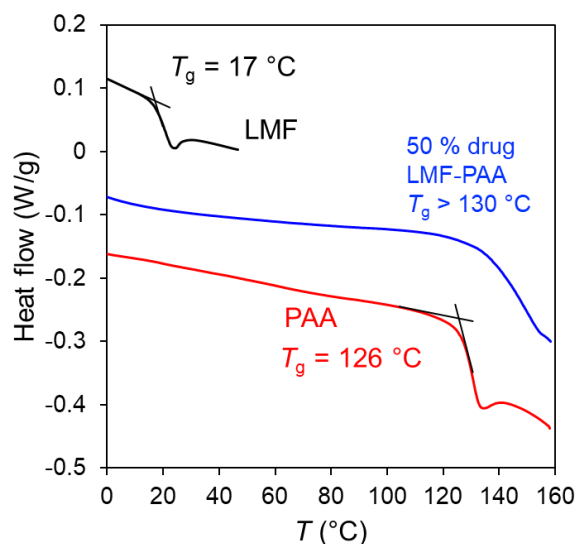


**Figure 3.** DSC traces of amorphous LMF, LMF-PAA salt, and PAA. The LMF-PAA salt has a higher  $T_g$  than LMF and PAA, indicating salt formation.

Figure 3 shows the DSC traces of amorphous LMF, an amorphous LMF-PAA salt (50 % drug loading), and PAA. The glass transition is detected as a step in heat flow. The  $T_g$  of LMF is 17 °C; the  $T_g$  of PAA is 126 °C. In contrast, the LMF-PAA salt does not show a glass transition below 130 °C, indicating its  $T_g$  is at a higher temperature (the downward signal above 140 °C is caused by the decomposition of PAA and obscures the detection of  $T_g$ ). This lower bound of  $T_g$  for the amorphous salt is much higher than the  $T_g$ s of LMF and PAA, consistent with salt formation. In a binary system without salt formation, the mixture's  $T_g$  is a weighted average of the  $T_g$ s of the pure components given by mixing rules such as the Fox equation. For example, the Fox equation correctly predicts the  $T_g$  of LMF-PVP K30 at 50 % drug loading (58 °C), which lies between the  $T_g$ s of PVP K30 (164 °C) and LMF (17 °C). The anomalously high  $T_g$  of LMF-PAA results from the strong ionic interactions between the drug and the polymer, after proton exchange and salt formation.<sup>17, 23</sup> This conclusion is consistent with the IR results described

above and with the expected proton transfer due to the larger-than-2 difference between the  $pK_a$  values of LMF (8.5) and PAA (4.5).<sup>18, 19</sup>

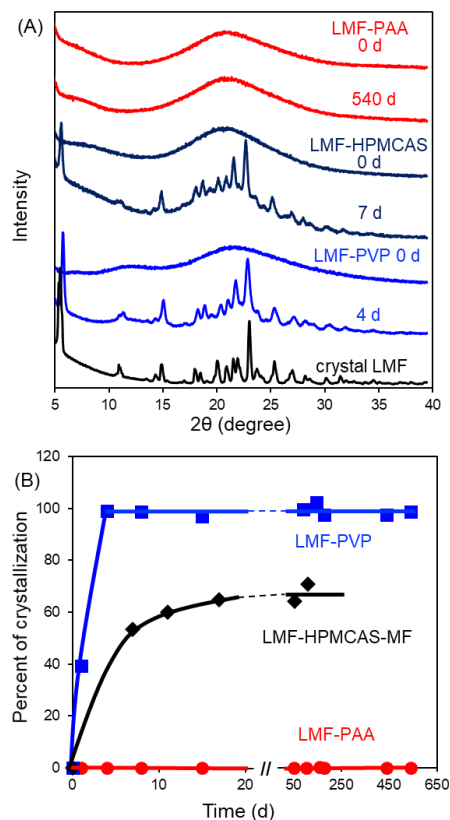


**Figure 4.** (A) PXRD patterns of amorphous LMF-PAA (amorphous salt), LMF-PVP (neutral dispersion), and LMF-HPMCAS after storage at 40 °C and 75 % RH. 50 % drug loading in both cases. (B) Percentage of crystallization as a function of time. The LMF-PAA salt did not crystallize, while the LMF-PVP ASD crystallized in 4 d and LMF-HPMCAS ASD crystallized in 7 d, demonstrating the stability of the drug-polymer salt at high temperature and humidity.

**Physical Stability.** The amorphous salt of LMF and PAA has remarkable stability against crystallization under the highly stressful condition of 40 °C and 75 % RH. Figure 4(A) shows the PXRD pattern of the amorphous salt as a function of storage time. No crystallization was detected in 540 d. In comparison, the amorphous dispersion of neutral LMF in PVP at the same drug loading (50 %) crystallized in 4 d, and the dispersion in HPMCAS, a weak polyelectrolyte

having much lower charge density than PAA, crystallized by 50 % in 7 d. In Figure 4(B), the percentage of crystallization is plotted against time for the two materials. Here the percentage of crystallization was calculated from the total intensity of the crystalline diffraction peaks relative to the amorphous halo. In addition, the stability of the LMF-PAA salt was tested at the highest drug loading attempted (75 %) (see Figure S2). The material remained mostly amorphous with only small and slow-changing crystalline peaks after 18 months of storage at 40 °C and 75 % RH. Thus, the formation of a drug-polymer salt vastly improves the stability of amorphous LMF against crystallization under a highly stressful condition. This result is consistent with a previous report on the enhanced stability of clofazimine upon salt formation with PAA.<sup>32</sup> It is noteworthy that although HPMCAS contains acidic groups, it has a much weaker stabilizing effect than PAA, presumably a result of its lower charge density.

Another indication of the physical stability of the amorphous drug-polymer salt is the integrity of the amorphous particles after storage at high temperature and humidity. After a few d at 40 °C and 75 % RH, the particles of LMF-PVP (the neutral ASD) became sticky and fused together. Over time, the material hardened again as crystallization occurred. In contrast, the particles of LMF-PAA (the drug-polymer salt) remained well separated and free flowing throughout storage. The transformation of the LMF-PVP particles is due to ~10 % moisture absorption, see Figure S2, which lowers the dry material's  $T_g$  (58 °C) below the storage temperature of 40 °C. This creates a sticky, viscous, easy-to-crystallize liquid; this liquid solidifies again upon crystallization. In the case of LMF-PAA, the  $T_g$  is elevated so much that moisture sorption (~4 %, see Figure S2) fails to lower it below the storage temperature and the material remains a free-

flowing powder. The physical stability of amorphous particles under harsh environmental conditions is important for pharmaceutical manufacturing and shelf stability in tropical climates.

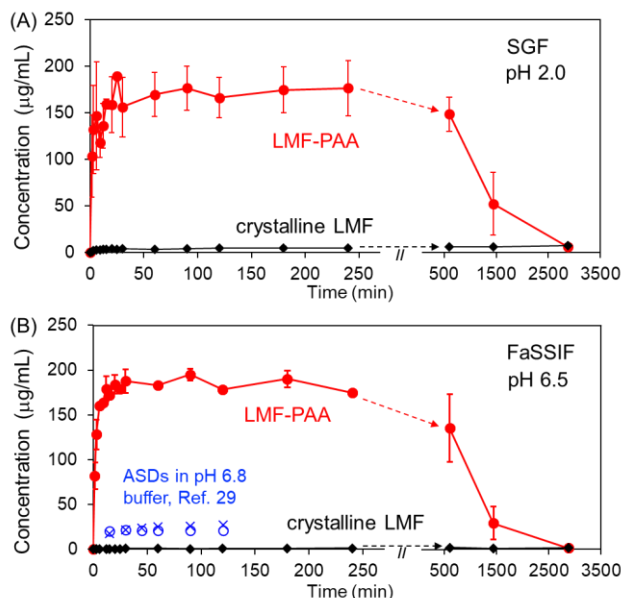


**Figure 5.** Dissolution kinetics of the amorphous LMF-PAA salt (50 % drug) and crystalline LMF in SGF (A) and FaSSIF (B). The amorphous salt reached much higher concentration than crystalline LMF. Within 4 h (stomach emptying time), the AUC of amorphous LMF-PAA is 30 times that of crystalline LMF in SGF and ~200 times in FaSSIF. Data from Ref. 29 are included in (B) for LMF-Eudragit L100 (X) and LMF-HPMCAS (O) dissolving in a pH 6.8 phosphate buffer.

**Dissolution.** The amorphous salt of LMF and PAA shows significantly faster dissolution than crystalline LMF. Figure 5 shows the dissolution kinetics of the amorphous salt at 50 % drug loading in Simulated Gastric Fluid (SGF) and Fasted State Simulated Intestinal Fluid (FaSSIF). In both media, the amorphous salt reached a substantially higher concentration than crystalline LMF in 30 min and maintained that concentration for at least 4 h. Within 4 h (the normal stomach emptying time), the area under the curve (AUC) of LMF-PAA amorphous salt is 30 times that of crystalline LMF in SGF and 200 times in FaSSIF.

After an extended plateau, the solution concentration gradually dropped over two d, finally arriving at the same concentration reached by LMF crystals. Upon equilibration, crystalline LMF reached a higher concentration in SGF (6  $\mu\text{g}/\text{mL}$ ) than in FaSSIF (1  $\mu\text{g}/\text{mL}$ ). To understand this difference, we analyzed the residual solids by PXRD, and the results (Figure 6) show that the residual solid after dissolution in SGF is different from the initial crystalline LMF, whereas the residual solid in FaSSIF is the same as the initial LMF crystal. That is, the final concentration in FaSSIF is the same as the initial LMF crystal. That is, the final concentration in FaSSIF is the solubility of crystalline LMF in the same medium, whereas the final concentration in SGF is the solubility of a different solid phase. Thus, we interpret the different final concentrations in SGF and FaSSIF as follows. The solubility of the LMF free base changes with pH according to:  $S_t = S_0(1 + 10^{\text{p}K_a - \text{pH}})$ , where  $S_0$  is the free-base solubility at high pH and  $\text{p}K_a = 8.5$ . Based on computer prediction,<sup>35</sup>  $S_0 = 0.03 \mu\text{g}/\text{mL}$ . At the FaSSIF pH (6.5), the solubility of

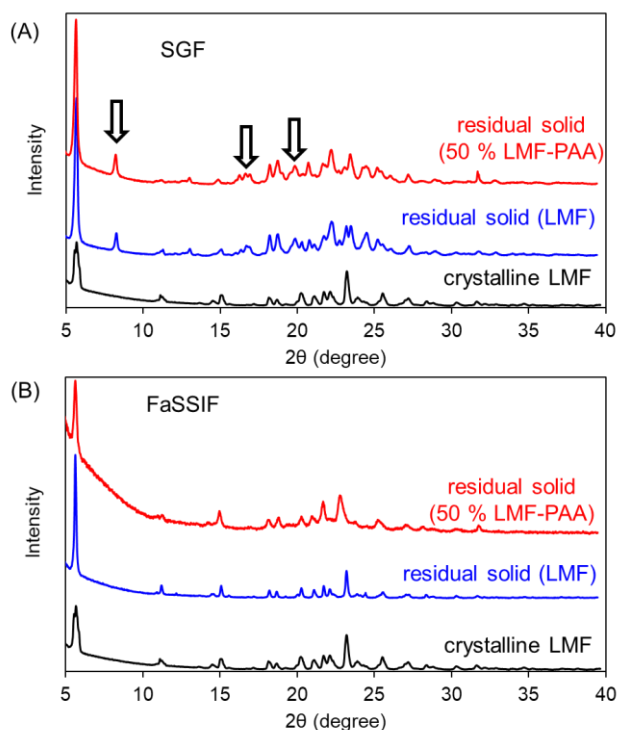


**Figure 6.** XRPD patterns of residual solids after dissolution. The final solid phase is crystalline LMF after equilibration with FaSSIF (B), but a different phase after equilibration with SGF (A). The peaks indicating a new solid form are labelled by the arrows.

LMF is elevated to  $S_t = 3 \mu\text{g/mL}$ , which roughly agrees with observed value of  $1 \mu\text{g/mL}$ . We interpret the new solid phase in equilibrium with SGF as a salt of LMF (not the amorphous drug-polymer salt), whose solubility is  $6 \mu\text{g/mL}$ .

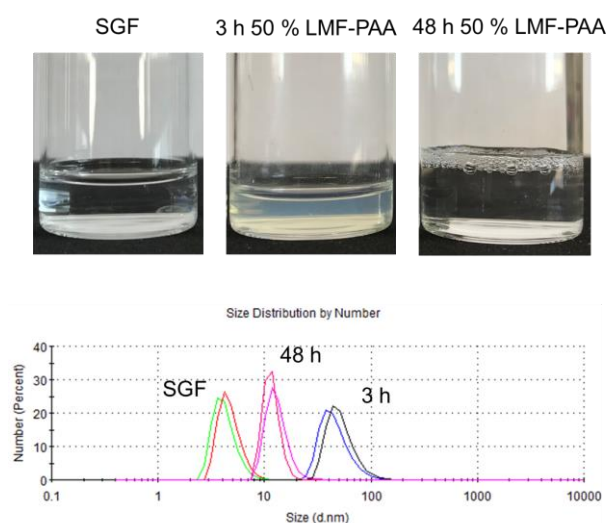


**Figure 7.** (A) Photographs of the pure SGF and the SGF containing dissolved LMF-PAA withdrawn after 3 and 48 h during the dissolution test. (B) DLS results of the three samples in (A). The results indicate the formation of nanodroplets during dissolution tests. Nanodroplets may play a role in the enhancement of dissolution.

Trasi et al. reported the dissolution kinetics of LMF-polymer ASDs in a pH 6.8 phosphate buffer,<sup>31</sup> and it is of interest to compare their result with ours. As dispersion polymers, Trasi et al. employed Eudragit L100 and HPMCAS, both having carboxylic acid groups but at a lower density than in PAA. Their result is plotted in Figure 5B since the pH of their medium (6.8) is close to that of FaSSIF (6.5). We observe that the amorphous salt of LMF and PAA reached a much higher solution concentration, by a factor of 9, than the ASDs of Trasi et al. Given that different dissolution conditions were used, we make no inference from this that the PAA formulation is superior.

It is noteworthy that the high density of acid groups in PAA means stronger ionic interactions in our amorphous salt, consistent with its high stability against crystallization. From this, one might expect *reduced* solubility and dissolution rate, but the data in Figure 5B indicate the opposite: the drug-polymer amorphous salt not only has high stability but also fast dissolution.

**Nano-Droplet Formation during Dissolution.** During dissolution in SGF, we noticed that the solution of the LMF-PAA amorphous salt appeared cloudy after 3 h, see Figure 7(A). The cloudiness persisted after filtration through a 0.45  $\mu\text{m}$  filter. On further equilibration, the cloudiness disappeared after 48 h, coincident with drop of solution concentration. DLS of the filtered solutions during dissolution test indicated formation of nano-droplets with a diameter of

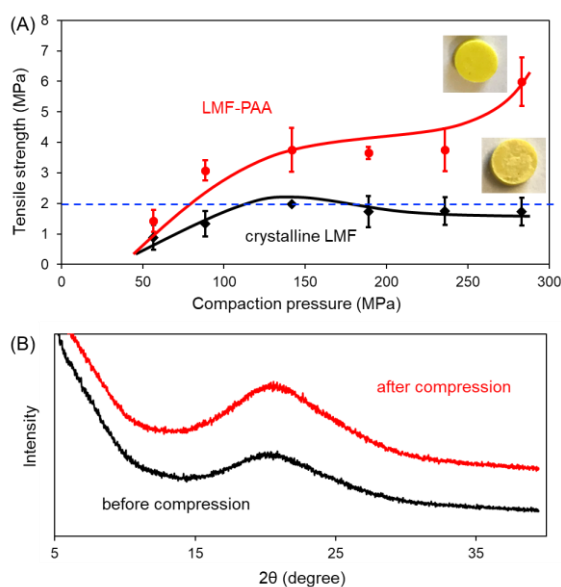


**Figure 8.** (A) Tensile strength of tablets prepared with crystalline LMF and amorphous LMF-PAA salt (50 % drug) as a function of compaction pressure. The LMF-PAA salt makes stronger tablets (red circles) than crystalline LMF (black diamonds) at all compaction pressures. The photographs show the tablets produced. (B) PXRD patterns of the amorphous drug-polymer salt before and after compression, indicating no crystallization during tableting.

~50 nm after 3 h, see Figure 7(B). After 48 h, the droplet size in the solution decreased to ~10 nm. The DLS results corroborated the visual observation and together they indicate the formation of colloidal particles during dissolution. As discussed below, these nano-droplets could play a role in the high concentration attained by LMF-PAA amorphous salt.<sup>36,37</sup> We did not perform the same analysis on the FaSSIF solutions because the medium was already cloudy after preparation, containing colloidal particles formed by bile salts and phospholipids.<sup>38,39</sup>

**Tabletability.** The LMF-PAA amorphous salt shows better tabletability than crystalline LMF. Figure 8 shows the tensile strengths of tablets formed at different compaction pressures. Tablets of the LMF-PAA salt were consistently stronger than those of the crystalline drug under all studied compaction pressures. The salt produced well-formed tablets with smooth surfaces, while crystalline LMF yielded chipped tablets with pitted surfaces (see pictures in Figure 8A). This is in part a result of crystalline LMF sticking to the punch and the die, while the LMF-PAA salt did not. The horizontal line in Figure 8 indicates the acceptable tensile strength for tablets (2 MPa). Except at the lowest compaction pressure, all tablets of LMF-PAA amorphous salt met the requirement, while the tablets of crystalline LMF did not.

During tableting, a large pressure is applied, potentially causing amorphous drugs to crystallize.<sup>40</sup> This possibility was tested for the LMF-PAA amorphous salt under a pressure of 350 MPa, much higher than the 100 MPa commonly used for tableting. No crystallization was detected after compression, see Figure 8 (B), indicating the LMF-PAA amorphous salt is stable under severe compression during tableting.



## 6.5. Discussion

This work has shown that the amorphous LMF-PAA salt has extraordinary stability against crystallization under the stressful condition of 40 °C and 75 % RH. The amorphous salt showed no crystallization for at least 540 d, while the neutral LMF-PVP dispersion fully crystallized in 4 d and LMF-HPMCAS, which forms slight acid-base interaction, crystallized by 50 % in 7 d. The finding is consistent with our previous work on CFZ using a similar approach,<sup>32</sup> but as noted earlier, LMF is a more challenging drug with sub-ambient  $T_g$  and this work performed the stability test for the longest time (540 d). The high stability against crystallization of the amorphous drug-polymer salt is manifest even in contact with a dissolution medium (Figures 5 and 6), where high supersaturation can be sustained for 10 h before gradually declining due to crystallization. These results argue that salt formation with a polymer can significantly improve the stability of an amorphous drug against crystallization.

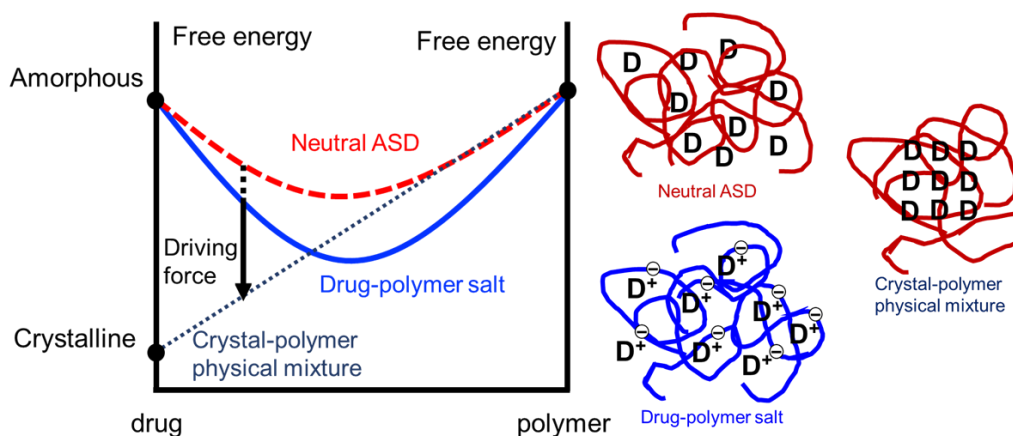


**Figure 9.** Free-energy diagram for crystallization. A drug-polymer salt has lower driving force for crystallization than a neutral ASD because of the strong ionic interactions. The drawings on the side represent a neutral ASD, a drug-polymer salt and the crystallized drug in a polymer matrix. “D” denotes a drug molecule. The drug is assumed to be a base and the polymer an acid.

Why is an amorphous drug-polymer salt so stable against crystallization at high temperature and high humidity? Crystallization requires a driving force as well as molecular mobility. The formation of a drug-polymer salt simultaneously reduces the driving force and the molecular mobility that enables crystallization. Because of strong ionic interactions, salt formation reduces the system's free energy to a greater extent than the mixing of neutral components. This is illustrated in Figure 9. This translates to a lower (even zero or negative) driving force for crystallization. In drawing Figure 9, we imagine a drug dissolved in a non-crystallizing polymer like PVP and PAA, for which the only practical pathway of crystallization is the formation of drug crystals. This is because it is nearly impossible for the drug and the polymer to crystallize together in the same unit cell.

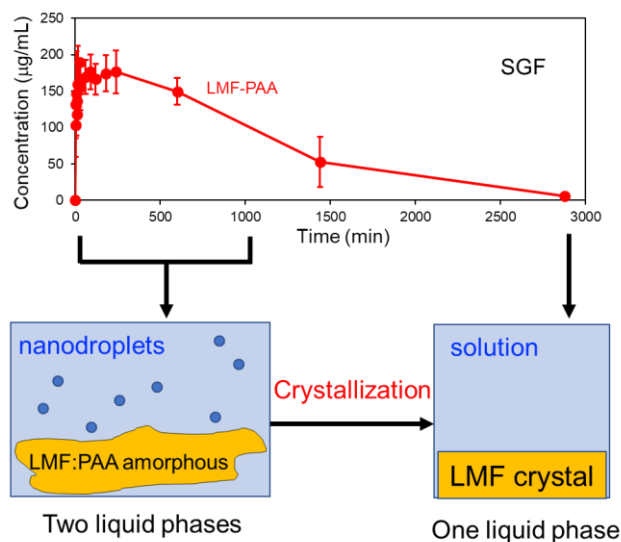


**Figure 10.** Diagram of the proposed dissolution process. Nanodroplets formed and contributed to the measured concentration. Crystallization happens over time and consumes the nanodroplets.

The low molecular mobility of an amorphous salt is a consequence of its high  $T_g$ . Forming a salt with PAA increases the  $T_g$  of LMF to a greater extent than forming a neutral ASD with PVP.

This means that at the same storage temperature, the amorphous salt is at a lower temperature relative to  $T_g$  than the neutral ASD. Given that amorphous systems have similar mobility at  $T_g$ , this means the amorphous salt has substantially lower mobility than the neutral ASD when stored at the same temperature. For the basic drug ketoconazole dispersed in various polymers,<sup>23</sup> the acidic polymer PAA slows down the relaxation time the most among the polymers tested, a result of ionic interactions. Our discussion above indicates that by forming a salt with a polymer, a drug has lower driving force to crystallize, as well as lower mobility to allow crystallization. This leads to high stability against crystallization.

We have observed the formation of nanodroplets during dissolution and this may be relevant for understanding the dissolution process. Despite the enhanced stability against crystallization, the amorphous drug-polymer salt offers large enhancement of solubility relative to the crystalline drug. It is possible that this good dissolution performance owes in part to the creation of colloidal particles. As shown in Figure 10, we imagine a dissolution process involving nano-droplets to occur as follows. At the beginning of dissolution, drug-rich nano-droplets form and they contribute to the high solution concentration measured. Crystallization occurs over time and the nanodroplets are gradually consumed. The final solution concentration is determined by the crystal solubility. It has been theorized that nanodroplets can serve as quick-response reservoirs in drug release.<sup>41</sup> In this regard, it may be of interest to learn whether a drug-polymer salt is more efficient in creating colloidal particles.

## 6.6. Conclusions

This work has shown that the important malaria drug lumefantrine (LMF) can form an amorphous salt with the polymer PAA through acid-base reaction. The amorphous salt can be conveniently synthesized up to 75 % drug loading using a simple slurry method suitable for thermally labile compounds and for deployment in basic facilities. The salt had remarkable stability against crystallization at high temperature and high humidity, as well as fast dissolution in bio-relevant media. The amorphous salt (50 % drug loading) resisted crystallization for at least 18 months at 40 °C with 75 % RH, while the dispersion in neutral PVP fully crystallized in 4 d and the dispersion in HPMCAS, a weak polyelectrolyte with lower charge density than PAA, crystallized by 50 % in 7 d. The enhanced stability owes to salt formation, which simultaneously lowers the driving force for crystallization and the molecular mobility enabling crystallization. Despite its outstanding stability, the amorphous drug-polymer salt showed high apparent solubility and fast dissolution, potentially a result of the formation of nanodroplets during dissolution that contributed to the solution concentration measured. The high resistance to crystallization allowed the amorphous drug-polymer salt to sustain high supersaturation during dissolution, a desirable feature for enhancing the bioavailability of LMF. Overall, the amorphous drug-polymer salt is a promising approach for formulating LMF-based malaria drugs and other medicines for global health to provide good stability under tropical conditions and fast dissolution. Among the questions raised by this work are: What is the optimal molecular weight of the polymer for salt formation that balances pharmaceutical performance and process convenience? Is an amorphous drug-polymer salt more likely to create stable colloidal particles during dissolution than a neutral ASD?

## 6.7. Acknowledgments

We thank the Bill and Melinda Gates Foundation (OPP1160408) for financial support, and Niya Bowers, Phil Goliber, and Ellen Harrington for helpful discussions. We also thank the Zeeh Pharmaceutical Experiment Station and the Analytical Instrumentation Center in School of Pharmacy at University of Wisconsin-Madison for instrument support, and Changlin Yao, Hao Wu, and Lauren Repp for experimental assistance.

## 6.8. Supporting Information

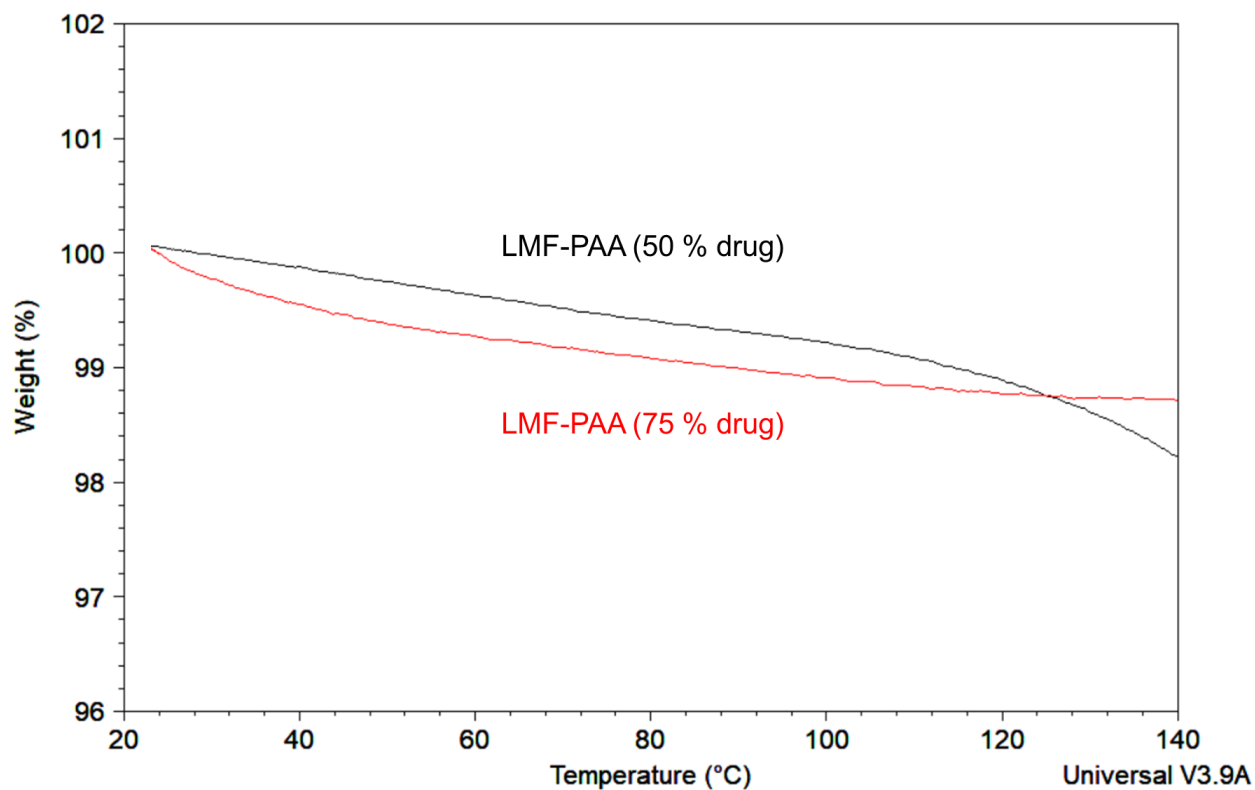


**Figure S1.** TGA traces of LMF-PAA salts with 50% and 75% drug loading. The residual solvent after preparation is 1% at 120 °C.

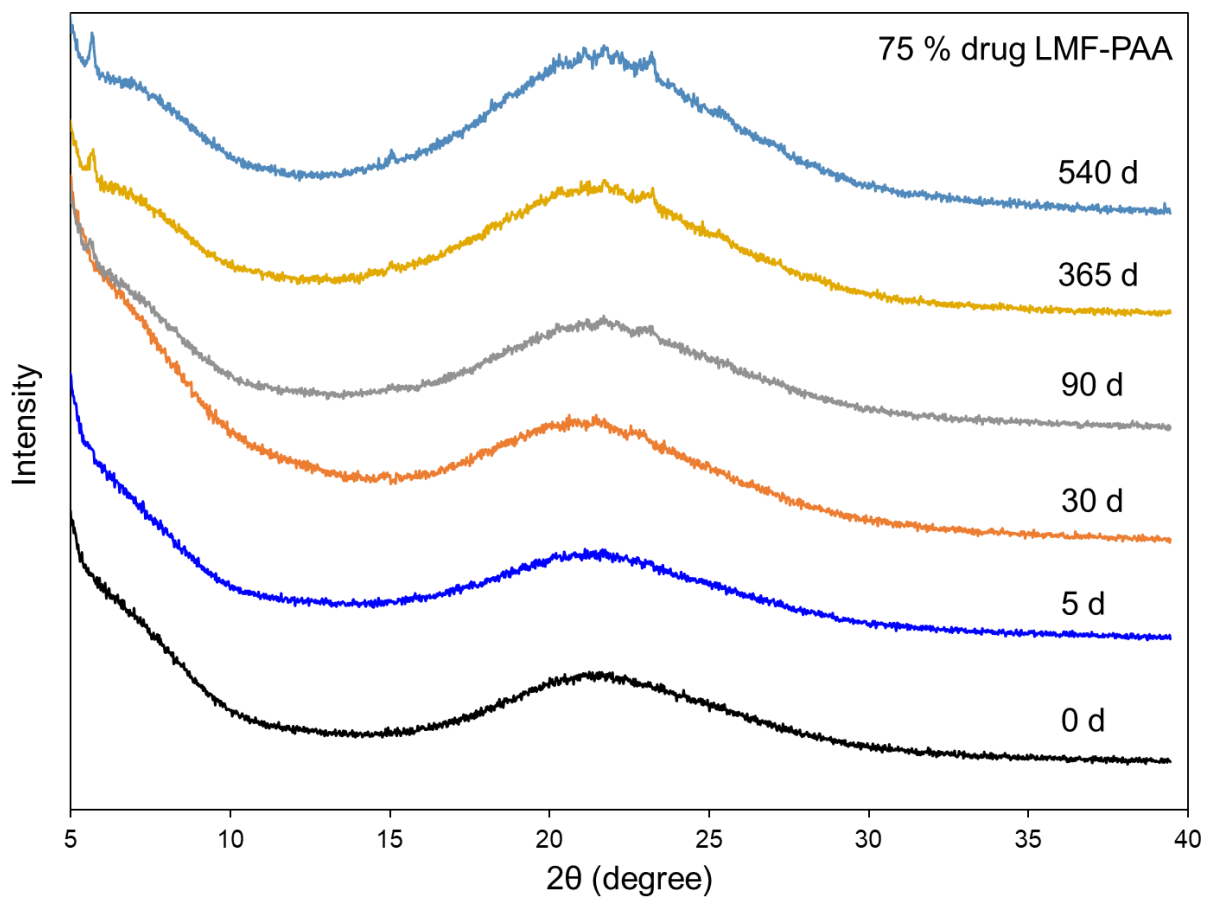


**Figure S2.** PXRD patterns of LMF-PAA salt at 75% drug loading during storage at 40 °C and 75% RH. Small peaks appeared after 90 d and grew very slowly afterward, with the material remaining mostly amorphous.

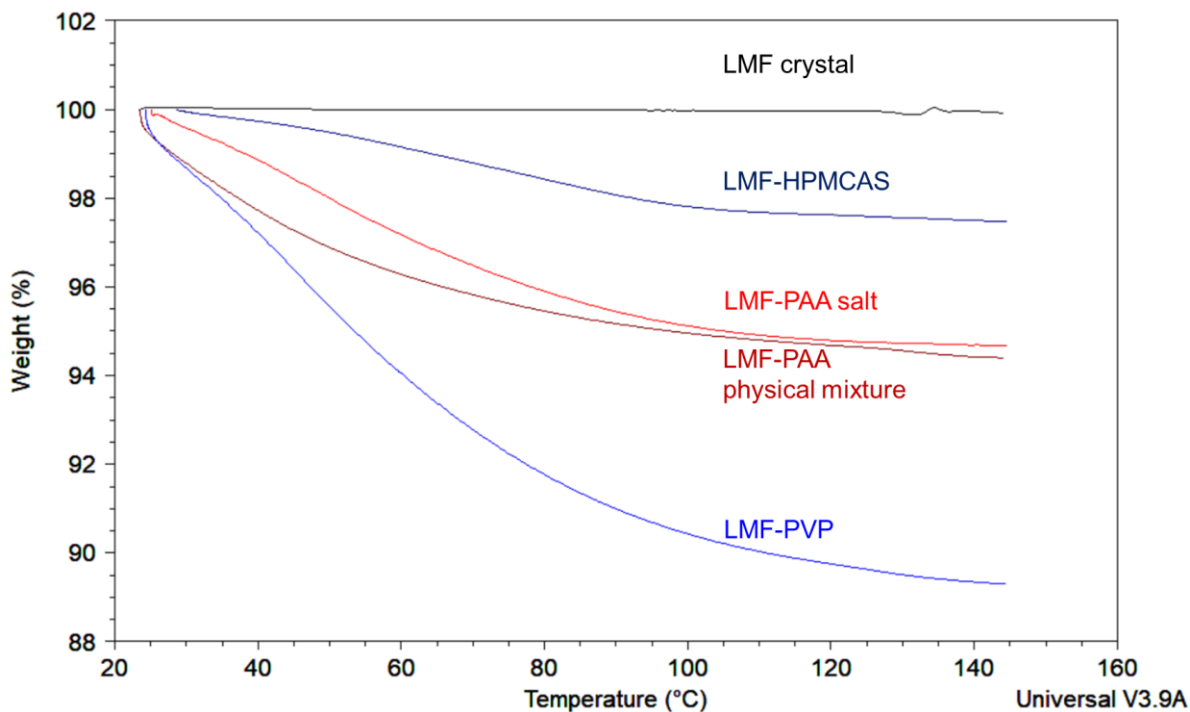


**Figure S3.** Water weight loss of crystalline LMF, LMF-PVP, LMF-HPMCAS, and LMF-PAA salt, and the LMF-PAA physical mixture after storage at 40 °C and 75% RH for at least 2 d. 50 % drug loading in all cases. Water absorption during storage ranged from 2% to 10%, depending on the polymer used.

## 6.9. References

1. Organization, W. H., World Malaria Report: World Health Organization. **2019**.
2. Lefèvre, G.; Thomsen, M. S., Clinical pharmacokinetics of artemether and lumefantrine (Riamet®). *Clinical Drug Investigation* **1999**, *18* (6), 467-480.
3. White, N. J.; van Vugt, M.; Ezzet, F. D., Clinical pharmacokinetics and pharmacodynamics of artemether-lumefantrine. *Clinical pharmacokinetics* **1999**, *37* (2), 105-125.
4. Omari, A. A.; Gamble, C.; Garner, P., Artemether-lumefantrine for uncomplicated malaria: a systematic review. *Tropical Medicine & International Health* **2004**, *9* (2), 192-199.
5. Organization, W. H., *Guidelines for the treatment of malaria*. World Health Organization: 2015.
6. Novartis. Annual report 2015. Novartis Pharma AG, Basel, Switzerland.
7. Lindenberg, M.; Kopp, S.; Dressman, J. B., Classification of orally administered drugs on the World Health Organization Model list of Essential Medicines according to the biopharmaceutics classification system. *European Journal of Pharmaceutics and Biopharmaceutics* **2004**, *58* (2), 265-278.

8. Anna, B.; Harisha, K.; Uday, K., Development, characterization and evaluation of solid dispersion of Artemether and Lumefantrine solvent evaporation method using hydrophilic polymers. *Int. J Pharm Pharm Sci* **2014**, *6* (2), 180-185.
9. Borrmann, S.; Sallas, W. M.; Machevo, S.; González, R.; Björkman, A.; Mårtensson, A.; Hamel, M.; Juma, E.; Peshu, J.; Ogutu, B., The effect of food consumption on lumefantrine bioavailability in African children receiving artemether–lumefantrine crushed or dispersible tablets (Coartem®) for acute uncomplicated Plasmodium falciparum malaria. *Tropical Medicine & International Health* **2010**, *15* (4), 434-441.
10. Ashley, E. A.; Stepniewska, K.; Lindegårdh, N.; Annerberg, A.; Kham, A.; Brockman, A.; Singhasivanon, P.; White, N. J.; Nosten, F., How much fat is necessary to optimize lumefantrine oral bioavailability? *Tropical Medicine & International Health* **2007**, *12* (2), 195-200.
11. Yu, L., Amorphous pharmaceutical solids: preparation, characterization and stabilization. *Advanced drug delivery reviews* **2001**, *48* (1), 27-42.
12. Baghel, S.; Cathcart, H.; O'Reilly, N. J., Polymeric amorphous solid dispersions: a review of amorphization, crystallization, stabilization, solid-state characterization, and aqueous solubilization of biopharmaceutical classification system class II drugs. *Journal of pharmaceutical sciences* **2016**, *105* (9), 2527-2544.
13. Jain, J. P.; Leong, F. J.; Chen, L.; Kalluri, S.; Koradia, V.; Stein, D. S.; Wolf, M.-C.; Sunkara, G.; Kota, J., Bioavailability of lumefantrine is significantly enhanced with a novel formulation approach, an outcome from a randomized, open-label pharmacokinetic study in healthy volunteers. *Antimicrobial agents and chemotherapy* **2017**, *61* (9), e00868-17.
14. Levine, H.; SLADE, L., Water as a plasticizer: physico-chemical aspects of. *Water Science Reviews 3: Volume 3: Water Dynamics* **1988**, (3), 79.
15. Andronis, V.; Yoshioka, M.; Zografis, G., Effects of sorbed water on the crystallization of indomethacin from the amorphous state. *Journal of pharmaceutical sciences* **1997**, *86* (3), 346-351.
16. Song, Y.; Zemlyanov, D.; Chen, X.; Su, Z.; Nie, H.; Lubach, J. W.; Smith, D.; Byrn, S.; Pinal, R., Acid-base interactions in amorphous solid dispersions of lumefantrine prepared by spray-drying and hot-melt extrusion using X-ray photoelectron spectroscopy. *International journal of pharmaceutics* **2016**, *514* (2), 456-464.
17. Duggirala, N. K.; Li, J.; Kumar, N. K.; Gopinath, T.; Suryanarayanan, R., A supramolecular synthon approach to design amorphous solid dispersions with exceptional physical stability. *Chemical Communications* **2019**, *55* (39), 5551-5554.
18. Cruz-Cabeza, A. J., Acid–base crystalline complexes and the p K a rule. *CrystEngComm* **2012**, *14* (20), 6362-6365.
19. Li, Z. J.; Abramov, Y.; Bordner, J.; Leonard, J.; Medek, A.; Trask, A. V., Solid-state acid– base interactions in complexes of heterocyclic bases with dicarboxylic acids: crystallography, hydrogen bond analysis, and 15N NMR spectroscopy. *Journal of the American Chemical Society* **2006**, *128* (25), 8199-8210.
20. Telang, C.; Mujumdar, S.; Mathew, M., Improved physical stability of amorphous state through acid base interactions. *Journal of pharmaceutical sciences* **2009**, *98* (6), 2149-2159.
21. Tong, P.; Zografis, G., Solid-state characteristics of amorphous sodium indomethacin relative to its free acid. *Pharmaceutical research* **1999**, *16* (8), 1186-1192.
22. Tong, P.; Zografis, G., A study of amorphous molecular dispersions of indomethacin and its sodium salt. *Journal of pharmaceutical sciences* **2001**, *90* (12), 1991-2004.



23. Mistry, P.; Mohapatra, S.; Gopinath, T.; Vogt, F. G.; Suryanarayanan, R., Role of the strength of drug–polymer interactions on the molecular mobility and crystallization inhibition in ketoconazole solid dispersions. *Molecular pharmaceutics* **2015**, *12* (9), 3339-3350.
24. Stahl, P. H.; Wermuth, C. G., *Pharmaceutical salts: Properties, selection and use*. John Wiley & Sons: 2002.
25. Wu, T.; Sun, Y.; Li, N.; de Villiers, M. M.; Yu, L., Inhibiting surface crystallization of amorphous indomethacin by nanocoating. *Langmuir* **2007**, *23* (9), 5148-5153.
26. Li, Y.; Yu, J.; Hu, S.; Chen, Z.; Sacchetti, M.; Sun, C. C.; Yu, L., Polymer nanocoating of amorphous drugs for improving stability, dissolution, powder flow, and tabletability: The case of chitosan-coated indomethacin. *Molecular pharmaceutics* **2019**, *16* (3), 1305-1311.
27. Gui, Y.; Chen, Y.; Chen, Z.; Jones, K. J.; Yu, L., Improving stability and dissolution of amorphous cefazolin by polymer nano-coating. *Pharmaceutical research* **2019**, *36* (5), 1-7.
28. Zeng, A.; Yao, X.; Gui, Y.; Li, Y.; Jones, K. J.; Yu, L., Inhibiting surface crystallization and improving dissolution of amorphous lorazepam by dextran sulfate nanocoating. *Journal of Pharmaceutical Sciences* **2019**, *108* (7), 2391-2396.
29. Song, Y.; Zemlyanov, D.; Chen, X.; Nie, H.; Su, Z.; Fang, K.; Yang, X.; Smith, D.; Byrn, S.; Lubach, J. W., Acid–base interactions of polystyrene sulfonic acid in amorphous solid dispersions using a combined UV/FTIR/XPS/ssNMR study. *Molecular pharmaceutics* **2016**, *13* (2), 483-492.
30. Nie, H.; Su, Y.; Zhang, M.; Song, Y.; Leone, A.; Taylor, L. S.; Marsac, P. J.; Li, T.; Byrn, S. R., Solid-state spectroscopic investigation of molecular interactions between cefazolin and hypromellose phthalate in amorphous solid dispersions. *Molecular pharmaceutics* **2016**, *13* (11), 3964-3975.
31. Trasi, N. S.; Bhujbal, S. V.; Zemlyanov, D. Y.; Zhou, Q. T.; Taylor, L. S., Physical stability and release properties of lomefentanyl amorphous solid dispersion granules prepared by a simple solvent evaporation approach. *International journal of pharmaceutics: X* **2020**, *2*, 100052.
32. Gui, Y.; McCann, E. C.; Yao, X.; Li, Y.; Jones, K. J.; Yu, L., Amorphous drug–polymer salt with high stability under tropical conditions and fast dissolution: the case of cefazolin and poly (acrylic acid). *Molecular pharmaceutics* **2021**, *18* (3), 1364-1372.
33. Fule, R. A.; Meer, T. S.; Sav, A. R.; Amin, P. D., Dissolution rate enhancement and physicochemical characterization of artemether and lomefentanyl solid dispersions. *International Journal of Drug Delivery* **2012**, *4* (1), 95.
34. Kirwan, L. J.; Fawell, P. D.; van Bronswijk, W., In situ FTIR-ATR examination of poly (acrylic acid) adsorbed onto hematite at low pH. *Langmuir* **2003**, *19* (14), 5802-5807.
35. Tetko, I. V.; Tanchuk, V. Y., Application of associative neural networks for prediction of lipophilicity in ALOGPS 2.1 program. *Journal of chemical information and computer sciences* **2002**, *42* (5), 1136-1145.
36. Alonzo, D. E.; Gao, Y.; Zhou, D.; Mo, H.; Zhang, G. G.; Taylor, L. S., Dissolution and precipitation behavior of amorphous solid dispersions. *Journal of pharmaceutical sciences* **2011**, *100* (8), 3316-3331.
37. Jackson, M. J.; Kestur, U. S.; Hussain, M. A.; Taylor, L. S., Dissolution of danazol amorphous solid dispersions: supersaturation and phase behavior as a function of drug loading and polymer type. *Molecular pharmaceutics* **2016**, *13* (1), 223-231.

38. Roos, C.; Dahlgren, D.; Sjögren, E.; Sjöblom, M.; Hedeland, M.; Lennernäs, H., Jejunal absorption of aprepitant from nanosuspensions: Role of particle size, prandial state and mucus layer. *European Journal of Pharmaceutics and Biopharmaceutics* **2018**, *132*, 222-230.
39. Fatouros, D. G.; Walrand, I.; Bergenstahl, B.; Müllertz, A., Colloidal structures in media simulating intestinal fed state conditions with and without lipolysis products. *Pharmaceutical research* **2009**, *26* (2), 361-374.
40. Thakral, N. K.; Mohapatra, S.; Stephenson, G. A.; Suryanarayanan, R., Compression-induced crystallization of amorphous indomethacin in tablets: characterization of spatial heterogeneity by two-dimensional X-ray diffractometry. *Molecular pharmaceutics* **2015**, *12* (1), 253-263.
41. Indulkar, A. S.; Gao, Y.; Raina, S. A.; Zhang, G. G.; Taylor, L. S., Exploiting the phenomenon of liquid–liquid phase separation for enhanced and sustained membrane transport of a poorly water-soluble drug. *Molecular pharmaceutics* **2016**, *13* (6), 2059-2069.

## Chapter 7. Amorphous Drug–Polymer Salts

Xin Yao, Amy Lan Neusaenger, Lian Yu

As published in:

*Pharmaceutics*. **2021** 13(8):1271.

DOI: 10.3390/pharmaceutics13081271

## 7.1. Abstract

Amorphous formulations provide a general approach to improving the solubility and bioavailability of drugs. Amorphous medicines for global health should resist crystallization under the stressful tropical conditions (high temperature and humidity) and often require high drug loading. We discuss the recent progress in employing drug–polymer salts to meet these goals. Through local salt formation, an ultra-thin polyelectrolyte coating can form on the surface of amorphous drugs, immobilizing interfacial molecules and inhibiting fast crystal growth at the surface. The coated particles show improved wetting and dissolution. By forming an amorphous drug–polymer salt throughout the bulk, stability can be vastly enhanced against crystallization under tropical conditions without sacrificing the dissolution rate. Examples of these approaches are given, along with suggestions for future work.

**Keywords:** amorphous; crystallization; tropical conditions; global health; polyelectrolytes; coating; drug–polymer salt

## 7.2. Introduction

An amorphous drug has a higher solubility than its crystalline counterpart, providing a general approach to improving the solubility and bioavailability of drugs <sup>1-3</sup>. Drugs considered for amorphous formulations are often hydrophobic and poorly water soluble, belonging to Class II and IV of the Biopharmaceuticals Classification System. These drugs are often dispersed in hydrophilic polymers, producing the so-called amorphous solid dispersions (ASDs), to help their dispersion and dissolution in water.

Medicines for global health should be stable under the highly stressful tropical conditions (high temperature and high humidity) and often require high drug loading. These requirements present additional challenges for amorphous formulations. Moisture is a potent mobility-enhancer and can dramatically accelerate the crystallization of amorphous drugs <sup>4,5</sup>, especially when combined with high temperature. For this reason, the combination of 40 °C and 75% RH (the “G condition”) is the harshest for pharmaceutical stability testing and the highest bar for the stability of amorphous drugs. High drug loading is desirable for those global-health medicines that have a high pill burden; for example, treatment for HIV requires 3–12 pills per day <sup>6,7</sup>. High drug loading in a single dosage form reduces patient discomfort and improves compliance.

Here, we discuss our recent work performed with support from the Gates Foundation to develop stable amorphous formulations for global health. Based on the needs for global health discussed above, our goal is a low-cost manufacturing strategy for amorphous formulations with high drug loading and high stability under tropical conditions. We show that amorphous drug–polymer salts offer a promising approach toward this goal. This strategy can be implemented by (1) local salt formation (polyelectrolyte coating) on the surface of an amorphous drug and (2) uniform salt formation throughout the bulk. We provide examples that illustrate this strategy and the improvement of formulation performance as a result.

A drug–polymer salt is produced by an acid-base reaction between a small-molecule drug and an ionizable polymer (polyelectrolyte). Although salt formation is a common approach in drug development,<sup>8-11</sup> the counterions are typically small inorganic ions or small organic ions, not

charged polymers. We will demonstrate the special advantages of polymeric counterions in salt formation. In the context of amorphous formulations, a salt formed with a polymeric counterion has greater resistance to crystallization than a salt formed with a small inorganic or organic counterion. This is a result of the awkward packing required for a drug and a polymer to crystallize together. Additionally, polyelectrolytes tend to be hydrophilic, and their incorporation into a drug formulation improves wetting and dispersion in water. A polymer has a lower solubility than its monomer or oligomers and provides stronger adhesion to solid surfaces. As a result, polyelectrolytes are often good coating materials, while low-molecular-weight materials could fail for this purpose.

A polyelectrolyte is a polymer in which all (or nearly all) monomer units can be ionized depending on pH. Polyelectrolytes are useful as viscosity enhancers (thickeners), emulsifiers, modifiers/stabilizers of colloidal structures, and coating materials. They have many applications in a vast array of industries. Many polyelectrolytes are acceptable ingredients in food and drugs; for example, pectin as a thickener and gelling agent in jams and jellies.<sup>12</sup> Polyelectrolytes are used to stabilize nanoparticle suspensions.<sup>13</sup> They play an important role in the formulation of hydrogels with unique characteristics such as self-healing and viscoelasticity (important for bioplastics)<sup>14</sup> and responsiveness to external stimuli (useful for sensors and drug delivery vehicles).<sup>15-18</sup> A key application of polyelectrolytes for this work is their ability to produce ultra-thin coatings through electrostatic deposition and layer-by-layer assembly.<sup>19</sup> The ultra-thin coatings have been used to control drug release,<sup>20</sup> stabilize drug delivery vehicles,<sup>21</sup> and protect medical devices from causing fungal infections.<sup>22</sup> This work is concerned with the applications of polyelectrolytes in stabilizing amorphous drugs.

As illustrated in Figure 1, we investigate two modes of salt formation between an amorphous drug and a polymer. Polyelectrolytes are used to form ultra-thin coatings on the surface of amorphous drugs (left). An acidic drug exposes negative charges in an aqueous medium (with  $\text{pH} > \text{pK}_a$ ) and can be coated with polycations. Likewise, a basic drug exposes positive charges in an aqueous medium (with  $\text{pH} < \text{pK}_a$ ) and can be coated with polyanions. Due to charge neutralization, a polyelectrolyte coating is extremely thin, approximately a monolayer, a property useful for achieving a high drug loading. On the right of Figure 1, we show similar processes of salt formation but shift our focus to the bulk material. By reacting acidic (basic) drugs with basic (acidic) polymers, amorphous salts can be formed throughout the materials, not just on the surface. These two modes of salt formation will be discussed in Sections 2 and 3.

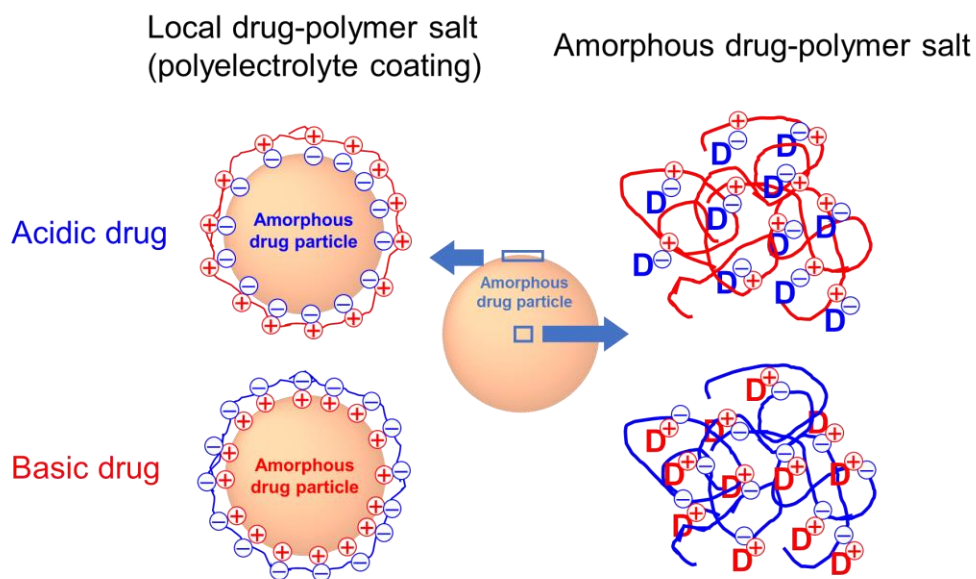


**Figure 1.** The two types of salt formation between drugs and polyelectrolytes investigated in this work. Left: Local salt formation (polyelectrolytes coating) on the surface of amorphous particles. Right: Uniform amorphous drug-polymer salt throughout the bulk. Each sphere represents an amorphous solid particle. “D” designates a drug molecule.

### 7.3. Polyelectrolyte Coating

Recent work has shown that amorphous drugs can grow crystals much faster at the free surface than in the bulk.<sup>23-28</sup> This is a result of the high mobility of molecules on the surface<sup>29-33</sup> and has motivated the development of surface coatings to stabilize amorphous drugs. Figure 2A shows the diffusion constants measured on the surface and in the interior of molecular glasses, many of which are amorphous drugs. Surface diffusion can be much faster than bulk diffusion by up to eight orders of magnitude when compared at the glass transition temperature  $T_g$ , and the difference increases with cooling.<sup>34, 35</sup> High surface mobility is a result of fewer neighbors surrounding a surface molecule relative to a bulk molecule, making it freer to move. The greater variation of surface mobility relative to bulk mobility is a consequence of the different degrees to which surface molecules are liberated relative to bulk molecules.

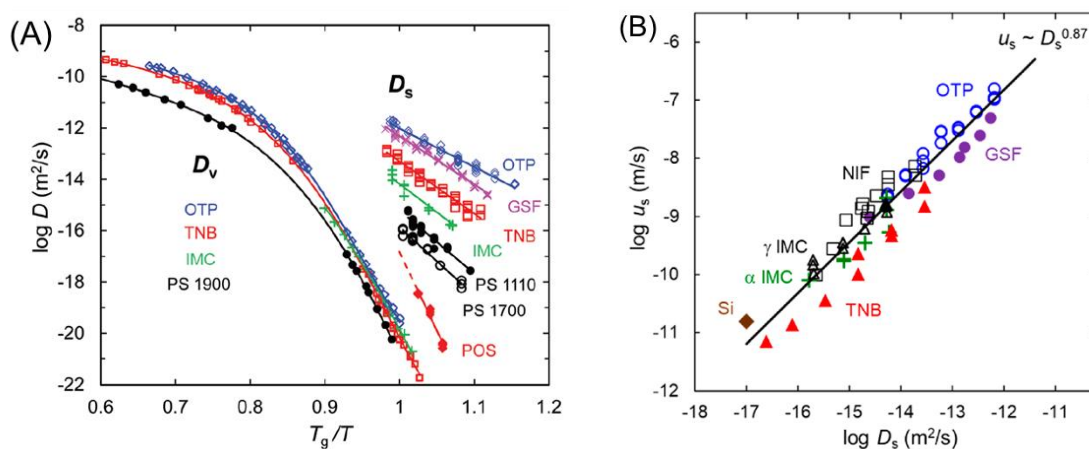


**Figure 2.** (A) Diffusion coefficient on the surface ( $D_s$ ) and in the bulk ( $D_v$ ) of several glass-forming molecular liquids against a  $T_g$ -scaled temperature [33]. Reproduced with permission from [33], Royal Society of Chemistry, 2020. (B) Crystal growth rate on the surface  $u_s$  plotted against the surface diffusion coefficient  $D_s$  for molecular glasses and amorphous silicon. OTP: ortho-terphenyl. GSF: griseofulvin. TNB: tris-naphthyl benzene. NIF: nifedipine. IMC: indomethacin. POS: posaconazole. PS: polystyrene oligomers [35]. Reproduced with permission from [35], American Chemical Society, 2017.



Fast surface diffusion leads to fast surface crystal growth. In Figure 2B, the surface crystal growth rate  $u_s$  is plotted against the surface diffusion coefficient  $D_s$ , and we observe a nearly proportional relation,  $u_s \sim D_s^{0.87}$ . That is, the faster the surface diffusion, the faster the surface crystal growth by about the same factor. This supports the notion that surface crystal growth is controlled by surface diffusion.<sup>34, 35</sup> This conclusion is further supported by the fact that surface crystals grow upward and laterally without deep penetration into the bulk and are surrounded by grooves created by the surface motion of molecules toward the crystal.<sup>36, 37</sup>

Fast surface crystallization presents a significant threat to the stability of amorphous drugs. All amorphous formulations have free surfaces and internal voids where crystallization can be accelerated by enhanced surface mobility. The problem worsens for formulations with high surface-to-volume ratios, including powders, thin films, and nanoparticles.<sup>23</sup> However, since surface crystallization is highly localized, the problem can be solved with a local solution—surface coatings. A coating, in essence, converts surface molecules into bulk molecules, thus eliminating surface crystallization. As we discuss below, surface coating by polyelectrolytes provides an ultra-thin nano-coating with many advantages: stability against crystallization, high drug loading, improved wetting, fast dissolution, good powder flow, and direct tabletability. Table 1 shows examples of the polyelectrolyte coating of amorphous drugs. Specific examples are discussed below.

**Table 1.** Examples of polyelectrolyte-coated amorphous drugs.

<b>Drug</b>	<b>Polymer</b>	<b>Stability Against Crystallization</b>	<b>Other Benefits</b>	<b>Ref.</b>
<i>Acids</i>				
Indomethacin	PDDA	Stable at 40 °C/dry for 20 d, while uncoated sample fully crystallized	Improved flowability	[38]
Indomethacin	Eudragit EPO (dry coating)	Improved stability at 30 °C/23% or 42% RH, outperforming neutral polymer Soluplus	No tests performed	[39]
Indomethacin	Gelatin A and B	Inhibited surface crystal growth at 40 °C/dry	No tests performed	[40]
Indomethacin	Chitosan, gelatin A and B	Improved stability at 40 °C/dry, 40 °C/75% RH, and 30 °C/75% RH; chitosan outperformed gelatins	Improved powder flow, tabletability, and wetting and dissolution	[41]
<i>Bases</i>				
Clofazimine	Alginic acid	Stable at 90 °C/dry for 60 d, while the uncoated particles fully crystallized. Improved stability at 40 °C/75% RH	Improved wetting and dissolution	[42]
Nifedipine	Gelatin A and B	Inhibited surface crystal growth at 40 °C/dry	No tests performed	[40]
Loratadine	Dextran sulfate (DTS)	Improved stability at 40 °C/dry	No tests performed	[43]

Wu et al. first demonstrated the use of a polyelectrolyte coating to inhibit surface crystal growth on an amorphous drug.<sup>38</sup> They coated amorphous indomethacin (IMC), a weak acid with  $pK_a = 4.5$ , with the polycation PDDA (polydiallyldimethylammonium) in an aqueous solution. At the

coating pH (6.1), the IMC and PDDA are oppositely charged, allowing for electrostatic deposition and the reversal of surface charge (Figure 3). In contrast, the polyanion PSS (poly(styrenesulfonate)) cannot directly coat IMC due to charge repulsion, but it can deposit on a previously coated layer of PDDA. A multilayer coat can be produced by alternate deposition of PDDA and PSS. Wu et al. found that coated amorphous IMC is significantly more stable against crystallization than uncoated amorphous IMC. The effect is pronounced even with a single coat of PDDA: after 20 days at 40 °C, an uncoated sample is fully covered by crystals, while a coated sample has a coverage of only several percent. This ultra-thin coating helps achieve a very high drug loading and improves the flowability of drug powders (the angle of repose is reduced from 36° to 18°).

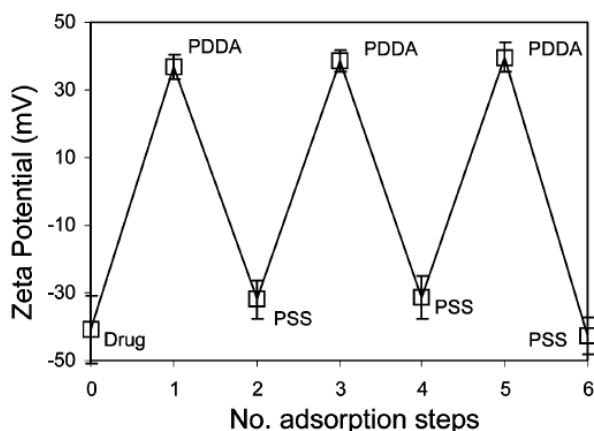


**Figure 3.** Zeta potential of amorphous IMC particles versus the number of adsorption steps [38]. Reproduced with permission from [38], American Chemical Society, 2007.

Further work on surface coating employed amorphous IMC as a model substrate and pharmaceutically acceptable polymers as coating materials (PDDA is not a pharmaceutical excipient). For example, Li et al. performed a comprehensive study of the effect of chitosan coating on the properties of amorphous IMC.<sup>41</sup> Chitosan is a natural basic polymer ( $pK_a = 6.5$ ).

Though weaker than PDDA as a polyelectrolyte, a chitosan coating similarly eliminates surface crystallization in IMC for samples tested in both film and particle geometries. Li et al. also compared chitosan with gelatin, an even weaker polyelectrolyte, as coating materials and found chitosan-coated particles to be more stable against crystallization and to remain free-flowing upon storage, whereas gelatin-coated particles became sticky after storage at high humidity and clumped together. Importantly, chitosan-coated amorphous particles dissolved in water faster than uncoated particles (Figure 4).<sup>41</sup> The improvement is a result of better wetting and the slower crystallization of coated particles during dissolution. These effects apparently outweigh the barrier effect of the polymer coating in drug release. The thin chitosan coating also improved powder flow and tableability.

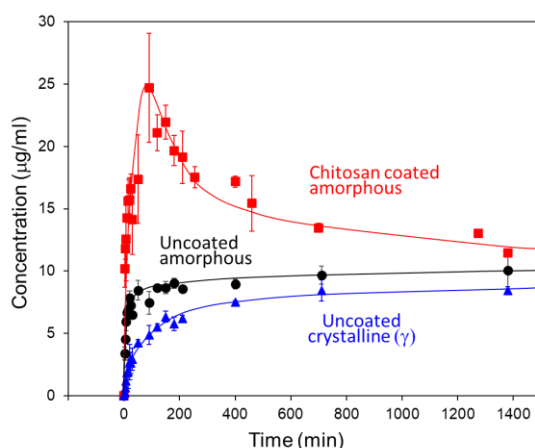


**Figure 4.** The effect of chitosan coating on the dissolution rate of amorphous IMC particles at 37 °C [41]. Reproduced with permission from [41], American Chemical Society, 2019.

Subsequent work on polyelectrolyte coating extended beyond the acidic drug IMC to include basic drugs (Table 1). These studies applied the same principle of coating illustrated in Figure 1 but used polyanions to coat the positively charged surfaces of basic drugs. For the basic drug clofazimine (CFZ,  $pK_a = 8.5$ ), Gui et al. investigated the coating of alginic acid ( $pK_a = 3.5$ ).<sup>42</sup>

They performed the coating in an aqueous solution at pH 7 so that the drug and the polymer were oppositely charged to allow for electrostatic deposition. The coating effect on stability was evaluated for particles stored at 90 °C and 40 °C/75% RH. At 90 °C, the coated particles did not crystallize in 60 days, while the uncoated particles fully crystallized. At 40 °C/75% RH, the coated particles crystallized approximately three times slower than the uncoated particles. The coated particles dissolved faster in Simulated Gastric Fluid (SGF) than the uncoated particles and showed more prolonged supersaturation (the “spring-and-parachute” profile). Within one hour, the coated particles dissolved two times faster than the uncoated amorphous particles and three times faster than the uncoated crystalline particles. As in the case of chitosan-coated IMC, the alginate coating improved the wetting of the coated particles and slowed their crystallization during dissolution.

Besides polyelectrolyte coatings, other coating methods have been used to improve the properties of amorphous formulations, both solvent-based<sup>44-48</sup> and solvent-free.<sup>39, 49-52</sup> Relative to the other methods, polyelectrolyte coatings applied via electrostatic deposition are characterized by extremely small thickness (several to tens of nanometers per layer). Even at this thickness, the coating eliminates surface crystallization. This coating method differs from many others in that an aqueous coating solution is used. An aqueous medium is compatible with poorly water-soluble drugs, in which they are present as undissolved, solid particles to be coated, while the use of organic solvents may dissolve the drugs. Polyelectrolyte coating is applied using a simple dip-coating process, which ensures coating uniformity. Owing to the small amount of coating material in the final product, this method helps achieve high drug loading while saving room in the formulation for other functional excipients. Enumerating these advantages is not to

imply that polyelectrolyte coating is superior to other coating methods in all respects. A thicker coating is required for applications where solid particles collide, causing coatings to wear off, and where a thicker layer is needed for the passage through the stomach for controlled release.

#### **7.4. Amorphous Drug–Polymer Salts in the Bulk**

Although a thin surface coating can eliminate surface crystallization, many amorphous drugs crystallize so rapidly in the bulk (especially under the stressful tropical conditions) that additional protection is needed. Furthermore, what appears to be a contiguous bulk material may, in fact, contain voids and fractures that lead to fast local crystallization.<sup>53</sup> This internal process can propagate in a vicious cycle through additional fracture and additional crystal growth.<sup>53</sup> There has been extensive work on the use of polymers as inhibitors of bulk crystallization.<sup>54-56</sup> The ensuing discussion focuses on the use of drug–polymer salts to stabilize amorphous formulations under what is perhaps the harshest condition for stability testing, 40 °C/75% RH, without sacrificing dissolution performance. This condition presents an ultimate separator for stabilization strategies. For example, surface-coated amorphous IMC is quite stable at 40 °C and in low humidity but quickly crystallizes at 40 °C/75% RH,<sup>41</sup> indicating the need for further stabilization.

In Table 2, we summarize the examples of amorphous drug–polymer salts with attention to synthetic methods, drug loading, stability at 40 °C/75% RH, and dissolution performance. This is followed by case studies and general comments.

**Table 2.** Examples of amorphous drug–polymer salts.

<b>Drug, % Loading</b>	<b>Polymer</b>	<b>Synthesis Method</b>	<b>Physical Stability</b>	<b>Other Benefits</b>	<b>Ref.</b>
<i>Acids</i>					
Naproxen, 42%	Eudragit EPO	Hot melt extrusion	Stable at 20 °C/60% RH for 12 mo.	Drug release triggered by inorganic salts	[57]
Mefenamic acid, 24%	Eudragit EPO, Eudragit L100	Cryogenic grinding	Stable at 25 °C/75% RH for 10 mo.	Extended supersaturation, enhanced dissolution	[58]
Lapatinib, 40% Gefitinib, 40%	PSSA	Solvent evaporation, cryogenic grinding	Stable at 40 °C/75% RH for 6 mo.	Faster dissolution than crystalline form	[59]
Indomethacin, 30%	Eudragit EPO	Solvent evaporation, cryogenic grinding	Stable at 40 °C/75% RH for 100 d. Neutral ASDs less stable	Enhanced dissolution	[60]
<i>Bases</i>					
Pyrimethamine, Lamotrigine, Trimethoprim, <65%	Polyacrylic acid (PAA)	Melt quench	Stable at 40 °C/75% RH for 6 mo. Pure drugs, neutral ASDs less stable	Fast dissolution relative to the crystalline and persisting supersaturation	[61]
Lumefantrine, 40%	CAP, HPMCP, Eudragit L100	Solvent evaporation	Stable at 40 °C/75% RH for 6 mo. Neutral ASDs less stable	CAP dispersion shows slow dissolution; others perform better	[62]
Clofazimine, 33–57%	HPMCP	Solvent evaporation	Not performed	Not performed	[63]
Clofazimine, 75%	PAA	Slurry conversion	Stable at 40 °C/75% RH for 6 mo. Neutral ASDs less stable	Improved flow, tableability, wetting, and dissolution	[64]

Lumefantrine, 50%	PAA	Slurry conversion	Stable at 40 °C/75% RH for 18 mo. Neutral ASDs less stable	Improved flow, tableability, and dissolution	[65]
Ciprofloxacin, 40%	Eudragit L	Ball milling	Stable at 25 °C/90% RH for 90 min. Improved stability over pure drug at 40 °C/75% RH	Improved solubility and drug permeability, persistent supersaturation	[66]
Ciprofloxacin, 80%	DTS	Precipitation by mixing drug and polymer solutions	Stable at 25 °C/55% RH for 1 mo.	Improved dissolution and supersaturation	[67]

Given the difficulty of processing high polymers, the method of forming drug–polymer salts deserves some discussion. According to the literature, drug–polymer salts can be prepared using many methods, including hot-melt extrusion (HME), ball milling, cryogenic milling, solvent evaporation such as spray- and freeze-drying, mixing solutions, and slurry conversion. The first two methods require no solvents. HME achieves the uniform mixing of components by heat, pressure, and physical mixing.<sup>68</sup> In ball milling and cryogenic grinding, solid components are mixed along with particle size reduction.<sup>69</sup> The other methods on the list above require the use of solvents, which help lower the processing temperature (necessary for thermally labile drugs and polymers) and increase the rate of mass transport.<sup>70</sup> The solvent evaporation method requires a common solvent for the drug and the polymer, which could be difficult to find when the polymer is hydrophilic (an electrolyte) and the drug is hydrophobic and poorly water soluble. The mixing of two solutions, one of the drug and the other of the polymer, has been used to prepare drug–polymer salts (“complexes”) and nanoparticles.<sup>64</sup> In our work, slurry conversion was used as a low-cost method to prepare amorphous drug–polymer salts.<sup>64</sup> In this method, solid components are mixed in the presence of a small amount of solvent with mild heating and stirring. Since



equilibration is slow in a polymer system, there is room for future optimization and innovation in engineering the structures of amorphous drug–polymer salts.

We illustrate the formation of amorphous drug–polymer salts and their pharmaceutical benefits using the reaction of the acidic polymer poly(acrylic acid) (PAA) with two basic drugs, clofazimine (CFZ)<sup>64</sup> and lumefantrine (LMF).<sup>65</sup> For both systems, a simple slurry method was used to produce the amorphous salt at a high drug loading (75% for CFZ–PAA and 50% for LMF–PAA). The synthesis was performed under a mild condition suitable for thermally unstable drugs and polymers. The salt formation was confirmed by spectroscopy, and we illustrate this for CFZ–PAA (Figure 5).<sup>64</sup> With increasing drug loading, the visible absorption spectrum initially does not change much but then undergoes a blue shift, eventually becoming the spectrum of the free base. The evolution is well fitted by a two-state model and exhibits an isosbestic point, indicating an equilibrium between the neutral and the ionized drug molecules. The spectral shift indicates a saturation drug loading of 70%, above which the drug–polymer mixture contains neutral drug molecules. For both CFZ and LMF, the salt formation with PAA elevates the glass transition temperature  $T_g$  above the  $T_g$  of the polymer (126 °C), indicating significant reduction of molecular mobility.

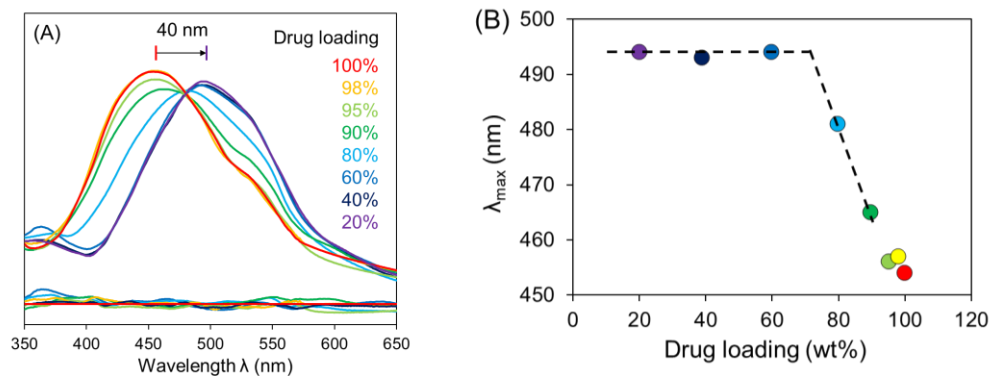


**Figure 5.** (A) Visible absorption spectra of amorphous CFZ–PAA films at different drug loading. (B)  $\lambda_{\text{max}}$  (wavelength of maximal absorption) vs. drug loading. The same color coding is used in (A) and (B). By extrapolation, the saturation drug loading is determined at 70% [64]. Reproduced with permission from [64], American Chemical Society, 2021.

For both CFZ and LMF, salt formation vastly improves the stability against crystallization at 40 °C/75% RH (Figure 6). No crystallization was observed in CFZ–PAA at 75% drug loading for at least 6 months, while the neutral dispersion of unionized CFZ in PVP or PVP/VA began crystallizing within weeks. In the case of the amorphous LMF–PAA salt (50% drug loading), no crystallization was observed for at least 18 months, while the neutral dispersion in PVP or HPMCAS began to crystallize within weeks. Despite the higher stability, these amorphous drug–polymer salts showed fast dissolution and extended supersaturation in biorelevant media SGF and FaSSIF.<sup>64, 65</sup> Their solid particles remained free flowing after storage at 40 °C/75% RH and showed improved tableability.

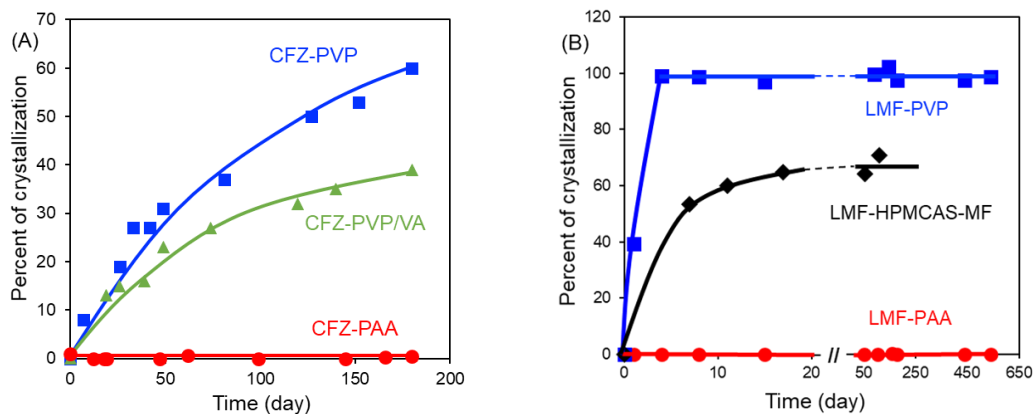


**Figure 6.** Stability of amorphous drug–polymer salts at 40 °C/75% RH. **(A)** CFZ–PAA (75% drug loading) [64]. No crystallization was observed in 6 months, while the neutral CFZ–PVP and CFZ–PVP/VA dispersions at the same drug loading both crystallized. Reproduced with permission from [64], American Chemical Society, 2021. **(B)** LMF–PAA salt (50% drug loading) [65]. No crystallization was observed after 18 months for LMF–PAA, while the neutral LMF–PVP and partially ionized LMF–HPMCAS dispersions at the same drug loading both crystallized. Reproduced with permission from [65], Elsevier, 2021.

When a comparison is possible, polymers that allow for salt formation with the drug appear to inhibit crystallization better than those that do not. Some of these cases are given in Table 2. For example, indomethacin is more stable when formulated with Eudragit EPO, a salt former, than with HPMC, a neutral, non-salt-forming polymer.<sup>60</sup> Clofazimine and lumefantrine, both bases, are more stable when formulated with an acidic polymer than with a neutral polymer.<sup>62, 64, 65</sup> This confirms the importance of salt formation on the stability of amorphous drug–polymer formulations.

Why is an amorphous drug–polymer salt so stable against crystallization at high temperatures and in high humidity? Crystallization requires a driving force and molecular mobility. The formation of a drug–polymer salt simultaneously reduces the driving force and molecular

mobility. Because of strong ionic interactions, salt formation reduces the system's free energy to a greater extent than the mixing of neutral components. This is illustrated in Figure 7. The large free energy of mixing leads to a lower (even zero or negative) driving force for crystallization. In Figure 7, we imagine a drug dissolved in a non-crystallizing polymer such as PVP and PAA, for which the only practical pathway of crystallization is the formation of drug crystals. This is because it is nearly impossible for the drug and the polymer to crystallize together in the same unit cell.

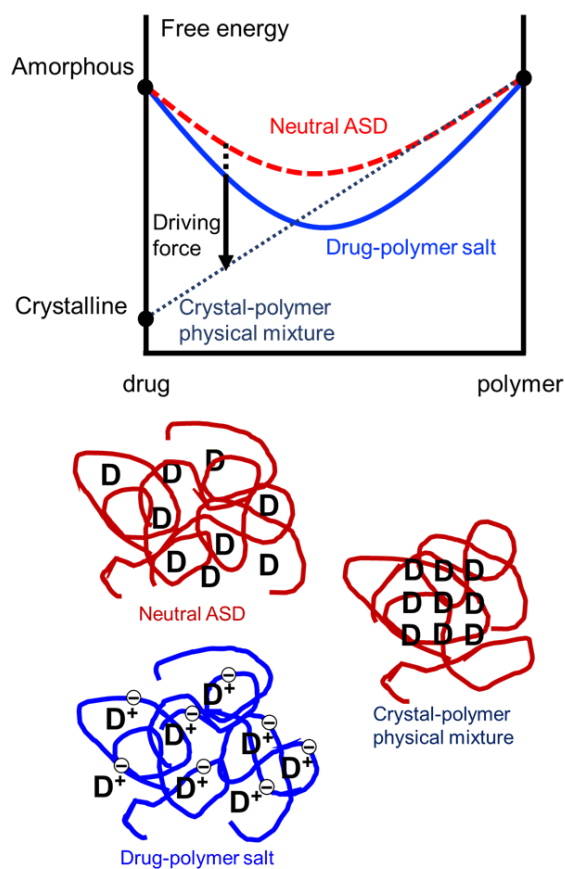


**Figure 7.** Free-energy diagram for crystallization in an amorphous salt and a neutral ASD. A drug–polymer salt has lower free energy than a neutral ASD because of the strong ionic interactions, leading to a lower driving force for crystallization. The drug is assumed to be a base. The drawings on the bottom represent a neutral ASD, a drug–polymer salt, and the crystallized drug in a polymer matrix [65]. Reproduced with permission from [65], Elsevier, 2021.

The low molecular mobility of an amorphous salt is a consequence of its high  $T_g$ . Salt formation is observed to elevate the  $T_g$  to a greater extent than the mixing of neutral components.<sup>64, 65</sup> Given that amorphous systems have similar mobility at  $T_g$ , this means that an amorphous salt has substantially lower mobility than a neutral dispersion when stored at the same temperature. Our discussion above indicates that by forming a salt with a polymer, a drug has a lower driving force to crystallize, as well as lower mobility available for crystallization. This leads to high stability against crystallization even under the highly stressful tropical conditions.

### **7.5. Concluding Remarks**

In this perspective, we discussed the role of drug–polymer salts in stabilizing amorphous drug formulations and improving other pharmaceutical properties. Through local salt formation, an ultra-thin layer of polyelectrolyte can be coated on the surface of amorphous drugs. The thin coating inhibits surface crystallization with a minute amount of coating material and improves wetting, dissolution, power flow, and tableting. With uniform salt formation throughout the bulk, stability against crystallization can be vastly improved under the harshest condition for stability testing, 40 °C/75% RH, without sacrificing the dissolution rate. This effect arises because of the difficulty or inability for the drug and the polymer to crystallize together, the significantly reduced driving force for crystallization, and the increased kinetic barrier for molecular motions. Despite their greater stability, amorphous drug–polymer salts can dissolve rapidly.

One possible area for future work is the optimization of the salt-forming process. The low mobility of high polymers makes the state of a drug–polymer mixture not only a matter of

thermodynamics (the tendency for mixing) but also a matter of kinetics (the rate of mixing). To illustrate the kinetic control in this context, consider the different manners in which a small amount (~1%) of the acidic polymer PAA can be incorporated into the basic drug clofazimine: depending on the processing conditions, PAA can be introduced as a surface coating or a bulk additive, both products being kinetically stable.<sup>64</sup> Such flexibility would be difficult to achieve with a small-molecule second component. At present, there are many methods for forming drug–polymer salts, both solvent-free and solvent-assisted. It is of interest to characterize the microstructures of these products for the uniformity and degree of ionization. One parameter to be optimized is the molecular weight of the polyelectrolyte for salt formation. A higher molecular weight could mean a higher  $T_g$  and better stability of the amorphous salt, but it might also lead to low solubility, slow drug release, and high viscosity of manufacturing solutions.<sup>71, 72</sup> Another parameter to be optimized is the drug–polymer ratio. For clofazimine–PAA (Figure 6), 70% is the maximal drug loading that ensures full ionization. It is of interest to learn whether this should be viewed as the upper limit for drug loading or if even higher loading should be attempted, yielding a mixture of salt and free base without sacrificing stability. These formulation parameters will need to be weighed against their impact on product performance, including stability and dissolution.

Another area of potential future work is the application of polyelectrolyte chemistry to improve drug delivery. Polyelectrolytes have been used to stabilize nanoparticle suspensions<sup>13</sup> and form hydrogels.<sup>14</sup> This property could be related to the observation of colloidal particles during the dissolution of amorphous drug–polymer salts.<sup>62, 65</sup> It is of interest to learn whether this is a general property of drug–polymer salts and, if so, whether it has any pharmaceutical applications.

An interesting property of drug–polymer salts is that drug release can be triggered by the increase in ionic strength.<sup>67</sup> This property could be useful for the controlled release of drugs.

## 7.6. Acknowledgments

We thank the Bill and Melinda Gates Foundation (OPP1160408) for financial support. We thank Niya Bowers, Phil Goliber, and Ellen Harrington for helpful discussions. We also thank Tian Wu, Rattavut Teerakapibal, Chengbin Huang, Yue Gui, Yuhui Li, Changquan Calvin Sun, and Aiguo Zeng for their contributions to the content of this perspective.

## 7.7. References

1. Yu, L., Amorphous pharmaceutical solids: preparation, characterization and stabilization. *Advanced drug delivery reviews* **2001**, *48* (1), 27-42.
2. Pandi, P.; Bulusu, R.; Kommineni, N.; Khan, W.; Singh, M., Amorphous solid dispersions: An update for preparation, characterization, mechanism on bioavailability, stability, regulatory considerations and marketed products. *International journal of pharmaceutics* **2020**, *586*, 119560.
3. Van den Mooter, G., The use of amorphous solid dispersions: A formulation strategy to overcome poor solubility and dissolution rate. *Drug Discovery Today: Technologies* **2012**, *9* (2), e79-e85.
4. Levine, H.; SLADE, L., Water as a plasticizer: physico-chemical aspects of. *Water Science Reviews 3: Volume 3: Water Dynamics* **1988**, (3), 79.
5. Andronis, V.; Yoshioka, M.; Zografu, G., Effects of sorbed water on the crystallization of indomethacin from the amorphous state. *Journal of pharmaceutical sciences* **1997**, *86* (3), 346-351.
6. Krentz, H. B.; Cosman, I.; Lee, K.; Ming, J. M.; Gill, M. J., Pill burden in HIV infection: 20 years of experience. *Antiviral therapy* **2012**, *17* (5), 833-840.
7. Hagedorff, A.; Freytag, S.; Müller, A.; Klebs, S., Pill burden in hypertensive patients treated with single-pill combination therapy—an observational study. *Advances in therapy* **2013**, *30* (4), 406-419.
8. Stahl, P. H.; Wermuth, C. G., *Pharmaceutical salts: Properties, selection and use*. John Wiley & sons: 2002.
9. Serajuddin, A. T., Salt formation to improve drug solubility. *Advanced drug delivery reviews* **2007**, *59* (7), 603-616.
10. Sun, C. C., Cocrystallization for successful drug delivery. *Expert opinion on drug delivery* **2013**, *10* (2), 201-213.

11. Karimi-Jafari, M.; Padrela, L.; Walker, G. M.; Croker, D. M., Creating cocrystals: A review of pharmaceutical cocrystal preparation routes and applications. *Crystal Growth & Design* **2018**, *18* (10), 6370-6387.
12. Thakur, B. R.; Singh, R. K.; Handa, A. K.; Rao, M., Chemistry and uses of pectin—a review. *Critical Reviews in Food Science & Nutrition* **1997**, *37* (1), 47-73.
13. Liufu, S.; Xiao, H.; Li, Y., Adsorption of poly (acrylic acid) onto the surface of titanium dioxide and the colloidal stability of aqueous suspension. *Journal of colloid and interface science* **2005**, *281* (1), 155-163.
14. Sun, S.; Mao, L. B.; Lei, Z.; Yu, S. H.; Cölfen, H., Hydrogels from amorphous calcium carbonate and polyacrylic acid: bio-inspired materials for "mineral plastics". *Angewandte Chemie International Edition* **2016**, *55* (39), 11765-11769.
15. Shang, J.; Shao, Z.; Chen, X., Electrical behavior of a natural polyelectrolyte hydrogel: chitosan/carboxymethylcellulose hydrogel. *Biomacromolecules* **2008**, *9* (4), 1208-1213.
16. Tan, C.; Wang, Q., Reversible terbium luminescent polyelectrolyte hydrogels for detection of H<sub>2</sub>PO<sub>4</sub><sup>-</sup> and HSO<sub>4</sub><sup>-</sup> in water. *Inorganic Chemistry* **2011**, *50* (7), 2953-2956.
17. Zhao, C.; Zhuang, X.; He, P.; Xiao, C.; He, C.; Sun, J.; Chen, X.; Jing, X., Synthesis of biodegradable thermo- and pH-responsive hydrogels for controlled drug release. *Polymer* **2009**, *50* (18), 4308-4316.
18. Shchukin, D. G.; Sukhorukov, G. B., Selective YF<sub>3</sub> nanoparticle formation in polyelectrolyte capsules as microcontainers for yttrium recovery from aqueous solutions. *Langmuir* **2003**, *19* (10), 4427-4431.
19. Lvov, Y.; Decher, G.; Moehwald, H., Assembly, structural characterization, and thermal behavior of layer-by-layer deposited ultrathin films of poly (vinyl sulfate) and poly (allylamine). *Langmuir* **1993**, *9* (2), 481-486.
20. Polomska, A.; Leroux, J. C.; Brambilla, D., Layer-by-Layer Coating of Solid Drug Cores: A Versatile Method to Improve Stability, Control Release and Tune Surface Properties. *Macromolecular Bioscience* **2017**, *17* (1), 1600228.
21. Donatan, S.; Yashchenok, A.; Khan, N.; Parakhonskiy, B.; Cocquyt, M.; Pinchasik, B.-E.; Khalkenow, D.; Möhwald, H.; Konrad, M.; Skirtach, A., Loading capacity versus enzyme activity in anisotropic and spherical calcium carbonate microparticles. *ACS applied materials & interfaces* **2016**, *8* (22), 14284-14292.
22. Karlsson, A. J.; Flessner, R. M.; Gellman, S. H.; Lynn, D. M.; Palecek, S. P., Polyelectrolyte multilayers fabricated from antifungal  $\beta$ -peptides: design of surfaces that exhibit antifungal activity against *Candida albicans*. *Biomacromolecules* **2010**, *11* (9), 2321-2328.
23. Wu, T.; Yu, L., Surface crystallization of indomethacin below T<sub>g</sub>. *Pharmaceutical research* **2006**, *23* (10), 2350-2355.
24. Zhu, L.; Wong, L.; Yu, L., Surface-enhanced crystallization of amorphous nifedipine. *Molecular pharmaceuticals* **2008**, *5* (6), 921-926.
25. Zhu, L.; Jona, J.; Nagapudi, K.; Wu, T., Fast surface crystallization of amorphous griseofulvin below T<sub>g</sub>. *Pharmaceutical research* **2010**, *27* (8), 1558-1567.
26. M. Gunn, E.; A. Guzei, I.; Yu, L., Does crystal density control fast surface crystal growth in glasses? A study with polymorphs. *Crystal growth & design* **2011**, *11* (9), 3979-3984.
27. Kestur, U. S.; Taylor, L. S., Evaluation of the crystal growth rate of felodipine polymorphs in the presence and absence of additives as a function of temperature. *Crystal growth & design* **2013**, *13* (10), 4349-4354.



28. Hasebe, M.; Musumeci, D.; Powell, C. T.; Cai, T.; Gunn, E.; Zhu, L.; Yu, L., Fast surface crystal growth on molecular glasses and its termination by the onset of fluidity. *The Journal of Physical Chemistry B* **2014**, *118* (27), 7638-7646.
29. Zhu, L.; Brian, C.; Swallen, S.; Straus, P.; Ediger, M.; Yu, L., Surface self-diffusion of an organic glass. *Physical Review Letters* **2011**, *106* (25), 256103.
30. Brian, C. W.; Yu, L., Surface self-diffusion of organic glasses. *The Journal of Physical Chemistry A* **2013**, *117* (50), 13303-13309.
31. Zhang, W.; Brian, C. W.; Yu, L., Fast surface diffusion of amorphous o-terphenyl and its competition with viscous flow in surface evolution. *The Journal of Physical Chemistry B* **2015**, *119* (15), 5071-5078.
32. Chen, Y.; Zhu, M.; Laventure, A.; Lebel, O.; Ediger, M.; Yu, L., Influence of hydrogen bonding on the surface diffusion of molecular glasses: Comparison of three triazines. *The Journal of Physical Chemistry B* **2017**, *121* (29), 7221-7227.
33. Li, Y.; Zhang, W.; Bishop, C.; Huang, C.; Ediger, M.; Yu, L., Surface diffusion in glasses of rod-like molecules posaconazole and itraconazole: Effect of interfacial molecular alignment and bulk penetration. *Soft Matter* **2020**, *16* (21), 5062-5070.
34. Yu, L., Surface mobility of molecular glasses and its importance in physical stability. *Advanced drug delivery reviews* **2016**, *100*, 3-9.
35. Huang, C.; Ruan, S.; Cai, T.; Yu, L., Fast surface diffusion and crystallization of amorphous griseofulvin. *The Journal of Physical Chemistry B* **2017**, *121* (40), 9463-9468.
36. Sun, Y.; Zhu, L.; Kearns, K. L.; Ediger, M. D.; Yu, L., Glasses crystallize rapidly at free surfaces by growing crystals upward. *Proceedings of the National Academy of Sciences* **2011**, *108* (15), 5990-5995.
37. Hasebe, M.; Musumeci, D.; Yu, L., Fast surface crystallization of molecular glasses: creation of depletion zones by surface diffusion and crystallization flux. *The Journal of Physical Chemistry B* **2015**, *119* (7), 3304-3311.
38. Wu, T.; Sun, Y.; Li, N.; de Villiers, M. M.; Yu, L., Inhibiting surface crystallization of amorphous indomethacin by nanocoating. *Langmuir* **2007**, *23* (9), 5148-5153.
39. Priemel, P. A.; Laitinen, R.; Barthold, S.; Grohganz, H.; Lehto, V.-P.; Rades, T.; Strachan, C. J., Inhibition of surface crystallisation of amorphous indomethacin particles in physical drug-polymer mixtures. *International journal of pharmaceutics* **2013**, *456* (2), 301-306.
40. Teerakapibal, R.; Gui, Y.; Yu, L., Gelatin nano-coating for inhibiting surface crystallization of amorphous drugs. *Pharmaceutical Research* **2018**, *35* (1), 1-7.
41. Li, Y.; Yu, J.; Hu, S.; Chen, Z.; Sachetti, M.; Sun, C. C.; Yu, L., Polymer nanocoating of amorphous drugs for improving stability, dissolution, powder flow, and tabletability: The case of chitosan-coated indomethacin. *Molecular pharmaceutics* **2019**, *16* (3), 1305-1311.
42. Gui, Y.; Chen, Y.; Chen, Z.; Jones, K. J.; Yu, L., Improving stability and dissolution of amorphous clofazimine by polymer nano-coating. *Pharmaceutical research* **2019**, *36* (5), 1-7.
43. Zeng, A.; Yao, X.; Gui, Y.; Li, Y.; Jones, K. J.; Yu, L., Inhibiting surface crystallization and improving dissolution of amorphous loratadine by dextran sulfate nanocoating. *Journal of Pharmaceutical Sciences* **2019**, *108* (7), 2391-2396.

44. Strydom, S.; Liebenberg, W.; Yu, L.; De Villiers, M., The effect of temperature and moisture on the amorphous-to-crystalline transformation of stavudine. *International journal of pharmaceutics* **2009**, *379* (1), 72-81.
45. Puri, V.; Dantuluri, A. K.; Bansal, A. K., Barrier coated drug layered particles for enhanced performance of amorphous solid dispersion dosage form. *Journal of pharmaceutical sciences* **2012**, *101* (1), 342-353.
46. Kawakami, K., Surface effects on the crystallization of ritonavir glass. *Journal of Pharmaceutical Sciences* **2015**, *104* (1), 276-279.
47. Hellrup, J.; Alderborn, G.; Mahlin, D., Inhibition of recrystallization of amorphous lactose in nanocomposites formed by spray-drying. *Journal of Pharmaceutical Sciences* **2015**, *104* (11), 3760-3769.
48. Novakovic, D.; Peltonen, L.; Isomäki, A.; Fraser-Miller, S. J.; Nielsen, L. H.; Laaksonen, T.; Strachan, C. J., Surface stabilization and dissolution rate improvement of amorphous compacts with thin polymer coatings: can we have it all? *Molecular pharmaceutics* **2020**, *17* (4), 1248-1260.
49. Capece, M.; Davé, R., Enhanced physical stability of amorphous drug formulations via dry polymer coating. *Journal of Pharmaceutical Sciences* **2015**, *104* (6), 2076-2084.
50. Chen, L.; Ding, X.; He, Z.; Fan, S.; Kunnath, K. T.; Zheng, K.; Davé, R. N., Surface engineered excipients: II. Simultaneous milling and dry coating for preparation of fine-grade microcrystalline cellulose with enhanced properties. *International journal of pharmaceutics* **2018**, *546* (1-2), 125-136.
51. Bannow, J.; Koren, L.; Salar-Behzadi, S.; Löbmann, K.; Zimmer, A.; Rades, T., Hot melt coating of amorphous Carvedilol. *Pharmaceutics* **2020**, *12* (6), 519.
52. Bosselmann, S.; Owens III, D. E.; Kennedy, R. L.; Herpin, M. J.; Williams III, R. O., Plasma deposited stability enhancement coating for amorphous ketoprofen. *European Journal of Pharmaceutics and Biopharmaceutics* **2011**, *78* (1), 67-74.
53. Powell, C. T.; Cai, T.; Hasebe, M.; Gunn, E. M.; Gao, P.; Zhang, G.; Gong, Y.; Yu, L., Low-concentration polymers inhibit and accelerate crystal growth in organic glasses in correlation with segmental mobility. *The Journal of Physical Chemistry B* **2013**, *117* (35), 10334-10341.
54. Kestur, U. S.; Lee, H.; Santiago, D.; Rinaldi, C.; Won, Y.-Y.; Taylor, L. S., Effects of the molecular weight and concentration of polymer additives, and temperature on the melt crystallization kinetics of a small drug molecule. *Crystal growth & design* **2010**, *10* (8), 3585-3595.
55. Kothari, K.; Ragoonanan, V.; Suryanarayanan, R., The role of drug-polymer hydrogen bonding interactions on the molecular mobility and physical stability of nifedipine solid dispersions. *Molecular pharmaceutics* **2015**, *12* (1), 162-170.
56. Huang, C.; Powell, C. T.; Sun, Y.; Cai, T.; Yu, L., Effect of low-concentration polymers on crystal growth in molecular glasses: a controlling role for polymer segmental mobility relative to host dynamics. *The Journal of Physical Chemistry B* **2017**, *121* (8), 1963-1971.
57. Kindermann, C.; Matthée, K.; Strohmeyer, J.; Sievert, F.; Breitzkreutz, J., Tailor-made release triggering from hot-melt extruded complexes of basic polyelectrolyte and poorly water-soluble drugs. *European journal of pharmaceutics and biopharmaceutics* **2011**, *79* (2), 372-381.
58. Kojima, T.; Higashi, K.; Suzuki, T.; Tomono, K.; Moribe, K.; Yamamoto, K., Stabilization of a supersaturated solution of mefenamic acid from a solid dispersion with EUDRAGIT® EPO. *Pharmaceutical research* **2012**, *29* (10), 2777-2791.

59. Song, Y.; Zemlyanov, D.; Chen, X.; Nie, H.; Su, Z.; Fang, K.; Yang, X.; Smith, D.; Byrn, S.; Lubach, J. W., Acid–base interactions of polystyrene sulfonic acid in amorphous solid dispersions using a combined UV/FTIR/XPS/ssNMR study. *Molecular pharmaceutics* **2016**, *13* (2), 483-492.
60. Xie, T.; Gao, W.; Taylor, L. S., Impact of Eudragit EPO and hydroxypropyl methylcellulose on drug release rate, supersaturation, precipitation outcome and redissolution rate of indomethacin amorphous solid dispersions. *International journal of pharmaceutics* **2017**, *531* (1), 313-323.
61. Duggirala, N. K.; Li, J.; Kumar, N. K.; Gopinath, T.; Suryanarayanan, R., A supramolecular synthon approach to design amorphous solid dispersions with exceptional physical stability. *Chemical Communications* **2019**, *55* (39), 5551-5554.
62. Trasi, N. S.; Bhujbal, S. V.; Zemlyanov, D. Y.; Zhou, Q. T.; Taylor, L. S., Physical stability and release properties of lumefantrine amorphous solid dispersion granules prepared by a simple solvent evaporation approach. *International journal of pharmaceutics: X* **2020**, *2*, 100052.
63. Nie, H.; Su, Y.; Zhang, M.; Song, Y.; Leone, A.; Taylor, L. S.; Marsac, P. J.; Li, T.; Byrn, S. R., Solid-state spectroscopic investigation of molecular interactions between clofazimine and hypromellose phthalate in amorphous solid dispersions. *Molecular pharmaceutics* **2016**, *13* (11), 3964-3975.
64. Gui, Y.; McCann, E. C.; Yao, X.; Li, Y.; Jones, K. J.; Yu, L., Amorphous drug–polymer salt with high stability under tropical conditions and fast dissolution: the case of clofazimine and poly (acrylic acid). *Molecular pharmaceutics* **2021**, *18* (3), 1364-1372.
65. Yao, X.; Kim, S.; Gui, Y.; Chen, Z.; Yu, J.; Jones, K. J.; Yu, L., Amorphous Drug–Polymer Salt with High Stability under Tropical Conditions and Fast Dissolution: The Challenging Case of Lumefantrine-PAA. *Journal of Pharmaceutical Sciences* **2021**, *110* (11), 3670-3677.
66. Mesallati, H.; Umerska, A.; Paluch, K. J.; Tajber, L., Amorphous polymeric drug salts as ionic solid dispersion forms of ciprofloxacin. *Molecular pharmaceutics* **2017**, *14* (7), 2209-2223.
67. Cheow, W. S.; Hadinoto, K., Self-assembled amorphous drug–polyelectrolyte nanoparticle complex with enhanced dissolution rate and saturation solubility. *Journal of colloid and interface science* **2012**, *367* (1), 518-526.
68. Chen, Y.-C.; Ho, H.-O.; Chiou, J.-D.; Sheu, M.-T., Physical and dissolution characterization of cilostazol solid dispersions prepared by hot melt granulation (HMG) and thermal adhesion granulation (TAG) methods. *International journal of pharmaceutics* **2014**, *473* (1-2), 458-468.
69. Caron, V.; Hu, Y.; Tajber, L.; Erxleben, A.; Corrigan, O. I.; McArdle, P.; Healy, A. M., Amorphous solid dispersions of sulfonamide/Soluplus® and sulfonamide/PVP prepared by ball milling. *Aaps Pharmscitech* **2013**, *14* (1), 464-474.
70. Szafraniec, J.; Antosik, A.; Knapik-Kowalczyk, J.; Gawlak, K.; Kurek, M.; Szlęk, J.; Jamróz, W.; Paluch, M.; Jachowicz, R., Molecular disorder of bicalutamide—amorphous solid dispersions obtained by solvent methods. *Pharmaceutics* **2018**, *10* (4), 194.
71. Puttipipatkachorn, S.; Nunthanid, J.; Yamamoto, K.; Peck, G., Drug physical state and drug–polymer interaction on drug release from chitosan matrix films. *Journal of controlled release* **2001**, *75* (1-2), 143-153.
72. Ko, J.; Park, H. J.; Hwang, S. J.; Park, J.; Lee, J., Preparation and characterization of chitosan microparticles intended for controlled drug delivery. *International journal of pharmaceutics* **2002**, *249* (1-2), 165-174.

## **Chapter 8. Conclusions and Future Work**

Xin Yao

This thesis considers the effect of Liquid/Vapor interfaces and dopants on the crystal nucleation and growth in the condensed phases of organic molecules. In Chapters 2 and 3, we demonstrate that the anisotropic organization at the surface can significantly alter the crystal nucleation rate and the polymorph outcome. The surface effect can vary significantly among different materials (water, acetomenonphen, D-arabitol and posaconazole) and strong surface effect requires (1) significant reconstruction at the surface and (2) a polymorph having molecular packing similar to the surface organization. In Chapter 4 and 5, we study the effect of dopants on crystal nucleation and growth. Chapter 4 and 5 together show that a dopant at low concentrations under deep supercooling alters crystal nucleation and growth always by a similar factor as mobility modifier (enhancer or inhibitor). In Chapter 6, we show one example of amorphous drug-polymer salts for global health. By forming ionic interactions between drug and polymer, amorphous lumefantrine (LMF) can be stable under tropical conditions and dissolve fast. In this last Chapter, we will discuss the possible future work and some preliminary results.

### **8.1. Surface Nucleation in Different Molecular Liquids.**

Chapter 2 and 3 show the surface effect can vary significantly among different materials. Although it is hard to predict the effect quantitatively and precisely, we may be able to classify the surface effect on crystal nucleation and predict the class with given the chemical structure of a molecule and the solved crystal structures of polymorphs.

The effect of surface nucleation can be classified based on nucleation rate enhancement ( $J_{s0}/J_{v0}$ ) and polymorph selection, as shown in Figure 1. Class 1: rate enhancement  $< 10^6$  and no

polymorphic change; Class 2: rate enhancement  $\geq 10^6$  and no polymorphic change; Class 3: rate enhancement  $< 10^6$  and polymorphic change; Class 4: rate enhancement  $\geq 10^6$  and polymorphic change. Following the classification, D-arabitol and posaconazole are Class 4 and acetaminophen and water are Class 1. Class 4 features (1) Molecules significantly reconstruct at the surface than in the bulk, (2) a polymorph has molecular packing similar to the surface organization, and (3) another polymorph mimics the isotropic packing in the bulk. Class 1 features mild reconstruction at the surface.

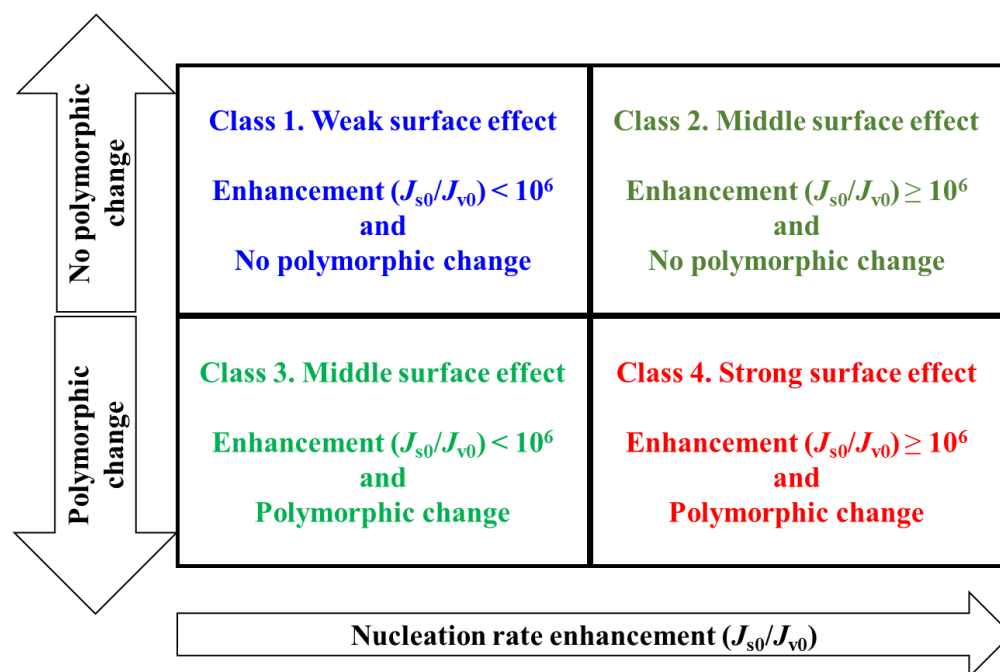


**Figure 1.** Classification of surface effect on crystal nucleation

We can predict the molecular orientation at the surface with our chemistry knowledge, search the crystal structures in database, and then predict the category of the surface effect. We test the prediction by comparing it to the real observation and measurements. If a nucleation rate is too fast or too slow to be measured, we do not include it in the prediction test.

As a start, we tested two materials: Benzyl  $\beta$ -L-arabinopyranoside (BAP) and Fucitol. Their chemical and crystal structures are shown in Figure 2. Both molecules should have strong preferred orientation at the surface with the hydrophobic end pointing outside the liquid. The two polymorphs both have *one* polymorph in the CSD database, and the polymorphs have similar molecular orientation to the expected orientation at the liquid surfaces, see Figure 2. Thus, we predict the surface effect should be Class 2.

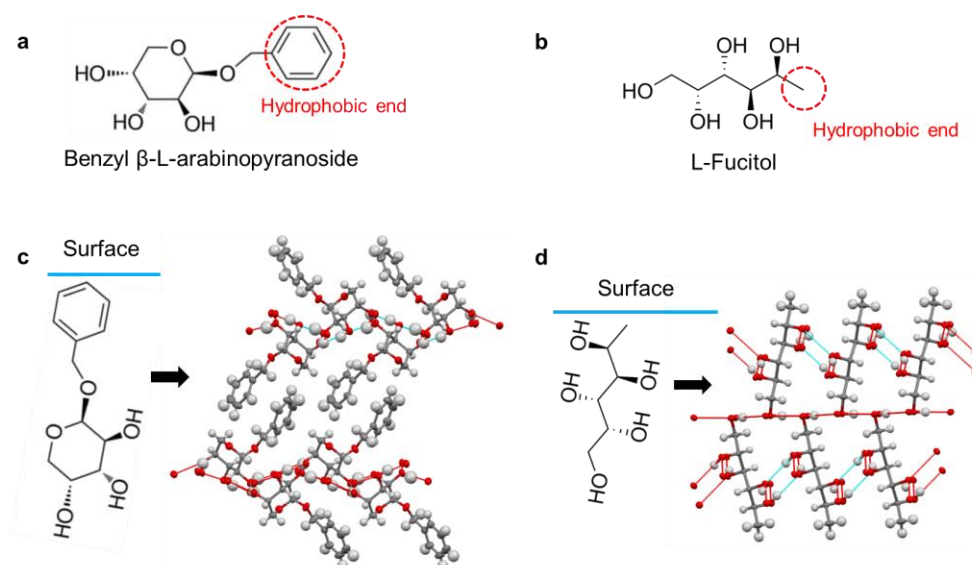


**Figure 2.** (a,b) Chemical and (c,d) crystal structures of Benzyl  $\beta$ -L-arabinopyranoside and L-Fucitol. The predicted orientation of molecules at the liquid surfaces are given and compared to crystal structures.

We measured the nucleation rates of benzyl  $\beta$ -L-arabinopyranoside and Fucitol. We only observed one polymorph nucleating in BAP. The nucleation surface and bulk rates are plotted in Figure 3. The enhancement is bigger than 6 orders of magnitude but with no polymorphic change. Thus, the surface effect on BAP should be Class 2, the same as the prediction. In the case of Fucitol, the crystallization rate is too fast to be measured, and thus not suitable for testing the prediction.

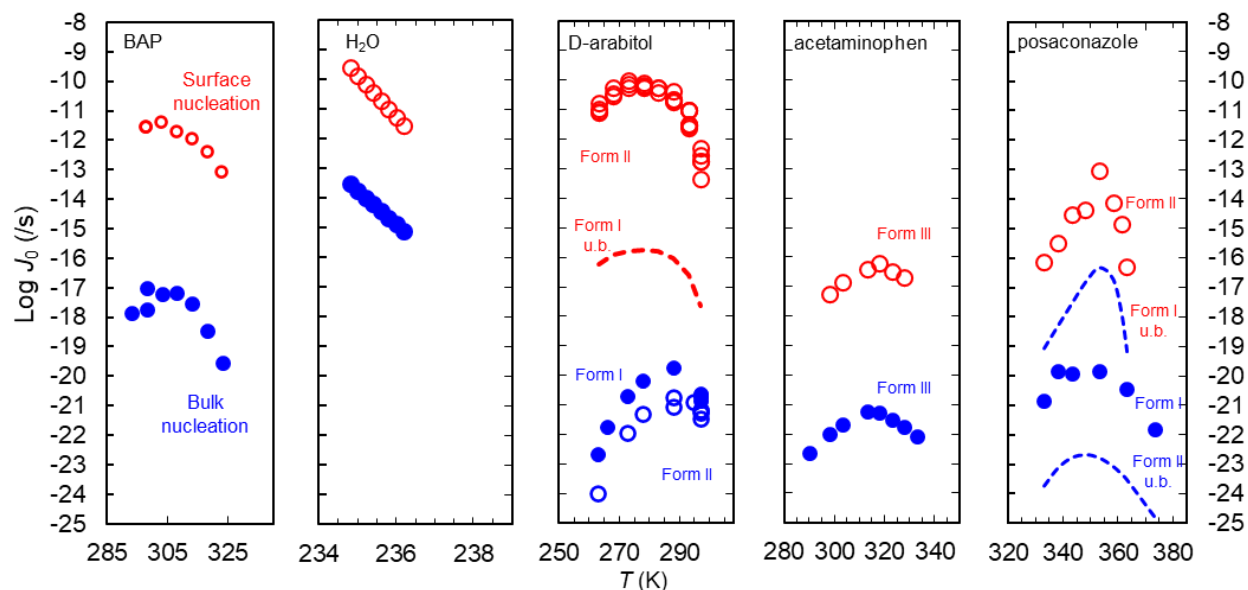


**Figure 3.** Per-molecule surface and bulk nucleation rates of benzyl  $\beta$ -L-arabinopyranoside (BAP) and other materials as a comparison.

Interestingly, the bulk liquid structure of BAP is investigated by small-angle X-ray scattering. The liquid shows a scattering peak at  $d$  spacing of  $17 \text{ \AA}$  (Figure 4), roughly equal to 2 times of the molecular length of  $10 \text{ \AA}$ . The X-ray scattering results indicate the bulk liquid has certain structure, which has two-molecule size domains. It is reasonable that the hydrophilic parts (sugar rings) are contacted, and hydrophobic parts (phenyl rings) are contacted separately. This bulk liquid structure may have similarity to the crystal structure (Figure 2) and cause fast *bulk* nucleation of BAP relative to other organic molecules, and the same polymorph as its surface nucleation. Besides the effect of liquid structure at the surface on crystal nucleation, it is interesting to know the relationship between liquid structure and crystal nucleation in the *bulk*, in the respects of absolute rate and polymorph outcome.



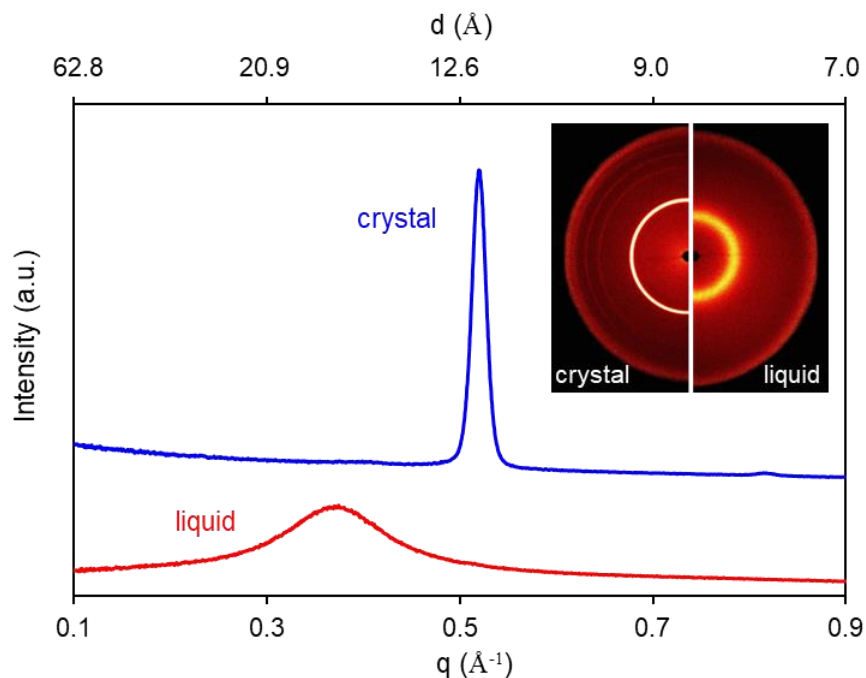


**Figure 4.** Small-angle X-ray scattering of benzyl  $\beta$ -L-arabinopyranoside crystal and liquid at room temperature.

## 8.2. Effect of Dopants on Surface Nucleation

We consider the effect of surface and polymers on crystal nucleation separately in the previous chapters. Now we are in a good position to consider more complicated situations, the effect of a dopant on surface nucleation. The surface effect on crystal nucleation and growth in multi-component systems is important in real applications, e.g., alloys and amorphous solid dispersions (ASDs). ASDs powders usually contain a dissolved polymer and a surfactant, and have large surface/volume ratio. Understanding the surface crystallization with the presence of polymers and surfactants is important for controlling the physical stability of amorphous formulations.

Yu et al. found that surfactants can concentrate at the surface of molecular liquids,<sup>1</sup> and later measured the kinetics of surface enrichment of a polymer in D-mannitol.<sup>2</sup> Thus, two research

topics can be considered: (1) the surface composition at equilibrium *vs.* surface nucleation and (2) crystal nucleation and growth at the surface as a function of time in glasses after surfaces are freshly created. Regarding to the first topic, one example has been shown in Chapter 2. Polymer PVP can concentrate at the surface of D-arabitol and inhibit surface nucleation of D-arabitol significantly.

In the future work, we will measure the surface and bulk nucleation rates in acetaminophen and nifedipine with the presence of polymer and surfactants to understand their effect on surface crystal nucleation and growth. This understanding can provide valid information for predicting the stability of ASDs powders.

### **8.3. Effects of Molecular Weight, Drug Loading, and Synthesis Process on the Protonation Ratio and Performance of Amorphous Drug-Polymer Salts**

In Chapter 6, we show the amorphous LMF-PAA salt is a promising formulation aligned with the global health aims. However, few studies were performed on the details of amorphous drug-polymer salts. What are the effects of molecular weight, drug loading, and synthesis process on stability, dissolution or protonation ratio? Do the stability, dissolution and protonation ratio correlate to each other or not? Taking LMF-PAA as a good model, we vary the molecular weight of PAA, drug loading, and synthesis process, and measure the protonation ratio, long-term stability and dissolution of those varied LMF-PAA salts.

Our preliminary results show that protonation ratio decreases with the increase of drug loading, and cannot reach the ideal stoichiometry (LMF:COOH of PAA = 1:1). When drug loading increases, there are less COOH groups available to the reaction, leading to the decrease of protonation ratio. LMF molecule is much bigger than acrylic acid (monomer of PAA), thus the protonation ratio cannot reach the ideal stoichiometry due to the steric effect. Even though the unprotonated LMF exists at 50% and 75% drug loading, the amorphous LMF-PAA salt is still stable under the tropical condition, indicating 100% protonation ratio is not required for good stability. At the meantime, if we decrease the molecular weight of polymer to the monomer size (propanoic acid or acrylic acid), the stability of amorphous salt is much worse (crystallized in several days), indicating that the molecular weight of PAA impacts the stability of amorphous drug-polymer salt.

With more data collected, we would be able to have a comprehensive answer to the beginning question of this section. This future work is important for designing better amorphous drug-polymer salt.

#### 8.4. References

1. Yu, J.; Li, Y.; Yao, X.; Que, C.; Huang, L.; Hui, H.-W.; Gong, Y. G.; Yu, L., Surface Enrichment of Surfactants in Amorphous Drugs: An X-Ray Photoelectron Spectroscopy Study. *Molecular pharmaceutics* **2022**, *19* (2), 654-660.
2. Yu, J.; Yao, X.; Chailu, Q.; Hunag, L.; Hui, H.-W.; Gong, Y.; Qian, F.; Yu, L., Kinetics of Surface Enrichment of a Polymer in a Glass-Forming Molecular Liquid. *Molecular pharmaceutics* **2022**, *Under review*.